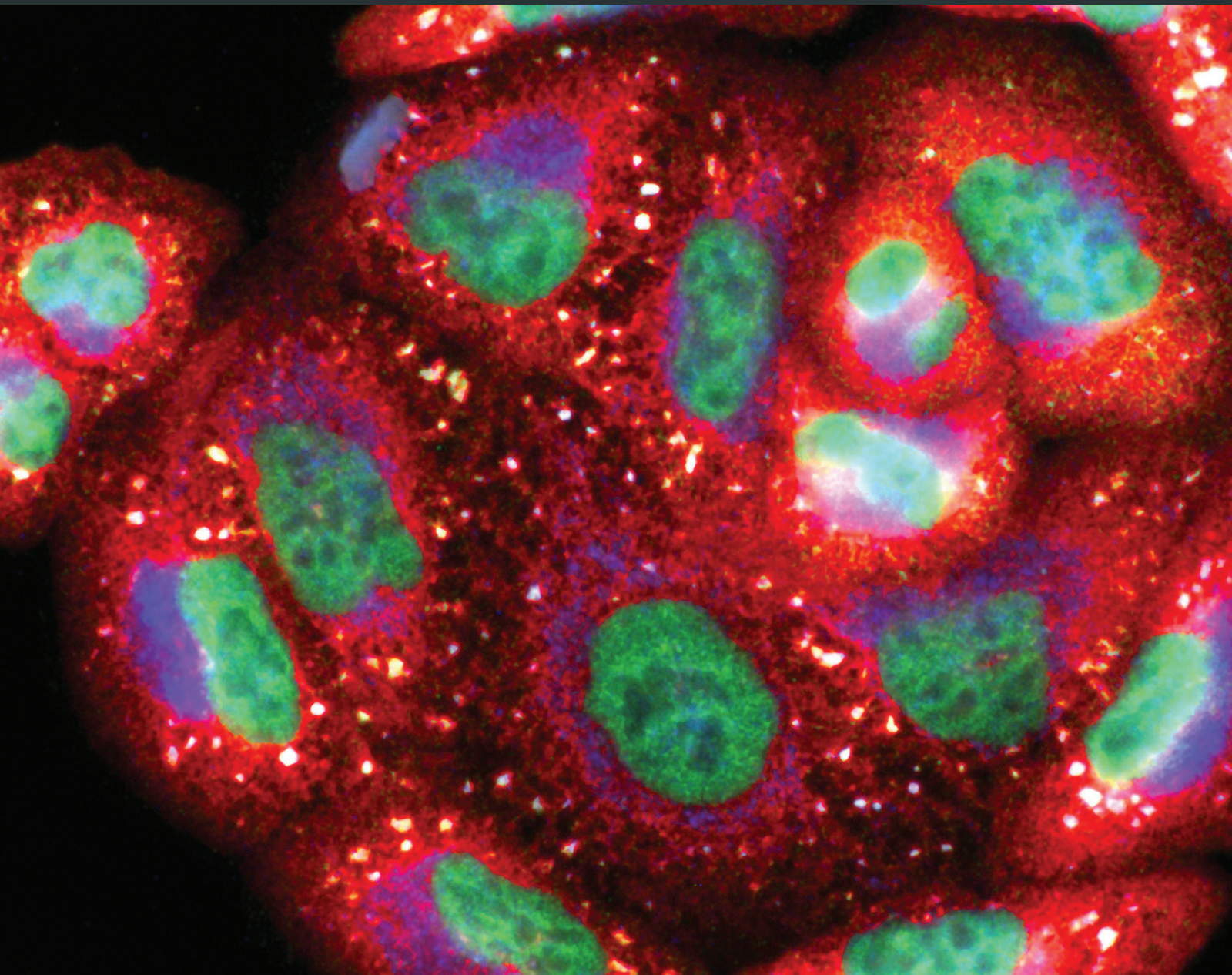


Oxidative Medicine and Cellular Longevity

Mitochondrial Bioenergetics and Quality Control Mechanisms in Health and Disease

Lead Guest Editor: Julio C. B. Ferreira

Guest Editors: Eric Gross and Marcelo Mori






**Mitochondrial Bioenergetics and Quality
Control Mechanisms in Health and Disease**

Oxidative Medicine and Cellular Longevity

Mitochondrial Bioenergetics and Quality Control Mechanisms in Health and Disease

Lead Guest Editor: Julio C. B. Ferreira

Guest Editors: Eric Gross and Marcelo Mori



Copyright © 2019 Hindawi. All rights reserved.

This is a special issue published in “Oxidative Medicine and Cellular Longevity.” All articles are open access articles distributed under the Creative Commons Attribution License, which permits unrestricted use, distribution, and reproduction in any medium, provided the original work is properly cited.

Editorial Board

- Fabio Altieri, Italy
Fernanda Amicarelli, Italy
José P. Andrade, Portugal
Cristina Angeloni, Italy
Antonio Ayala, Spain
Elena Azzini, Italy
Peter Backx, Canada
Damian Bailey, UK
Grzegorz Bartosz, Poland
Sander Bekeschus, Germany
Ji C. Bihl, USA
Consuelo Borrás, Spain
Nady Braidy, Australia
Darrell W. Brann, USA
Ralf Braun, Germany
Laura Bravo, Spain
Vittorio Calabrese, Italy
Amadou Camara, USA
Gianluca Carnevale, Italy
Roberto Carnevale, Italy
Angel Catalá, Argentina
Giulio Ceolotto, Italy
Shao-Yu Chen, USA
Ferdinando Chiaradonna, Italy
Zhao Zhong Chong, USA
Alin Ciobica, Romania
Ana Cipak Gasparovic, Croatia
Giuseppe Cirillo, Italy
Maria R. Ciriolo, Italy
Massimo Collino, Italy
Manuela Corte-Real, Portugal
Mark Crabtree, UK
Manuela Curcio, Italy
Andreas Daiber, Germany
Felipe Dal Pizzol, Brazil
Francesca Danesi, Italy
Domenico D'Arca, Italy
Claudio De Lucia, Italy
Yolanda de Pablo, Sweden
Sonia de Pascual-Teresa, Spain
Cinzia Domenicotti, Italy
Joël R. Drevet, France
Grégory Durand, France
Javier Egea, Spain
- Ersin Fadillioglu, Turkey
Ioannis G. Fatouros, Greece
Qingping Feng, Canada
Gianna Ferretti, Italy
Giuseppe Filomeni, Italy
Swaran J. S. Flora, India
Teresa I. Fortoul, Mexico
Jeferson L. Franco, Brazil
Rodrigo Franco, USA
Joaquin Gadea, Spain
Juan Gambini, Spain
José Luís García-Giménez, Spain
Gerardo García-Rivas, Mexico
Janusz Gebicki, Australia
Alexandros Georgakilas, Greece
Husam Ghanim, USA
Rajeshwary Ghosh, USA
Eloisa Gitto, Italy
Daniela Giustarini, Italy
Saeid Golbidi, Canada
Aldrin V. Gomes, USA
Tilman Grune, Germany
Nicoletta Guaragnella, Italy
Solomon Habtemariam, UK
Eva-Maria Hanschmann, Germany
Tim Hofer, Norway
John D. Horowitz, Australia
Silvana Hrelia, Italy
Stephan Immenschuh, Germany
Maria Isagulians, Latvia
Luigi Iuliano, Italy
Vladimir Jakovljevic, Serbia
Marianna Jung, USA
Peeter Karihtala, Finland
Eric E. Kelley, USA
Kum Kum Khanna, Australia
Neelam Khaper, Canada
Thomas Kietzmann, Finland
Demetrios Kouretas, Greece
Andrey V. Kozlov, Austria
Jean-Claude Lavoie, Canada
Simon Lees, Canada
Ch. Horst Lillig, Germany
Paloma B. Liton, USA
- Ana Lloret, Spain
Lorenzo Loffredo, Italy
Daniel Lopez-Malo, Spain
Antonello Lorenzini, Italy
Nageswara Madamanchi, USA
Kenneth Maiese, USA
Marco Malaguti, Italy
Tullia Maraldi, Italy
Reiko Matsui, USA
Juan C. Mayo, Spain
Steven McAnulty, USA
Antonio Desmond McCarthy, Argentina
Bruno Meloni, Australia
Pedro Mena, Italy
Víctor Manuel Mendoza-Núñez, Mexico
Maria U Moreno, Spain
Trevor A. Mori, Australia
Ryuichi Morishita, Japan
Fabiana Morroni, Italy
Luciana Mosca, Italy
Ange Mouithys-Mickalad, Belgium
Iordanis Mourouzis, Greece
Danina Muntean, Romania
Colin Murdoch, UK
Pablo Muriel, Mexico
Ryoji Nagai, Japan
David Nieman, USA
Hassan Obied, Australia
Julio J. Ochoa, Spain
Pál Pacher, USA
Pasquale Pagliaro, Italy
Valentina Pallottini, Italy
Rosalba Parenti, Italy
Vassilis Paschalis, Greece
Daniela Pellegrino, Italy
Ilaria Peluso, Italy
Claudia Penna, Italy
Serafina Perrone, Italy
Tiziana Persichini, Italy
Shazib Pervaiz, Singapore
Vincent PIALoux, France
Ada Popolo, Italy
José L. Quiles, Spain
Walid Rachidi, France



Zsolt Radak, Hungary
Namakkal S. Rajasekaran, USA
Kota V. Ramana, USA
Sid D. Ray, USA
Hamid Reza Rezvani, France
Alessandra Ricelli, Italy
Paola Rizzo, Italy
Francisco J. Romero, Spain
Joan Roselló-Catafau, Spain
H. P. Vasantha Rupasinghe, Canada
Gabriele Saretzki, UK
Nadja Schroder, Brazil
Sebastiano Sciarretta, Italy

Ratanesh K. Seth, USA
Honglian Shi, USA
Cinzia Signorini, Italy
Mithun Sinha, USA
Carla Tatone, Italy
Frank Thévenod, Germany
Shane Thomas, Australia
Carlo Tocchetti, Italy
Angela Trovato Salinaro, Jamaica
Paolo Tucci, Italy
Rosa Tundis, Italy
Giuseppe Valacchi, Italy
Jeannette Vasquez-Vivar, USA

Daniele Vergara, Italy
Victor M. Victor, Spain
László Virág, Hungary
Natalie Ward, Australia
Philip Wenzel, Germany
Anthony R. White, Australia
Georg T. Wondrak, USA
Michal Wozniak, Poland
Sho-ichi Yamagishi, Japan
Liang-Jun Yan, USA
Guillermo Zalba, Spain
Jacek Zielonka, USA
Mario Zoratti, Italy

Contents

Mitochondrial Bioenergetics and Quality Control Mechanisms in Health and Disease

Julio C. B. Ferreira , Marcelo A. Mori , and Eric R. Gross 

Editorial (3 pages), Article ID 5406751, Volume 2019 (2019)

Melatonin and Docosahexaenoic Acid Decrease Proliferation of PNT1A Prostate Benign Cells via Modulation of Mitochondrial Bioenergetics and ROS Production

Guilherme H. Tamarindo , Daniele L. Ribeiro , Marina G. Gobbo , Luiz H. A. Guerra ,

Paula Rahal , Sebastião R. Taboga , Fernanda R. Gadelha , and Rejane M. Góes 

Research Article (15 pages), Article ID 5080798, Volume 2019 (2019)

Association of Impaired Reactive Aldehyde Metabolism with Delayed Graft Function in Human Kidney Transplantation

Leonie G. M. Wijermars, Alexander F. Schaapherder, Thomas George, Pritam Sinharoy, and Eric R. Gross 

Research Article (10 pages), Article ID 3704129, Volume 2018 (2019)

Increased Mitochondrial Protein Levels and Bioenergetics in the *Musculus Rectus Femoris* of Wfs1-Deficient Mice

Margus Eimre , Kalju Paju, Nadežda Peet , Lumme Kadaja , Marian Tarrend, Sergo Kasvandik ,

Joosep Seppet, Marilin Ivask , Ehte Orlova , and Sulev Kõks 

Research Article (12 pages), Article ID 3175313, Volume 2018 (2019)

Reduced Levels of ATP Synthase Subunit ATP5F1A Correlate with Earlier-Onset Prostate Cancer

René G. Feichtinger , Georg Schäfer, Christof Seifarth, Johannes A. Mayr , Barbara Kofler ,

and Helmut Klocker

Research Article (10 pages), Article ID 1347174, Volume 2018 (2019)


Possible Clues for Brain Energy Translation via Endolysosomal Trafficking of APP-CTFs in Alzheimer's Disease

Senthilkumar Sivanesan , Ravi Mundugaru, and Jayakumar Rajadas 

Review Article (11 pages), Article ID 2764831, Volume 2018 (2019)

The Causal Role of Mitochondrial Dynamics in Regulating Insulin Resistance in Diabetes: Link through Mitochondrial Reactive Oxygen Species

Hung-Yu Lin , Shao-Wen Weng, Yen-Hsiang Chang, Yu-Jih Su , Chih-Min Chang, Chia-Jen Tsai,

Feng-Chih Shen, Jiin-Haur Chuang, Tsu-Kung Lin, Chia-Wei Liou, Ching-Yi Lin, and Pei-Wen Wang 

Research Article (14 pages), Article ID 7514383, Volume 2018 (2019)

Superoxide Anion Production and Bioenergetic Profile in Young and Elderly Human Primary Myoblasts

Mariangela Marrone, Rita Maria Laura La Rovere, Simone Guarnieri , Ester Sara Di Filippo,

Giovanni Monaco, Tiziana Pietrangelo, Geert Bultynck, Stefania Fulle , and Rosa Mancinelli

Research Article (16 pages), Article ID 2615372, Volume 2018 (2019)

Mitochondrial Antioxidants and the Maintenance of Cellular Hydrogen Peroxide Levels

Ryan J. Mailloux 

Review Article (10 pages), Article ID 7857251, Volume 2018 (2019)

Editorial

Mitochondrial Bioenergetics and Quality Control Mechanisms in Health and Disease

Julio C. B. Ferreira ^{1,2} **Marcelo A. Mori** ³ and **Eric R. Gross** ⁴

¹Department of Anatomy, Institute of Biomedical Sciences, University of Sao Paulo, SP, Brazil

²School of Medicine, University of Sao Paulo, SP, Brazil

³Department of Biochemistry and Tissue Biology, Institute of Biology, University of Campinas (Unicamp), SP, Brazil

⁴Department of Anesthesiology, Stanford University School of Medicine, Stanford, California, USA

Correspondence should be addressed to Julio C. B. Ferreira; jcesarbf@usp.br, Marcelo A. Mori; morima@unicamp.br, and Eric R. Gross; ergross@stanford.edu

Received 26 December 2018; Accepted 27 December 2018; Published 20 January 2019

Copyright © 2019 Julio C. B. Ferreira et al. This is an open access article distributed under the Creative Commons Attribution License, which permits unrestricted use, distribution, and reproduction in any medium, provided the original work is properly cited.

Since the first endosymbiotic event occurred, where a proteobacterium was engulfed by larger cells, evolutionary pressure was imposed into mitochondria in order to facilitate the higher energy output required for the evolution of complexity. As a result, mitochondria are also a primary source of reactive molecules involved in physiologic redox signaling and the cause of oxidative stress from pathological events [1]. Besides their central role in ensuring that energy demands are met, mitochondria also contribute to intercellular and intracellular processes such as controlling nuclear gene expression, ion homeostasis, and apoptosis [2]. Thus, maintaining mitochondrial integrity and functionality is critical for cellular homeostasis. As shown by the manuscripts assembled for this special issue, mechanisms for surveillance of mitochondria are complex and diverse. However, these manuscripts together echo the importance of assessing mitochondria for integrity and functionality to identify aberrant redox signaling or early signs of pathology [3]. In general, mitochondrial quality is controlled by a myriad of interconnected systems including (1) enzymatic and nonenzymatic elements capable of fighting oxygen-mediated mitochondrial toxicity [4], (2) mitochondrial proteases and chaperones responsible for the maintenance of mitochondrial proteostasis [5], and (3) a multilayer network of proteins involved in the control of mitochondrial morphology, location, and number [6]. Disruption of mitochondrial quality control mechanisms

in general results in adverse effects that contribute to the establishment and progression of several diseases [7, 8]. Therefore, the development of pharmacological and non-pharmacological approaches capable of optimizing mitochondrial surveillance and quality control mechanisms is a promising tool to treat diseases [9, 10].

This special issue consists of 6 original articles and 2 review articles that broaden our understanding of the regulatory processes involved in mitochondrial bioenergetics, surveillance, and quality control mechanisms of mitochondria in health and disease. In turn, these manuscripts bring new insights into mitochondrial signaling mechanisms and for proposing novel approaches for diagnostics and therapeutics. They cover the topics of (1) redox signaling and oxidative stress, (2) mitochondrial proteostasis, (3) mitochondria-nucleus communication (mitochondrial retrograde signaling), (4) mitochondrial dynamics: mitochondrial biogenesis, fusion, and fission, (5) mitochondrial clearance (mitophagy), and (6) mitochondrial bioenergetics.

Two articles in this special issue focus on the interplay between mitochondria bioenergetics and oxidative stress in skeletal muscle physiology. M. Marrone et al. demonstrate that sarcopenia (i.e., age-related loss of skeletal muscle mass and function) is paralleled by impaired mitochondrial bioenergetics and excessive superoxide levels in both myoblasts and myotubes from skeletal muscle of elderly subjects. However, the direct impact of mitochondrial

dysfunction on skeletal muscle regenerative capacity in ageing still needs to be addressed. M. Eimre et al. provide evidence that *Wfs1*-deficient mice, which display progressive loss of plasma insulin concentration, exhibit reduced mitochondrial oxygen consumption, with no changes in mass of the *soleus* skeletal muscle (abundant in slow twitch muscle fibers). In contrast, the *rectus femoris* skeletal muscle (abundant in fast twitch muscle fibers) has a significant reduction in mass along with increased mitochondrial content and improved bioenergetics. These differences in skeletal muscle metabolism in *Wfs1*-deficient mice should be further explored in order to understanding its possible contribution to diabetes or Wolfram syndrome.

Two other articles in this special issue focus on the role of mitochondrial metabolism in tumor biology. Many tumors are characterized by changes in the mitochondrial electron transport chain composition, which might have either positive or negative impact on energy production. R. G. Feichtinger et al. investigate the expression of oxidative phosphorylation complexes in human prostate carcinomas. There is an accumulation of oxidative phosphorylation complexes I, II, and V in carcinomas compared with benign tissue. Moreover, complex V levels (i.e., ATP5F1A subunit) have a positive correlation with early-onset prostate cancer. Whether these changes in complex abundance reflect functional alterations in mitochondria of tumor cells remains to be determined, although this is likely given the rate limiting characteristic of some of these complexes. In another article, G. H. Tamarindo et al. show that melatonin or docosahexaenoic acid supplementation reduces proliferation of PNT1A cancer cell line. Of interest, melatonin and docosahexaenoic acid have opposite effects on mitochondrial bioenergetics and hydrogen peroxide production in this cell line. Nonetheless, the contribution of mitochondrial biology to the impact of such interventions in PNT1A cancer cell line is still unclear.

Finally, two other articles in this special issue focus on the role of mitochondria as detoxifying systems capable of fighting aldehyde- and oxygen- mediated toxicity. L. G. M. Wijermars et al. demonstrates that impaired aldehyde metabolism, characterized by reduced activity of aldehyde dehydrogenase enzyme and accumulation of toxic reactive aldehydes, is associated with delayed graft function following kidney transplantation in humans. These findings suggest that measuring aldehyde metabolism can be a possible strategy to develop biomarkers to assess delayed graft function from a kidney transplant. In another article, R. J. Mailloux provides an updated view on the critical contribution of mitochondria to the degradation of intracellular hydrogen peroxide as well as its contribution to both redox signaling and oxidative stress. Considering that mitochondria have a high concentration of antioxidant defense enzymes, it is expected that therapies capable of changing mitochondrial content, number, and function will play a critical role in redox biology [1, 2, 6, 10]. In that sense, H.-Y. Lin et al. demonstrate that the reestablishment of mitochondrial network through overexpression of mitochondrial fusion-related proteins or down-regulation of mitochondrial fission-related proteins reduces oxidative stress and improves insulin signaling in cybrid cells

harboring diabetes mellitus-susceptible mtDNA haplogroup. Finally, S. Sivanesan et al. describe in a review article some possible connections between impaired energy metabolism and Alzheimer's disease.

We hope that this special issue provided new insights and fostered new ideas into mitochondrial biology and how it associates with health and disease.

Conflicts of Interest

No potential conflicts of interest were disclosed.

Acknowledgments

We would like to thank the expert reviewers that provided feedback to all manuscripts submitted to this special issue. J.C.B.F. and M.A.M. are supported by the Fundação de Amparo à Pesquisa do Estado de São Paulo, Brazil (FAPESP #2012/05765-2, #2015/20783-5, #2017/16694-2, #2017/01184-9, #2017/07975-8, and #2018/18627-3), the Conselho Nacional de Pesquisa e Desenvolvimento (CNPq), Brazil (#303281/2015-4, #470880/2012-0, #407306/2013-7, and #305069/2015-2), the Coordenação de Aperfeiçoamento de Pessoal de Nível Superior, Brazil (CAPES), Finance Code 001, and Centro de Pesquisa e Desenvolvimento de Processos Redox em Biomedicina (CEPID-Redoxoma). E.R.G. is supported by the National Institutes of Health, National Institute of General Medical Sciences (GM119522).

Julio C. B. Ferreira
Marcelo A. Mori
Eric R. Gross

References

- [1] J. C. Campos, L. H. M. Bozi, L. R. G. Bechara, V. M. Lima, and J. C. B. Ferreira, "Mitochondrial quality control in cardiac diseases," *Frontiers in Physiology*, vol. 7, p. 479, 2016.
- [2] L. A. Kiyuna, R. P. Albuquerque, C. H. Chen, D. Mochly-Rosen, and J. C. B. Ferreira, "Targeting mitochondrial dysfunction and oxidative stress in heart failure: challenges and opportunities," *Free Radical Biology & Medicine*, vol. 129, pp. 155–168, 2018.
- [3] C. B. Ueta, K. S. Gomes, M. A. Ribeiro, D. Mochly-Rosen, and J. C. B. Ferreira, "Disruption of mitochondrial quality control in peripheral artery disease: new therapeutic opportunities," *Pharmacological Research*, vol. 115, pp. 96–106, 2017.
- [4] T. Fernandes, L. R. G. Bechara, N. A. da Paixão, P. C. Brum, E. M. de Oliveira, and J. C. B. Ferreira, "Increased clearance of reactive aldehydes and damaged proteins in hypertension-induced compensated cardiac hypertrophy: impact of exercise training," *Oxidative Medicine and Cellular Longevity*, vol. 2015, Article ID 464195, 11 pages, 2015.
- [5] L. Sun, J. C. Ferreira, and D. Mochly-Rosen, "ALDH2 activator inhibits increased myocardial infarction injury by nitroglycerin tolerance," *Science Translational Medicine*, vol. 3, no. 107, article 107ra111, 2011.
- [6] J. C. Campos, B. B. Queliconi, L. H. M. Bozi et al., "Exercise reestablishes autophagic flux and mitochondrial quality control in heart failure," *Autophagy*, vol. 13, no. 8, pp. 1304–1317, 2017.

- [7] G. Budas, H. M. Costa Jr., J. C. B. Ferreira et al., "Identification of ϵ PKC targets during cardiac ischemic injury," *Circulation Journal*, vol. 76, no. 6, pp. 1476–1485, 2012.
- [8] K. M. S. Gomes, L. R. G. Bechara, V. M. Lima et al., "Aldehydic load and aldehyde dehydrogenase 2 profile during the progression of post-myocardial infarction cardiomyopathy: benefits of Alda-1," *International Journal of Cardiology*, vol. 179, pp. 129–138, 2015.
- [9] M. H. Disatnik, S. Hwang, J. C. B. Ferreira, and D. Mochly-Rosen, "New therapeutics to modulate mitochondrial dynamics and mitophagy in cardiac diseases," *Journal of Molecular Medicine*, vol. 93, no. 3, pp. 279–287, 2015.
- [10] C. B. Ueta, J. C. Campos, R. P. Albuquerque et al., "Cardioprotection induced by a brief exposure to acetaldehyde: role of aldehyde dehydrogenase 2," *Cardiovascular Research*, vol. 114, no. 7, pp. 1006–1015, 2018.

Research Article

Melatonin and Docosahexaenoic Acid Decrease Proliferation of PNT1A Prostate Benign Cells via Modulation of Mitochondrial Bioenergetics and ROS Production

Guilherme H. Tamarindo ¹, Daniele L. Ribeiro ², Marina G. Gobbo ³,
Luiz H. A. Guerra ³, Paula Rahal ³, Sebastião R. Taboga ³, Fernanda R. Gadelha ⁴,
and Rejane M. Góes ³

¹Institute of Biology, State University of Campinas, Campinas, SP, Brazil

²Department of Histology, Institute of Biomedical Sciences, Federal University of Uberlândia, Uberlândia, MG, Brazil

³Department of Biology, Institute of Biosciences, Humanities and Exact Sciences, São Paulo State University, São José do Rio Preto, SP, Brazil

⁴Department of Biochemistry and Tissue Biology, Institute of Biology, State University of Campinas, Campinas, SP, Brazil

Correspondence should be addressed to Rejane M. Góes; remagoes@ibilce.unesp.br

Received 12 June 2018; Revised 20 July 2018; Accepted 18 September 2018; Published 9 January 2019

Academic Editor: Ana Cipak Gasparovic

Copyright © 2019 Guilherme H. Tamarindo et al. This is an open access article distributed under the Creative Commons Attribution License, which permits unrestricted use, distribution, and reproduction in any medium, provided the original work is properly cited.

Prostate cancer development has been associated with changes in mitochondrial activity and reactive oxygen species (ROS) production. Melatonin (MLT) and docosahexaenoic acid (DHA) have properties to modulate both, but their protective role, mainly at early stages of prostate cancer, remains unclear. In this study, the effects of MLT and DHA, combined or not, on PNT1A cells with regard to mitochondria bioenergetics, ROS production, and proliferation-related pathways were examined. Based on dose response and lipid accumulation assays, DHA at 100 μM and MLT at 1 μM for 48 h were chosen. DHA doubled and MLT reduced (40%) superoxide anion production, but coinubation (DM) did not normalize to control. Hydrogen peroxide production decreased after MLT incubation only ($p < 0.01$). These alterations affected the area and perimeter of mitochondria, since DHA increased whereas MLT decreased, but such hormone has no effect on coinubation. DHA isolated did not change the oxidative phosphorylation rate (OXPHOS), but decreased ($p < 0.001$) the mitochondrial bioenergetic reserve capacity (MBRC) which is closely related to cell responsiveness to stress conditions. MLT, regardless of DHA, ameliorated OXPHOS and recovered MBRC after coinubation. All incubations decreased AKT phosphorylation; however, only MLT alone inhibited p-mTOR. MLT increased p-ERK1/2 and, when combined to DHA, increased GSTP1 expression ($p < 0.01$). DHA did not change the testosterone levels in the medium, whereas MLT alone or coinubated decreased by about 20%; however, any incubation affected AR expression. Moreover, incubation with luzindole revealed that MLT effects were MTR1/2-independent. In conclusion, DHA increased ROS production and impaired mitochondrial function which was probably related to AKT inactivation; MLT improved OXPHOS and decreased ROS which was related to AKT/mTOR dephosphorylation, and when coinubated, the antiproliferative action was related to mitochondrial bioenergetic modulation associated to AKT and ERK1/2 regulation. Together, these findings point to the potential application of DHA and MLT towards the prevention of proliferative prostate diseases.

1. Introduction

Despite its multifactorial etiology, progression and aggressiveness of prostate cancer (PCa) have been related to oxidative stress [1, 2] and the increased production of reactive

oxygen species (ROS) is closely associated to alterations in the mitochondria [3]. Such organelles play a crucial role in all stages of malign transformation [3] and have been associated to PCa due to reduction in apoptotic potential [4], pathogenic mutations in genes encoding the electron transport

chain (ETC) respiratory complexes, and loss of mitochondrial DNA and integrity [5]. Therefore, modulation of mitochondria physiology may be a good therapeutic target, either in the prevention of tumor development or in the induction of cancer cell death.

Melatonin (MLT) is a pleiotropic hormone with antioxidant properties that regulate mitochondrial activity [6–10] and has been investigated as a PCa suppressor [11]. Patients with PCa exhibit low MLT serum levels when compared to healthy individuals, with a notable decrease when benign prostatic hyperplasia (BPH) progresses to adenocarcinoma [11, 12]. Most cases of PCa (75%) are diagnosed in men over 65 years [11], coincidental to the period when MLT synthesis is reduced [13] and mitochondrial dysfunction increases due to ROS production [14, 15]. Regarding this evidence, MLT supplementation in patients within risk age of PCa (30–40 years old) may be an interesting chemoprevention strategy [16]. Apart from its own anticancer properties, MLT has also been investigated in combination with other compounds, due to its ability to sensitize cells and potentialize the antiproliferative effect of these compounds by inhibition of survival pathways, e.g., AKT [17]. In this context, polyunsaturated fatty acids omega-3 (PUFA ω -3), mainly docosahexaenoic acid (DHA), have been reported to increase mitochondrial ROS in tumor cells through AKT/mTOR inhibition [18], leading to cell death. Furthermore, DHA catabolism occurs in the peroxisome and mitochondria [19] and is very susceptible to oxidation caused by reactive species [20] leading to generation of cyto- and genotoxic hydroperoxides and aldehydes [21]. Although evidence suggests that DHA, a fatty acid present in the human diet and usually adopted as nutritional supplementation, can exert antiproliferative effects, it has not yet been investigated in early stages of prostate proliferative disorders, such as benign hyperplasia.

The treatment adopted in most cases of androgen-dependent PCa is androgen ablation, which can lead to selective advantage to androgen-independent cancer cells that eventually proliferate and promote the recurrence of a more aggressive phenotype [22]. Administration of compounds that affect sexual steroid pathways also have been a strategy in prevention and treatment of PCa, but the mechanisms triggered are still not fully elucidated and their safety is uncertain [23]. In this context, one of the avenues to decrease the high mortality rate caused by PCa [24] may be the chemoprevention focused on the suppression of growth or survival of abnormal cells at early stages. Therefore, our aim was to test, *in vitro*, the antiproliferative potential of MLT and DHA, combined or not, in early stages of prostate proliferative disorders. For this purpose, the proliferation of PNT1A cells, an epithelial benign prostate line sensitive to androgen, and the correlations to ROS production, mitochondrial bioenergetics, and proliferative signaling pathways were evaluated.

2. Material and Methods

2.1. Cell Culture and Treatments. PNT1A cells (#95012614—Health Protection Agency, England, UK) were seeded in RPMI 1640 medium (#R6504—Sigma-Aldrich, St.

Louis, Missouri, EUA) enriched with 10% fetal bovine serum (#S0011—Vitrocell, Campinas, São Paulo, Brazil), 1% of penicillin, streptomycin, and amphotericin B (#15240062—Life Technologies, Paisley, UK) and incubated in a wet incubator with 5% of CO₂ at 37°C. For cell maintenance, the medium was replaced every 2–3 days and subculture was done when 70–85% confluence was reached. For the experiments, the cells were incubated at the desired density and were allowed to attach during 24 hours.

DHA (#D2534—Sigma-Aldrich, St. Louis, Missouri, EUA) concentrations (10 μ M, 20 μ M, 50 μ M, and 100 μ M) were freshly prepared in RPMI 1640 culture medium from a stock solution of 20 mM DHA in anhydrous ethanol (vehicle), and the effects on cell proliferation at 24 h, 48 h, and 72 h were tested. These concentrations were chosen according to previous experiments with normal epithelial prostatic cells RWPE-1 [25]. DHA concentration and time of incubation that first exerted antiproliferative effects, combined to higher lipid accumulation, were chosen to perform all forward assays.

Because there are several studies reporting major pathways triggered by MLT (#M5250—Sigma-Aldrich, St. Louis, Missouri, EUA) in different concentrations [26, 27], we first evaluated physiologic (pM–nM), supraphysiologic (nM– μ M), and pharmacologic (μ M–mM) ranges on cell proliferation. Then, the effects of 1 pM, 1 nM, 1 μ M, and 1 mM of MLT were tested alone or in coinubation with DHA. These MLT concentrations in the medium were freshly prepared from a stock solution at 100 mM in anhydrous ethanol (vehicle), and the first that exerted antiproliferative effects, alone and combined to DHA, were chosen for forward assays. For coinubation assays, DHA and MLT at the desired concentration were added to the medium at the same time. Proliferation assay with luzindole (#15998—Cayman Chemical, MI, USA), a nonselective antagonist of MTR1 and MTR2 membrane receptors, 100-fold higher than the MLT work concentration, was performed in control (vehicle incubation only), melatonin (MLT), DHA, and coinubation (DM) to determine the pathways of hormone action.

To ensure that the mechanisms observed were not due to vehicle, all control assays were incubated with anhydrous ethanol at the same volume of DHA, MLT, or DM added to the cells. Also, the concentration of vehicle in the medium never exceeded 0.5% which did not exert alteration on cell proliferation (data not shown).

2.2. Cell Proliferation Assay. The effects of treatments were evaluated after incubation of 1×10^4 cells/well with commercial colorimetric kit CellTiter 96® Aqueous One Solution Cell Proliferation Assay (#G3580—Promega Corporation, Madison, WI, USA), according to the manufacturer's instructions. Absorbance was determined at 490 nm in an Epoch microplate reader (BioTek Instruments Inc., Winooski, VT, EUA). Three independent experiments in triplicate were performed for statistical analysis.

2.3. Lipid Accumulation. Qualitative evaluation of lipid uptake was assessed by light microscopic analysis after incubation with Oil Red O (#O0625—Sigma-Aldrich, St. Louis,

Missouri, EUA). Cells were seeded at 1×10^4 cells/well followed by incubation with DHA (10 μ M, 20 μ M, 50 μ M, and 100 μ M) or vehicle (control). After incubation, the medium was removed, and the cells were washed with PBS and fixed with paraformaldehyde 4% for 10 minutes. Then, cells were immersed in isopropanol 60% for 5 minutes at room temperature (RT) followed by incubation for 60 minutes with fresh Oil Red O prepared at 0.03% in isopropanol. After two independent experiments performed in duplicate, the most representative profile of lipid accumulation was considered for each DHA concentration.

Quantitative evaluation of intracellular lipids was assessed after incubation (5×10^4 cells/well) with 5 μ M of BODIPY™ Lipid Probes 493/503 (#D3922—Molecular Probes®, Invitrogen) prepared in serum-free medium for 5 minutes at RT, according to the manufacturer's instructions. Immediately, images were captured with an inverted fluorescence microscope (Axio Vert.A1 Carl Zeiss AG, DE) with the same time of exposure (280 ms). Quantification of total fluorescence intensity was assessed with ImageJ software, and at least four hundred cells per treatment from three consecutive passages were considered.

2.4. ROS Determination. Hydrogen peroxide (H_2O_2) production was determined after incubation of 10^6 cells/mL in PBS/ Mg^{+2} , 5 mM of succinate, 1 U/mL of HRP, and 25 μ M of Amplex Red (Molecular Probes®, Thermo Fisher Inc.). Fluorescence intensity was assessed at 563 nm excitation and 587 nm emission, using a Cytation 3 Cell Imaging Multi-Mode Reader (BioTek Instruments Inc., Winooski, VT, EUA). Cell H_2O_2 production was correlated to fluorescence intensity and calculated as described previously [28]. Three independent experiments in triplicate were considered for statistical analysis.

Superoxide anion production ($O_2^{\bullet-}$) was assessed after incubation with MitoSOX® Red dye (#M36008—Molecular Probes, Thermo Fisher Inc.), according to the manufacturer's instructions. After treatments, the medium was removed, and the cells (5×10^4 /well) were washed twice with KH buffer (NaCl 120 mM, $NaHCO_3$ 15 mM, KCl 5 mM, NaH_2PO_4 1.5 mM, and Na_2HPO_4 0.7 mM) and incubated with the dye at 3 μ M for 15 minutes at 37°C in an incubator with 5% CO_2 . Then, cells were washed twice with KH buffer to remove the dye that did not enter the mitochondria. A total of fifteen images from wells containing cells of consecutive passages were captured at the same exposure time (1200 ms) with an inverted fluorescence microscope (Axio Vert.A1 Carl Zeiss AG, DE). Total field fluorescence intensity was measured with ImageJ software and normalized with the number of cells per field. At least 250 cells were counted in each treatment.

2.5. Morphometric Analysis of Mitochondria. Cells were seeded at a density 5×10^4 cells/well in a CELL^{view} bottom glass (Greiner Bio-One) and, after treatments, incubated with MitoTracker Orange CMTMRos (#M7510 Molecular Probes, Invitrogen) at 50 nM in a serum-free medium at 37°C and 5% CO_2 , according to the manufacturer's instructions. After 15 minutes, media were replaced and live cells were immediately

analyzed with an inverted fluorescence microscope (Axio Observer Z1 Carl Zeiss AG, DE). Morphometric evaluation of mitochondria was done with a macro created for ImageJ software by Dagda and colleagues [29]. This tool was previously validated [29] and allows measuring mitochondria stained with the specific fluorescent dye and determining the area and perimeter of the organelle. Measurements were performed in at least fifteen images captured with 40x objective. Fluorescent regions of each image were measured followed by normalization of number of cells per field. At least 100 cells were considered for statistical analysis.

2.6. Mitochondrial Membrane Potential Determination. After incubations, cells were centrifuged at 2000 rpm for 5 minutes at 4°C, then the pellets were washed and resuspended in PBS. Respiration buffer (sucrose 125 mM, KCl 65 mM, HEPES 10 mM pH 7.2, $MgCl_2$ 1 mM, KH_2PO_4 2 mM, EGTA 0.5 mM, and BSA 0.15%), 10^6 cells/mL, succinate 5 mM, safranin O 5 μ M, and digitonin 20 μ M were added to a cuvette, as described by Holden and Sze [30] (concentrations of cells, succinate, safranin O, and digitonin were adapted for increased effectiveness without damaging the integrity of the mitochondria). For analysis, ADP 50 μ M, oligomycin 1 μ g/mL (OLG), and antimycin A 1 μ g/mL (AA) were added to the incubation medium. Values were recorded in a fluorescence spectrophotometer (F-2500 Hitachi) with 495 nm and 589 nm excitation and emission, respectively. The most representative profile of mitochondrial membrane potential of three independent experiments performed in duplicate was plotted and values shown in arbitrary fluorescence units.

2.7. Oxygen Consumption Rate. Oxygen consumption rate (OCR) was assessed in a Hansatech Oxygraph (Yellow Springs Corporation) as described by Silva and colleagues [31]. Basal state (S2) was determined after incubation of 10^6 cells/mL in respiration buffer (sucrose 125 mM, KCl 65 mM, HEPES 10 mM pH 7.2, $MgCl_2$ 1 mM, KH_2PO_4 2 mM, EGTA 0.5 mM, and BSA 0.15%) in the presence of digitonin at 20 μ M and succinate 5 mM. State 3 (S3) was determined by OCR and assessed after the addition of 50 μ M ADP and state 4 (S4) with oligomycin 1 μ g/mL. Respiratory control (RC) was calculated as $RC = (\text{state 3 OCR} / \text{state 4 OCR})$ and indicates the oxidative phosphorylation rate. ETC maximum velocity (S3U) was determined by OCR and assessed after the addition of mitochondrial uncoupler carbonyl cyanide m-chlorophenyl hydrazone (CCCP) at 1 μ M. Mitochondrial bioenergetic reserve capacity was calculated as $MBRC = (S3U - S2)$, as described by Vayalil and Landar [32], considering nonmitochondrial oxygen consumption. At least three experiments in triplicate were considered for statistical analysis.

2.8. Testosterone Level in the Medium. After incubations, the medium was removed from the wells and testosterone levels were measured with ELISA assay from an AccuBind Testosterone System Microwells (#3725300—Monobind Inc., Lake Forest, CA, USA) commercial kit, according to the manufacturer's instructions. Concentrations of testosterone (ng/mL) were normalized by protein amount in the cell lysate from

the correspondent well. Three independent experiments were performed in triplicate for statistical analysis.

2.9. Western Blotting. After incubations, cells (5×10^4 /well) were lysed in RIPA buffer in the presence of 10% protease inhibitor cocktail, sodium orthovanadate (1:100), and PMSF (1:1000). All reagents were obtained from Sigma-Aldrich (St. Louis, Missouri, EUA). Protein quantification was performed in an Epoch microplate reader coupled to Take3 Micro-Volume (BioTek Instruments Inc., Winooski, VT, EUA) at 280 nm. After electrophoresis in SDS-PAGE, proteins (50 or 100 $\mu\text{g}/\mu\text{L}$) were transferred to the nitrocellulose membrane for 1 hour and 40 minutes in a semidry system. Nonspecific bindings were blocked with BSA 5% in TBST for 1 h (phosphorylated proteins) or nonfat milk at 5% in TBST for 30 minutes (for nonphosphorylated proteins), at RT in a shaker. Primary antibodies anti-phospho-mTOR (rabbit monoclonal, Santa Cruz Biotechnology, 1:400), anti-phospho-AKT (rabbit polyclonal, Santa Cruz Biotechnology, 1:400), anti-phospho-ERK1/2 (rabbit polyclonal, Cell Signaling, 1:1000), anti-GSTP1 (rabbit polyclonal, Cell Signaling, 1:1000), and anti- β -actin (mouse monoclonal, Santa Cruz Biotechnology, 1:1000) were incubated overnight at 4°C. Secondary antibodies were prepared at 10x dilution of the respective primary antibody and incubated at 4°C for 1 h. The ECL system was applied for band visualization and image capture. All incubations were analyzed in triplicate ($n = 3$) in the same gel, and one protein per gel in addition to β -actin for loading control was quantified. Relative densitometry was assessed using ImageJ software.

2.10. Statistical Analyses. Statistical analyses were performed with GraphPad Prism® software (GraphPad Prism software, v.5.0). First, distribution of samples was analyzed with Kolmogorov-Smirnov and Shapiro-Wilk normality tests. Parametric distributions were submitted to *T* test or one-way ANOVA followed by Tukey test (post hoc); nonparametric distributions to Mann-Whitney or Kruskal-Wallis test followed by Dunn test (post hoc). $p < 0.05$ was considered statistically different.

3. Results

3.1. Pro- or Antimitogenic Actions of DHA in PNT1A Cells Are Time- and Concentration-Dependent. All DHA concentrations tested within 24 h, except 10 μM , increased the proliferation of PNT1A cells. Stimulation of the clonogenic rate at 48 h was only observed with 20 and 50 μM as well as 10 and 20 μM at 72 h (Figure 1(a)). At 100 μM , the highest concentration tested, cell proliferation (Figure 1(a)) reduced only after 48 h (control: 0.41 ± 0.01 ; DHA 0.34 ± 0.01 abs) and 72 h (control: 0.36 ± 0.01 ; DHA: 0.20 ± 0.01 abs). DHA also stimulated lipid accumulation in a dose- and time-dependent pattern, as represented in Figure 1(b) for 48 h incubation. Therefore, 100 μM of DHA at 48 h was selected to perform all forward assays.

3.2. MLT Decreased PNT1A Cell Proliferation. MLT at physiological concentrations (1 pM and 1 nM) had no effect on cell proliferation (Figure 1(c)) but decreased at 1 μM

(control: 0.87 ± 0.02 ; MLT 0.74 ± 0.02 abs) and 1 mM (control: 0.81 ± 0.02 ; MLT: 0.50 ± 0.005 abs). At 1 μM , MLT exerted the most antiproliferative effect in comparison to all concentrations analyzed (Figure 1(c)). We chose MLT at the concentration of 1 μM because it was the first to exert an antiproliferative effect. Also, our aim was to evaluate the MLT effects, regardless of membrane receptor activation, which occurs mainly in the pM–nM range.

3.3. MLT Improved Antiproliferative Effect When Combined to DHA. MLT coincubated with DHA 100 μM for 48 h roughly decreased cell proliferation (Figure 1(c)) at 1 μM (control: 0.87 ± 0.02 ; DM: 0.58 ± 0.02 abs) and 1 mM (control: 0.81 ± 0.02 ; DM: 0.29 ± 0.01 abs). Coincubation with MLT at 1 mM exhibited the most antiproliferative effect, decreasing by 50% the cell proliferation rate compared to DM at 1 μM (Figure 1(c)).

3.4. DHA Alone or Coincubated with MLT Increased Lipid Intracellular Amount. Incubation with DHA alone (100 μM) increased by 62% lipid accumulation in PNT1A cells after 48 h and, when coincubated with MLT 1 μM , raised to 82% (control: 3.97 ± 0.19 , DHA: 6.66 ± 0.14 , and DM: 7.34 ± 0.16 FI/cell $\times 10^5$). MLT alone did not affect intracellular lipid storage (Figure 2).

3.5. DHA Increased Superoxide Anion Production and MLT Alleviated ROS Generation. DHA did not alter H_2O_2 production by PNT1A cells when compared to control (Figure 3(a)). MLT reduced 62% of total H_2O_2 production, but when coincubated with DHA, H_2O_2 generation increased compared to control, as shown in Figure 3(a) (control: 0.098 ± 0.007 , MLT: 0.037 ± 0.008 , and DM: 0.144 ± 0.009 pmol/min/ 10^6 cells).

DHA doubled whereas MLT alone reduced 40% of superoxide anion production (Figures 3(b) and 3(c)) by PNT1A cells when compared to control. Coincubation attenuated such ROS production compared to DHA alone, but did not normalize to control (control: 7.91 ± 0.73 , DHA: 16.78 ± 1.30 , MLT: 4.75 ± 0.39 , and DM: 12.26 ± 0.65 FI/cell $\times 10^4$).

3.6. MLT Improved Oxidative Phosphorylation and Alleviated Mitochondrial Damage Caused by DHA. None of the incubations altered basal OCR in PNT1A cells (S2—Figure 4(a)). Respiratory control (Figure 4(b)) was increased by MLT alone or coincubated whereas DHA did not promote any change on OCR when compared to control (control: 3.13 ± 0.08 , MLT: 4.89 ± 0.23 , and DM: 3.71 ± 0.13). Mitochondrial bioenergetic reserve capacity (MBRC) of PNT1A cells (Figure 4(d)) was unaffected by MLT alone, decreased 2-fold after incubation only with DHA, and raised roughly by 130% in DM compared to control (control: 2.90 ± 0.27 , DHA: 1.59 ± 0.11 , and DM: 3.77 ± 0.07 nmol $\text{O}_2/10^6$ cells/min). MLT alone decreased both mitochondrial area and perimeter, and DHA alone increased as well as coincubation when compared to control (area—control: 122.1 ± 5.79 , DHA: 147.1 ± 5.33 , MLT: 89.55 ± 4.05 , and DM: 146.3 ± 8.04 μm^2 /perimeter—control: 8.02 ± 0.28 , DHA: 10.03 ± 0.21 , MLT: 6.23 ± 0.23 , and DM: 9.47 ± 0.48 μm), as shown in Figures 5(a)–5(c).

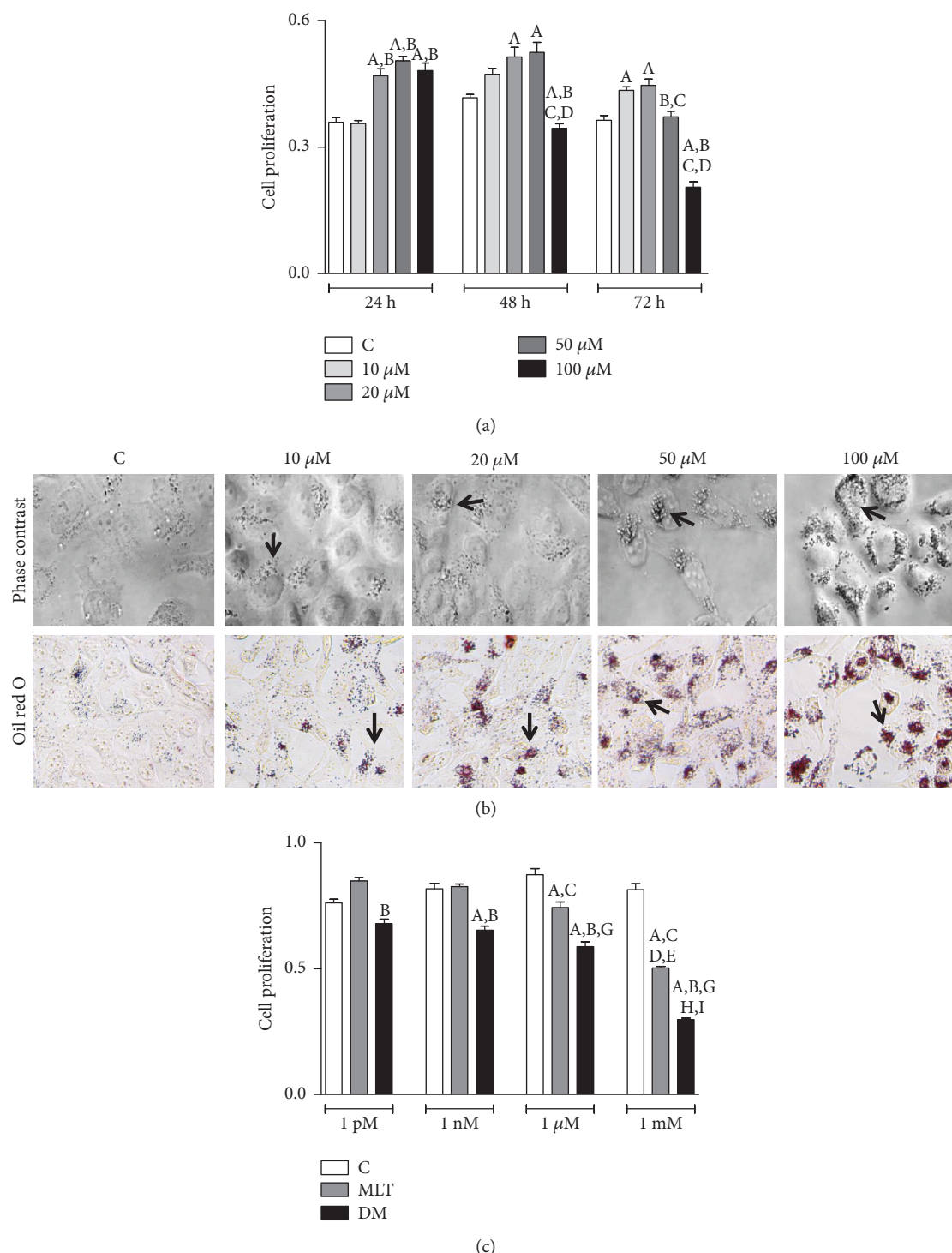


FIGURE 1: DHA and MLT antiproliferative effect. (a) PNT1A cell proliferation incubated with 10, 20, 50, and 100 μM of DHA after 24, 48, and 72 h. Legend of panel (a): C: control (vehicle incubation). Statistical analysis of panel (a): (A) different from C; (B) different from 10 μM ; (C) different from 20 μM ; (D) different from 50 μM . (b) Lipid droplets (arrow) stained (red) with Oil Red O (bottom row) after incubation with vehicle (C) or DHA at 10, 20, 50, and 100 μM for 48 h. Images captured with 40x objective. For qualitative analysis, two independent experiments were performed in duplicate, and the most representative lipid accumulation for each DHA concentration is shown. (c) PNT1A cell proliferation incubated with 1 pM, 1 nM, 1 μM , and 1 mM of MLT after 48 h. Legend of panel (c): C: control (vehicle incubation); MLT: melatonin incubation; DM: coincubation with 100 μM of DHA and melatonin. Statistical analysis of panel (c): (A) different from C; (B) different from MLT considering same concentration range; (C) different from MLT-1 pM; (D) different from MLT-1 nM; (E) different from MLT-1 μM ; (G) different from DM-1 pM; (H) different from DM-1 nM; (I) different from DM-1 μM ; $p < 0.05$ was determined as statistically different. All proliferation assays were performed in triplicate, and three independent events considered for statistical analysis. Values show the mean of absorbance and SEM.

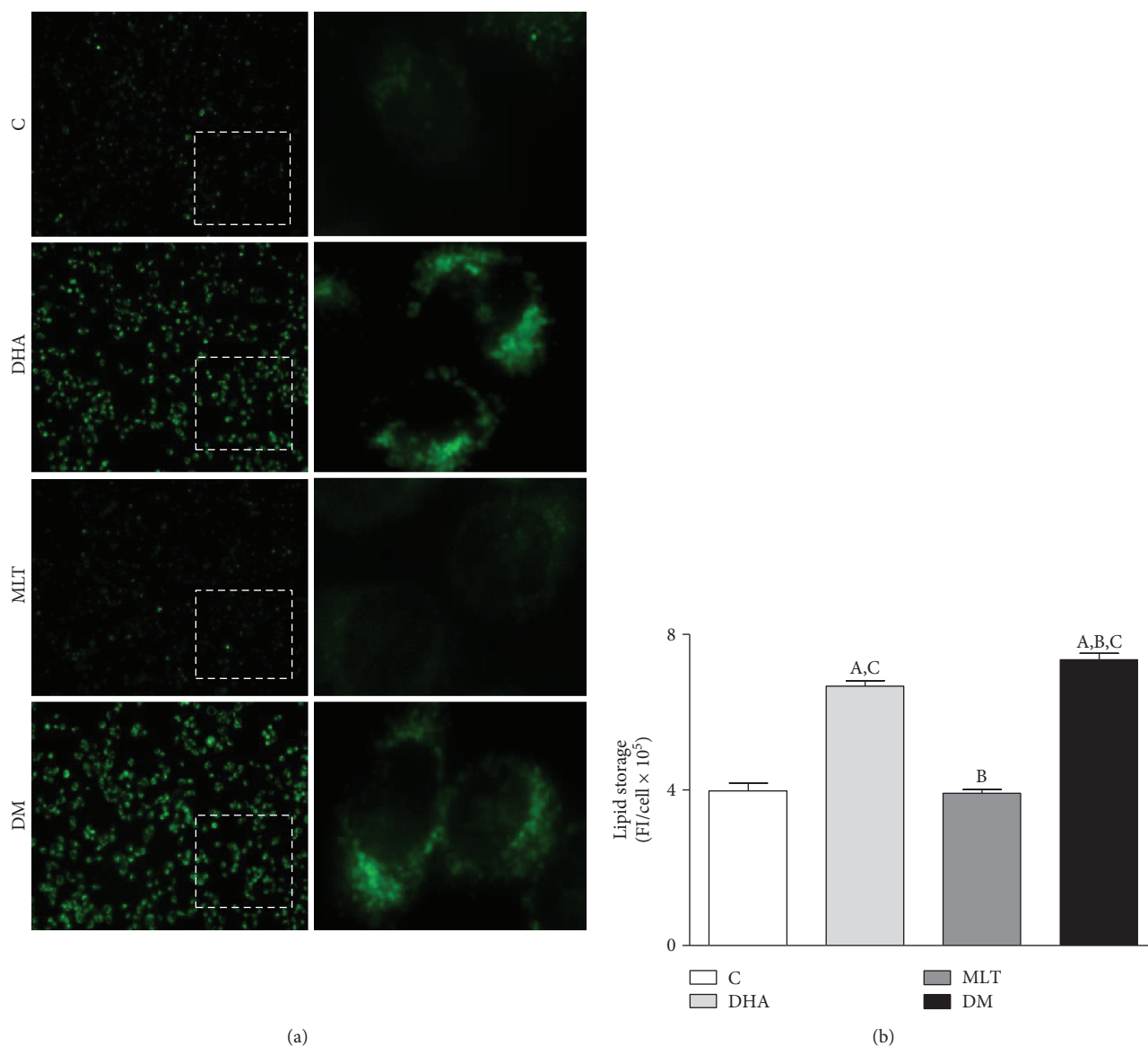


FIGURE 2: Lipid accumulation. (a) Detection of lipids (green) in PNT1A cells with BODIPY. Cells were incubated with 100 μM of DHA and 1 μM of MLT for 48 h before the dye. Images of left column were captured with 10x objective and right column (insets) with 40x. (b) Lipid storage quantification. C: control (vehicle incubation); DHA: incubation with 100 μM of DHA for 48 h; MLT: incubation with 1 μM of melatonin for 48 h; DM: coincubation with 100 μM of DHA and 1 μM of melatonin for 48 h. Statistical analysis: (A) different from C; (B) different from DHA; (C) different from MLT. $p < 0.05$ was considered statistically different. At least four hundred cells per treatment from three consecutive passages were analyzed. Values show the mean of fluorescent units per cell and SEM.

3.7. MLT and DHA Modulated the Survivor and Cell Proliferation-Related Pathways Regardless of MTR1 or MTR2 Sensitization. Luzindole did not change cell proliferation (Figure 6(f)) in control or MLT, but was reduced when incubated with DHA (control: 0.65 ± 0.02 ; DHA: 0.48 ± 0.02 abs) and DM (control: 0.51 ± 0.03 ; DM: 0.35 ± 0.02 abs) compared to incubations without the antagonist.

DHA and MLT alone suppressed AKT phosphorylation (Figure 6(a)) when compared to control, as well as coincubation, which did not show a synergistic effect (control: 2.17 ± 0.12 , DHA: 1.33 ± 0.18 , MLT: 1.31 ± 0.03 , and DM: 1.51 ± 0.15). MLT alone also inhibited mTOR activation (Figure 6(b)) compared to control, whereas DHA alone or

in coincubation did not change (control: 0.150 ± 0.015 ; MLT: 0.082 ± 0.003). On the other hand, MLT alone increased ERK1/2 phosphorylation (Figure 6(c)) compared to control and coincubation with DHA amplified this effect (control: 0.045 ± 0.005 , MLT: 0.125 ± 0.009 , and DM: 0.223 ± 0.021). GSTP1 expression (Figure 6(d)) did not change in isolated incubations, but together, MLT and DHA increased 20% compared to MLT alone (MLT: 1.69 ± 0.10 ; DM: 2.34 ± 0.17).

3.8. MLT May Influence the Androgen Pathway. Testosterone levels in culture medium (Figure 7) decreased by 25% after MLT incubation compared to control and 20% when

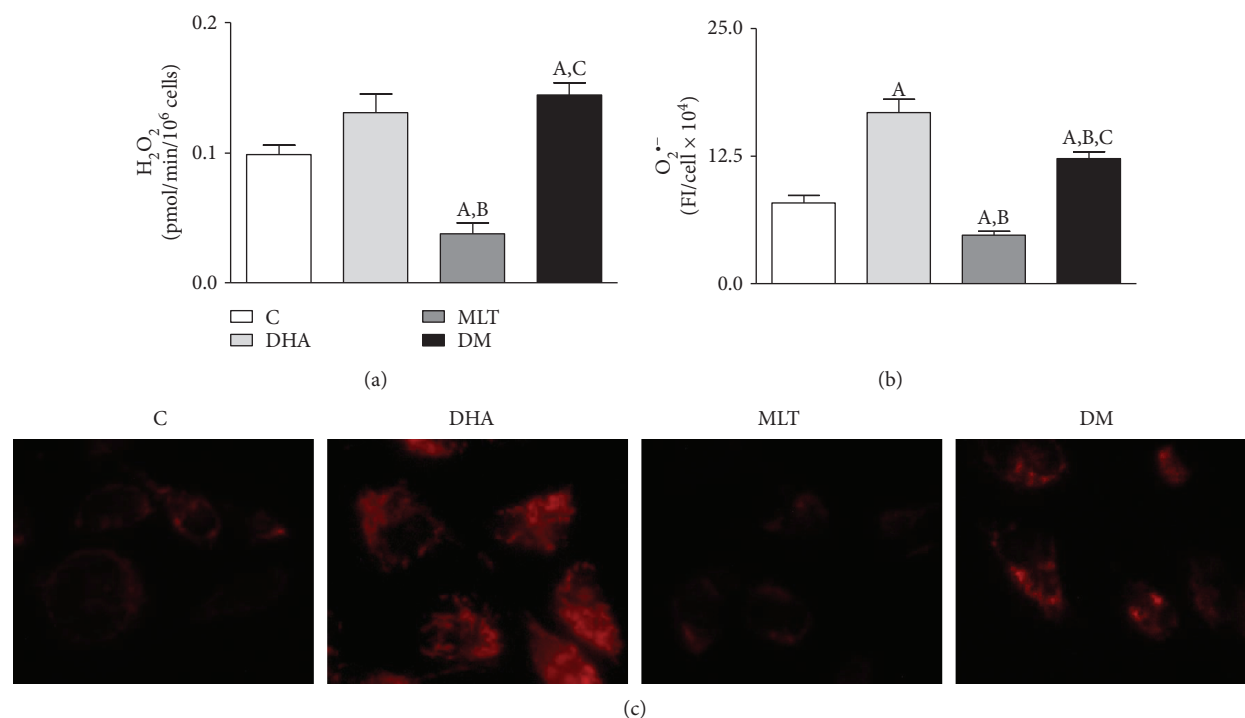


FIGURE 3: ROS determination. Production of (a) hydrogen peroxide (H_2O_2)—values show pmol of $\text{H}_2\text{O}_2/\text{min}/10^6$ cells and SEM; production of (b) superoxide anion ($\text{O}_2^{\bullet-}$)—values show the fluorescence intensity (FI) per cell $\times 10^4$. Legend of panels (a) and (b): C: control (vehicle incubation); DHA: incubation with $100 \mu\text{M}$ of DHA for 48 h; MLT: incubation with $1 \mu\text{M}$ of melatonin for 48 h; DM: coincubation with $100 \mu\text{M}$ of DHA and $1 \mu\text{M}$ of melatonin for 48 h. Statistical analysis: (A) different from C; (B) different from DHA; (C) different from MLT. $p < 0.05$ was considered statistically different. Three independent experiments in triplicate were considered for statistical analysis of H_2O_2 production and at least 250 cells for $\text{O}_2^{\bullet-}$. (c) Detection of $\text{O}_2^{\bullet-}$ production after MitoSOX incubation. Images captured with 40x objective with an inverted fluorescence microscope.

coincubated with DHA, whereas no alteration was observed for DHA alone (control: 11.20 ± 0.15 , MLT: 8.60 ± 0.64 , DM: $9.18 \pm 0.43 \text{ ng/mL} \times 10^{-5}$). AR expression did not change among any incubation (Figure 6(e)).

4. Discussion

Considering that the available strategies against PCa are still highly inefficient and may lead to the recurrence of more aggressive phenotypes [22, 23], we investigated, *in vitro*, the potential of DHA and MLT to decrease cell survival at early stages of proliferative disorders. PNT1A cells were chosen due to their normal secretory phenotype but also nonmalignant alterations, allowing study growth and survival of high proliferative prostate cells which are sensitive to androgen, as described in early stages of prostate cancer progression and BHP [33]. Furthermore, this cell line retains AR expression, whose activity is closely related to cell metabolism, and the loss thereof affects mitochondria yields and dynamics among PCa progression. Due to their antiproliferative properties, DHA and MLT have been investigated as PCa suppressors in experimental studies [11, 18], but their combined action in benign prostate cells has not yet been evaluated. In this study, we observed that ROS generation and mitochondrial function play a pivotal role in determination of PNT1A cell proliferation. On the one hand, DHA had

an antiproliferative effect at the highest concentration tested ($100 \mu\text{M}$) after 48 h of incubation, mainly due to the increase in ROS production, probably related to mitochondrial function impairment and AKT inactivation. On the other hand, MLT, at the pharmacologic range, improved oxidative phosphorylation and decreased ROS production, but reduced cell proliferation due to inhibition of survival pathways. Moreover, MLT improved the DHA antiproliferative effect in PNT1A cells.

4.1. Benign Epithelial Prostatic Cells Respond Differently to DHA than Tumor Cells. DHA has been described to have antimitotic and proapoptotic effects on malignant prostate cell lines using different concentrations [18, 34, 35]. However, in this study DHA had a hormetic behavior on nontumor PNT1A cells, since an inhibitory effect on proliferation was detected at a higher concentration ($100 \mu\text{M}$) for longer exposures (48 and 72 h), whereas a proliferative stimulus was triggered at lower concentrations (20 and $50 \mu\text{M}$). Despite not being the aim of our study, it is worth mentioning that the results from our laboratory (not shown) with DHA $50 \mu\text{M}$ for 48 h suggest that such an increase in cell proliferation may be related to deregulation of peroxisome proliferator-activated receptor gamma ($\text{PPAR}\gamma$), which is still under investigation. Regarding DHA at $100 \mu\text{M}$ for 48 h, it is possible to suggest two key factors in cytotoxic effect: the

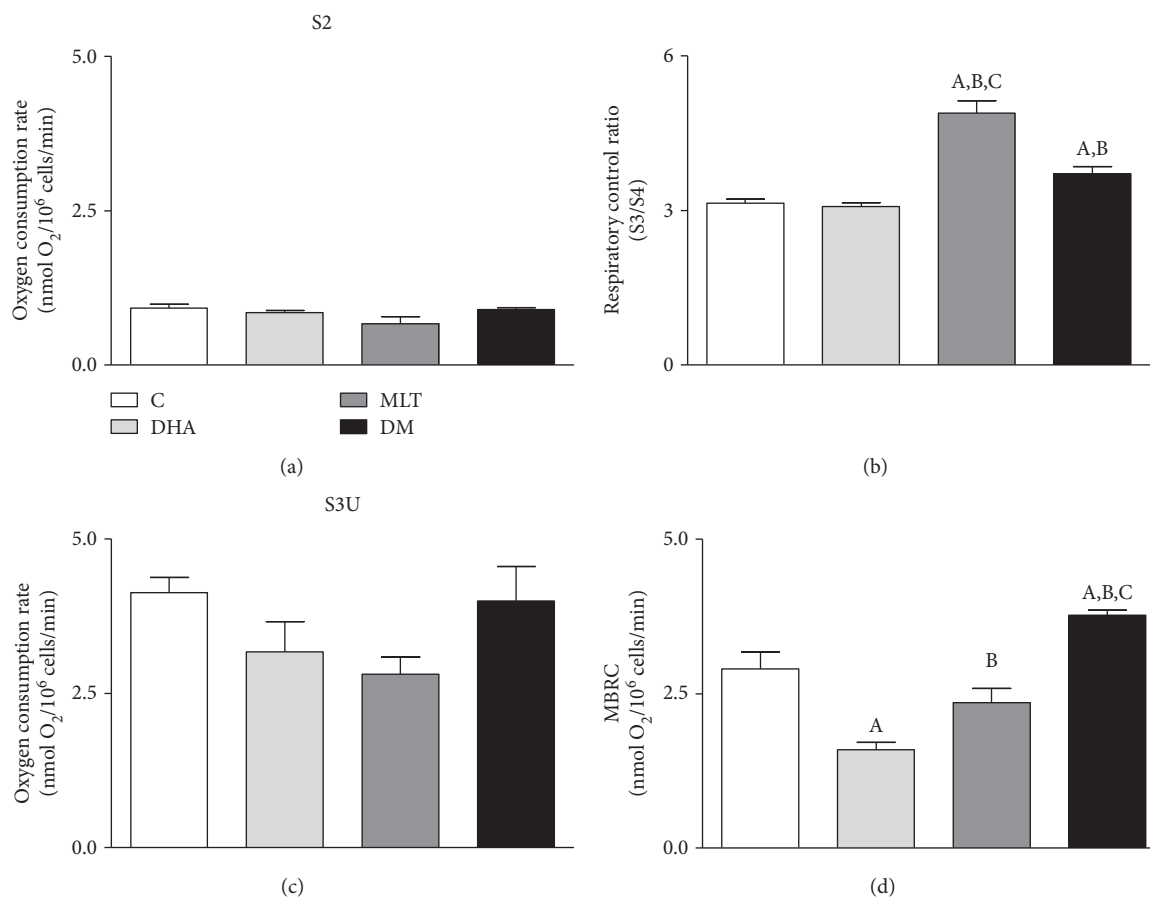


FIGURE 4: Oxygen consumption rate of PNT1A cells after incubations. (a) Basal state (S2), (b) respiratory control ratio (OCR), (c) maximum velocity of respiratory chain (S3U), and (d) mitochondrial bioenergetic reserve capacity (MBRC). Values show the mean of nmol of O₂/10⁶ cells/min and SEM. C: control (vehicle incubation); DHA: incubation with 100 μ M of DHA for 48 h; MLT: incubation with 1 μ M of melatonin for 48 h; DM: coincubation with 100 μ M of DHA and 1 μ M of melatonin for 48 h. Statistical analysis: (A) different from C; (B) different from DHA; (C) different from MLT. $p < 0.05$ was considered statistically different. Three independent experiments were performed in triplicate for statistical analysis.

increase in ROS production and the inactivation of AKT (Figure 8(a)). Interestingly, previous studies demonstrated that 50 μ M of DHA led to death of PC3 and DU145 cells [18] whereas in our study this concentration stimulated PNT1A to proliferate and cytotoxic effects were observed solely at 100 μ M. In PCa, oxidative stress is increased and it is possible that incubation with DHA enhanced cellular damage, activating cell death even at lower concentrations. Furthermore, this susceptibility may also rely on metabolic changes among malignant transformations known as the Warburg effect [36]. Regarding PCa, these changes may be related to several mechanisms [37], as increased β -oxidation [38], higher amounts of mitochondria and lower complex I activity [4], mutations in ETC complexes [5], and alterations in mitochondria dynamics [39] which may be related to different responses between benign and prostate tumor cells.

4.2. DHA Raised ROS Production and Mitochondrial Rearrangement. To the best of our knowledge, this is the first evidence that DHA increases ROS generation and decreases cell proliferation in PNT1A benign prostate cells. Such effects

were probably associated to higher O₂^{•-} production, which is related to the increase in mitochondrial membrane potential (Figure 5(d)) [40]. It is currently known that higher oxidative stress levels commonly exhibit impairment of mitochondrial activity [41]. In response to oxidative damage or metabolic changes, mitochondrial fusion may be triggered as tentative to restoration of organelle function [42]. In this context, we hypothesize that DHA raised oxidative stress, therefore impairing mitochondrial function, which then stimulated organelle fusion and led to area and perimeter increase as well as the recovery of oxidative phosphorylation (OXPHOS). Mitochondrial morphology alterations described here are in line with previous reports, since DHA upregulated the protein related to mitochondrial fusion MFN2 [43]. It is worth mentioning that despite that OXPHOS was unchanged after 48 h of incubation, mitochondrial integrity probably remained damaged because DHA strongly impaired MBRC, an index of cell potential to respond upon stress conditions, which is decreased under oxidative stress [44]. In this context, *in vitro* studies from our research group found that half of DHA concentrations used here remarkably decreased the

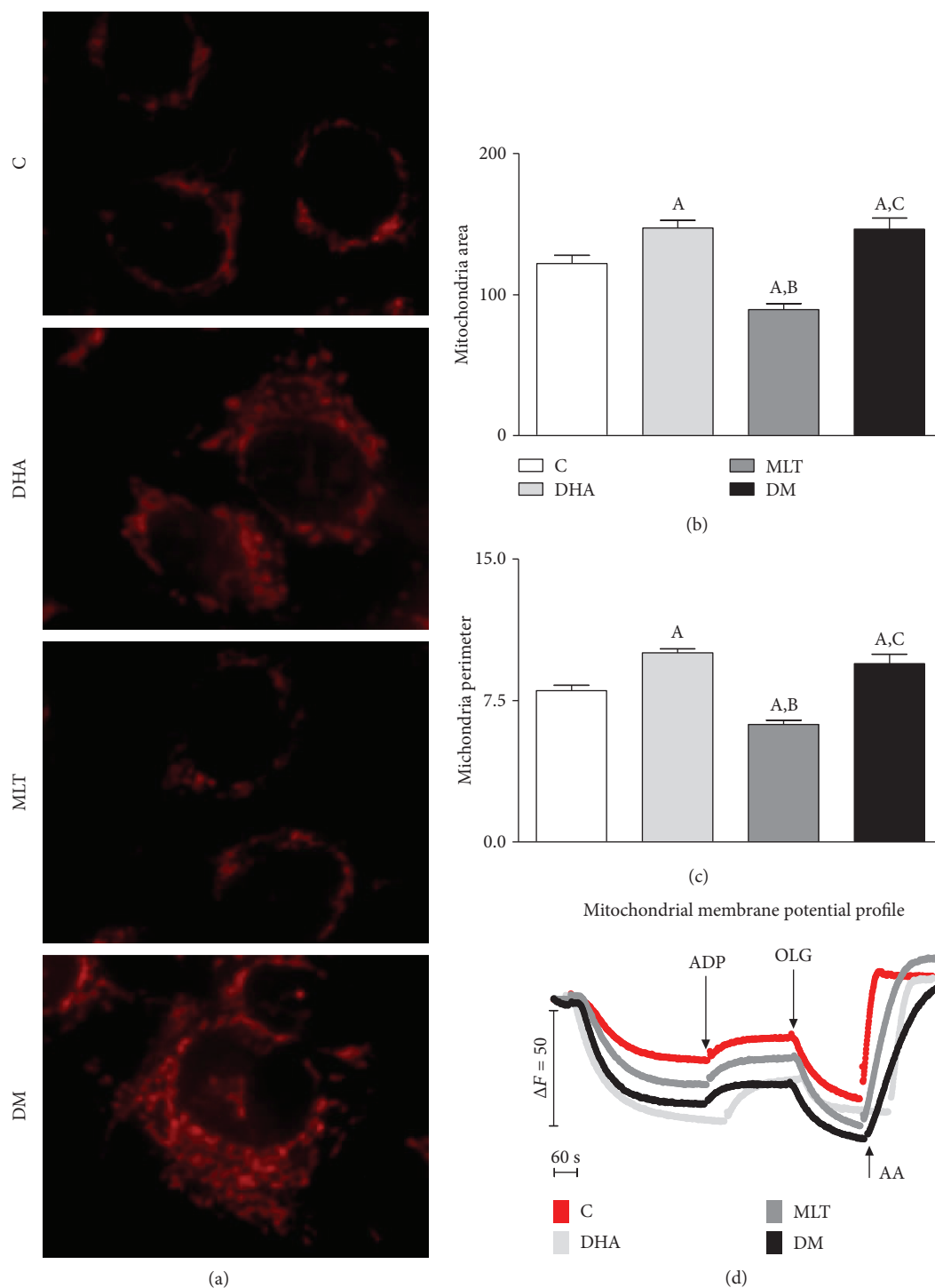


FIGURE 5: Morphometric analysis of mitochondria. (a) Mitochondria labeling with MitoTracker, (b) area (μm^2), (c) perimeter (μm), and (d) mitochondrial membrane potential assessed with Safranin O. Images captured with 40x objective with an inverted fluorescence microscope for morphological analysis. Legend: C: control (vehicle incubation); DHA: incubation with $100 \mu\text{M}$ of DHA for 48 h; MLT: incubation with $1 \mu\text{M}$ of melatonin for 48 h; DM: coinubation with $100 \mu\text{M}$ of DHA and $1 \mu\text{M}$ of melatonin for 48 h; ADP: adenosine diphosphate; OLG: oligomycin; AA: antimycin A. At least 100 cells from consecutive passages were considered for statistical analysis. Values show the mean and SEM. Statistical analysis: (A) different from C; (B) different from DHA; (C) different from MLT. $p < 0.05$ was considered statistically different.

viability of the testis cell population in fetal mice and, when combined to 2-monoethylhexyl phthalate (MEHP), strongly impaired the survival of male germ cells

(gonocytes). Therefore, the data highlights the ability of DHA to induce cell sensitization to other cytotoxic compounds (data not published).

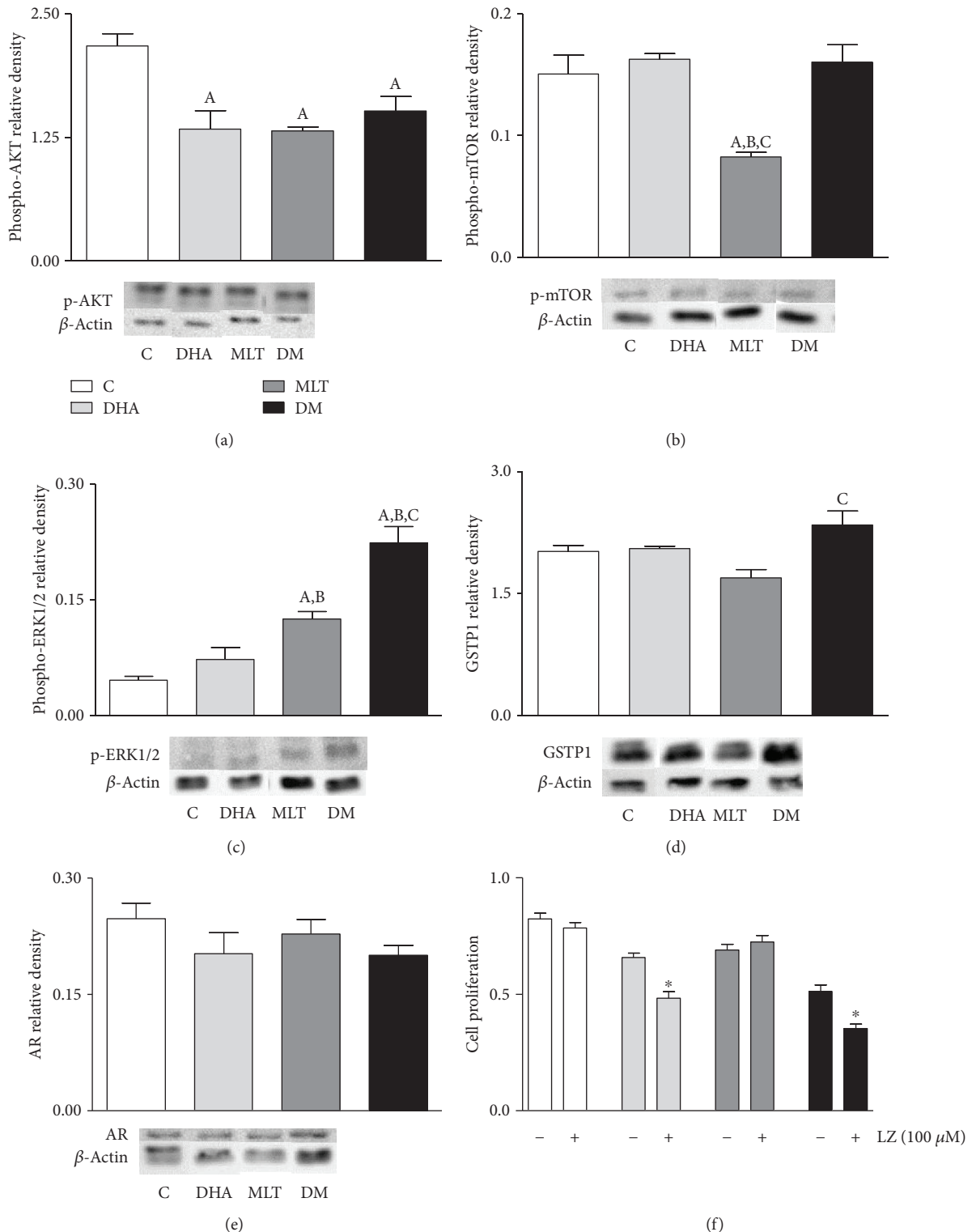


FIGURE 6: Signaling pathways. (a) AKT, (b) mTOR, and (c) ERK1/2 activation. (d) GSTP1 and (e) AR expression. Legend of panels (a)–(e): C: control (vehicle incubation); DHA: incubation with 100 μ M of DHA for 48 h; MLT: incubation with 1 μ M of melatonin for 48 h; DM: coinubation with 100 μ M of DHA and 1 μ M of melatonin for 48 h. Values show the mean of relative density and SEM from three different samples normalized to β -actin. For each blotting, the samples run in the same electrophoresis, and except for AR, the bands were cropped, for group standard purposes. Statistical analysis of panels (a)–(e): (A) different from C; (B) different from DHA; (C) different from MLT. (f) Cell proliferation rate after incubation with luzindole. Values show the mean of absorbance and SEM. Legend of panel (f): LZ: luzindole. Statistical analysis of panel (f): * different from incubation without luzindole. $p < 0.05$ was considered statistically different. Three independent experiments were performed in triplicate ($n = 9$) for statistical analysis.

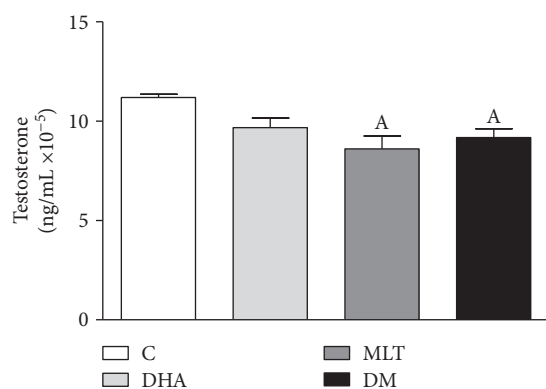


FIGURE 7: Testosterone level in the medium. After incubations, the medium was removed and testosterone level assessed by ELISA assay. Values show mean of ng of testosterone/mL $\times 10^{-5}$ normalized by protein amount from cell lysate and SEM. Legend: C: control (vehicle incubation); DHA: incubation with 100 μ M of DHA for 48 h; MLT: incubation with 1 μ M of melatonin for 48 h; DM: coincubation with 100 μ M of DHA and 1 μ M of melatonin for 48 h. Statistical analysis: (A) different from C. $p < 0.05$ was considered statistically different. Three independent experiments were performed in triplicate for statistical analysis.

4.3. Decrease in ROS Production by MLT Alone Is Associated to Lower Cell Proliferation Rates. Because oxidative stress apparently is a key factor for cell survival [18], we evaluated the antioxidant potential of MLT. MLT is an expected antioxidant agent which can scavenge free radicals directly or by its metabolites [45], upregulate the expression and activity of antioxidant enzymes, such as superoxide dismutase, glutathione peroxidase, and catalase [46], or modulate mitochondrial activity [6, 47]. In the present study, our aim was to validate on PNT1A cells the MLT antioxidant action and not the mechanisms per se. Indeed, MLT was able to decrease H_2O_2 and $O_2^{\bullet-}$ production, combined or not to DHA. Our data are in line with previous literature, since it was reported that MLT, at the same concentration, decreased ROS in isolated mitochondria from the liver [10]. Such an effect on oxidative stress attenuation may be associated to the attenuation of proton leak in mitochondria [48] or even decrease in mitochondrial membrane potential, a well-known contributor to $O_2^{\bullet-}$ production *in vitro* and *in vivo* [40]. Levels of ROS production are closely related to OXPHOS [6], and decrease in H_2O_2 and $O_2^{\bullet-}$ described may be related to improvement of the respiratory control ratio. It is worth mentioning that complex II-supported respiration was chosen based on the fact that such complex is invariable among cancer cells [49] and it is an important site for ROS generation, while it also contributes to ROS either directly or indirectly via reverse electron transfer [50]. To our knowledge, this is the first report to show antioxidant properties of MLT in PNT1A cells associated to improvement of the mitochondrial physiology. Because the increase in ROS generation had been related to expansion of mitochondrial area and perimeter, we investigated if the decreased production of reactive species associated to OXPHOS improvement also affected organelle morphology. Thus, it was possible to observe that mitochondrial function enhancement was

followed by decrease in organelle area and perimeter. The findings herein suggest a quality control system that removes fractions or the entirety of mitochondria with higher ROS generation which may be harmful to organelle homeostasis. On the other hand, we cannot discard that MLT effects on mitochondria physiology may be a consequence of first changes in organelle dynamics, as well as contribution of antioxidant system enzyme modulation. Therefore, the present study highlights new possibilities of MLT's role as a regulator of mitochondrial function in prostatic epithelial cells.

The results observed here regarding proliferation of PNT1A cells were different from the previous results [51], since it was reported that MLT at 500 μ M or 10 mM did not affect cell proliferation. Such differences may be due to conditions of incubation but also to higher cell density seeded (10^4 cells/well) than what Gobbo and colleagues [51] performed (3×10^3 cells/well), which may be more suitable to clarify the differences between proliferation rates among incubations. In the present study, OXPHOS improvement and decrease in ROS production by MLT was probably associated to AKT inactivation and decrease in cell proliferation. Our data may suggest an association with ATP, since its increase may be associated to cell death [52]. MLT's property of modulating ATP levels was reported at different concentrations and systems due to several mechanisms, such as a raise in ADP/O ratio and upregulation of β subunit of ATP synthase [7–10]. Despite not being assessed, it is suggested that OXPHOS improvement may be related to increase in ATP levels in the cells. This hypothesis is in line with previous literature, since MLT in the liver and brain tissue, even at lower concentrations (100 nM), was able to improve OXPHOS through stimulation of complexes I and IV and protection of these enzymes against oxidative damage, which was closely related to increase in ATP production [7]. In this context, the increase in ATP levels may suppress the AKT pathway [53] and decrease survival, as observed here and reported in breast cancer cells after administration of extracellular ATP to the medium [54]. Therefore, this hormone decreased cell proliferation probably due to the decrease in ROS production that affected pathways of mitosis stimulation and cell survivor. PCa progression is related to the rise in oxidative stress and, together with our data, point to mitochondrial bioenergetics' role on cell arrest and suggest that MLT is effective as antiproliferative agent acting in this pathway (Figure 8(b)).

4.4. MLT Antioxidant Ability Apparently Is More Efficient at the Mitochondrial Compartment. Higher lipid accumulation probably was related to increased amounts of DHA. Such omega-3 is metabolized primarily at the peroxisome fraction, a well-known site of H_2O_2 generation, due to long-chain fatty acid structure [19]. Regarding coincubation, H_2O_2 production was increased and MLT was not able to decrease it. Therefore, the antioxidant effects of MLT in the presence of DHA were mainly at the mitochondrial compartment since, despite not recovering to control levels, such hormone decreased $O_2^{\bullet-}$ levels possibly related to OXPHOS improvement in DM. In addition, such decrease may attenuate

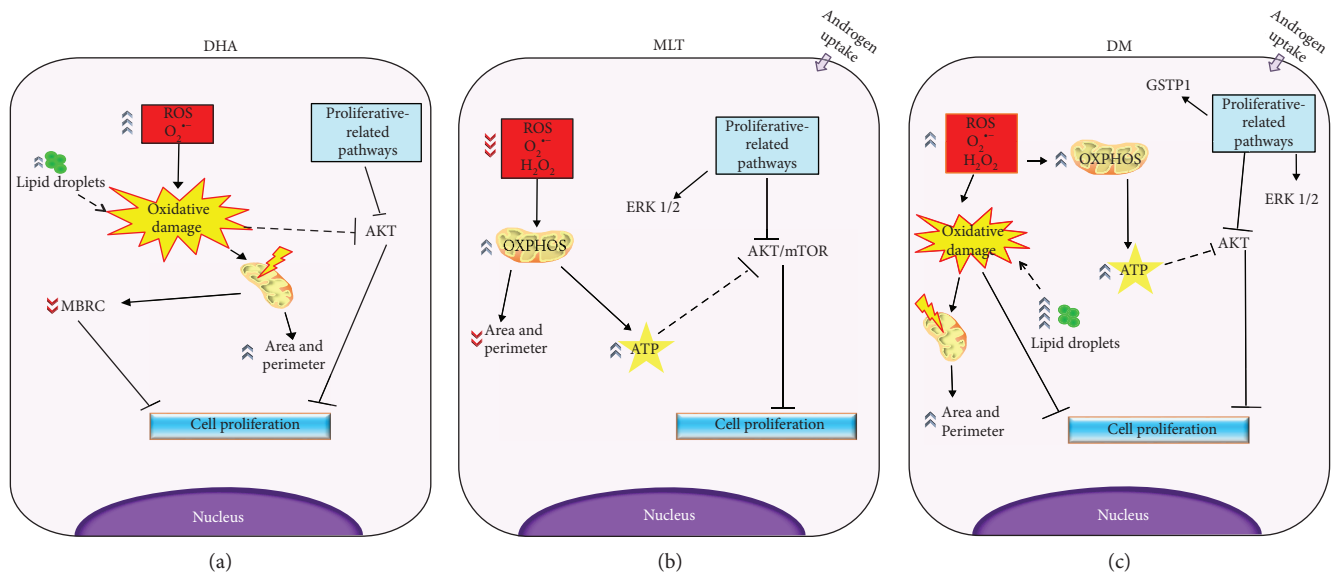


FIGURE 8: Proposed mechanism. (a) DHA increased ROS production, mainly O₂^{•-}, leading to oxidative damage that may trigger mitochondrial fusion as tentative to restoration of organelle function. Also, such fatty acid increased lipid accumulation which may increase ROS. In this context, we hypothesize that DHA raised oxidative stress, therefore impairing mitochondrial function, which then stimulated organelle fusion and led to area and perimeter increase as well as the recovery of OXPHOS, but not MBRC. In addition, DHA also inhibited AKT activation which may be related to increase in oxidative damage and decrease in cell proliferation. (b) MLT decreased ROS production, both O₂^{•-} and H₂O₂, and improved OXPHOS which may be associated to AKT/mTOR inactivation. (c) DHA increased oxidative damage which was not neutralized by MLT, but together (DM) amplified the antiproliferative effect probably due to AKT and ERK1/2 regulation. MLT, alone or coincubated, stimulated ERK1/2 activation as well as androgen uptake, but the mechanism is not clear. Also, MLT coincubated with DHA-stimulated GSTP1 expression probably due to ROS increase. Legend: DHA: docosahexaenoic acid; MLT: melatonin; DM: coincubation; O₂^{•-}: superoxide anion production; H₂O₂: hydrogen peroxide; ATP: adenosine triphosphate; OXPHOS: oxidative phosphorylation; MBRC: mitochondrial bioenergetics reserve capacity; ROS: reactive oxygen species. Dashed lines, mechanism proposed based on the literature; solid lines, effects and correlations based on observed results.

mitochondrial oxidative damage, which can be related to the enhancement of MBRC observed in coincubation.

4.5. DHA and MLT Downregulate Cell Proliferation and Survival Pathways. In PC3 and DU145 lines, DHA led to AKT/mTOR suppression [18], whereas in PNT1A only the activation of AKT decreased. This evidence may suggest a different action of such omega-3 when distinct stages of proliferative disorders are considered. Concerning MLT alone, it suppressed the AKT/mTOR pathway, which is closely related to decrease in cell proliferation. However, when coincubated to DHA, MLT enhances the decrease in proliferation by activating ERK1/2. Despite being generally associated to proliferation stimulus, activation of ERK1/2 may also lead to cell death mainly under stress conditions [55]. In PC3 cells, the increase in oxidative stress reduced AKT activation, followed by increased phosphorylation of ERK and cell proliferation arrest [56], similar to what was observed in PNT1A in our study after coincubation. Despite the fact that DHA alone did not stimulate ERK1/2 activation, even under high ROS production, in our *in vitro* model, this evidence highlights that MLT could play a key role in the modulation of such pathway. In addition, we also suggest that MLT combined to increased oxidative stress, the ERK1/2 pathway is strongly activated and therefore controls cell survival, as reported previously [57]. It is worth mentioning that

higher levels of ERK activation may also be related to GSTP1 upregulation [58].

Because androgen regulation is important for the survival of prostate cells and PCa development, we analyzed if incubation effects were related to the alteration in this pathway. In the present incubations, DHA did not change testosterone levels in medium or AR expression, which supports the hypothesis that the antimetabolic property of this omega-3 in PNT1A cells was mainly due to alterations on oxidative status. AR expression was also unchanged after MLT exposure, regardless of DHA incubation. However, MLT influenced the androgen levels in the medium, but due to methodologic limitations, it is not clear if the release of testosterone or its uptake was affected by MLT. Furthermore, Estrada and colleagues [59] demonstrated that in the presence of androgen, ERK activation was increased and followed by cell proliferation decrease. Therefore, our study suggests that MLT may improve antiproliferative effects due to an association between mitochondrial bioenergetics, androgen pathway, and ERK pathway, even in nontumor cells (Figure 8(c)), although additional studies are needed to better understand this issue.

Finally, we proved that PNT1A proliferation, when incubated with MLT, was independent of MTR1 and MTR2 activation, both expressed in the prostate gland [60]. This demonstrates that MLT uptake by PNT1A cells, already

reported previously [26], activated pathways regardless of membrane receptors and had a key role in mitochondrial activity modulation and oxidative stress control.

5. Conclusion

Our data indicates that PNT1A cells are less sensitive to DHA than advanced cancer cell lines; however, at 100 μ M this omega-3 reduced the proliferation rate due to the increase in ROS production at cytotoxic levels and possibly associated to the inhibition of AKT activation. It is important to emphasize DHA hormetic behavior in PNT1A cells, because at lower concentrations it stimulated cell proliferation. This finding highlights the need for further studies, concerning dietary supplementation with this PUFA, mainly in men at risk of PCa development. Furthermore, MLT at 1 μ M increased OXPHOS, decreased ROS production, and exerted an antimutagenic effect via AKT inactivation and ERK1/2 activation regardless of binding in MTR1 or MTR2. Moreover, MLT improved *in vitro* DHA antiproliferative effect, which may open new possibilities of chemopreventive strategies, mainly at early stages of prostate proliferative disorders.

Data Availability

The data used to support the findings of this study are available from the corresponding author upon request.

Conflicts of Interest

None of the authors has been commissioned to perform or publish this work and have no conflict of interest. All authors approved the final version of the manuscript.

Acknowledgments

The authors are grateful to Dr. Nishtman Dizeyi (Lund University, Malmo, Sweden) for kindly providing the PNT1A cells and for the collaboration of Dr. Hernandez Faustino Carvalho (Institute of Biology, State University of Campinas, São Paulo, Brazil) and Dr. Marilia de Freitas Calmon Saiki (Institute of Biosciences, Humanities and Exact Sciences, São Paulo State University, São José do Rio Preto, São Paulo, Brazil) in cell culture. Financial support was provided by São Paulo Research Foundation (FAPESP) and the National Research Council (CNPq). The authors have received fellowships as follows: Dr. Rejane Maira Góes (Grant number 308367/2014-6 — CNPq; 2013/16368-7 and 2018/19590-6 — FAPESP), Msc. Guilherme Henrique Tamarindo (Grant number 2015/13371-2 FAPESP) and Dr. Fernanda Ramos Gadelha (Grant number 2015/24595-9 FAPESP and 309764/2015-7 CNPq). The authors also thank the Coordination for the Improvement of Higher Education Personnel (CAPES) for scholarship (Finance Code 001), São José do Rio Preto Extension and Research Foundation (FAPERP) for their partial financial support (Grant number 002/2018), and Mr. Angel Esteban Van Nynatten, a native speaker and professional translator, for extensively revising the manuscript.

References

- [1] T. D. Oberley, W. Zhong, L. I. Szveda, and L. W. Oberley, "Localization of antioxidant enzymes and oxidative damage products in normal and malignant prostate epithelium," *The Prostate*, vol. 44, no. 2, pp. 144–155, 2000.
- [2] O. Yossepowitch, I. Pinchuk, U. Gur, A. Neumann, D. Lichtenberg, and J. Baniel, "Advanced but not localized prostate cancer is associated with increased oxidative stress," *The Journal of Urology*, vol. 178, no. 4, pp. 1238–1244, 2007.
- [3] P. E. Porporato, N. Filigheddu, J. M. B. S. Pedro, G. Kroemer, and L. Galluzzi, "Mitochondrial metabolism and cancer," *Cell Research*, vol. 28, no. 3, pp. 265–280, 2017.
- [4] A. Panov and Z. Orynbayeva, "Bioenergetic and antiapoptotic properties of mitochondria from cultured human prostate cancer cell lines PC-3, DU145 and LNCaP," *PLoS One*, vol. 8, no. 8, article e72078, 2013.
- [5] J. V. Phillely, A. Kannan, W. Qin et al., "Complex-I alteration and enhanced mitochondrial fusion are associated with prostate cancer progression," *Journal of Cellular Physiology*, vol. 231, no. 6, pp. 1364–1374, 2016.
- [6] D. Acuna-Castroviejo, M. Martín, M. Macías et al., "Melatonin, mitochondria, and cellular bioenergetics," *Journal of Pineal Research*, vol. 30, no. 2, pp. 65–74, 2001.
- [7] M. Martín, M. Macías, J. León, G. Escames, H. Khaldy, and D. Acuña-Castroviejo, "Melatonin increases the activity of the oxidative phosphorylation enzymes and the production of ATP in rat brain and liver mitochondria," *International Journal of Biochemistry and Cell Biology*, vol. 34, no. 4, pp. 348–357, 2002.
- [8] L. G. A. Chuffa, L. A. Lupi Júnior, F. R. F. Seiva et al., "Quantitative proteomic profiling reveals that diverse metabolic pathways are influenced by melatonin in an *in vivo* model of ovarian carcinoma," *Journal of Proteome Research*, vol. 15, no. 10, pp. 3872–3882, 2016.
- [9] C. Castillo, V. Salazar, C. Ariznavarreta, E. Vara, and J. A. F. Tresguerres, "Effect of melatonin administration on parameters related to oxidative damage in hepatocytes isolated from old Wistar rats," *Journal of Pineal Research*, vol. 38, no. 4, pp. 240–246, 2005.
- [10] A. López, J. A. García, G. Escames et al., "Melatonin protects the mitochondria from oxidative damage reducing oxygen consumption, membrane potential, and superoxide anion production," *Journal of Pineal Research*, vol. 46, no. 2, pp. 188–198, 2009.
- [11] S. Y. W. Shiu, "Towards rational and evidence-based use of melatonin in prostate cancer prevention and treatment," *Journal of Pineal Research*, vol. 43, no. 1, pp. 1–9, 2007.
- [12] C. Bartsch, H. Bartsch, A. Schmidt, S. Ilg, K. H. Bichler, and S. H. Flüchter, "Melatonin and 6-sulfatoxymelatonin circadian rhythms in serum and urine of primary prostate cancer patients: evidence for reduced pineal activity and relevance of urinary determinations," *Clinica Chimica Acta*, vol. 209, no. 3, pp. 153–167, 1992.
- [13] H. Iguchi, K.-I. Kato, and H. Ibayashi, "Age-dependent reduction in serum melatonin concentrations in healthy human subjects," *Journal of Clinical Endocrinology and Metabolism*, vol. 55, no. 1, pp. 27–29, 1982.
- [14] R. S. Sohal and R. Weindruch, "Oxidative stress, caloric restriction, and aging," *Science*, vol. 273, no. 5271, pp. 59–63, 1996.

- [15] F. Scialò, D. J. Fernández-Ayala, and A. Sanz, "Role of mitochondrial reverse electron transport in ROS signaling: potential roles in health and disease," *Frontiers in Physiology*, vol. 8, no. 428, pp. 1–7, 2017.
- [16] W. A. Sakr, G. P. Haas, B. F. Cassin, J. E. Pontes, and J. D. Crissman, "The frequency of carcinoma and intraepithelial neoplasia of the prostate in young male patients," *The Journal of Urology*, vol. 150, no. 2, pp. 379–385, 1993.
- [17] Y.-X. Lu, D.-L. Chen, D.-S. Wang et al., "Melatonin enhances sensitivity to fluorouracil in oesophageal squamous cell carcinoma through inhibition of Erk and Akt pathway," *Cell Death & Disease*, vol. 7, no. 10, pp. e2432–e2412, 2016.
- [18] S. Shin, K. Jing, S. Jeong et al., "The omega-3 polyunsaturated fatty acid DHA induces simultaneous apoptosis and autophagy via mitochondrial ROS-mediated Akt-mTOR signaling in prostate cancer cells expressing mutant p53," *BioMed Research International*, vol. 2013, Article ID 538529, 11 pages, 2013.
- [19] L. Hou, K. Lian, M. Yao et al., "Reduction of n-3 PUFAs, specifically DHA and EPA, and enhancement of peroxisomal beta-oxidation in type 2 diabetic rat heart," *Cardiovascular Diabetology*, vol. 11, no. 1, p. 126, 2012.
- [20] A. M. Lyberg and P. Adlerceutz, "Monitoring monohydroperoxides in docosahexaenoic acid using high-performance liquid chromatography," *Lipids*, vol. 41, no. 1, pp. 67–76, 2006.
- [21] H. Esterbauer, R. J. Schaur, and H. Zollner, "Chemistry and biochemistry of 4-hydroxynonenal, malonaldehyde and related aldehydes," *Free Radical Biology & Medicine*, vol. 11, no. 1, pp. 81–128, 1991.
- [22] M. Kirby, C. Hirst, and E. D. Crawford, "Characterising the castration-resistant prostate cancer population: a systematic review," *International Journal of Clinical Practice*, vol. 65, no. 11, pp. 1180–1192, 2011.
- [23] K. Cui, X. Li, Y. du et al., "Chemoprevention of prostate cancer in men with high-grade prostatic intraepithelial neoplasia (HGPIN): a systematic review and adjusted indirect treatment comparison," *Oncotarget*, vol. 8, no. 22, pp. 36674–36684, 2017.
- [24] D. Cunningham and Z. You, "In vitro and in vivo model systems used in prostate cancer research," *Journal of Biological Methods*, vol. 2, no. 1, pp. 17–28, 2015.
- [25] H. Meng, Y. Shen, J. Shen, F. Zhou, S. Shen, and U. N. Das, "Effect of n-3 and n-6 unsaturated fatty acids on prostate cancer (PC-3) and prostate epithelial (RWPE-1) cells in vitro," *Lipids in Health and Disease*, vol. 12, no. 1, p. 160, 2013.
- [26] D. Hevia, J. C. Mayo, I. Quiros, C. Gomez-Cordoves, and R. M. Sainz, "Monitoring intracellular melatonin levels in human prostate normal and cancer cells by HPLC," *Analytical and Bioanalytical Chemistry*, vol. 397, no. 3, pp. 1235–1244, 2010.
- [27] R. J. Reiter, D. X. Tan, and M. D. Maldonado, "Melatonin as an antioxidant: physiology versus pharmacology," *Journal of Pineal Research*, vol. 39, no. 2, pp. 215–216, 2005.
- [28] M. H. Barros, B. Bandy, E. B. Tahara, and A. J. Kowaltowski, "Higher respiratory activity decreases mitochondrial reactive oxygen release and increases life span in *Saccharomyces cerevisiae*," *Journal of Biological Chemistry*, vol. 279, no. 48, pp. 49883–49888, 2004.
- [29] R. K. Dagda, S. J. Cherra III, S. M. Kulich, A. Tandon, D. Park, and C. T. Chu, "Loss of PINK1 function promotes mitophagy through effects on oxidative stress and mitochondrial fission," *Journal of Biological Chemistry*, vol. 284, no. 20, pp. 13843–13855, 2009.
- [30] M. J. Holden and H. Sze, "Effects of *Helminthosporium maydis* race t toxin on electron transport in susceptible corn mitochondria and prevention of toxin actions by dicyclohexylcarbodiimide," *Plant Physiology*, vol. 91, no. 4, pp. 1296–1302, 1989.
- [31] T. M. Silva, E. F. Peloso, S. C. Vitor, L. H. G. Ribeiro, and F. R. Gadelha, "O₂ consumption rates along the growth curve: new insights into *Trypanosoma cruzi* mitochondrial respiratory chain," *Journal of Bioenergetics and Biomembranes*, vol. 43, no. 4, pp. 409–417, 2011.
- [32] P. K. Vayalil and A. Landar, "Mitochondrial oncobiogenic index: a potential biomarker to predict progression from indolent to aggressive prostate cancer," *Oncotarget*, vol. 6, no. 40, pp. 43065–43080, 2015.
- [33] A. Degeorges, F. Hoffschir, O. Cussenot et al., "Recurrent cytogenetic alterations of prostate carcinoma and amplification of c-myc or epidermal growth factor receptor in subclones of immortalized PNT1 human prostate epithelial cell line," *International Journal of Cancer*, vol. 62, no. 6, pp. 724–731, 1995.
- [34] W. Friedrichs, S. B. Ruparel, R. A. Marciniak, and L. deGraffenried, "Omega-3 fatty acid inhibition of prostate cancer progression to hormone independence is associated with suppression of mTOR signaling and androgen receptor expression," *Nutrition and Cancer*, vol. 63, no. 5, pp. 771–777, 2011.
- [35] K. Oono, K. Takahashi, S. Sukehara et al., "Inhibition of PC3 human prostate cancer cell proliferation, invasion and migration by eicosapentaenoic acid and docosahexaenoic acid," *Molecular and Clinical Oncology*, vol. 7, no. 2, pp. 217–220, 2017.
- [36] M. G. Vander Heiden, L. C. Cantley, and C. B. Thompson, "Understanding the Warburg effect: the metabolic requirements of cell proliferation," *Science*, vol. 324, no. 5930, pp. 1029–1033, 2009.
- [37] E. Eidelman, J. Twum-Ampofo, J. Ansari, and M. M. Siddiqui, "The metabolic phenotype of prostate cancer," *Frontiers in Oncology*, vol. 7, pp. 1–6, 2017.
- [38] I. Valença, N. Pértega-Gomes, J. R. Vizcaino et al., "Localization of MCT2 at peroxisomes is associated with malignant transformation in prostate cancer," *Journal of Cellular and Molecular Medicine*, vol. 19, no. 4, pp. 723–733, 2015.
- [39] V. Choudhary, I. Kaddour-Djebbar, V. Lakshminathan et al., "Novel role of androgens in mitochondrial fission and apoptosis," *Molecular Cancer Research*, vol. 9, no. 8, pp. 1067–1077, 2011.
- [40] H. Rottenberg, R. Covian, and B. L. Trumpower, "Membrane potential greatly enhances superoxide generation by the cytochrome_c complex reconstituted into phospholipid vesicles," *Journal of Biological Chemistry*, vol. 284, no. 29, pp. 19203–19210, 2009.
- [41] S. Banerjee, N. Aykin-Burns, K. J. Krager et al., "Loss of C/EBP δ enhances IR-induced cell death by promoting oxidative stress and mitochondrial dysfunction," *Free Radical Biology & Medicine*, vol. 99, pp. 296–307, 2016.
- [42] R. J. Youle and A. M. van der Bliek, "Mitochondrial fission, fusion, and stress," *Science*, vol. 337, no. 6098, pp. 1062–1065, 2012.
- [43] Y. Zhang, L. Jiang, W. Hu, Q. Zheng, and W. Xiang, "Mitochondrial dysfunction during in vitro hepatocyte steatosis is

- reversed by omega-3 fatty acid-induced up-regulation of mitofusin 2," *Metabolism: Clinical and Experimental*, vol. 60, no. 6, pp. 767–775, 2011.
- [44] B. K. Chacko, P. A. Kramer, S. Ravi et al., "The bioenergetic health index: a new concept in mitochondrial translational research," *Clinical Science*, vol. 127, no. 6, pp. 367–373, 2014.
- [45] D. X. Tan, L. C. Manchester, M. P. Terron, L. J. Flores, and R. J. Reiter, "One molecule, many derivatives: a never-ending interaction of melatonin with reactive oxygen and nitrogen species?," *Journal of Pineal Research*, vol. 42, no. 1, pp. 28–42, 2007.
- [46] C. Tomás-Zapico and A. Coto-Montes, "A proposed mechanism to explain the stimulatory effect of melatonin on antioxidant enzymes," *Journal of Pineal Research*, vol. 39, no. 2, pp. 99–104, 2005.
- [47] M. Martin, M. Macias, G. Escames et al., "Melatonin-induced increased activity of the respiratory chain complexes I and IV can prevent mitochondrial damage induced by ruthenium red in vivo," *Journal of Pineal Research*, vol. 28, no. 4, pp. 242–248, 2000.
- [48] A. Jimenez-Aranda, G. Fernández-Vázquez, M. Mohammad A-Serrano, R. J. Reiter, and A. Agil, "Melatonin improves mitochondrial function in inguinal white adipose tissue of Zucker diabetic fatty rats," *Journal of Pineal Research*, vol. 57, no. 1, pp. 103–109, 2014.
- [49] K. Kluckova, A. Bezawork-Geleta, J. Rohlena, L. Dong, and J. Neuzil, "Mitochondrial complex II, a novel target for anti-cancer agents," *Biochimica et Biophysica Acta-Bioenergetics*, vol. 1827, no. 5, pp. 552–564, 2013.
- [50] A. Bezawork-Geleta, J. Rohlena, L. Dong, K. Pacak, and J. Neuzil, "Mitochondrial complex II: at the crossroads," *Trends in Biochemical Sciences*, vol. 42, no. 4, pp. 312–325, 2017.
- [51] M. G. Gobbo, N. Dizayi, P. A. Abrahamsson et al., "Influence of melatonin on the proliferative and apoptotic responses of the prostate under normal and hyperglycemic conditions," *Journal of Diabetes Research*, vol. 2015, Article ID 538529, 18 pages, 2015.
- [52] M. V. Zamaraeva, R. Z. Sabirov, E. Maeno, Y. Ando-Akatsuka, S. V. Bessonova, and Y. Okada, "Cells die with increased cytosolic ATP during apoptosis: a bioluminescence study with intracellular luciferase," *Cell Death and Differentiation*, vol. 12, no. 11, pp. 1390–1397, 2005.
- [53] Z. Yang, Y. Liu, C. Shi et al., "Suppression of PTEN/AKT signaling decreases the expression of TUBB3 and TOP2A with subsequent inhibition of cell growth and induction of apoptosis in human breast cancer MCF-7 cells via ATP and caspase-3 signaling pathways," *Oncology Reports*, vol. 37, no. 2, pp. 1011–1019, 2017.
- [54] Y. Zhang, K. Chin-Quee, R. C. Riddle, Z. Li, Z. Zhou, and H. J. Donahue, "BRMS1 sensitizes breast cancer cells to ATP-induced growth suppression," *BioResearch Open Access*, vol. 2, no. 2, pp. 77–83, 2013.
- [55] Y. Mebratu and Y. Tesfaigzi, "How ERK1/2 activation controls cell proliferation and cell death is subcellular localization the answer?," *Cell Cycle*, vol. 8, no. 8, pp. 1168–1175, 2009.
- [56] K.-H. Yan, C.-J. Yao, C.-H. Hsiao et al., "Mefloquine exerts anticancer activity in prostate cancer cells via ROS-mediated modulation of AKT, ERK, JNK and AMPK signaling," *Oncology Letters*, vol. 5, no. 5, pp. 1541–5, 2013.
- [57] S. Cagnol and J. C. Chambard, "ERK and cell death: mechanisms of ERK-induced cell death - apoptosis, autophagy and senescence," *FEBS Journal*, vol. 277, no. 1, pp. 2–21, 2010.
- [58] Z. Yin, V. N. Ivanov, H. Habelhah, K. Tew, and Z. Ronai, "Glutathione S-transferase p elicits protection against H₂O₂-induced cell death via coordinated regulation of stress kinases," *Cancer Research*, vol. 60, no. 15, pp. 4053–4057, 2000.
- [59] M. Estrada, A. Espinosa, M. Müller, and E. Jaimovich, "Testosterone stimulates intracellular calcium release and mitogen-activated protein kinases via a G protein-coupled receptor in skeletal muscle cells," *Endocrinology*, vol. 144, no. 8, pp. 3586–3597, 2003.
- [60] E. Gilad, E. Pick, H. Matzkin, and N. Zisapel, "Melatonin receptors in benign prostate epithelial cells: evidence for the involvement of cholera and pertussis toxins-sensitive G proteins in their signal transduction pathways," *The Prostate*, vol. 35, no. 1, pp. 27–34, 1998.

Research Article

Association of Impaired Reactive Aldehyde Metabolism with Delayed Graft Function in Human Kidney Transplantation

Leonie G. M. Wijermars,¹ Alexander F. Schaapherder,¹ Thomas George,² Pritam Sinharoy,² and Eric R. Gross ²

¹Department of Surgery, Leiden University Medical Center, PO Box 9600, 2300 RC Leiden, Netherlands

²Department of Anesthesiology, Perioperative and Pain Medicine, School of Medicine, Stanford University, 300 Pasteur Drive H3580, Stanford, 94305-5640 California, USA

Correspondence should be addressed to Eric R. Gross; ergross@stanford.edu

Received 17 June 2018; Revised 2 September 2018; Accepted 27 September 2018; Published 23 December 2018

Academic Editor: Luigi Iuliano

Copyright © 2018 Leonie G. M. Wijermars et al. This is an open access article distributed under the Creative Commons Attribution License, which permits unrestricted use, distribution, and reproduction in any medium, provided the original work is properly cited.

Delayed graft function is an early complication following kidney transplantation with an unclear molecular mechanism. Here we determined whether impaired reactive aldehyde metabolism is associated with delayed graft function. Human kidney biopsies from grafts with delayed graft function were compared with grafts that did not develop delayed graft function by Ingenuity gene pathway analysis. A second series of grafts with delayed graft function ($n = 10$) were compared to grafts that did not develop delayed graft function ($n = 10$) by measuring reactive aldehyde metabolism, reactive aldehyde-induced protein adduct formation, and aldehyde dehydrogenase (ALDH) gene and protein expression. In the first series of kidney biopsies, several gene families known for metabolizing reactive aldehydes, such as aldehyde dehydrogenase (ALDH), aldo-keto reductase (AKR), and glutathione-S transferase (GSTA), were upregulated in kidneys that did not develop delayed graft function versus those that did. In the second series of kidney grafts, we focused on measuring aldehyde-induced protein adducts and ALDH enzymatic activity. The reactive aldehyde metabolism by ALDH enzymes was reduced in kidneys with delayed graft function compared to those that did not ($37 \pm 12^*$ vs. $79 \pm 5 \mu\text{g}/\text{min}/\text{mg}$ tissue, $*P < 0.005$, respectively). ALDH enzymatic activity was also negatively correlated with length of hospital stay after a kidney transplant. Together, our study identifies a reduced ALDH enzymatic activity with kidneys developing delayed graft function compared to those that did not. Measuring ALDH enzymatic activity and reactive aldehyde-induced protein adducts can potentially be further developed as a biomarker to assess for delayed graft function and recovery from a kidney transplant.

1. Introduction

Organ transplantation, including kidney transplantation, is a known and planned occurrence of organ reperfusion injury. Reperfusion injury in turn can trigger delayed graft function, resulting in the deferred functional recovery of the donor kidney following kidney transplantation.

Delayed graft function detrimentally affects renal function and graft longevity and is a risk factor for acute kidney rejection [1, 2]. The incidence of delayed graft function in deceased donor kidneys is ~25% and perhaps as high as 50% for kidneys from cardiac death donor organs [3, 4]. Additionally, the incidence of delayed graft function is

steadily rising due to the increased use of marginal donor grafts secondary to organ transplant shortages. As a consequence, delayed graft function leads to reduced graft function, prolonged hospital admissions, increased demand of donor kidneys for retransplantation secondary to rejection, and a higher economic societal burden [5]. Several definitions exist for delayed graft function [6]. For this manuscript, we define delayed graft function as the requirement of dialysis within the first 7 postoperative days of a kidney transplant [6].

During reperfusion of an organ, reactive oxygen species produced at the mitochondria causes lipid peroxidation which generates reactive aldehydes which can impair cellular

functions [7–9]. The reactive aldehydes produced include acetaldehyde, malondialdehyde (MDA), and 4-hydroxynonenal (4-HNE). To metabolize these reactive aldehydes, several protein families such as glutathione-S reductase, aldo-keto reductase, and aldehyde dehydrogenase gene families contribute to metabolizing aldehydes produced within the cell [7, 10, 11].

Although kidney transplants from living donors are less susceptible to delayed graft function when compared to grafts from deceased donors [1], the differences in molecular biology have not been extensively studied. Here we used human renal biopsies from transplanted deceased donor kidneys who developed delayed graft function and compared the molecular differences using gene arrays to kidneys from living donor transplants that did not develop delayed graft function. From this approach, we here suggest that impaired reactive aldehyde metabolism by ALDH enzymes is associated with delayed graft function.

2. Materials and Methods

2.1. Patient Enrollment. The study protocol was approved by the medical ethics committee at the Leiden University Medical Center. Written informed consent was obtained from each patient.

Paired renal cortical biopsies were obtained at the end of the cold ischemic period (prior to implantation) and 45 min after reperfusion of the kidney in the recipient. Kidney biopsies from an initial 18 donor kidneys were used to conduct the whole genome array portion of the study (Figure 1(a)). We then obtained an additional 10 paired renal biopsies from living donor kidneys that did not develop delayed graft function and 10 paired renal biopsies from deceased donor kidneys that developed delayed graft function. Details regarding enrollment and patient demographics are described in detail (Tables 1 and 2).

Renal allografts were perfused and stored with either University of Wisconsin solution or Custodiol® HTK (histidine-tryptophan-ketoglutarate) solution. None of the grafts were machine perfused. For renal transplantation, all patients were induced by propofol, sufentanil, and atracurium. Patients were intubated in addition to a central venous catheter used for intraoperative monitoring. Patients received basiliximab (day 0 and 4) as immunosuppressive induction. Patients were maintained on tacrolimus or cyclosporine A, mycophenolate mofetil, and steroids for immunosuppression.

Biopsies were taken from the upper pole of the kidney. For biopsies taken after reperfusion, a spring-loaded automatic biopsy needle was used (16 Ga Travenol). Tissue was snap frozen in liquid nitrogen and stored at -80°C and labeled with a unique identifier, blinding the person performing the analysis. For the genome array studies, all samples were analyzed together after the groups were collected. The validation studies were also performed after the tissue was obtained, selectively using only tissue from deceased donors who developed delayed graft function after transplantation.

The transplanted patients were also followed during their hospital stay. The length of hospital stay after transplantation

in addition to glomerular filtration rate at postoperative day 7 was also assessed. Patients were considered as developing delayed graft function if they were in need of dialysis within the first week after transplantation. For those requiring dialysis, acute rejection was excluded as a cause of delayed graft function by renal biopsy. Surgical complications of the transplant procedure were also excluded as a source of delayed graft function. Further, if transplant recipients required one episode of dialysis after transplantation due to incident hyperkalemia, these grafts were also not included as having delayed graft function.

2.2. Genome Array. Paired biopsies were taken for the patients undergoing renal transplantation with one biopsy prior to transplantation and one biopsy 45 minutes after transplant reperfusion. From these renal biopsies, total RNA was extracted using RNazol (Campro Scientific, Veenendaal, Netherlands) and glass beads. The integrity of each RNA sample was examined by Agilent Lab-on-a-chip technology using the RNA 6000 Nano LabChip kit and a Bioanalyzer 2100 (Agilent Technologies, Amstelveen, Netherlands). RNA preparations were considered suitable for array hybridization only if samples showed intact 18S and 28S rRNA bands and displayed no chromosomal peaks or RNA degradation products (RNA integrity number >8.0). Microarray analysis was performed using Illumina whole-genome gene expression BeadChips (Illumina BeadArray®, San Diego, USA) according to the manufacturer's instructions at the Service XS facility in Leiden.

The tissue biopsies collected from the two groups were run on separate gene arrays. The 2 paired tissue biopsies obtained for each transplanted kidney resulted in running 36 gene arrays for the tissue biopsies that were collected. The gene arrays obtained were analyzed by a statistician at the University of Leiden blinded to the identification of the groups of tissue biopsies collected. An average replicate value was calculated and \log_2 ratios were computed by comparing the matched pair biopsies and the gene expression differences for each transplanted kidney prior to and after reperfusion. One value per gene was calculated for the average expression of multiple probes with the same Entrez gene identification, resulting in 15,093 unique gene profiles. The unique gene profiles obtained from the whole genome array were analyzed by Ingenuity pathway analysis (Redwood City, CA, USA).

2.3. Biochemical Assays. In addition to biopsies collected for gene array studies, 20 transplanted kidneys were used to perform further biochemical analysis which included qPCR, western blot (for aldehyde-induced protein adduct and protein expression), and aldehyde enzymatic activity assays.

For qPCR, RNA was isolated from kidney biopsies taken at the end of the cold ischemic period. Kidney biopsy lysates were made by sonification, and RNA was isolated by the use of Ambion® RNAqueous Kit. To substantially reduce the possibility of DNA contamination in the preparations, the isolated total RNA was subject to precipitation with lithium chloride and DNase digestion (Ambion DNase-free). cDNA was made using the Takara® Primescript cDNA synthesis

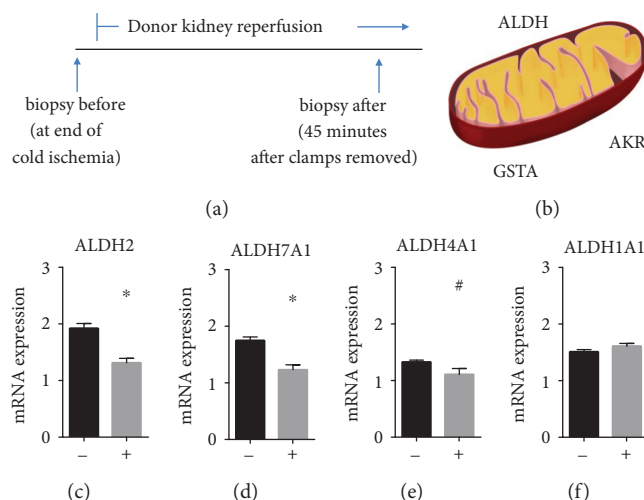


FIGURE 1: Changes in ALDH enzymes found by gene array studies. (a) Experimental scheme for biopsies. 10 paired renal biopsies from kidneys that did not develop delayed graft function and 8 paired renal biopsies that developed delayed graft function were obtained. One biopsy was taken prior to transplant at the end of cold ischemia. The second biopsy was taken after transplant and reperfusion 45 minutes after the cross-clamp was removed. (b) Of the genes identified by Ingenuity pathway analysis, several gene families are identified to be involved in reactive aldehyde metabolism. (c), (d) ALDH2 and ALDH7A1 were statistically significant between kidneys that did not develop delayed graft function compared to kidneys developing delayed graft function ($*P < 0.01$). (e) ALDH4A1 nearly reached statistical significance ($\#P = 0.05$). (f) ALDH1A1, another ALDH family member, did not change between living donor kidneys compared to kidneys that developed delayed graft function. (-) = donor kidneys without delayed graft function; (+) = donor kidneys with delayed graft function.

kit with oligo dT primers. qPCR reactions were performed in a final volume of 20 μ l that contained 15 μ l of Fast SYBR® Green Master Mix (Life Technologies), 1000 nM primer (ALDH2, ALDH7A1, or GAPDH) or 500 nM primer (ALDH4A1), and 10 ng cDNA. The cycling protocol was 20 seconds at 95°C, followed by 40 cycles of 3 seconds at 95°C and 30 seconds at 61°C. The melt curve protocol was 15 seconds at 95°C, followed by a minute at 60°C, followed by a gradual temperature increase from 60°C to 95°C (+0.03°C per 15 seconds) in 42 minutes.

Western blot analysis was used to quantify 4-HNE-induced protein adducts in addition to protein expression of ALDH enzymes. For western blot analysis, kidney biopsies taken 45 minutes after reperfusion were homogenized in mannitol-sucrose buffer (210 mM mannitol, 70 mM sucrose, MOPS 5 mM, and EDTA 1 mM, pH 7.4) with protease and phosphatase inhibitors (1:300, Sigma protease inhibitor cocktail, Sigma phosphatase inhibitor cocktail 2, and phosphatase inhibitor cocktail 3) using a glass homogenizer (Wheaton, 1 mL tissue grinder). Homogenates were subsequently collected and spun at 800 g \times 10 minutes to remove nuclei and debris. The supernatant was collected and protein counts were obtained by Bradford assay and samples were normalized to μ g protein. Western blot was performed as described [12]. Primary antibodies used included anti-4HNE (rabbit, Alpha Diagnostics, 1:500), ALDH2 (goat, Santa Cruz, 1:1000), ALDH4A1 (rabbit, Abcam #EPR14287, 1:1000), ALDH7A1 (rabbit, Abcam, #EP1934Y, 1:1000), and ALDH1A1 (rabbit, Abcam, #EP1993Y, 1:1000). Secondary antibodies were used at 1:3000 consisting of anti-goat (Santa Cruz) and anti-rabbit (Sigma). Density of bands was measured by ImageJ and normalized to GAPDH (Santa Cruz, #47724, 1:3000).

To determine ALDH enzyme activity, 25 μ g of protein were used. ALDH enzyme activity was measured spectrophotometrically (340 nm) by analyzing the reaction of NAD⁺ to NADH as previously described [7, 12]. The activity assay was performed at 25°C in 50 mM sodium pyrophosphate buffer (pH 9.4), 2.5 mM NAD⁺, and 10 mM acetaldehyde was used as substrate. ALDH enzyme activity was converted to μ mole NADH/min/mg of protein.

2.4. Statistical Analysis. Sample sizes were chosen for this study based on previous experience the University of Leiden has on conducting clinical studies regarding ischemia-reperfusion injury in human kidney transplantation [13, 14]. SPSS 22.0 (SPSS, Chicago, IL) was used for gene array statistical analysis. For pathway analysis, data is represented as P values for the change in expression comparing the paired biopsies, fitting into predefined pathways. P values are expressed as the $-\log P$ value. Results were then analyzed by biostatistical methods using average replicate values for each group of samples. Log₂ ratios were computed and one value per gene was calculated for the average expression of probes with the same Entrez gene ID. For qPCR and protein assays, data was analyzed with GraphPad prism.

3. Results

Changes in gene pathway p -values using Ingenuity pathway analysis were calculated and initially reported [15]. Here, we analyzed the gene array data by comparing the gene array of a biopsy taken 45 minutes after reperfusion compared to the paired biopsy gene array taken at the end of cold ischemia. When looking at these differences for each group, we identified 10 signaling pathways that were induced with the

TABLE 1: Patient characteristics for gene array studies.

	Living donor kidney transplant (<i>n</i> = 10)	Deceased donor kidney transplant (<i>n</i> = 8)
Age of recipient (yrs)	49 ± 5	56 ± 4
Sex of recipient (% males)	60%	50%
Age of donor (yrs)	52 ± 2	49 ± 6
Sex of donor (% males)	30%	75%
Cold ischemia time (min)	213 ± 12	1001 ± 96*
Hospital stay (days)	8 ± 1	15 ± 2*
<i>Recipient cause of renal failure</i>		
Glomerulonephritis	40%	12.5%
Polycystic kidney disease	20%	25%
Diabetes mellitus type 2	10%	12.5%
Obstructive uropathy	10%	0%
Malignant hypertension	0%	0%
Renal failure	20%	50%
<i>Donor cause of death</i>		
Living donor	100%	
CVA		0%
SAB		25%
Trauma		37.5%
CA-OHCA-AMI		25%
Suicide		0%
Miscellaneous		12.5%
<i>Histocompatibility (HLA mismatches, %)</i>		
0	10%	12.5%
1	10%	25%
2	10%	25%
3	20%	25%
4	20%	12.5%
5	20%	0%
6	10%	0%

A total of 18 patients were included. When comparing recipients of a living donor transplant to recipients of a deceased donor transplant, significant differences were noted for duration of ischemia time, and length of posttransplantation hospital stay. **P* < 0.01, CVA = cerebral vascular accident, SAB = subarachnoid bleeding, CA = cardiac arrest, OHCA = out of hospital cardiac arrest, AMI = acute myocardial infarction. Data represents mean ± SEM.

highest differences in *p*-values in kidneys which did not develop delayed graft function compared to the kidneys which developed delayed graft function (Table 3). In particular, when examining these differences, distinct genes were upregulated for only the kidney biopsies that did not develop delayed graft function at reperfusion when compared to the kidney biopsies that developed delayed graft function for these pathways (Table 3).

Genes that contribute to aldehyde metabolism were identified in this gene array including the family of aldehyde dehydrogenase enzymes (ALDH2, ALDH4A1, and ALDH7A1), aldo-keto reductases (AKR1A1), and glutathione-S-transferases (GSTA1, GSTA2, GSTA3, and GST5) known to metabolize

TABLE 2: Patient characteristics for validation studies.

	Living donor kidney transplant (<i>n</i> = 10)	Deceased donor kidney transplant (<i>n</i> = 10)
Age of recipient (yrs)	58 ± 4	56 ± 4
Sex of recipient (% males)	70%	60%
Age of donor (yrs)	58 ± 2	57 ± 4
Sex of donor (% males)	50%	70%
Cold ischemia time (min)	221 ± 18	900 ± 88*
Hospital stay (days)	8 ± 2	15 ± 3*
<i>Recipient cause of renal failure</i>		
Glomerulonephritis	40%	30%
Polycystic kidney disease	20%	20%
Diabetes mellitus type 2	0%	20%
Obstructive uropathy	10%	10%
Malignant hypertension	10%	10%
Renal failure	20%	10%
<i>Donor cause of death</i>		
Living donor	100%	
CVA		20%
SAB		20%
Trauma		20%
CA-OHCA-AMI		30%
Suicide		10%
Miscellaneous		0%
<i>Histocompatibility (HLA mismatches, %)</i>		
0	0%	10%
1	10%	10%
2	0%	30%
3	10%	40%
4	20%	0%
5	40%	10%
6	20%	0%

A total of 20 patients were recruited. When comparing recipients of a living donor transplant to recipients of a deceased donor transplant, significant differences were noted for developing delayed graft function, duration of ischemia, and length of posttransplantation hospital stay. **P* < 0.01, CVA = cerebrovascular accident, SAB = subarachnoid bleeding, CA = cardiac arrest, OHCA = out of hospital cardiac arrest, AMI = acute myocardial infarction.

reactive aldehydes typically generated by the mitochondria during reperfusion (Figure 1(b)). Together, these results suggest that differences exist in the reactive aldehyde production and metabolism within donor kidneys that developed delayed graft function versus those that did not.

We further examined the gene array expression for ALDH2, ALDH4A1, and ALDH7A1 in addition to the other ALDH family of enzymes. Other ALDH enzymes (besides the cytosolic enzymes ALDH3A2 and ALDH1L1 unknown to be involved in aldehyde metabolism) remained unchanged (Supplemental Figure 1). ALDH2 and ALDH7A1 were significantly higher in the living donor grafts compared to the grafts with delayed graft function (ALDH2: 1919.4 ± 86.7

TABLE 3: Gene array differences from living compared to deceased donor kidney biopsies.

Pathway	Difference in value	Genes only upregulated in living donor	Genes only upregulated in deceased donor	Common
Serotonin degradation	6.59	ALDH4A1, ALDH2, ALDH7A1, ALDH3A2, ADH6, UGT2B7, UGT2B10, UGT2A3, UGT1A9, AKR1A1, SMOX, DHRS4	None	None
Tryptophan degradation	5.54	ALDH4A1, ALDH2, ALDH7A1, ALDH3A2, AKR1A1, DDC, SMOX	None	None
Histamine degradation	5.34	ALDH4A1, ALDH2, ALDH7A1, ALDH3A2, HNMT, ABP1	None	None
Ethanol degradation II	5.03	ALDH4A1, ALDH2, ALDH7A1, ALDH3A2, ADH6, AKR1A1, ACSS2, DHRS4	None	None
NRF-2-mediated oxidative stress response	4.82	AKR7A2, AKR1A1, FTL, NQO2, ABCC2, MAF, GSTA5, SCARB1, FMO1, GSTA1, GSTA2, GSTA3, MGST1, PRKCQ, ACTB, ACTG1, MGST2, MAP2K3, SQSTM1, AOX1, EIF2AK3, EPHX1	UBB, JUNB, DNAJA1, DNA	FOS, JUN, JUND, DNAJA4, DNAJB11, MAFF
Xenobiotic metabolism signaling	4.63	ALDH4A1, ALDH7A1, ALDH3A2, ALDH8A1, FTL, UGT2B7, NQO2, ABCC2, MAF, GSTA5, CYP3A7, HS6ST2, SMOX, FMO1, GSTA1, GSTA2, GSTA3, MGST1, PRKCQ, UGT2B10, UGT8, PPP2R5A, MGST2, MAP2K3, EIF2AK3, UGT1A9	CITED2, MAP3K8, TNF, HSP90AB1, HSP90AA1	None
Noradrenaline and adrenaline degradation	4.33	ALDH4A1, ALDH2, ALDH7A1, ALDH3A2, ALDH8A1, ADH6, AKR1A1, SMOX, DHRS4	None	None
LPS/IL-1-mediated inhibition of RXR function	4.14	ALDH4A1, ALDH7A1, ALDH3A2, ALDH8A1, GSTA1, GSTA2, GSTA3, GSTA5, APOE, MGST1, SLC27A2, ACOX2, ABCC2, CYP3A7, IL1R2, MGST2, SCARB1, NR5A2, HS6ST2, FMO1, SMOX	ALAS1, HMGCS1, TNF	ACSL3, JUN, NR0B2
Glutathione-mediated detoxification	4.12	GSTA1, GSTA2, GSTA3, GSTA5, MGST1, MGST2, GGH	None	None
Oxidative ethanol degradation	3.98	ALDH4A1, ALDH2, ALDH7A1, ALDH3A2, ACSS2	None	ACSL3

Whole genome array changes before and after kidney transplantation were compared from each donor kidney that did not develop delayed graft function (living donor) with those that did develop delayed graft function (deceased donor) using Ingenuity pathway analysis. The difference in *P*-values between gene arrays sets were the highest for the 10 signaling pathways listed. Specific genes that were only upregulated in living donor kidneys and deceased donor kidneys are listed. Further, genes that were upregulated in both kidneys that developed delayed graft function versus those that did not are also listed.

versus $1314.5 \pm 76.6^*$, ALDH7A1: 1739.9 ± 65.5 versus $1230.4 \pm 83.1^*$, $*P = 0.001$) with ALDH4A1 just at statistical significance (1324.1 ± 34.7 versus 1102.9 ± 105.9 ; $p = 0.05$, Figures 1(c)–1(e)). As a comparison, no differences were seen for the cytosolic ALDH enzyme ALDH1A1 (Figure 1(f)).

Since the gene array findings suggest a link to reactive aldehyde metabolism, we further examined reactive aldehyde metabolism and aldehyde-induced protein adducts by obtaining paired biopsies from additional grafts that did not develop delayed graft function and donor kidney grafts that developed delayed graft function. For these biopsies, we determined the ALDH-dependent enzymatic activity to metabolize reactive aldehydes (using the substrate NAD⁺) in addition to 4-hydroxynonenal- (4-HNE-) induced protein adducts for biopsies taken 45 minutes after reperfusion. The total ALDH enzymatic activity was significantly higher for donor kidney biopsies without delayed graft function when compared to biopsies from kidneys that developed delayed graft function (Figure 2(a): 78.6 ± 4.7 vs. $36.9 \pm 11.5^* \mu\text{g}/\text{min}/\text{mg}$ protein, $n = 8/\text{group}$, $*P < 0.005$). Additionally, the amount of 4-hydroxynonenal-induced protein adducts in the reperfused

kidneys was significantly higher for kidneys developing delayed graft function versus those that did not (Figure 2(b), 4-HNE adducts: 1.2 ± 0.2 vs. $1.9 \pm 0.3^*$, $n = 10/\text{group}$, $*P < 0.028$, $n = 10/\text{group}$).

Since a full analysis of the ALDH, AKR, and GSTA enzyme classes identified through gene array was not feasible to examine in human tissue biopsies based upon the biopsy sample size, we chose 3 candidate genes from our array that appeared in high frequency within the signaling pathways. These members of the aldehyde dehydrogenase gene family, ALDH2, ALDH7A1, and ALDH4A1, metabolize reactive aldehydes in a NAD-dependent fashion and can protect against cellular stress [7, 8, 16, 17]. Therefore, we focused on examining expression for the ALDH enzymes ALDH2, ALDH4A1, and ALDH7A1 with ALDH1A1 used as a control.

We performed qPCR on all biopsy samples obtained prior to kidney transplantation. The details of the primer design and validation for ALDH2, ALDH4A1, ALDH7A1, and ALDH1A1 are described (Figure 3(a) and Supplemental Figure 2). Significant differences were noted when calculating

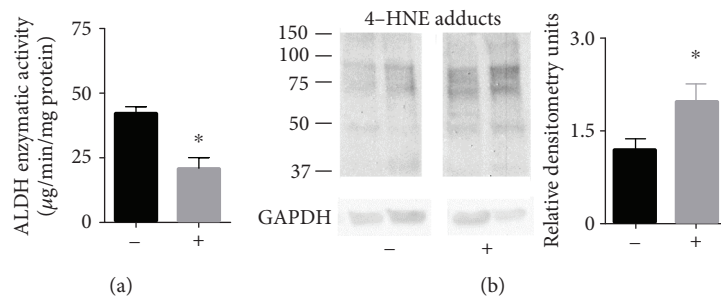


FIGURE 2: ALDH enzyme activity and 4-HNE protein-induced adduct formation taken from biopsies of kidneys 45 minutes after reperfusion. (a) ALDH enzymatic activity when challenged with acetaldehyde. $n = 8/\text{group}$, $*P < 0.005$; (b) 4-hydroxynonenal-induced protein adducts. Representative western blot in addition to quantification by densitometry. Western blots were normalized to GAPDH. (-) = donor kidneys without delayed graft function; (+) = donor kidneys with delayed graft function, $n = 10/\text{group}$, $*P < 0.05$.

Target	NCBI code	Forward primer	Reverse primer
ALDH2	NM_000690.3	CCGAGGTCTTCTGCAACCAG	AAGGCCTTGCCCTTCAG
ALDH7A1	NM_001182.4	CTTGCCCCATAGACCACTG	GCACAGATCCGAGTTGGGAA
ALDH4A1	NM_170726.2	GGTCCTTGCTCTCCACGATG	CTGCAGTGATTGATGCCAAGTC
ALDH1A1	NM_000689.4	ATCAAAGAAGCTGCCGGGAA	GCATTGTCCAAGTCGGCATC
GAPDH	NM_002046.5	GAGAAGGCTGGGGCTCATT	AGTGATGGCATGGACTGTGG

(a)

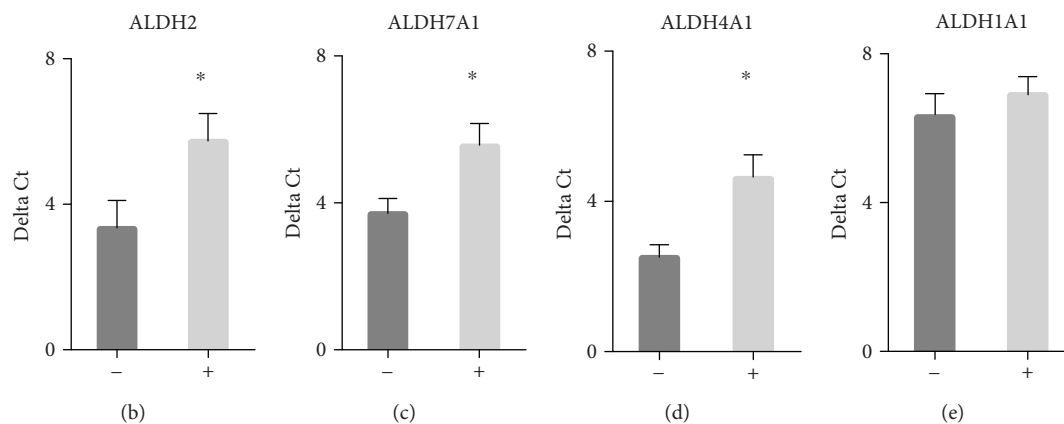


FIGURE 3: qPCR studies for kidney biopsies taken prior to transplant. For a separate series of kidney transplants, biopsies were collected for qPCR. (a) PCR primers used for qPCR. qPCR reactions were performed in a final volume of $20 \mu\text{l}$ that contained $15 \mu\text{l}$ of Fast SYBR® Green Master Mix (Life Technologies), 1000 nM primer (ALDH2, ALDH7A1 or GAPDH) or 500 nM primer (ALDH4A1), and 10 ng cDNA. (b–e) qPCR results for (b) ALDH2, (c) ALDH7A1, (d) ALDH4A1, and (e) ALDH1A1. ALDH2, ALDH7A1, and ALDH4A1 by qPCR were significantly elevated in kidneys that did not develop delayed graft function versus those kidneys that developed delayed graft function ($n = 10/\text{group}$, $*P < 0.05$). Ct values of each gene were normalized to GAPDH to calculate the delta Ct value. (-) = donor kidneys without delayed graft function; (+) = donor kidneys with delayed graft function.

a delta Ct (normalized to GAPDH) for donor kidneys that did not develop delayed graft function when compared to those donor kidneys that developed delayed graft function (Figures 3(b)–3(d), $n = 10/\text{group}$, ALDH2: 3.3 ± 0.8 vs. $5.7 \pm 0.8^*$, ALDH7A1 3.7 ± 0.4 vs. $5.6 \pm 0.6^*$, and ALDH4A1: 2.5 ± 0.3 vs. $4.6 \pm 0.6^{**}$, $*P < 0.01$, $**P < 0.001$, reported as delta Ct values normalized to GAPDH). As a comparison, ALDH1A1 was unchanged (Figure 3(e)).

We also quantified the levels of protein expression by western blot for ALDH2, ALDH7A1, and ALDH4A1. Both

ALDH7A1 and ALDH4A1 had significant changes in protein expression between the two groups (Figure 4(a), ALDH7A1: $1.2 \pm 0.1^*$ vs. 0.7 ± 0.07 , $*P < 0.001$, Figure 4(b), ALDH4A1: $1.7 \pm 0.3^*$ vs. 0.9 ± 0.1 , $*P < 0.017$). Western blot for ALDH2 also showed a relative change in expression that did not reach statistical significance (Figure 4(c), ALDH2: 5.2 ± 1.1 vs. 4.0 ± 0.6).

Since our results suggested that impaired reactive aldehyde metabolism may be associated with delayed graft function, we further examined whether cold ischemia times

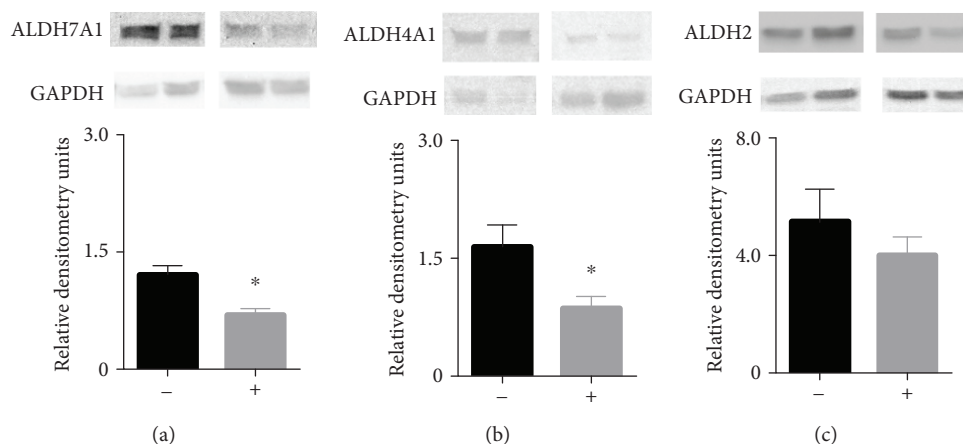


FIGURE 4: Western blot of ALDH7A1, ALDH4A1, and ALDH2 taken from biopsies of kidneys 45 minutes after reperfusion. (a–c) Western blots for (a) ALDH7A1, (b) ALDH4A1, and (c) ALDH2. All western blots were normalized to GAPDH. Both ALDH7A1 and ALDH4A1 were significantly different in kidneys that did not develop delayed graft function versus those kidneys that developed delayed graft function. (-) = donor kidneys without delayed graft function; (+) = donor kidneys with delayed graft function, $n = 10/\text{group}$, $*P < 0.05$.

influenced ALDH enzymatic activity. Generally, the cold ischemia times in the kidneys that did not develop delayed graft function was less compared to the kidneys that developed delayed graft function (Table 2, living donor without delayed graft function: 221 ± 18 minutes versus deceased donor with delayed graft function: $900 \pm 88^*$ minutes, $*P < 0.01$). No correlation between ALDH enzymatic activity and cold ischemia times for living donor grafts without delayed graft function was found, and the range of cold ischemia time for these kidneys was small (Figure 5(a) 6 of 8 samples had cold ischemia times between 210–240 minutes). Further, in grafts that did develop delayed graft function, a wider range of cold ischemia times existed; however, no association between ALDH enzymatic activity and cold ischemia times was found (Figure 5(b)).

However, ALDH enzymatic activity was also examined in relation to glomerular filtration rate (GFR) measured in patients at postoperative day 7 and length of hospital stay. Interestingly, those kidney biopsies that had lower ALDH enzymatic activity also had a lower GFR at day 7 (Figure 5(c): GFR <10: $30 \pm 12^*$, GFR 10–60: 49 ± 25 , GFR >60: $79 \pm 5 \mu\text{g}/\text{min}/\text{mg}$ protein, $n = 5$, $n = 3$, and $n = 8$, respectively, $*P = 0.013$ vs. GFR >60 group). In addition, an inverse association also existed with ALDH enzymatic activity when compared to the length of hospital stay (Figure 5(d): $r = -0.58$ by Pearson coefficient, $P = 0.0183$).

4. Discussion

Here we describe an important role by enzymes within the human kidney to metabolize reactive aldehydes produced during reperfusion of an organ transplant. We suggest quantifying the enzymatic activity to metabolize reactive aldehydes coupled with reactive aldehyde-induced protein adduct levels may be useful in possibly predicting delayed graft function and recovery from a kidney transplant. Our results suggest that measuring the overall reactive aldehyde balance within the donor kidney may be important in understanding which transplants may be at risk for

developing delayed graft function. These initial findings may potentially lead to developing a cellular biomarker based on reactive aldehyde production and metabolism to predict delayed graft function.

Presently, several biomarkers are being investigated for their ability to predict delayed graft function including neutrophil gelatinase-associated lipocalin (NGAL), kidney injury molecule 1 (KIM-1), interleukin18 (IL-18), klotho, cystatin C, and liver type fatty acid binding protein (L-FABP) [18–20]. Recently, NGAL blood levels taken from brain-dead kidney donors prior to kidney graft harvesting could not predict the development of delayed graft function [20]. Additionally, the idea of combining several biomarkers to detect delayed graft function was proposed, with a possible triple biomarker approach of serum malondialdehyde, cystatin C, and creatinine [21].

Although associations exist between serum malondialdehyde levels and delayed graft function [21, 22], serum malondialdehyde may underestimate the cellular damage contributed to lipid peroxidation. This is since ~95% of malondialdehyde is in the bound form with only 5% being free to measure in the serum for patients with end-stage renal disease [23]. Therefore, assessing both reactive aldehyde-induced protein levels and reactive aldehyde metabolism may provide a means to develop complementary biomarkers in order to predict delayed graft function. Even though our results were from kidney biopsies and not measured from circulating blood levels, we suggest that measuring the state of reactive aldehyde production and metabolism may potentially be useful in predicting delayed graft function rather than assessing specific protein biomarkers or reactive aldehyde levels within the blood.

Our data also examined ALDH7A1, ALDH4A1, and ALDH2 within the ALDH enzyme family suggesting that these enzymes are involved and contribute to a decreased reactive aldehyde metabolism seen in kidneys developing delayed graft function. However, the contribution of other families of enzymes such as AKR and GSTA cannot be excluded. Although protein expression was not significantly

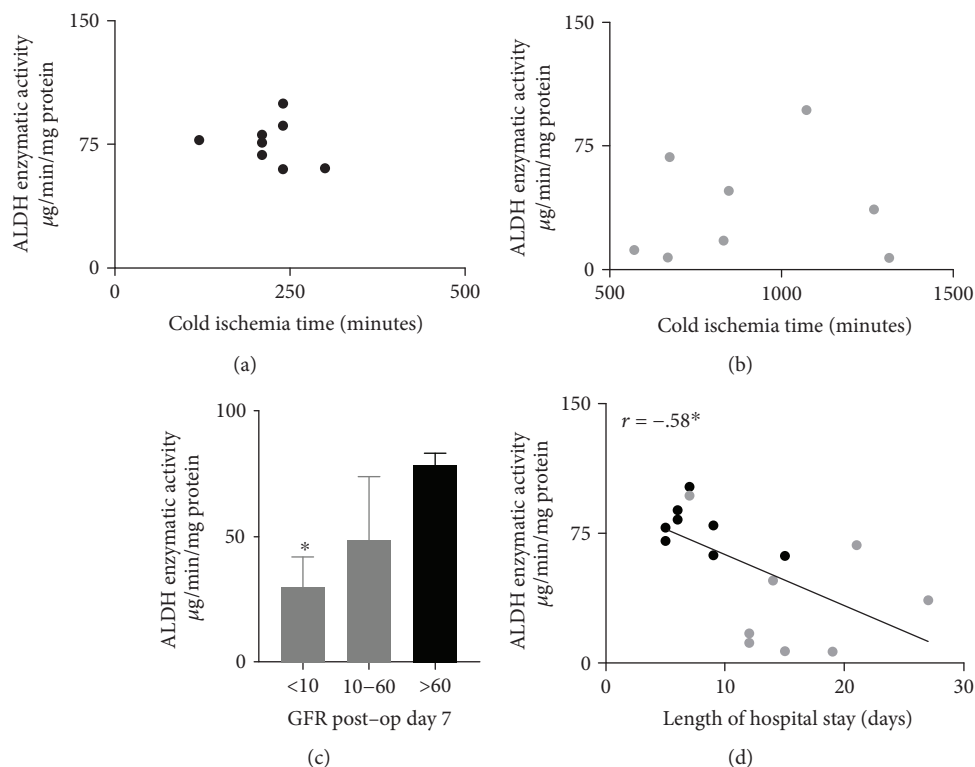


FIGURE 5: Association of ALDH enzymatic activity with transplant outcomes. (a) The level of ALDH enzymatic activity measured from the renal biopsy at 45 minutes after reperfusion during transplantation was associated with GFR at day 7 (GFR <10 $n = 5$, GFR 10-6 $n = 3$, GFR >60 $n = 8$). $*P = 0.013$ versus >60 GFR group). (b) ALDH enzymatic activity was also negatively correlated with the length of hospital stay. $n = 16$, $*P = 0.0183$.

changed for ALDH2 in our study, it cannot be ruled out that ALDH2 was posttranslationally modified by reactive aldehydes. To identify posttranslational modifications, immunoprecipitation of an enzyme (such as ALDH2) followed by western blot for aldehyde-induced protein adducts could be performed. However, the amount of protein needed to conduct this type of study exceeded the amount obtained from a renal biopsy for our study. Based upon prior studies performed *in vitro*, 4-HNE can inhibit human recombinant ALDH2 resulting in a decreased capability for the enzyme to metabolize reactive aldehydes [24]. At 50 μM 4-HNE, most of the effect is reversible; however, at 500 μM 4-HNE concentrations, this effect is noted to be irreversible [24]. Since with increases in oxidative stress blood levels of 4-HNE in humans can increase 10- to 100-fold [25], the reactive aldehydes generated during kidney reperfusion likely can cause a partial inhibition of ALDH enzymes. This inhibition can potentially contribute to the decreased reactive aldehyde metabolism we identified for our study in kidneys that developed delayed graft function.

In the era of precision medicine, it is also important to determine how genetic polymorphisms in mitochondrial ALDH enzymes may affect reactive aldehyde metabolism and delay graft function. In particular, ~560 million people in the world have a genetic variant of ALDH2, ALDH2*2, which severely limits the metabolism of reactive aldehydes [26]. Although no study has associated with an ALDH2*2 variant as a predictor of delayed graft function, this may

be due to organ transplantation (and in particular kidney transplantation) numbers that are traditionally low in East Asia compared to the rest of the world secondary to cultural reasons [27]. Further, very little is known regarding whether a genetic polymorphism in ALDH7A1 which decreases the enzymatic activity may also affect cellular function during organ transplantation. However, ALDH7A1 overexpression protects from both cellular toxicity and hyperosmotic stress [16, 28]. Therefore, the effects of either the donor or recipient having a genetic polymorphism in mitochondrial ALDH enzymes warrants further study [7, 12].

Our study does have a number of potential limitations that need to be considered when interpreting the data presented. Although we show an importance of reactive aldehyde production and metabolism in delayed graft function, we could not conclusively identify all the enzymes involved based on the size of the kidney biopsy obtained. Therefore, we only focused on 3 ALDH enzymes even though AKR and GSTA family members also had an increased gene expression for kidneys that did not develop delayed graft function. Additionally, the decreased protein expression observed might also be due to loss of cell and mitochondrial integrity since donor death itself induces metabolic dysregulation and mitochondrial dysfunction. We also compared grafts from living donor kidneys to deceased donor kidneys that developed delayed graft function. Further studies will be needed to compare reactive aldehyde production and

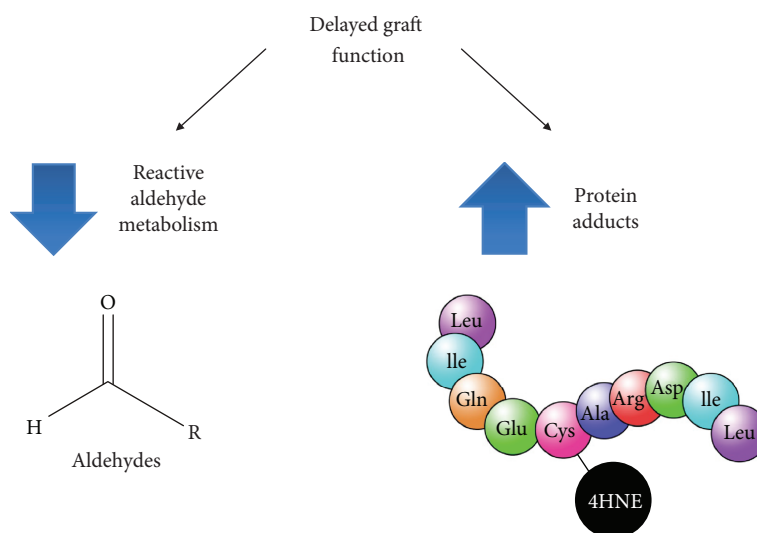


FIGURE 6: Summary. Reactive aldehyde metabolism is important in clearing toxic reactive aldehydes including 4-HNE in transplanted kidneys. Impaired reactive aldehyde metabolism and an increase in 4-HNE-induced protein adducts were found to be associated with delayed graft function.

metabolism also in deceased donor kidneys that did not develop delayed graft function as the effect we identify may be secondary to comparing living donor kidneys to deceased donor kidneys.

The study is also an association study and will require further validation both in experimental models and in the clinical realm. Although we did find associations for aldehyde enzymatic activity with GFR and length of hospital stay, these associations should be considered with caution as many factors contribute to the postoperative recovery from a kidney transplant and a larger study would be important to confirm these findings.

Together, we suggest that a decreased ability to metabolize reactive aldehydes in donor kidneys that develop delayed graft function occurs (Figure 6). This diminished metabolism of reactive aldehydes can result in aldehyde adducts forming on proteins that can potentially impair cellular functions by producing changes in enzyme activity, ion channel gating, and mitochondrial energetics [7, 29–31].

Data Availability

The data used to support the findings of this study are included within the article, supplemental information, and are cited at relevant places within the text as reference [13].

Conflicts of Interest

The authors declare that they have no conflicts of interest.

Acknowledgments

We thank all LUMCs transplantation surgeons who are greatly acknowledged for their assistance in obtaining tissue biopsies for this study. Funding support for this study was through the Dutch Kidney Foundation, the Catharina van Tussenbroek Fund, the Jo Kolk Studiefonds, the Michael

van Vloten Fund, and the Foundation “De Drie Lichten” in Netherlands (LGMW). This work was also supported by the National Institute of General Medical Sciences GM119522 (ERG).

Supplementary Materials

Microarray studies: microarray analysis was performed using Illumina whole-genome gene expression BeadChips. The gene array expression for the other ALDH family of enzymes on the microarray (besides ALDH2, ALDH4A1, and ALDH7A1 that were presented in the nonsupplemental portion of the manuscript) is presented in Supplemental Figure 1. qPCR primer validation: primer design and validation for ALDH2, ALDH4A1, ALDH7A1, and ALDH1A1 are presented in Supplemental Figure 2. (*Supplementary Materials*)

References

- [1] W. K. Wu, O. Famure, Y. Li, and S. J. Kim, “Delayed graft function and the risk of acute rejection in the modern era of kidney transplantation,” *Kidney International*, vol. 88, no. 4, pp. 851–858, 2015.
- [2] M. Hassanain, J. I. Tchervenkov, M. Cantarovich et al., “Recovery of graft function early posttransplant determines long-term graft survival in deceased donor renal transplants,” *Transplantation Proceedings*, vol. 41, no. 1, pp. 124–126, 2009.
- [3] M. Hassanain, J. Tchervenkov, M. Cantarovich et al., “Delayed graft function has an equally bad impact on deceased donor renal graft survival in both standard criteria donors and expanded criteria donors,” *Transplantation Proceedings*, vol. 41, no. 1, pp. 133–134, 2009.
- [4] M. M. Sainz, J. C. Toro, H. B. Poblete, L. F. Perez, V. H. Nicovani, and M. G. Carrera, “Incidence and factors associated with delayed graft function in renal transplantation at Carlos Van Buren Hospital, January 2000 to June 2008,” *Transplantation Proceedings*, vol. 41, no. 6, pp. 2655–2658, 2009.

- [5] B. Schroppel and C. Legendre, "Delayed kidney graft function: from mechanism to translation," *Kidney International*, vol. 86, no. 2, pp. 251–258, 2014.
- [6] D. H. Mallon, D. M. Summers, J. A. Bradley, and G. J. Pettigrew, "Defining delayed graft function after renal transplantation: simplest is best," *Transplantation*, vol. 96, no. 10, pp. 885–889, 2013.
- [7] C. H. Chen, G. R. Budas, E. N. Churchill, M. H. Disatnik, T. D. Hurley, and D. Mochly-Rosen, "Activation of aldehyde dehydrogenase-2 reduces ischemic damage to the heart," *Science*, vol. 321, no. 5895, pp. 1493–1495, 2008.
- [8] C.-H. Chen, J. C. B. Ferreira, E. R. Gross, and D. Mochly-Rosen, "Targeting aldehyde dehydrogenase 2: new therapeutic opportunities," *Physiological Reviews*, vol. 94, no. 1, pp. 1–34, 2014.
- [9] V. R. Mali and S. S. Palaniyandi, "Regulation and therapeutic strategies of 4-hydroxy-2-nonenal metabolism in heart disease," *Free Radical Research*, vol. 48, no. 3, pp. 251–263, 2014.
- [10] S. Srivastava, A. Chandra, H. N. Ansari, K. S. Srivastava, and A. Bhatnagar, "Identification of cardiac oxidoreductase(s) involved in the metabolism of the lipid peroxidation-derived aldehyde-4-hydroxynonenal," *Biochemical Journal*, vol. 329, no. 3, pp. 469–475, 1998.
- [11] Y. C. Awasthi, Y. Yang, N. K. Tiwari et al., "Regulation of 4-hydroxynonenal-mediated signaling by glutathione S-transferases," *Free Radical Biology & Medicine*, vol. 37, no. 5, pp. 607–619, 2004.
- [12] V. O. Zambelli, E. R. Gross, C. H. Chen, V. P. Gutierrez, Y. Cury, and D. Mochly-Rosen, "Aldehyde dehydrogenase-2 regulates nociception in rodent models of acute inflammatory pain," *Science Translational Medicine*, vol. 6, no. 251, article 251ra118, 2014.
- [13] D. K. de Vries, J. H. N. Lindeman, D. Tsikas et al., "Early renal ischemia-reperfusion injury in humans is dominated by IL-6 release from the allograft," *American Journal of Transplantation*, vol. 9, no. 7, pp. 1574–1584, 2009.
- [14] D. K. de Vries, P. van der Pol, G. E. van Anken et al., "Acute but transient release of terminal complement complex after reperfusion in clinical kidney transplantation," *Transplantation*, vol. 95, no. 6, pp. 816–820, 2013.
- [15] L. G. M. Wijermars, A. F. Schaapherder, D. K. de Vries et al., "Defective postreperfusion metabolic recovery directly associates with incident delayed graft function," *Kidney International*, vol. 90, no. 1, pp. 181–191, 2016.
- [16] C. Brocker, M. Cantore, P. Failli, and V. Vasiliou, "Aldehyde dehydrogenase 7A1 (ALDH7A1) attenuates reactive aldehyde and oxidative stress induced cytotoxicity," *Chemico-Biological Interactions*, vol. 191, no. 1–3, pp. 269–277, 2011.
- [17] K.-A. Yoon, Y. Nakamura, and H. Arakawa, "Identification of *ALDH4* as a p53-inducible gene and its protective role in cellular stresses," *Journal of Human Genetics*, vol. 49, no. 3, pp. 134–140, 2004.
- [18] J. Malyszko, E. Lukaszyk, I. Glowinska, and M. Durlik, "Biomarkers of delayed graft function as a form of acute kidney injury in kidney transplantation," *Scientific Reports*, vol. 5, no. 1, p. 11684, 2015.
- [19] G. Castellano, A. Intini, A. Stasi et al., "Complement modulation of anti-aging factor klotho in ischemia/reperfusion injury and delayed graft function," *American Journal of Transplantation*, vol. 16, no. 1, pp. 325–333, 2016.
- [20] L. Muller, A. Nicolas-Robin, S. Bastide et al., "Assessment of neutrophil gelatinase-associated lipocalin in the brain-dead organ donor to predict immediate graft function in kidney recipients: a prospective, multicenter study," *Anesthesiology*, vol. 122, no. 1, pp. 96–105, 2015.
- [21] I. Fonseca, H. Reguengo, J. C. Oliveira et al., "A triple-biomarker approach for the detection of delayed graft function after kidney transplantation using serum creatinine, cystatin C, and malondialdehyde," *Clinical Biochemistry*, vol. 48, no. 16–17, pp. 1033–1038, 2015.
- [22] I. Fonseca, H. Reguengo, M. Almeida et al., "Oxidative stress in kidney transplantation: malondialdehyde is an early predictive marker of graft dysfunction," *Transplantation*, vol. 97, no. 10, pp. 1058–1065, 2014.
- [23] A. F. De Vecchi, F. Bamonti, C. Novembrino et al., "Free and total plasma malondialdehyde in chronic renal insufficiency and in dialysis patients," *Nephrology Dialysis Transplantation*, vol. 24, no. 8, pp. 2524–2529, 2009.
- [24] J. A. Doorn, T. D. Hurley, and D. R. Petersen, "Inhibition of human mitochondrial aldehyde dehydrogenase by 4-hydroxy-non-2-enal and 4-oxonon-2-enal," *Chemical Research in Toxicology*, vol. 19, no. 1, pp. 102–110, 2006.
- [25] H. Esterbauer, R. J. Schaur, and H. Zollner, "Chemistry and biochemistry of 4-hydroxynonenal, malonaldehyde and related aldehydes," *Free Radical Biology & Medicine*, vol. 11, no. 1, pp. 81–128, 1991.
- [26] E. R. Gross, V. O. Zambelli, B. A. Small, J. C. B. Ferreira, C. H. Chen, and D. Mochly-Rosen, "A personalized medicine approach for Asian Americans with the aldehyde dehydrogenase 2*2 variant," *Annual Review of Pharmacology and Toxicology*, vol. 55, no. 1, pp. 107–127, 2015.
- [27] D. J. Rothman, "Ethical and social consequences of selling a kidney," *JAMA*, vol. 288, no. 13, pp. 1640–1641, 2002.
- [28] C. Brocker, N. Lassen, T. Estey et al., "Aldehyde dehydrogenase 7A1 (ALDH7A1) is a novel enzyme involved in cellular defense against hyperosmotic stress," *The Journal of Biological Chemistry*, vol. 285, no. 24, pp. 18452–18463, 2010.
- [29] K. Uchida and E. R. Stadtman, "Covalent attachment of 4-hydroxynonenal to glyceraldehyde-3-phosphate dehydrogenase. A possible involvement of intra- and intermolecular cross-linking reaction," *The Journal of Biological Chemistry*, vol. 268, no. 9, pp. 6388–6393, 1993.
- [30] S. Bang, K. Y. Kim, S. Yoo, Y. G. Kim, and S. W. Hwang, "Transient receptor potential A1 mediates acetaldehyde-evoked pain sensation," *The European Journal of Neuroscience*, vol. 26, no. 9, pp. 2516–2523, 2007.
- [31] B. G. Hill, B. P. Dranka, L. Zou, J. C. Chatham, and V. M. Darley-Usmar, "Importance of the bioenergetic reserve capacity in response to cardiomyocyte stress induced by 4-hydroxynonenal," *The Biochemical Journal*, vol. 424, no. 1, pp. 99–107, 2009.

Research Article

Increased Mitochondrial Protein Levels and Bioenergetics in the *Musculus Rectus Femoris* of *Wfs1*-Deficient Mice

Margus Eimre ¹, Kalju Paju,¹ Nadežda Peet ¹, Lumme Kadaja ¹, Marian Tarrend,¹
Sergo Kasvandik ², Joosep Seppet,³ Marilin Ivask ¹, Ehte Orlova ¹ and Sulev Kõks ¹

¹Chair of Pathological Physiology, Institute of Bio- and Translational Medicine, University of Tartu, Ravila 19, 50411 Tartu, Estonia

²Proteomics Core Facility, Institute of Technology, University of Tartu, Nooruse 1, 50411 Tartu, Estonia

³Department of Pathology, Tartu University Hospital, L. Puusepa 8, 51014 Tartu, Estonia

Correspondence should be addressed to Margus Eimre; margus.eimre@ut.ee

Received 14 June 2018; Revised 15 August 2018; Accepted 25 September 2018; Published 21 November 2018

Guest Editor: Julio C. B. Ferreira

Copyright © 2018 Margus Eimre et al. This is an open access article distributed under the Creative Commons Attribution License, which permits unrestricted use, distribution, and reproduction in any medium, provided the original work is properly cited.

Wfs1 deficiency leads to a progressive loss of plasma insulin concentration, which should reduce the consumption of glucose in insulin-dependent tissues, causing a variety of changes in intracellular energy metabolism. Our objective here was to assess the changes in the amount and function of mitochondrial proteins in different muscles of *Wfs1*-deficient mice. Mitochondrial functions were assayed by high-resolution oxygraphy of permeabilized muscle fibers; the protein amount was evaluated by liquid chromatography tandem mass spectrometry (LC/MS/MS) analysis and mRNA levels of the uncoupler proteins UCP2 and UCP3 by real-time PCR; and citrate synthase (CS) activity was determined spectrophotometrically in muscle homogenates. Compared to controls, there were no changes in proton leak and citrate synthase activity in the heart and *m. soleus* tissues of *Wfs1*-deficient mice, but significantly higher levels of both of these factors were observed in the *m. rectus femoris*; mitochondrial proteins and mRNA of UCP2 were also higher in the *m. rectus femoris*. ADP-stimulated state 3 respiration was lower in the *m. soleus*, remained unchanged in the heart, and was higher in the *m. rectus femoris*. The mitochondrial protein amount and activity are higher in *Wfs1*-deficient mice, as are mitochondrial proton leak and oxygen consumption in *m. rectus femoris*. These changes in muscle metabolism may be important for identifying the mechanisms responsible for Wolfram syndrome and diabetes.

1. Introduction

Wolframin, which is encoded by the *WFS1* gene, is a transmembrane glycoprotein found primarily in the endoplasmic reticulum (ER) and is ubiquitously expressed at high levels in the brain, pancreas, and heart but also has been observed in the liver, spleen, skeletal muscles, and kidney [1, 2]. Deficiency of wolframin induces ER stress and calcium depletion in cells [3, 4], which eventually may lead to the development of Wolfram syndrome type 1 (WS), a complex disease associated with diabetes insipidus, diabetes mellitus, optic atrophy, and deafness [5]. Short stature is also quite common in patients with WS [6–8], and people with WS often suffer from chronic and progressively increasing fatigue [9], as well as muscle spasms, which are common in most patients and can be very serious [10, 11].

The development of diabetes has been associated with increased ER stress and apoptosis in pancreatic beta cells, leading to insufficient insulin secretion [3, 12]. Wolfram syndrome-related diabetes (WSD) usually develops in childhood [13, 14] and tends to occur earlier than type 1 diabetes (5.4 vs. 7.9 years of age, respectively, $P < 0.001$) [15]. Normally, approximately three-quarters of the total body glucose uptake stimulated by insulin is mediated by the skeletal muscles [16–18], and therefore, deficit of insulin or resistance of muscle fibers to insulin in diabetes mellitus causes changes in muscle energy metabolism. Diabetic patients may experience muscular weakness in the ankles and knees [19]. Hand-grip strength values were also found to be lower in diabetes patients than in age-matched control subjects [20, 21]. Muscle weakness is related to signs and severity of polyneuropathy (PN), a frequent complication for people with diabetes.

In addition to PN, diabetes often leads to lower strength per unit of striated muscle and to the slowing of movements [22]. Accumulation of glycation end products may also be a cause of impaired muscle function in these patients [23].

Previous research has suggested a possible link between WS and mitochondrial DNA mutations [24], and patients with Wolfram syndrome have also been described as having heteroplasmic deletions of mtDNA in skeletal muscles [25, 26]. However, mitochondrial functioning has been poorly studied, with conflicting results [25, 27, 28]. Studies of muscle metabolism and mitochondrial function are limited by the small number of WS patients and a degree of randomness in the collection of biopsies from heterogeneous human muscles; in addition, it is also extremely difficult to analyze changes in different types of human muscle.

Several *Wfs1*-deficient mice models have been bred in order to study WS [3, 12, 29]. The mouse model we created exhibits a more severe phenotype than mutant mice developed by other labs and as such is a more precise model for the study of WS [30]. As *Wfs1* deficiency leads to a progressive loss of β -cells in the pancreas and lower concentrations of plasma insulin [29, 30], our mouse model can also be used to study the mechanisms responsible for type 1 diabetes. Our objective here was to assess changes in mitochondrial function and in the amounts and enzymatic activities of mitochondrial and glycolytic pathway proteins in muscles of *Wfs1*-deficient mice.

2. Materials and Methods

2.1. Animals. *Wfs1*-deficient (*Wfs1*KO) mice were generated as described previously [29, 31]. Experiments were performed with 9–12-month-old *Wfs1*KO male mice with a 129S6/SvEvTac background and their wild-type littermates. The animals were housed under standard laboratory conditions and kept on a 12 h light–dark cycle (lights on at 07:00) and were given free access to food and water. All experiments in this study involving animals were performed in accordance with the European Parliament Directive 2010/63/EU and under permit (no. 86, May 4, 2016) from the Estonian National Board of Animal Experiments.

2.2. Chemicals and Reagents. K-Lactobionate, ethylene glycol-bis(β -aminoethyl ether)-*N,N,N',N'*-tetraacetic acid (EGTA), and taurine were obtained from Fluka (Buchs, Switzerland); reduced nicotinamide adenine dinucleotide (NADH), pyruvate, and saponin were obtained from SERVA (Heidelberg, Germany); $MgCl_2$ and KCl were obtained from ACROS (Geel, Belgium); and leupeptin was obtained from Roche (Basel, Switzerland). All other reagents, ADP, ATP, bovine serum albumin, enzymes (glucose-6-phosphate dehydrogenase and lactate dehydrogenase), dithiothreitol, KH_2PO_4 , 4-(2-hydroxyethyl)-1-piperazineethanesulfonic acid (HEPES), L-glutamate, DL-malate, rotenone (Rot), succinate, atractyloside, antimycin A, *N,N,N',N'*-tetramethyl-p-phenylenediamine (TMPD), ascorbate, ethylenediaminetetraacetic acid (EDTA), glucose, Triton X-100, Tris, phosphoenolpyruvate (PEP), and NADP were obtained from Sigma (St. Louis, MO, United States).

2.3. Determination of Activities of the Respiratory Chain Complexes. Mice received 5 units/g b.wt. of heparin intraperitoneally and were killed by cervical dislocation. The heart, *m. soleus*, and white glycolytic section of the *m. rectus femoris* were excised and placed into ice-cold saline to ensure rapid cooling and blood removal. Thin muscle bundles from muscles were then excised in ice-cold solution A, which contained 2.77 mM CaK_2EGTA , 7.23 mM K_2EGTA 7.23 (free calcium concentration 0.1 μM), 6.56 mM $MgCl_2$, 0.5 mM dithiothreitol (DTT), 50 mM potassium 2-(*N*-morpholino)ethanesulfonate (K-MES), 20 mM imidazole, 20 mM taurine, 5.3 mM ATP, and 15 mM phosphocreatine, at pH 7.1 adjusted at 4°C. Muscle fibers were separated using sharp-ended needles, leaving only small areas of contact; the fibers were then transferred to vessels filled with solution A, to which an additional 50 μg of saponin per ml was added, and incubated with mild stirring for 30 min at 4°C for complete solubilization of the sarcolemma. Skinned (permeabilized) fibers were washed three times in solution B, which contained 0.5 mM EGTA, 3 mM $MgCl_2$, 60 mM K-lactobionate, 20 mM taurine, 3 mM KH_2PO_4 , 20 mM HEPES, 110 mM sucrose, and 5 mM pyruvate, and 1 mg/ml bovine serum albumin (BSA) and was set at pH 7.1 (adjusted at 25°C) for 10 min at 4°C by stirring to completely remove all metabolites, particularly trace amounts of ADP.

The activities of the mitochondrial respiratory chain segments in permeabilized muscle fibers were assessed using the polarographic method (Oroboros, Innsbruck, Austria) as respiration rates (VO_2) in solution B with 10 mM pyruvate or glutamate, 2 mM malate, and 0.2 μM free Ca^{2+} at 25°C. Following registration of mitochondrial respiration under nonphosphorylating conditions (basal respiration rate [V_{O_0}]) in the oxygraph chamber, 2 mM ADP was added to monitor the maximum rate of NADH-linked ADP-dependent respiration; subsequently, complex I was inhibited by 10 μM of rotenone (Rot). Then, 10 mM succinate was added to activate respiratory chain complex II-dependent respiration, 0.1 mM atractyloside (Atr) was added to assess respiratory control by adenine nucleotide translocase (ANT), 10 μM antimycin A was added to inhibit complex III and thereby block the electron flow from complex II to cytochrome c, and 0.5 mM tetramethylphenylene diamine (TMPD) with 2 mM ascorbate was added to activate cytochrome oxidase (COX). Activation of COX in the case of blocked oxidative phosphorylation (OXPHOS) in the presence of Atr was possible due to the smaller number of protons pumped by the respiratory chain per oxygen consumed [32]. In this case, the proton leak in the presence of TMPD was no longer a limiting factor for the respiratory chain. Finally, 5 mM sodium azide (NaN_3) was added to inhibit COX. Antimycin-sensitive respiration in the presence of atractyloside ($V_{Atr}-V_{Ant}$) was considered to represent the proton leak. The NaN_3 -sensitive portion of respiration with TMPD and ascorbate ($V_{TMPD}-V_{NaN_3}$) exhibits COX-related respiration.

2.4. Gene Expression Study. The *rectus femoris* muscles used in the gene expression analysis were suspended in RNAlater RNA Stabilization Reagent (Qiagen, Düsseldorf, Germany). Total RNA was isolated using the RNeasy Mini Kit (Qiagen).

Genomic DNA wipeout and reverse transcription were performed with QuantiTect® Reverse Transcription Kit (Qiagen), in accordance with the manufacturer's instructions (QuantiTect® Reverse Transcription Handbook, 2005). A QuantiTect SYBR Green PCR Kit (Qiagen, Düsseldorf, Germany) was used to perform real-time PCR amplification with mouse gene-specific primers (Table 1). Fluorescence data during PCR was collected with a StepOnePlus™ Real-Time PCR Instrument (Applied Biosystems, Foster City, CA, United States) and an intercalator-based approach (also known as the SYBR Green method). The comparative threshold cycle (ΔC_T , $\Delta\Delta C_T$) technique was used to determine the relative target quantities in samples [33], with all measurements normalized to the endogenous control gene ACTB. Relative target quantity in each sample was assessed by comparing normalized target quantity in each sample to normalized target quantity in the reference sample.

2.5. Determination of Enzymatic Activities. The heart muscle, *m. soleus*, and the glycolytic part of *m. rectus femoris* were frozen in liquid nitrogen and stored at -80°C ; these muscle tissues were later allowed to thaw at 0°C and homogenized by sonication (Bandelin Sonopuls HD 2200, probe MS 72, Sigma-Aldrich, St. Louis, MO, United States) on ice for 15 s in a medium containing 1 mM EDTA, 1 mM DTT, 10 mM glucose, 5 mM MgCl_2 , and 5 mM HEPES, at pH 8 (maintained by NaOH), with 0.1% Triton X-100 and 5 mg/ml leupeptin added to the mixture. After homogenization, the probe was kept on ice for an additional 30 s. The homogenization cycle was repeated twice thereafter, and the homogenates were left on ice for 1 h to allow complete extraction of the enzymes. Measurement of pyruvate kinase (PK) activity was performed using a spectrophotometric cuvette under stirring conditions in solution containing 26.7 mM KHPO_4 26.7 (pH 7.6, 37°C), 6.67 mM MgSO_4 , 0.24 mM NADH, 0.5 mM PEP, 3 mM ADP, and 10 IU/ml lactate dehydrogenase (LDH). After baseline registration, the reaction was initiated with the addition of the homogenate, and PK activity was derived from subsequent changes in NADH oxidation rates at 340 nm. Measurement of citrate synthase (CS) activity was performed using a Citrate Synthase Assay Kit (Sigma-Aldrich, St. Louis, MO, United States).

2.6. Proteomics Sample Preparation. Protein content of the homogenates was determined by precipitation with a methanol:chloroform:water solution in a 2:1:3 ratio, respectively, and suspended in digestion buffer (7 M thiourea, 2 M urea, and 100 mM ammonium bicarbonate). After reduction with 2.5 mM dithiothreitol and alkylation with 5 mM chloroacetamide, the samples were first predigested with 1:50 (protease:protein ratio) Lys-C (Wako Pure Chemical Industries, Osaka, Japan) for 4 h, diluted 5-fold with 100 mM ammonium bicarbonate, and then digested for 16 h with 1:50 trypsin at room temperature. Peptides were desalted using C18 (3M, Maplewood, Minnesota, United States) StageTips and reconstituted in 0.5% trifluoroacetic acid.

2.7. LC/MS/MS Analysis. Injected peptides were separated on an Ultimate 3000 RSLCnano system (Dionex, Sunnyvale,

TABLE 1: Primers for real-time PCR analysis.

Primer	Sequence 5' > 3'
UCP2	F: GCTGGTGGTGGTCGGAGAT
	R: TGAAGTGGCAAGGGAGG
UCP3	F: GCTGACACGAGAACTGAACTAAA
	R: GGAGTTGACTCTGGTTTTCTTTGT
ACTB	F: AGCCATGTACGTAGCCATCCA
	R: GACTTTGCTTTCCTTGGTGAGG

F: forward; R: reverse.

California, United States) using a C18 cartridge trap column (Dionex) in backflush configuration and an in-house packed ($3\ \mu\text{m}$ C18 particles, Dr. Maisch GmbH, Ammerbuch, Germany) analytical $50\ \text{cm} \times 75\ \mu\text{m}$ emitter column (New Objective Inc., Woburn, MA, United States). Peptides were eluted at 200 nl/min with a 5–35% B 180 min gradient (buffer B: 80% acetonitrile + 0.1% formic acid, buffer A: 0.1% formic acid) to a Q Exactive Plus (Thermo Fisher Scientific, Waltham, MA, United States) tandem mass spectrometer operating with a top 10 strategy. Briefly, one 350–1400 m/z MS scan at a resolution of $R = 70,000$ was followed by higher energy collisional dissociation fragmentation (normalized collision energy of 26) of the 10 most intense ions (charge states +2 to +6) at $R = 17,500$. MS and MS/MS ion target values were $3e6$ and $5e4$, respectively, and injection times were limited to 50 ms. Dynamic exclusion was set to 50 s.

2.8. Proteomics Data Analysis. Mass spectrometric raw data were processed with MaxQuant 1.5.3.17 software [34]. Label-free quantification with the MaxQuant LFQ algorithm [35] was enabled with default settings with the exception of the minimal ratio count (number of peptides quantified to report a protein quantification), which was set to 1 peptide. Methionine oxidation and protein N-terminal acetylation were set as variable modifications. Cysteine carbamidomethylation was defined as a fixed modification. Search was performed against the UniProt (<http://www.uniprot.org>) *Mus musculus* reference proteome database (downloaded on 11 November 2015; 57,320 entries) using the tryptic digestion rule Trypsin/P. Only identifications minimally 1 peptide 7 amino acids long were accepted, and transfer of identifications between runs was enabled. Peptide-spectrum match and protein false discovery rate (FDR) were kept below 1% using a target-decoy approach. All other parameters were kept at default settings.

2.9. Statistical Analysis. All statistical analyses were performed with Student's *t*-test, and data are presented as mean \pm SEM, with significance set at $P < 0.05$.

3. Results

3.1. Anatomical Data of *Wfs1*-Deficient and Wild-Type Mice. Body weights and muscle weights of *Wfs1*-deficient mice were significantly reduced compared to wild-type mice (Table 2); however, the heart-to-body weight and *soleus* muscle-to-body weight ratios were similar in both mice,

TABLE 2: Anatomical characteristics of Wfs1-deficient and wild-type mice.

Characteristic	WT ($n = 5$)	Wfs1KO ($n = 5$)
Body weight (g)	30.9 ± 1.1	19.9 ± 1.2***
Heart weight (mg)	161.5 ± 8.3	113.4 ± 7.6**
Heart/body weight ratio (mg/g)	5.59 ± 0.34	6.05 ± 0.06
Soleus muscle weight (mg)	5.47 ± 0.28	4.50 ± 0.41*
Soleus muscle/body weight ratio (mg/g)	0.189 ± 0.006	0.235 ± 0.020
Quadriceps femoris muscle weight (mg)	196.7 ± 5.93	100.3 ± 3.62***
Quadriceps femoris muscle/body weight ratio (mg/g)	6.05 ± 0.09	4.82 ± 0.27**

Means ± SEM are shown. Compared to wild type: * $P < 0.05$, ** $P < 0.01$, and *** $P < 0.001$.

suggesting that the absence of wolframin was not associated with atrophy of these muscles. In contrast, the *quadriceps femoris* muscle-to-body weight ratio was significantly reduced, indicating atrophy of this muscle and in part of the *m. rectus femoris*.

3.2. Mitochondrial Respiration in Muscles of Wfs1-Deficient Mice. The function of different respiratory chain complexes in the muscle fibers of saponin-skinned wild-type and Wfs1-deficient mice was assessed using a substrate/inhibitor titration protocol [36, 37] (Figure 1(a)). Mitochondrial respiration in the permeabilized muscle fibers increased over the basal levels following the addition of ADP, indicating a coupling of complex I-dependent respiration to ADP phosphorylation. After registration of respiration in the presence of ADP (Figure 1(a)), rotenone was added to inhibit complex I, and succinate was subsequently added to stimulate complex II-dependent respiration. Next, atractyloside was added, which strongly reduces succinate-dependent respiration; this was suppressed even further by the addition of 10 μ M antimycin A, which inhibits the electron flow from complex III to cytochrome c in mitochondria. Cytochrome c oxidase was activated with TMPD and ascorbate and then suppressed by NaN_3 (Figure 1(a)). As previous experiments have shown, V_{NaN_3} remains higher than V_0 [38, 39], a background respiration caused by strong autooxidation of TMPD [40]. We found that the basal respiration rate (V_0) was 2.59 times ($P < 0.001$) greater in Wfs1-deficient *m. rectus femoris* (Figure 1(d), Table S1) than in wild-type *m. rectus femoris*, whereas there were no differences in the heart and *m. soleus* between the two mice (Figures 1(b) and 1(c)). After the addition of ADP into the medium of wild-type *m. rectus femoris*, the rate of respiration increased to 1.06 ± 0.10 nmol $\text{O}_2/\text{min}/\text{mg}$ w.w. (Figure 1(d), Table S1), a rate lower than that of the corresponding increases in the other muscles. However, for the respiratory control index, the relative increase of 10.6 times with respect to V_0 for the wild-type *m. rectus femoris* was greater than that for the other muscles (Table S1). The corresponding relative increase of the respiration rate for the Wfs1-deficient *m. rectus femoris* was only 4.87 times, which was lower than in the *m. soleus*

and practically the same as in the heart. *Musculus rectus femoris* V_{ADP} was 40% higher in Wfs1-deficient mice than in wild-type mice ($P < 0.01$) (Figure 1(d)) but was 34% lower in Wfs1-deficient *m. soleus* than in wild-type *m. soleus* ($P < 0.01$) (Figure 1(c)). In addition, ADP- and complex II-dependent respirations were 62% higher in Wfs1-deficient *m. rectus femoris* ($P < 0.001$), whereas Wfs1-deficient *m. soleus* was 24% lower than in wild-type *m. soleus* ($P = 0.012$). Blocked OXPHOS (Atr) respiration was 75% higher in Wfs1-deficient *m. rectus femoris* than in wild-type *m. rectus femoris* ($P < 0.001$). The difference between V_{Atr} and V_{Ant} as proton leak-dependent respiration, was 73% greater in Wfs1-deficient *m. rectus femoris* than in wild-type *m. rectus femoris* ($P = 0.001$), and complex IV-dependent respiration (V_{COX}) was greater by 31% in Wfs1-deficient *m. rectus femoris*. There were no significant differences in complex I and OXPHOS-related oxygen flux ($V_{\text{ADP}} - V_0$) between wild-type and Wfs1-deficient *m. rectus femoris* (0.936 ± 0.08 and 1.171 ± 0.10 nmol $\text{O}_2/\text{min}/\text{mg}$ w.w., respectively).

3.3. Quantitative Real-Time RT-PCR Data Analysis. It is possible that the greater basal respiration (V_0) and differences in V_{Atr} and V_{Ant} in Wfs1-deficient *m. rectus femoris* compared to wild-type *m. rectus femoris* that we observed in the respiratory experiments were caused by increased proton leak in this muscle. Proton leak in skeletal muscles depends on uncoupler protein levels, and thus, we examined UCP2 and UCP3 expressions at the genetic level. We found that, relative to the housekeeping gene ACTB, UCP2 mRNA levels were 1.05 ± 0.37 in wild-type *m. rectus femoris* and 2.75 ± 0.30 in Wfs1-deficient *m. rectus femoris*, a difference of 2.6 times ($P < 0.05$). UCP3 expression was an order of magnitude lower than that of UCP2 and did not differ among the muscle types (Figure 2).

3.4. Enzymatic Activity. Citrate synthase activity was 77.0 ± 10.0 in wild-type heart muscles, but activity of this enzyme was 7.5 times lower (10.3 ± 1.1) in the *m. soleus* and 2 times lower still (4.4 ± 0.9) in the *m. rectus femoris* than in the *m. soleus* (Figure 3(a)). Compared with controls, there was no change in citrate synthase activity levels in Wfs1-deficient heart and *m. soleus* fibers, but activity levels were 1.46-fold ($P < 0.05$) higher in the Wfs1-deficient *m. rectus femoris*. Pyruvate kinase activity levels did not differ between wild-type and Wfs1-deficient muscles (Figure 3(b)).

3.5. Proteomics of Mitochondrial Proteins. We performed an LC/MS/MS analysis to confirm the results obtained from the oxygraphic experiments. Twenty-seven subunits of respiratory chain complex I were identified. In wild-type mice, protein amounts were determined to be ~ 5 times higher in the *m. soleus* than in the *m. rectus femoris* and ~ 5 times higher in the heart muscle than in the *m. soleus* (Figure S1). Amounts of typical representatives of the complex I proteins NADH dehydrogenase [ubiquinone] 1 alpha subcomplex subunit 2 (Ndufa2) and NADH dehydrogenase [ubiquinone] iron-sulfur protein 3 (Ndufs3) are shown in Figure 4. Respiratory chain complex II or succinate

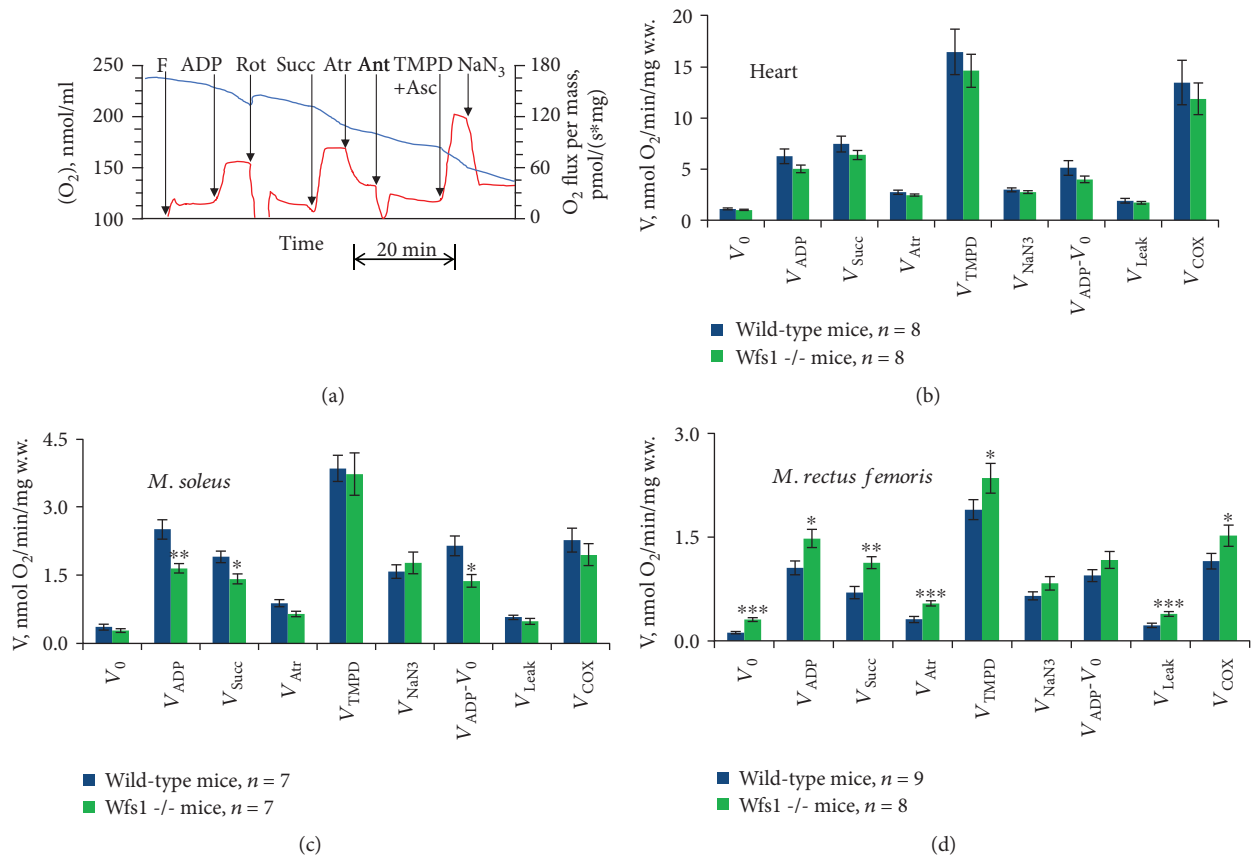


FIGURE 1: (a) Original recording of the assessment of the respiratory chain function in skinned muscle fibers. Additions: F: fibers; ADP: 2 mM ADP; Rot: 10 μ M rotenone; Succ: 10 mM succinate; Atr: 0.1 mM atractyloside; Ant: 10 μ M antimycin A; TMPD + Asc: 0.5 mM TMPD with 2 mM ascorbate; NaN_3 : 5 mM sodium azide. Upper, blue line: $[O_2]$; lower, red line: O_2 flux. Summary of results, which correspond to the experimental scheme shown in (a), is given in groups of permeabilized muscle fibers from the heart (b), *musculus soleus* (c), and *musculus rectus femoris* (d). V_0 : basal respiration; V_{ADP} : complex I- and ADP-dependent respirations; V_{Succ} : complex II-dependent respiration in the presence of rotenone with succinate; V_{Atr} : atractyloside-insensitive respiration rate; V_{TMPD} : respiration with TMPD and ascorbate in the presence of antimycin A; V_{NaN_3} : respiration in the presence of sodium azide; V_{Leak} : the difference between V_{Atr} and V_{Ant} , proton leak-dependent respiration; V_{COX} : sodium azide-sensitive portion of the respiration rate in the presence of TMPD and ascorbate. Data are mean \pm SEM. Compared to wild type: * $P < 0.05$, ** $P < 0.01$, and *** $P < 0.001$.

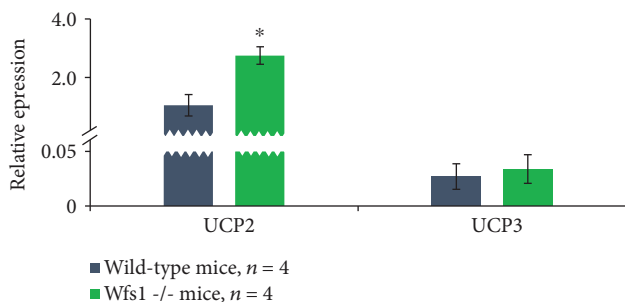


FIGURE 2: Relative expression of uncoupler proteins in homogenates of muscles in relation to housekeeping gene ACTB. * $P < 0.05$.

dehydrogenase is composed of four subunits consisting of the succinate dehydrogenase [ubiquinone] flavoprotein subunit SDHA, iron-sulfur protein SDHB, cytochrome b560 subunit SDHC, and cytochrome b small subunit SDHD. This enzyme plays a role in both the citric acid cycle and

the respiratory chain. Our LC/MS/MS analysis revealed the same increases (2.08 times) in both hydrophilic subunits SDHA and SDHB in *Wfs1*-deficient *m. rectus femoris* compared to wild-type *m. rectus femoris* and that the amounts of two hydrophobic subunits of succinate dehydrogenase, SDHC and SDHD, were more than an order of magnitude lower and did not differ significantly between wild-type and *Wfs1*-deficient muscles (Figure S4). Amounts of complex II protein and succinate dehydrogenase [ubiquinone] iron-sulfur subunit in wild-type and *Wfs1*-deficient mice muscles are shown in Figure 4. Eight components of the ubiquinol-cytochrome c reductase complex (complex III) were identified in *Wfs1*-deficient *m. rectus femoris*, of which amounts of six components were significantly higher by ~ 1.5 times (Figure S2). Similar results were obtained for respiratory chain complex IV, for which protein amounts were significantly higher in *Wfs1*-deficient *m. rectus femoris* than in wild-type *m. rectus femoris* (Figure S2). Amounts of typical representatives of complex IV are shown in

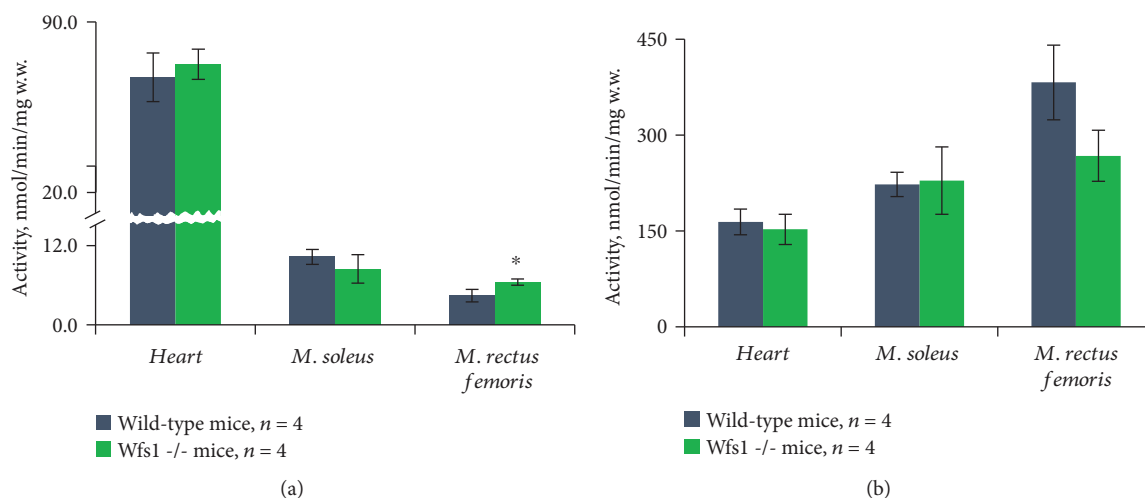


FIGURE 3: Citrate synthase (a) and pyruvate kinase (b) activity. Compared to wild type: * $P < 0.05$.

Figure 4. Mitochondrial membrane ATP synthase (F_1F_0 ATP synthase or complex V) consists of two structural domains, subunits alpha (Atp5a1) and beta (Atp5b), which form the catalytic core in the F_1 domain, which were compared to other subunits of F_1F_0 ATP synthase, and which are most abundant in muscle homogenates (Figure S3). The amounts of these subunits are shown in Figure 4. Abundance of subunit alpha Atp5a1 was 1.81 times ($P = 0.008$) and that of subunit beta 1.58 times ($P = 0.016$) higher in Wfs1-deficient *m. rectus femoris* than in wild-type *m. rectus femoris*. In the homogenates, H^+ transporting delta subunit of F_1 domain Atp5d; ATP synthase subunit gamma Atp5c1 of the central stalk; and several subunits of ATP synthase F_0 domain, namely, d Atp5h, e Atp5i, f Atp5j2, g Atp5l, o Atp5o, and ATP synthase-coupling factor 6 Atp5j, were also all detected at moderate levels. The amounts of all these subunits were higher in the *m. rectus femoris* of Wfs1-deficient mice than in that of wild-type mice (Figure S3).

The citric acid cycle is also an important mitochondrial enzymatic system that provides electrons to the respiratory chain. Citrate synthase, the first step of the citric acid cycle, is commonly used as a quantitative enzyme marker for the mitochondrial presence. As with enzyme activity, higher amounts of citrate synthase were present in Wfs1-deficient *m. rectus femoris* compared to wild-type *m. rectus femoris* (by 1.62 times, $P < 0.05$, Figure 5), as was also found for aconitate hydratase Aco2 (by 1.71 times, $P = 0.001$), isocitrate dehydrogenase [NAD] subunit gamma Idh3g (by 1.86 times, $P = 0.008$), 2-oxoglutarate dehydrogenase Ogdh (by 1.42 times, $P < 0.05$), succinyl-CoA ligase subunit beta (Sucla2) (by 1.42 times, $P < 0.05$), and mitochondrial malate dehydrogenase (by 1.93 times, $P = 0.001$) (Figure S4). Concentrations of pyruvate dehydrogenase, an enzyme closely linked to the citrate cycle, were also increased in Wfs1-deficient *m. rectus femoris* compared to wild-type *m. rectus femoris*, with pyruvate dehydrogenase E1 component subunit alpha 1.69 times ($P = 0.0021$) and subunit beta 1.56 times ($P = 0.018$) higher. Beta-oxidation of fatty acids takes place in the mitochondria, and all enzymes involved in beta-oxidation that were identified in our LC/MS/MS analysis were also

significantly higher (1.7–3.3 times, $P < 0.05$) in Wfs1-deficient *m. rectus femoris* than in wild-type *m. rectus femoris* (Figure S5). Amounts of the typical representative medium-chain-specific acyl-CoA dehydrogenase (Acadm) and hydroxyacyl-coenzyme A dehydrogenase (Hadh) are also shown in Figure 5.

3.6. Amounts of Indicators of Metabolic Profile and Regulators of Mitochondrial Function. Sirtuins are a class of proteins of relatively small molecular mass; these proteins have deacetylase activity and regulate important biological pathways [41]. Mitochondrial sirtuin 3 and sirtuin 5 amounts were 6.24 and 1.68 times higher, respectively, in Wfs1-deficient *m. rectus femoris* than in wild-type *m. rectus femoris* (Table 3), and sirtuin 5 was considerably more abundant than sirtuin 3 in all muscles. Amounts of cytoplasmic sirtuin 2 were lower than those of mitochondrial sirtuins in oxidative muscles. Both parvalbumin, a calcium-binding albumin protein, and sarcoplasmic reticulum calcium ATPase are normally found in greater quantities in fast-contracting glycolytic muscles. Parvalbumin alpha and sarcoplasmic reticulum calcium ATPase were 2.15 ($P = 0.01$) and 1.89 ($P = 0.0006$) times lower, respectively, in Wfs1-deficient *m. rectus femoris* than in wild-type *m. rectus femoris* (Table 3). Moreover, compared to the wild type, the abundance of some glycolytic enzymes was also lower in Wfs1-deficient *m. rectus femoris*; for instance, fructose-bisphosphate aldolase (Aldoa), alpha-enolase (Eno1), and L-lactate dehydrogenase A chain (Ldha) were reduced by 25% ($P = 0.003$), by 27% ($P = 0.0163$), and by 33% ($P = 0.0042$), respectively, in the *m. rectus femoris* of Wfs1-deficient mice relative to that of wild-type mice (Figure S6).

4. Discussion

To the best of our knowledge, this represents the first study in which the mitochondrial function and abundance of mitochondrial proteins in the muscles of Wfs1-deficient mice were characterized. Surprisingly, we found that, compared to the wild type, the amounts of the majority of the

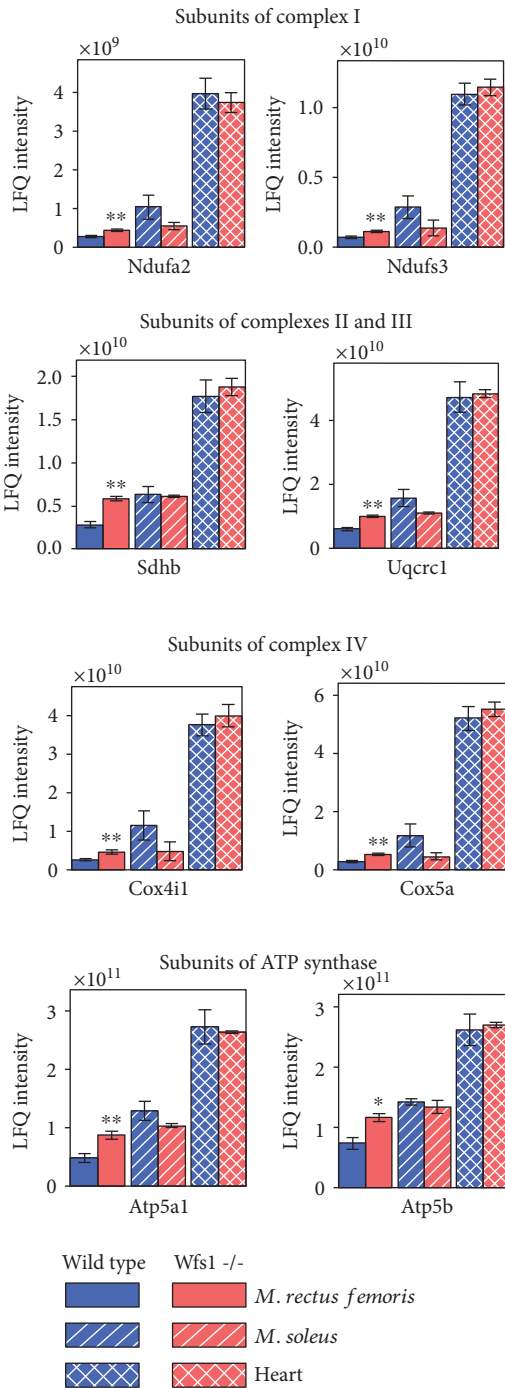


FIGURE 4: Amounts of some subunits of mitochondrial respiratory chain complexes. Ndufa2: NADH dehydrogenase [ubiquinone] 1 alpha subcomplex subunit 2; Ndufs3: NADH dehydrogenase [ubiquinone] iron-sulfur protein 3; SDHB: succinate dehydrogenase [ubiquinone] iron-sulfur subunit; Uqcrc1: cytochrome b-c1 complex subunit 1; Cox4i1: cytochrome c oxidase subunit 4 isoform 1; Cox5a: cytochrome c oxidase subunit 5A; Atp5a1: ATP synthase subunit alpha; Atp5b: ATP synthase subunit beta. Compared to wild type: * $P < 0.05$ and ** $P < 0.01$.

mitochondrial proteins and activity levels of citrate synthase were significantly higher in *Wfs1*-deficient glycolytic muscle tissues (~1.5-fold). ADP-dependent respiration with

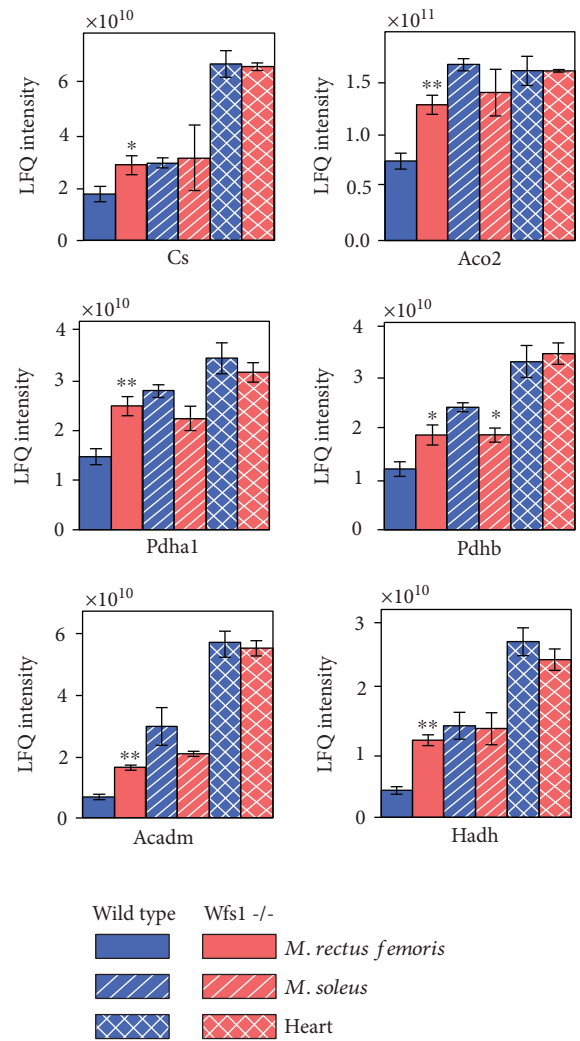


FIGURE 5: Amounts of some mitochondrial proteins and their subunits. Cs: citrate synthase; Aco2: aconitate hydratase; Pdha1: pyruvate dehydrogenase E1 component subunit alpha; Pdhb: pyruvate dehydrogenase E1 component subunit beta; Acadm: medium-chain specific acyl-CoA dehydrogenase; Hadh: hydroxyacyl-coenzyme A dehydrogenase. Compared to wild type: * $P < 0.05$ and ** $P < 0.01$.

complex I and II substrates was also higher in *Wfs1*-deficient *m. rectus femoris* than in wild-type *m. rectus femoris*, and complex IV-dependent respiration was one-third greater in this muscle in *Wfs1*-deficient mice than in wild-type mice (Figure 1(d)). As can be seen in Table 2, the quadriceps muscle-to-body weight ratio was lower in *Wfs1*-deficient mice. Similarly, STZ-induced type I diabetes produces profound atrophy of fast-twitch muscles and especially the fast glycolytic (FG) fibers [42–46]. Atrophy of glycolytic muscle fibers in our model mice most likely caused even higher rates of respiration and mitochondrial protein abundance in the *Wfs1*-deficient glycolytic *rectus femoris* muscle. Comparable results were reported from recent work, in which it was shown that basal oxygen consumption (measured at the whole-organism level) was 1.3 times higher in

TABLE 3: LFQ intensities of proteins determined by LC/MS/MS analysis.

Proteins	Genes	<i>M. rectus femoris</i>		<i>M. soleus</i>		Heart	
		Wfs1+/+ <i>n</i> = 8	Wfs1-/- <i>n</i> = 5	Wfs1+/+ <i>n</i> = 3	Wfs1-/- <i>n</i> = 2	Wfs1+/+ <i>n</i> = 4	Wfs1-/- <i>n</i> = 4
NAD-dependent protein deacylase sirtuin-5, mitochondrial	Sirt5	1.86E + 08 ± 2.17E + 07	3.13E + 08 ± 3.37E + 07*	4.05E + 08 ± 3.42E + 07	2.61E + 08 ± 1.15E + 08	8.24E + 08 ± 8.25E + 07	7.94E + 08 ± 3.06E + 07
NAD-dependent protein deacetylase sirtuin-3	Sirt3	3.81E + 06 ± 1.24E + 06	2.38E + 07 ± 6.73E + 06**	7.37E + 06 ± 4.10E + 06	8.22E + 06 ± 7.12E + 06	1.66E + 08 ± 6.67E + 07	2.83E + 08 ± 3.61E + 07
NAD-dependent protein deacetylase sirtuin-2	Sirt2	4.40E + 08 ± 3.34E + 07	3.39E + 08 ± 3.68E + 07	2.44E + 08 ± 1.94E + 07	2.17E + 08 ± 1.03E + 08	5.80E + 07 ± 5.74E + 06	6.03E + 07 ± 1.11E + 07
Parvalbumin alpha	Pvalb	4.30E + 11 ± 5.90E + 10	2.00E + 11 ± 2.24E + 10*	7.25E + 10 ± 6.04E + 10	5.54E + 10 ± 4.22E + 10	1.87E + 07 ± 1.43E + 07	0.00
Sarcoplasmic/endoplasmic reticulum calcium ATPase	Atp2a	3.86E + 11 ± 2.76E + 10	2.04E + 11 ± 1.84E + 10***	1.25E + 11 ± 7.08E + 10	3.00E + 10 ± 1.42E + 10	2.64E + 10 ± 4.81E + 09	2.85E + 10 ± 2.16E + 09

Values are means ± SEM; *n* = the number of specimens studied. Compared to wild type: **P* < 0.05, ***P* < 0.01, and ****P* < 0.001.

Wfs1-deficient mice, and heat production was also 1.3 times higher in Wfs1-deficient mice [47]. Transient receptor potential melastatin 8 (TRPM8) channels, which are activated by cold (8–28°C) and by some chemicals like menthol, are key pathways for heat production signaling [48–50]. Dietary menthol was shown to significantly increase oxygen consumption in WT mice but not in TRMP8KO mice, suggesting that dietary menthol increases the resting metabolic rate via TRPM8 activation [51]. Likewise, RNA sequencing analysis revealed increased expression of TRMP8 in the hippocampus of Wfs1-deficient mice, and metabolic studies have shown higher response to menthol administration in Wfs1-deficient mice compared to WT mice. Overexpressed TRMP8 in Wfs1-deficient mice might be the reason for the higher basal oxygen consumption and heat production in this type compared to WT mice [47]. Given that TRMP8-dependent thermogenesis is caused by activation of uncoupler protein 1 (UCP1) in brown adipose tissue [51], the enhanced heat production and oxygen consumption of Wfs1-deficient mice may be due to increased mitochondrial proton leak in BAT, but the results of our study suggest that elevated mitochondrial proton leak also occurs in the glycolytic muscle *rectus femoris*. Compared to the wild type, basal respiration without ADP was 2.5-folds higher and proton leak-dependent respiration 1.7-folds higher in Wfs1-deficient muscles. OXPHOS-related oxygen flux (V_{ADP-V_0}) did not differ significantly between wild-type and Wfs1-deficient *m. rectus femoris* muscles; thus, in the latter, the proportion of proton leak to OXPHOS was increased, and accordingly, the respiratory control index was 2 times lower in Wfs1-deficient *m. rectus femoris*. Increases in the relative proportion of proton leak in glycolytic skeletal muscle may depend on higher levels of UCP2, as we observed an increase in RNA levels of this protein; however, LC/MS/MS analysis failed to detect the presence of UCP2 proteins in any of the muscle types, indicating that increased proton leak simply damages mitochondria in Wfs1-deficient glycolytic muscles and that the increase in mitochondrial proteins is most likely compensating for decreasing mitochondrial quality. It has been shown that SIRT3 stimulates mitochondrial biogenesis [52–54], and thus, the higher levels of mitochondrial sirtuin 3 in Wfs1-deficient *m. rectus femoris* compared to wild-type *m. rectus femoris* likely stimulate mitochondrial biogenesis in this tissue. Concentrations of sirtuin 5 were also higher in Wfs1-deficient *m. rectus femoris*; like other sirtuins, sirtuin 5 has deacetylase activity and is capable of removing acetyl, succinyl, and malonyl groups from the lysine residues of proteins, but in contrast to sirtuin 3, it does not seem to be involved in mitochondrial biogenesis [55, 56]. Levels of cytoplasmic sirtuin 2 were roughly the same in Wfs1-deficient and wild-type *m. rectus femoris*, which may simply reflect a reduction in the amount of cytoplasm relative to mitochondria as levels of mitochondrial sirtuins and other mitochondrial proteins increased.

In contrast to glycolytic *rectus femoris*, either there were no changes in the oxidative muscles of Wfs1-deficient mice or changes occurred in the opposite direction. In the heart muscle, for instance, mitochondrial protein abundance, citrate synthase activity, and mitochondrial respiration

remained unchanged, and compared to the wild type, ADP-dependent respiration involving both complex I and complex II substrates was lower in Wfs1-deficient *m. soleus*. Furthermore, although we observed downward trends in the parameters of several mitochondrial proteins in Wfs1-deficient *m. soleus*, the amounts of other proteins and the activity level of citrate synthase did not change.

The Wfs1 protein interacts with sarco/endoplasmic reticulum ATPase (Atp2a) and negatively regulates Atp2a turnover, possibly via proteasome-mediated degradation. In Wfs1-depleted cells, Wfs1–Atp2a interaction is limited, and therefore, the amount of Atp2a is upregulated [57]; however, we did not observe higher levels of Atp2a in Wfs1-deficient muscles. In fact, Atp2a was lower in Wfs1-deficient *m. rectus femoris* than in wild-type *m. rectus femoris*, as was parvalbumin alpha (Pvalb), a protein involved in calcium signaling. Concentrations of parvalbumin are normally high in fast-contracting muscles and low in slow-contracting muscles [58], whereas slow-twitch muscles generally contain more mitochondria and less cytoplasm. We also found that, compared to the wild type, concentrations of some glycolytic enzymes were lower in Wfs1-deficient *m. rectus femoris*. As such, the reduced amounts of Atp2a1 and Pvalb may indicate a shift from fast-contracting glycolytic *m. rectus femoris* to slower oxidative muscles in Wfs1-deficient mice. Like type 1 diabetes, this shift in the glycolytic muscle type is probably triggered by insulin deficiency and the atrophy of FG fibers in Wfs1-deficient mice and missed in oxidative muscles [45, 46]. Increased relative proton leak, which reduces the efficiency of ATP synthesis, is another alteration in *m. rectus femoris* metabolism. It is possible that these same pathologies occur in patients suffering from WS; considering the high percentage of glycolytic muscles in the human body, such changes may be major causes of the chronic progressive fatigue and other muscle disorders experienced by WS patients [9].

5. Conclusions

Mitochondrial protein concentrations, citrate synthase activity, and mitochondrial respiration of permeabilized fibers were found to be significantly elevated in Wfs1-deficient *m. rectus femoris*. Compared to the wild type, efficiency of ATP synthesis declined in the mitochondria of Wfs1-deficient *m. rectus femoris* muscle due to higher proton leak-dependent respiration, whereas there was no difference in OXPHOS-dependent respiration.

Data Availability

The mass spectrometry proteomics data used to support the findings of this study have been deposited to the ProteomeXchange Consortium via the PRIDE [59] partner repository with the dataset identifier PXD011019 and will be published as data article [60]. The other data used to support the findings of this study are available from the corresponding author upon request.

Conflicts of Interest

The authors declare that they have no competing interests.

Acknowledgments

The authors thank Ellen Gvozdkova and Martin Eimre for technical assistance. This work was supported by the European Union's Horizon 2020 research and innovation programme TRANSGENO project under grant agreement No. 668989 and Institutional Research Funding IUT20-46 of the Haridus- ja Teadusministeerium.

Supplementary Materials

Table S1: rates of mitochondrial respiration. Figure S1: amounts of respiratory chain complex I subunits. Figure S2: amounts of respiratory chain complex III and IV subunits. Figure S3: amounts of respiratory chain complex V subunits. Figure S4: amounts of citrate cycle enzymes and their subunits. Figure S5: amounts of fatty acid beta-oxidation enzymes. Figure S6: amounts of glycolytic enzymes. (*Supplementary Materials*)

References



- [1] S. Hofmann, C. Philbrook, K. D. Gerbitz, and M. F. Bauer, "Wolfram syndrome: structural and functional analyses of mutant and wild-type wolframin, the WFS1 gene product," *Human Molecular Genetics*, vol. 12, no. 16, pp. 2003–2012, 2003.
- [2] H. Inoue, Y. Tanizawa, J. Wasson et al., "A gene encoding a transmembrane protein is mutated in patients with diabetes mellitus and optic atrophy (Wolfram syndrome)," *Nature Genetics*, vol. 20, no. 2, pp. 143–148, 1998.
- [3] A. C. Riggs, E. Bernal-Mizrachi, M. Ohsugi et al., "Mice conditionally lacking the Wolfram gene in pancreatic islet beta cells exhibit diabetes as a result of enhanced endoplasmic reticulum stress and apoptosis," *Diabetologia*, vol. 48, no. 11, pp. 2313–2321, 2005.
- [4] D. Takei, H. Ishihara, S. Yamaguchi et al., "WFS1 protein modulates the free Ca(2+) concentration in the endoplasmic reticulum," *FEBS Letters*, vol. 580, no. 24, pp. 5635–5640, 2006.
- [5] T. M. Strom, K. Hörtnagel, S. Hofmann et al., "Diabetes insipidus, diabetes mellitus, optic atrophy and deafness (DIDMOAD) caused by mutations in a novel gene (wolframin) coding for a predicted transmembrane protein," *Human Molecular Genetics*, vol. 7, no. 13, pp. 2021–2028, 1998.
- [6] E. Simsek, T. Simsek, S. Tekgül, S. Hosal, V. Seyrantepe, and G. Aktan, "Wolfram (DIDMOAD) syndrome: a multidisciplinary clinical study in nine Turkish patients and review of the literature," *Acta Paediatrica*, vol. 92, no. 1, pp. 55–61, 2003.
- [7] R. Medlej, J. Wasson, P. Baz et al., "Diabetes mellitus and optic atrophy: a study of Wolfram syndrome in the Lebanese population," *The Journal of Clinical Endocrinology & Metabolism*, vol. 89, no. 4, pp. 1656–1661, 2004.
- [8] M. A. Ganie, B. A. Laway, S. Nisar et al., "Presentation and clinical course of Wolfram (DIDMOAD) syndrome from North India," *Diabetic Medicine*, vol. 28, no. 11, pp. 1337–1342, 2011.
- [9] Diabetes UK, "Wolfram syndrome," <https://www.diabetes.org.uk/diabetes-the-basics/other-types-of-diabetes/wolfram-syndrome>.
- [10] Genetics Home Reference, "Wolfram syndrome," 2012, <http://ghr.nlm.nih.gov/condition/wolfram-syndrome>.
- [11] The Genetic and Rare Diseases Information Center, "Wolfram syndrome," 2018, https://rarediseases.info.nih.gov/diseases/7898/wolfram-syndrome#ref_7125.
- [12] H. Ishihara, S. Takeda, A. Tamura et al., "Disruption of the WFS1 gene in mice causes progressive beta-cell loss and impaired stimulus-secretion coupling in insulin secretion," *Human Molecular Genetics*, vol. 13, no. 11, pp. 1159–1170, 2004.
- [13] T. G. Barrett and S. E. Bunday, "Wolfram (DIDMOAD) syndrome," *Journal of Medical Genetics*, vol. 34, no. 10, pp. 838–841, 1997.
- [14] C. J. Smith, P. A. Crock, B. R. King, C. J. Meldrum, and R. J. Scott, "Phenotype-genotype correlations in a series of Wolfram syndrome families," *Diabetes Care*, vol. 27, no. 8, pp. 2003–2009, 2004.
- [15] J. Rohayem, C. Ehlers, B. Wiedemann et al., "Diabetes and neurodegeneration in Wolfram syndrome: a multicenter study of phenotype and genotype," *Diabetes Care*, vol. 34, no. 7, pp. 1503–1510, 2011.
- [16] A. D. Baron, G. Brechtel, P. Wallace, and S. V. Edelman, "Rates and tissue sites of non-insulin- and insulin-mediated glucose uptake in humans," *American Journal of Physiology-Endocrinology and Metabolism*, vol. 255, no. 6, pp. E769–E774, 1988.
- [17] P. Nuutila, V. A. Koivisto, J. Knuuti et al., "Glucose-free fatty acid cycle operates in human heart and skeletal muscle in vivo," *Journal of Clinical Investigation*, vol. 89, no. 6, pp. 1767–1774, 1992.
- [18] I. Idris, S. Gray, and R. Donnelly, "Insulin action in skeletal muscle: isozyme-specific effects of protein kinase C," *Annals of the New York Academy of Science*, vol. 967, no. 1, pp. 176–182, 2002.
- [19] H. Andersen, S. Nielsen, C. E. Mogensen, and J. Jakobsen, "Muscle strength in type 2 diabetes," *Diabetes*, vol. 53, no. 6, pp. 1543–1548, 2004.
- [20] E. Cetinus, M. A. Buyukbese, M. Uzel, H. Ekerbicer, and A. Karaoguz, "Hand grip strength in patients with type 2 diabetes mellitus," *Diabetes Research and Clinical Practice*, vol. 70, no. 3, pp. 278–286, 2005.
- [21] M. E. Khallaf, E. E. Fayed, and M. I. Al-Rashidi, "Effect of long-standing diabetes mellitus type II on hand grip strength and pinch power of females in the city of Hail-KSA," *IOSR Journal of Nursing and Health Science*, vol. 3, no. 1, pp. 41–44, 2014.
- [22] H. Andersen, "Motor dysfunction in diabetes," *Diabetes/Metabolism Research and Reviews*, vol. 28, Supplement 1, pp. 89–92, 2012.
- [23] H. Mori, A. Kuroda, M. Araki et al., "Advanced glycation end-products are a risk for muscle weakness in Japanese patients with type 1 diabetes," *Journal of Diabetes Investigation*, vol. 8, no. 3, pp. 377–382, 2017.
- [24] A. Barrientos, J. Casademont, A. Saiz et al., "Autosomal recessive Wolfram syndrome associated with an 8.5-kb mtDNA single deletion," *American Journal of Human Genetics*, vol. 58, no. 5, pp. 963–970, 1996.
- [25] A. Rötig, V. Cormier, P. Chatelain et al., "Deletion of mitochondrial DNA in a case of early-onset diabetes mellitus, optic

- atrophy, and deafness (Wolfram syndrome, MIM 222300),” *Journal of Clinical Investigation*, vol. 91, no. 3, pp. 1095–1098, 1993.
- [26] N. Mezghani, M. Mnif, E. Mkaouar-Rebai et al., “The mitochondrial ND1 m.3337G>A mutation associated to multiple mitochondrial DNA deletions in a patient with Wolfram syndrome and cardiomyopathy,” *Biochemical and Biophysical Research Communications*, vol. 411, no. 2, pp. 247–252, 2011.
- [27] M. J. Jackson, L. A. Bindoff, K. Weber et al., “Biochemical and molecular studies of mitochondrial function in diabetes insipidus, diabetes mellitus, optic atrophy, and deafness,” *Diabetes Care*, vol. 17, no. 7, pp. 728–733, 1994.
- [28] T. G. Barrett, M. Scott-Brown, A. Seller, A. Bednarz, K. Poulton, and J. Poulton, “The mitochondrial genome in Wolfram syndrome,” *Journal of Medical Genetics*, vol. 37, no. 6, pp. 463–466, 2000.
- [29] S. Köks, U. Soomets, J. L. Paya-Cano et al., “Wfs1 gene deletion causes growth retardation in mice and interferes with the growth hormone pathway,” *Physiological Genomics*, vol. 37, no. 3, pp. 249–259, 2009.
- [30] K. Noormets, S. Köks, M. Muldmaa, L. Muring, E. Vasar, and V. Tillmann, “Sex differences in the development of diabetes in mice with deleted wolframin (Wfs1) gene,” *Experimental and Clinical Endocrinology and Diabetes*, vol. 119, no. 5, pp. 271–275, 2011.
- [31] H. Luuk, S. Köks, M. Plaas, J. Hannibal, J. F. Rehfeld, and E. Vasar, “Distribution of Wfs1 protein in the central nervous system of the mouse and its relation to clinical symptoms of the Wolfram syndrome,” *Journal of Comparative Neurology*, vol. 509, no. 6, pp. 642–660, 2008.
- [32] S. Papa, N. Capitanio, G. Capitanio, E. De Nitto, and M. Minuto, “The cytochrome chain of mitochondria exhibits variable H^+/e^- stoichiometry,” *FEBS Letters*, vol. 288, no. 1–2, pp. 183–186, 1991.
- [33] K. J. Livak and T. D. Schmittgen, “Analysis of relative gene expression data using real-time quantitative PCR and the $2(-\Delta\Delta C(T))$ method,” *Methods*, vol. 25, no. 4, pp. 402–408, 2001.
- [34] J. Cox and M. Mann, “MaxQuant enables high peptide identification rates, individualized p.p.b.-range mass accuracies and proteome-wide protein quantification,” *Nature Biotechnology*, vol. 26, no. 12, pp. 1367–1372, 2008.
- [35] J. Cox, M. Y. Hein, C. A. Luber, I. Paron, N. Nagaraj, and M. Mann, “Accurate proteome-wide label-free quantification by delayed normalization and maximal peptide ratio extraction, termed MaxLFQ,” *Molecular and Cellular Proteomics*, vol. 13, no. 9, pp. 2513–2526, 2014.
- [36] W. Sperl, D. Skladal, E. Gnaiger et al., “High resolution respirometry of permeabilized skeletal muscle fibers in the diagnosis of neuromuscular disorders,” in *Detection of Mitochondrial Diseases*, F. N. Gellerich and S. Zierz, Eds., vol. 21 of *Developments in Molecular and Cellular Biochemistry*, pp. 71–78, Springer, Boston, MA, USA, 1997.
- [37] T. Regueira, P. M. Lepper, S. Brandt et al., “Hypoxia inducible factor-1 alpha induction by tumour necrosis factor-alpha, but not by toll-like receptor agonists, modulates cellular respiration in cultured human hepatocytes,” *Liver International*, vol. 29, no. 10, pp. 1582–1592, 2009.
- [38] M. Roosimaa, T. Põdrämägi, L. Kadaja et al., “Dilation of human atria: increased diffusion restrictions for ADP, overexpression of hexokinase 2 and its coupling to oxidative phosphorylation in cardiomyocytes,” *Mitochondrion*, vol. 13, no. 5, pp. 399–409, 2013.
- [39] R. Pääsuke, M. Eimre, A. Piirsoo et al., “Proliferation of human primary myoblasts is associated with altered energy metabolism in dependence on ageing in vivo and in vitro,” *Oxidative Medicine and Cellular Longevity*, vol. 2016, Article ID 8296150, 10 pages, 2016.
- [40] R. Munday, “Generation of superoxide radical, hydrogen peroxide and hydroxyl radical during the autoxidation of N,N,N',N' -tetramethyl-p-phenylenediamine,” *Chemico-Biological Interactions*, vol. 65, no. 2, pp. 133–143, 1988.
- [41] H. Yamamoto, K. Schoonjans, and J. Auwerx, “Sirtuin functions in health and disease,” *Molecular Endocrinology*, vol. 21, no. 8, pp. 1745–1755, 2007.
- [42] R. B. Armstrong, P. D. Gollnick, and C. D. Ianuzzo, “Histochemical properties of skeletal muscle fibers in streptozotocin-diabetic rats,” *Cell and Tissue Research*, vol. 162, no. 3, pp. 387–394, 1975.
- [43] M. Cotter, N. E. Cameron, D. R. Lean, and S. Robertson, “Effects of long-term streptozotocin diabetes on the contractile and histochemical properties of rat muscles,” *Quarterly Journal of Experimental Physiology*, vol. 74, no. 1, pp. 65–74, 1989.
- [44] M. Medina-Sanchez, C. Rodriguez-Sanchez, J. A. Vega-Alvarez, A. Menedez-Pelaez, and A. Perez-Casas, “Proximal skeletal muscle alterations in streptozotocin-diabetic rats: a histochemical and morphometric analysis,” *American Journal of Anatomy*, vol. 191, no. 1, pp. 48–56, 1991.
- [45] K. M. Klueber and J. D. Feczko, “Ultrastructural, histochemical, and morphometric analysis of skeletal muscle in a murine model of type I diabetes,” *The Anatomical Record*, vol. 239, no. 1, pp. 18–34, 1994.
- [46] A. A. Aughsteen, A. M. Khair, and A. A. Suleiman, “Quantitative morphometric study of the skeletal muscles of normal and streptozotocin-diabetic rats,” *Journal of the Pancreas*, vol. 10, no. 4, pp. 382–389, 2006.
- [47] M. Ehrlich, M. Ivask, A. Raasmaja, and S. Köks, “Analysis of metabolic effects of menthol on WFS1-deficient mice,” *Physiological Reports*, vol. 4, no. 1, article e12660, 2016.
- [48] D. D. McKemy, W. M. Neuhauser, and D. Julius, “Identification of a cold receptor reveals a general role for TRP channels in thermosensation,” *Nature*, vol. 416, no. 6876, pp. 52–58, 2002.
- [49] A. M. Peier, A. Moqrich, A. C. Hergarden et al., “A TRP channel that senses cold stimuli and menthol,” *Cell*, vol. 108, no. 5, pp. 705–715, 2002.
- [50] R. V. Olsen, H. H. Andersen, H. G. Møller, P. W. Eskelund, and L. Arendt-Nielsen, “Somatosensory and vasomotor manifestations of individual and combined stimulation of TRPM8 and TRPA1 using topical L-menthol and trans-cinnamaldehyde in healthy volunteers,” *European Journal of Pain*, vol. 18, no. 9, pp. 1333–1342, 2014.
- [51] S. Ma, H. Yu, Z. Zhao et al., “Activation of the cold-sensing TRPM8 channel triggers UCP1-dependent thermogenesis and prevents obesity,” *Journal of Molecular Cell Biology*, vol. 4, no. 2, pp. 88–96, 2012.
- [52] X. Kong, R. Wang, Y. Xue et al., “Sirtuin 3, a new target of PGC-1 α , plays an important role in the suppression of ROS and mitochondrial biogenesis,” *PLoS One*, vol. 22, no. 5, article e11707, 2010.

- [53] A. Giralt, E. Hondares, J. A. Villena et al., "Peroxisome proliferator-activated receptor-gamma coactivator-1alpha controls transcription of the Sirt3 gene, an essential component of the thermogenic brown adipocyte phenotype," *Journal of Biological Chemistry*, vol. 286, no. 19, pp. 16958–16966, 2011.
- [54] A. Giralt and F. Villarroya, "SIRT3, a pivotal actor in mitochondrial functions: metabolism, cell death and aging," *Biochemical Journal*, vol. 444, no. 1, pp. 1–10, 2012.
- [55] M. Gertz and C. Steegborn, "Function and regulation of the mitochondrial sirtuin isoform Sirt5 in Mammalia," *Biochimica et Biophysica Acta*, vol. 1804, no. 8, pp. 1658–1665, 2010.
- [56] J. Du, Y. Zhou, X. Su et al., "Sirt5 is a NAD-dependent protein lysine demalonylase and desuccinylase," *Science*, vol. 334, no. 6057, pp. 806–809, 2011.
- [57] M. Zatyka, X. G. Da Silva, E. A. Bellomo et al., "Sarco(endo)-plasmic reticulum ATPase is a molecular partner of Wolfram syndrome 1 protein, which negatively regulates its expression," *Human Molecular Genetics*, vol. 24, no. 3, pp. 814–827, 2015.
- [58] C. W. Heizmann, M. W. Berchtold, and A. M. Rowleson, "Correlation of parvalbumin concentration with relaxation speed in mammalian muscles," *Proceedings of the National Academy of Sciences of the United States of America*, vol. 79, no. 23, pp. 7243–7247, 1982.
- [59] J. A. Vizcaíno, A. Csordas, N. del-Toro et al., "2016 update of the PRIDE database and its related tools," *Nucleic Acids Research*, vol. 44, no. D1, pp. D447–D456, 2016.
- [60] M. Eimre, S. Kasvandik, M. Ivask, and S. Kõks, "Proteomic dataset of wolframin-deficient mouse heart and skeletal muscles," *Data in Brief*, vol. 21, pp. 616–619, 2018, submitted.

Research Article

Reduced Levels of ATP Synthase Subunit ATP5F1A Correlate with Earlier-Onset Prostate Cancer

René G. Feichtinger ^{1,2}, Georg Schäfer,^{3,4} Christof Seifarth,^{3,4} Johannes A. Mayr ²,
Barbara Kofler ^{1,2} and Helmut Klocker³

¹Research Program for Receptor Biochemistry and Tumor Metabolism, Department of Pediatrics, University Hospital Salzburg, Paracelsus Medical University, 5020 Salzburg, Austria

²Department of Pediatrics, University Hospital Salzburg, Paracelsus Medical University, 5020 Salzburg, Austria

³Division of Experimental Urology, Department of Urology, Medical University of Innsbruck, 6020 Innsbruck, Austria

⁴Department of Pathology, Medical University of Innsbruck, 6020 Innsbruck, Austria

Correspondence should be addressed to Barbara Kofler; b.kofler@salk.at

Received 14 June 2018; Revised 21 September 2018; Accepted 30 September 2018; Published 14 November 2018

Guest Editor: Marcelo Mori

Copyright © 2018 René G. Feichtinger et al. This is an open access article distributed under the Creative Commons Attribution License, which permits unrestricted use, distribution, and reproduction in any medium, provided the original work is properly cited.

Switching of cellular energy production from oxidative phosphorylation (OXPHOS) to aerobic glycolysis occurs in many types of tumors. However, the significance of energy metabolism for the development of prostate carcinoma is poorly understood. We investigated the expression of OXPHOS complexes in 94 human prostate carcinomas and paired benign tissue using immunohistochemistry. Overall mitochondrial mass was upregulated in carcinomas compared to benign prostate tissue in all Gleason grades. A significant direct correlation between the expression of OXPHOS complexes I, II, and V and the Gleason score was observed. However, 17% of prostate carcinomas and 18% of benign prostate tissues showed isolated or combined deficiency of OXPHOS complexes (one deficiency in 12% of the tumors, combined deficiencies in 5%). Complex I was absent in 9% of the samples, with only parts of the tumor affected. ATP5F1A, a complex V protein, was the most frequently affected subunit, in 10% of tumors and 11% of benign prostate tissues (but not both tissues in any single patient). A possible role of complex V in prostate cancer development is suggested by the significant positive correlation of ATP5F1A levels with earlier-onset prostate cancer (age at diagnosis and at prostatectomy) and free PSA percentage. The relatively high percentage (17%) of prostate carcinomas with regional foci of partial OXPHOS complex deficiencies could have important therapeutic implications.

1. Introduction

Metabolism, especially energy metabolism, is a hot topic in tumor biology. Many tumor entities are characterized by deficiencies and reprogramming of mitochondrial energy metabolism. Sometimes, a single tumor entity can be divided into subgroups, where one group shows high levels of oxidative phosphorylation (OXPHOS) and the other is deficient in one or more OXPHOS complexes, as found in melanomas [1]. Some tumor entities are very homogeneous in their OXPHOS signature; for example, neuroblastomas and renal cell carcinomas both show significant reductions of all OXPHOS complexes. In contrast, many other carcinomas (e.g., gastric carcinomas and colorectal carcinomas) show

a relatively constant number of OXPHOS defects [1–13]. Although the mode of downregulation of OXPHOS can vary (loss of mitochondria, loss of all complexes, isolated and combined deficiencies), nearly all tumors have one feature in common—disruption of respiratory chain complex I [1–13].

Mitochondrial complex I is clearly at the center of the OXPHOS deficiency landscape in cancer, and there are several explanations for this. Subunits of complex I, namely, NDUFS3 and NDUFS1, can be cleaved by granzyme A or granzyme B and caspase 3 to induce apoptosis [14, 15]. A lack of complex I might help shield tumor cells from apoptosis. Secondly, complex I is the most elaborate mitochondrial multisubunit protein, potentially making it more prone to damage [16]. Statistically, the large number of subunits might

also explain the higher incidence of genetic hits affecting complex I. It is also reported that complex I is the main production site of reactive oxygen species (ROS) within the respiratory chain [17]. Since ROS immediately react with biomolecules, complex I might be the first target of its own generated ROS. ROS also attack mtDNA, including the 7 mitochondrially encoded complex I subunits [18].

Combined OXPHOS deficiencies are the most frequent alteration with regard to tumors and patients with mitochondrial disease [19]. Fifty-seven percent of all patients diagnosed in our center with a mitochondrial disease show a combined reduction of OXPHOS complexes [19]. Combined OXPHOS deficiencies can arise from mitochondrial tRNA mutations, mtDNA deletions, and mtDNA depletion [19]. Since respiratory chain complexes are further organized into super/megacomplexes, mutations in complex III subunits typically also lead to secondary loss of complex I [20]. Furthermore, mutations in a number of genes involved in mitochondrial biogenesis, architecture, or protein transport can cause combined defects [19]. In total, mutations in more than 250 genes cause mitochondrial disorders [19]. Interestingly, unlike mutations in respiratory chain subunits, mutations affecting other mitochondrial proteins are generally not associated with tumors (exceptions include IDH2/isocitrate dehydrogenase 2, FH/fumarate dehydrogenase, and DGUOK/deoxyguanosine kinase) [21–23].

Prostate cancer is the most frequently diagnosed cancer in males in developed countries and responsible for more than 300,000 annual cancer deaths worldwide [24]. Mitochondrial DNA alterations are frequent in prostate cancer and have been correlated to pathological features, tumor progression, and worse outcomes [25–27]. The aim of the present study was to characterize the metabolic phenotype of prostate carcinomas and corresponding benign prostate tissue by immunohistochemical (IHC) staining of mitochondria and individual mitochondrial complexes. Previously, we demonstrated that semiquantitative IHC of homogeneous tissue samples correlates well with functional analysis, as the OXPHOS system is mainly regulated via protein amount [2, 3, 5–8, 13, 28]. Therefore, IHC of heterogeneous samples is the method of choice as it accurately reflects the *in vivo* situation at the cellular level and can detect small areas of OXPHOS deficiency in tumor samples.

2. Material and Methods

2.1. Ethics. Human tumors were obtained from the Institute of Pathology, Medical University Innsbruck. The study was performed according to the Austrian Gene Technology Act. Experiments were conducted in accordance with the Helsinki Declaration of 1975 (revised 2013) and the guidelines of the local ethics committee, being no clinical drug trial or epidemiological investigation. All patients signed an informed consent document concerning the surgical intervention. Furthermore, the study did not extend to the examination of individual case records. Patient anonymity was ensured at all times. The use of the archived tissue samples was approved by the ethics committee of the Medical University Innsbruck (AN 3174, AN 4837).

2.2. Samples. To evaluate differences in expression between malignant and benign prostate tissues, we constructed a tissue microarray (TMA) of formalin-fixed, paraffin-embedded tissue blocks from 94 previously untreated prostate cancer patients who had undergone radical prostatectomy after tumor diagnosis in a PSA screening program performed in Tyrol by the Department of Urology, Medical University Innsbruck [29]. The TMA was assembled using a manual tissue arrayer (Beecher Instruments, Sun Prairie, WI). Four punches of each case, 3 from the tumor and 1 from a benign area, were evaluated. In many cases, tissue cores contained tumor as well as benign regions.

2.3. AMACR/p63 Staining. Hematoxylin and eosin staining, basal cell marker p63 and tumor cell marker alpha-methylacyl-CoA racemase (AMACR) immunohistochemistry (IHC) double stains were used to confirm the histological diagnosis. IHC was performed on a Discovery-XT-automated staining device (Ventana, Tucson, AZ) using instrument standard protocols. Antibodies, suppliers, catalog numbers, and concentrations used were as follows: anti-p63, Sigma-Aldrich, #P3362, 1:200; anti-AMACR, Dako (Vienna, Austria), #M3616, 1:200. DAB (3,3'-diaminobenzidine; brown) was used for visualization of AMACR and nitroblue tetrazolium chloride (blue) for staining of p63.

2.4. Immunohistochemical Staining of OXPHOS Complex Subunits and Porin of FFPE Tissues. For IHC, the following antibodies were used: complex I subunit NDUFS4 (mouse monoclonal, 1:1000; Abcam, Cambridge, UK), complex II subunit SDHA (mouse monoclonal, 1:2000; MitoSciences, Eugene, Oregon), complex III subunit UQCRC2 (mouse monoclonal, 1:1500; MitoSciences), complex IV subunit MT-COI (mouse monoclonal, 1:1000; MitoSciences), complex V subunit ATP5F1A (mouse monoclonal, 1:2000; MitoSciences), and VDAC1 (mouse monoclonal, 1:3000; MitoSciences). All antibodies were diluted in Dako antibody diluent with background-reducing components (Dako, Glostrup, Denmark). IHC was performed as described previously [13]. For antigen retrieval, the sections were immersed for 45 min in 1 mM EDTA, 0.05% Tween-20, pH 8, at 95°C. Tissue sections were incubated for 30 min with the above-mentioned primary antibodies. The staining intensities of the tumor and control tissues were determined by two examiners using a stereomicroscope. Staining intensities were rated using a scoring system ranging from 0 to 4, with 0 indicating no staining, 1 mild, 2 moderate, 3 strong, and 4 very strong staining. Four punches of each tissue sample were analyzed, and for each punch, the lowest and highest intensities were scored. Staining intensities of each tissue punch, mean staining intensities of each sample, and clinical data are given in Supplementary Tables 1A and 1B. For statistical analysis (*t*-test, ANOVA, and correlations), the mean of the staining intensities of the four punches was used. For the frequency distribution, the lowest staining intensity of each sample was analyzed. The specificity of the antibodies used was previously shown in numerous articles by Western blot analysis: ([6]; Figure 3), ([5], Figure 2); NDUFS4 ([6]; Figure 3), ([5], Figure 2); SDHA ([6]; Figure 3),

([5], Figure 2); UQCRC2 ([6]; Figure 3), ([5], Figure 2); MT-CO1 ([30], Figure 2); ATP5F1A ([6]; Figure 3), ([31]; Figure 3). The punches were also stained with AMACR/p63 to distinguish between tumor and benign prostate tissue. All antibodies are suitable for the detection of assembly defects. If these subunits are missing, the respective complexes are not assembled and, therefore, no function is present. The antibodies were used to detect numerous defects caused by pathogenic mutations. The activity of the OXPHOS enzymes was determined in previous studies, underlining that the amount of protein and the level of activity are highly correlated and showing that loss of the subunits causes loss of activity [2, 3, 5, 7, 20, 28, 31, 32].

2.5. Statistical Analysis. For the comparison of tumors and benign prostate tissue, a *t*-test was applied. For multiple comparisons of tumors with different Gleason scores, one-way ANOVA and Bonferroni's correction were applied. Pearson's correlation was applied to analyze potential associations between the Gleason score and OXPHOS complex expression. In addition, the frequency distribution of the staining intensities was calculated.

3. Results

3.1. Increased Mitochondrial Biogenesis and Consistent Upregulation of OXPHOS Complexes in Carcinomas Compared to Adjacent Benign Prostate Tissue. To elucidate if prostate carcinomas and adjacent benign prostate tissue differ in terms of protein expression of the OXPHOS complexes and mitochondrial biogenesis, we immunohistochemically stained prostate carcinomas ($n=94$) and corresponding benign prostate tissue ($n=89$). The benign and cancerous tissues were distinguished by AMCR/p63 staining: the carcinoma stained brown and the epithelium of benign glands stained dark blue (Figure 1). We also stained for VDAC1, a protein of the outer mitochondrial membrane, as an indicator of mitochondrial mass and therefore mitochondrial biogenesis. Overall, we detected a significantly higher expression level of VDAC1 ($p=0.0009$) in carcinomas compared to adjacent benign prostate tissue ($n=62$) (Figure 2(a)), although the latter showed a significantly higher proportion of samples with "very strong staining" (score = 4) (24% of benign tissue vs. 6% of tumor tissue). In accordance, the staining levels of NDUFS4 ($p=0.01$), SDHA ($p<0.0001$), UQCRC2 ($p<0.05$), MT-CO1 ($p<0.05$), and ATP5F1A ($p<0.0001$) were all significantly higher in the prostate carcinomas compared to their benign counterparts (Figures 2(b)–2(f)). Since altogether the OXPHOS complexes and VDAC1 are increased in carcinomas, we conclude that mitochondrial mass is higher in carcinomas than in benign prostate tissue.

3.2. Comparison of Prostate Carcinomas and Adjacent Benign Prostate Tissue with respect to Tumor Malignancy. To test if the altered expression of subunits of the OXPHOS complexes is associated with malignancy of prostate carcinomas, we compared IHC immunoreactivities among the different pathological Gleason score (GS) grades. We found no clear-

cut association of complex marker expression with GS grade, except in the case of GS 7 tumors, which showed increased expression of all mitochondrial complex markers. Nonetheless, in agreement with the generalized increase in mitochondrial mass observed in prostate carcinomas, we detected overall trends to higher expression in all GS grades (Supplementary Table 2). The mean staining intensities over all tissue punches from each tumor case revealed no differences between prostate carcinomas of different GS grades for VDAC1, SDHA, MT-CO1, and ATP5F1A (Supplementary Figure 1). For NDUFS4, both GS 7 and 9 carcinomas showed significantly higher expression than GS 6 and 8 tumors (Supplementary Figure 1). A correlation analysis revealed increased expression with Gleason scores for NDUFS4 ($p<0.05$; $R=0.22$), SDHA ($p<0.05$; $R=0.25$), and ATP5F1A ($p<0.05$; $R=0.22$).

3.3. Frequency of OXPHOS Deficiencies. The overall analysis of staining intensities often masks important results when only the averages are used for calculation and variations within the analyzed tissue specimen are ignored. Tumors, especially prostate tumors, are heterogeneous, and alterations of protein expression in small areas of the tissue, indicating regional loss of expression, need to be considered separately. We analyzed expression heterogeneity in more detail in the four cores of each case to uncover regional OXPHOS deficiencies. The lowest staining intensity for each tumor or benign prostate tissue was identified, and the frequency distribution was evaluated to elucidate the percentage of specimens exhibiting OXPHOS deficiency (staining intensity = 0).

The tumors of 16 patients (17%) showed deficiencies of respiratory chain complexes. Eleven tumors showed deficiencies in one complex only, three tumors exhibited deficiencies in two complexes, and two tumors exhibited losses of three and four complexes, respectively. The frequency of partial mitochondrial complex loss in benign tissue was 18%, similar to that in tumors. Deficiency of complex I was present in 9% of carcinomas compared to 2% of benign prostate tissue samples (Figure 3, Supplementary Figures 2 and 3). Deficiency of SDHA (2% vs. 7%) and ATP5F1A (10% vs. 11%) (Figure 3) was more frequent in benign prostate tissue (Figure 4). ATP5F1A deficiency was never observed in both carcinoma and adjacent benign prostate tissue. UQCRC2 was lost in 2% of the tumors and in 1% of the benign prostate tissue, whereas MT-CO1 loss was observed only in carcinomas (4%). There was no clear association of complex loss with the tumor Gleason score (Supplementary Figure 2).

3.4. Correlation of Clinical Parameters and the Expression of OXPHOS Complexes. We analyzed the correlation of the expression of OXPHOS complexes and porin with age at prostatectomy, pathological tumor stage, serum PSA level, free to total PSA ratio, prostate size at radical prostatectomy, and time until biochemical tumor recurrence (PSA progression). A significant positive correlation was present between complex V expression and patient age at diagnosis ($p=0.0314$; $R=0.2297$) and at prostatectomy ($p=0.0206$;

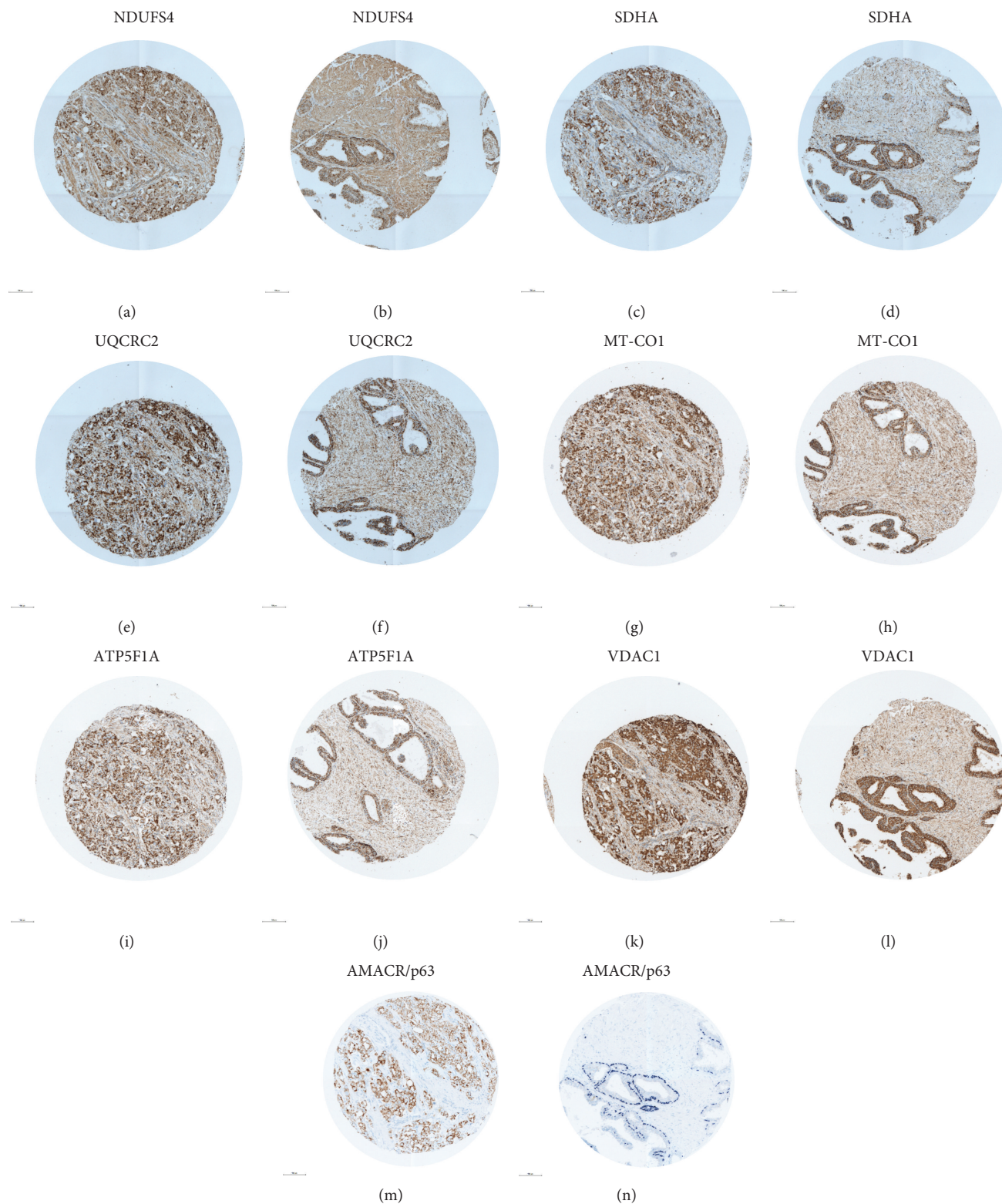


FIGURE 1: Staining of OXPHOS complexes, VDAC1, and AMACR/p63 in a prostate carcinoma of Gleason score 9 and adjacent benign prostate tissue. (a, b) NDUFS4; (c, d) SDHA; (e, f) UQCRC2; (g, h) MT-CO1; (i, j) ATP5F1A; (k, l) VDAC1; and (m, n) AMACR/p63. (a, c, e, g, i, k, m) carcinoma and (b, d, f, h, j, l, n) hyperplasia. The punches are 0.6 mm in diameter. AMACR/p63 staining was used to visualize carcinoma cells (brown) and benign prostate tissue (blue).

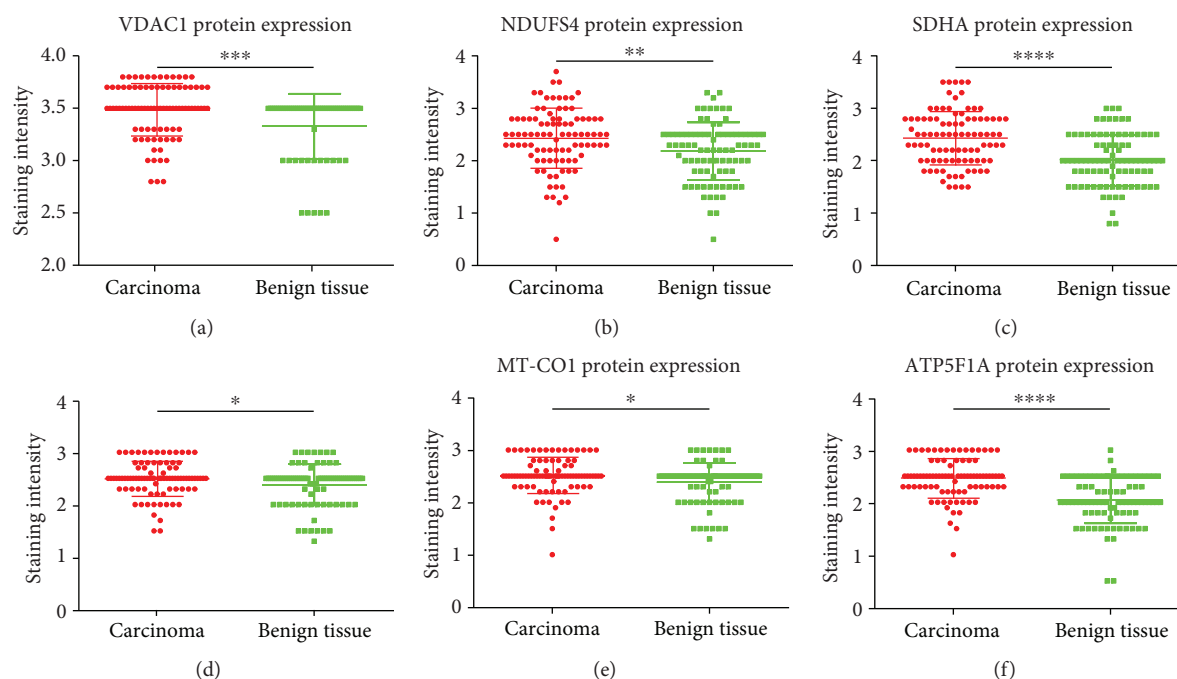


FIGURE 2: OXPPOS complex expression in prostate carcinomas and corresponding benign prostate tissue. (a) VDAC1, (b) NDUF54, (c) SDHA, (d) UQCRC2, (e) MT-CO1, and (f) ATP5F1A. The intensities of the stainings are given as the median \pm SD. **** $p < 0.0001$, *** $p < 0.001$, ** $p < 0.01$, and * $p < 0.05$.

$R = 0.2465$) (Figures 5(a) and 5(b)). Furthermore, complex V expression was significantly higher in individuals with high free to total PSA ratios ($p = 0.0425$; $R = 0.218$) (Figure 5(c)), whereas a negative correlation between prostate volume at prostatectomy and complex IV was found ($p = 0.0373$; $R = -0.225$) (Figure 5(d)).

No differences of OXPPOS complex levels in tumors were observed with respect to pathological stage, TNM (T: size or direct extent of the primary tumor; N: degree of spread to regional lymph nodes; and M: presence of distant metastasis) or biochemical tumor recurrence.

4. Discussion

Analysis of mitochondrial mass and individual mitochondrial OXPPOS complexes using surrogate protein markers detected by IHC revealed an increased mitochondrial mass in prostate carcinomas in comparison to their benign tissue counterparts. VDAC1 was used as a marker for the mitochondrial mass. It was previously shown that it correlates excellently with citrate synthase activity, which is also used as a marker for the mitochondrial amount in functional studies [2, 3, 5, 7, 20, 28]. mtDNA is not a reliable marker for mitochondrial mass since many solid tumor entities have a high or normal mitochondrial mass but a reduced mtDNA copy number [5, 7]. Also, patients with mitochondrial diseases affecting muscle argue against this (TK2, SUCLA2, SUCLG1, RRM2B, DGUOK, and TYMP) [32, 33]. Patients with an mtDNA depletion disorder show a normal mitochondrial amount but a reduction of one or more OXPPOS complexes (e.g., DGUOK) [32, 33].

In addition, our analysis identified a subgroup of about one-sixth of the analyzed prostate carcinoma specimens harboring areas of isolated or combined loss of OXPPOS complexes.

The most frequent alterations of the OXPPOS system in our cohort were the loss of complex I and complex V. The absence of complex I protein and potentially pathogenic mutations of mitochondrial complex I genes have been consistently reported for numerous tumor entities [1, 4–6, 10, 12, 13, 28, 33]. A very recent study sequenced mtDNA in 384 prostate carcinoma patients and identified 129 nonsynonymous mitochondrial single-nucleotide variants in protein-coding regions, including six premature stop codons and two mutated stop codons [25]. The most frequently affected protein-coding gene was MT-ND5 (30 out of 157 mitochondrial synonymous and nonsynonymous single nucleotide variants). In addition, 8 mutations in the anticodon stem of mitochondrial tRNA genes were present. As a consequence, combined OXPPOS complex deficiencies would be expected, as observed in 5 cases in our study. According to a recent review, 749 mtDNA mutations have been described for prostate cancer [34]. Only 80 of these were found in two or more patients, 15 of which are potentially pathogenic according to commonly used prediction tools [34]. We are not aware of any previous study correlating nuclear OXPPOS subunit gene alterations to the frequency of OXPPOS deficiency in prostate carcinomas.

In line with many other studies, the loss of complex I was the most frequent event in our cohort of primary prostate tumors. An explanation might be that complex I deficiency confers a selective advantage on tumor cells since

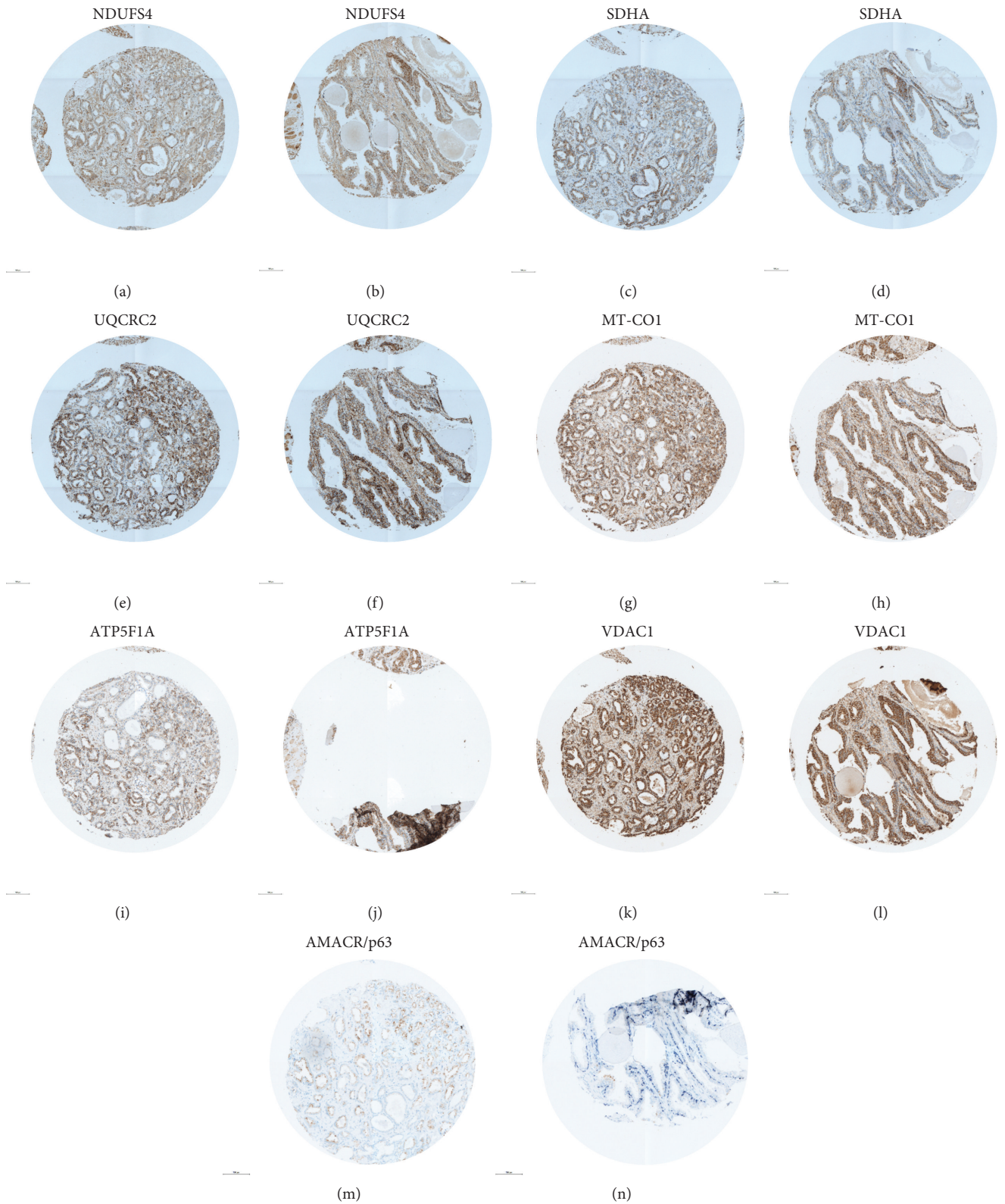


FIGURE 3: Staining of OXPHOS complexes, VDAC1, and AMACR/p63 in a prostate carcinoma with partial loss of ATP5F1A and adjacent benign prostate tissue. (a, b) NDUFS4; (c, d) SDHA; (e, f) UQCRC2; (g, h) MT-CO1; (i, j) ATP5F1A; (k, l) VDAC1; and (m, n) AMACR/p63. (a, c, e, g, i, k, m) carcinoma and (b, d, f, h, j, l, n) benign prostate tissue. The punches are 0.6 mm in diameter. AMACR/p63 staining was used to visualize carcinoma cells (brown) and benign prostate tissue (blue).

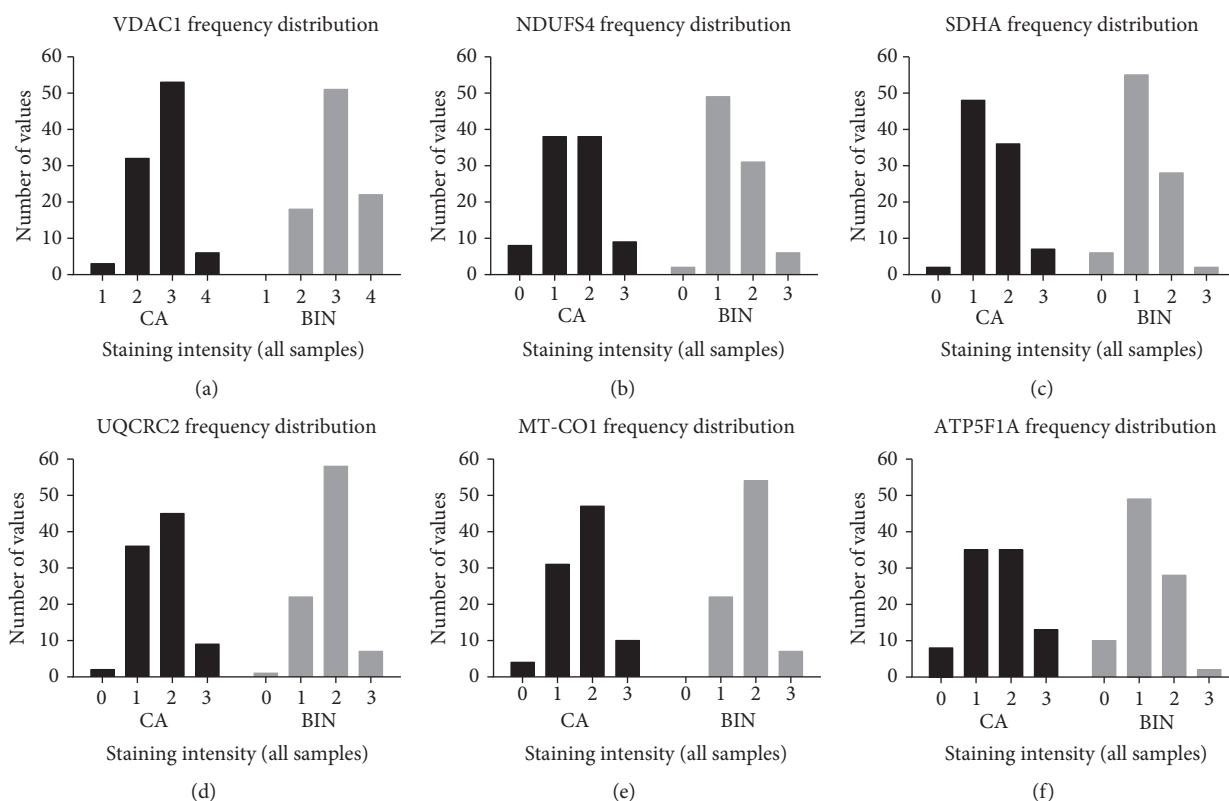


FIGURE 4: Frequency distribution of the lowest staining intensities found in prostate carcinoma and corresponding benign prostate tissue punches. (a) VDAC1, (b) NDUFS4, (c) SDHA, (d) UQCRC2, (e) MT-CO1, and (f) ATP5F1A. The frequencies are given in percent. The staining intensities are as follows: 0 = no staining, 1 = weak staining, 2 = moderate staining, 3 = strong staining, and 4 = very strong staining. CA, prostate carcinoma; BIN, benign prostate tissue.

it is part of an important apoptosis pathway. The NDUFS1 subunit of complex I can be cleaved by caspase 3 to induce apoptosis [15].

Interestingly, ATP synthase (complex V) staining was decreased in a substantial number of prostate carcinomas (10%) and benign prostate tissues (11%). We have previously shown that the loss of complex V is a rare event in different solid tumors [1, 4–6, 10, 12, 13, 28, 33]. In contrast to these tumor entities, a significant percentage of prostate tumors is characterized by this relatively rare bioenergetic phenotype. Overall, the level of complex V subunit ATP5F1A was increased in our prostate cancer cohort. Up- or downregulation of specific subunits of ATP synthase was reported depending on the tumor entity [35–40]. Increased levels of ATP synthase subunits α and d were present in 76–79% of colorectal carcinomas [41]. ATP synthase d was significantly overexpressed in 93 lung adenocarcinomas [39]. We also found that complex V and complex II usually correlate with mitochondrial mass, as indicated by VDAC1 and citrate synthase activity [4, 5, 12, 13, 28, 42].

To our knowledge, this is the first report of the total lack of complex V in a subset of prostate tumors. Interestingly, complex V defects are very rare among patients with mitochondrial diseases compared to defects of the other four complexes of the OXPHOS system. Mutations in patients have been reported only for the mitochondrial genes MT-ATP6 and MT-ATP8 and the nuclear genes ATP5F1A

and ATP5E [43–45]. In this context, the ATP synthase inhibitory factor 1 (IF₁) is of interest because it is upregulated in many human carcinomas and implicated in the control of mitochondrial bioenergetics and structure by regulating the activity and oligomerization of ATP synthase [46–48]. IF₁ suppresses programmed cell death, thereby enhancing tumor invasion and chemoresistance. Indeed, a possible role of complex V in prostate cancer development is also suggested by the significant positive correlation we detected between ATP5F1A level and age at diagnosis/prostatectomy as well as ATP5F1A level and percentage of free PSA in relationship to total PSA.

One of every six men will be diagnosed with prostate carcinoma during his lifetime (<https://www.cancer.org/cancer/prostate-cancer/about/key-statistics.html>), and prostate cancer accounts for 8% of all new cancer cases. Therefore, the finding that a high percentage of prostate carcinomas and the corresponding benign prostate tissues show OXPHOS deficiency warrants consideration in therapeutic strategies.

5. Conclusions

Based on our own studies, we estimate that at least 10% of all tumor cases show low levels of OXPHOS similar to those we detected in prostate carcinomas. Since most diagnosed tumors are carcinomas, this is a very conservative estimate. Therefore, the therapeutic implications of OXPHOS

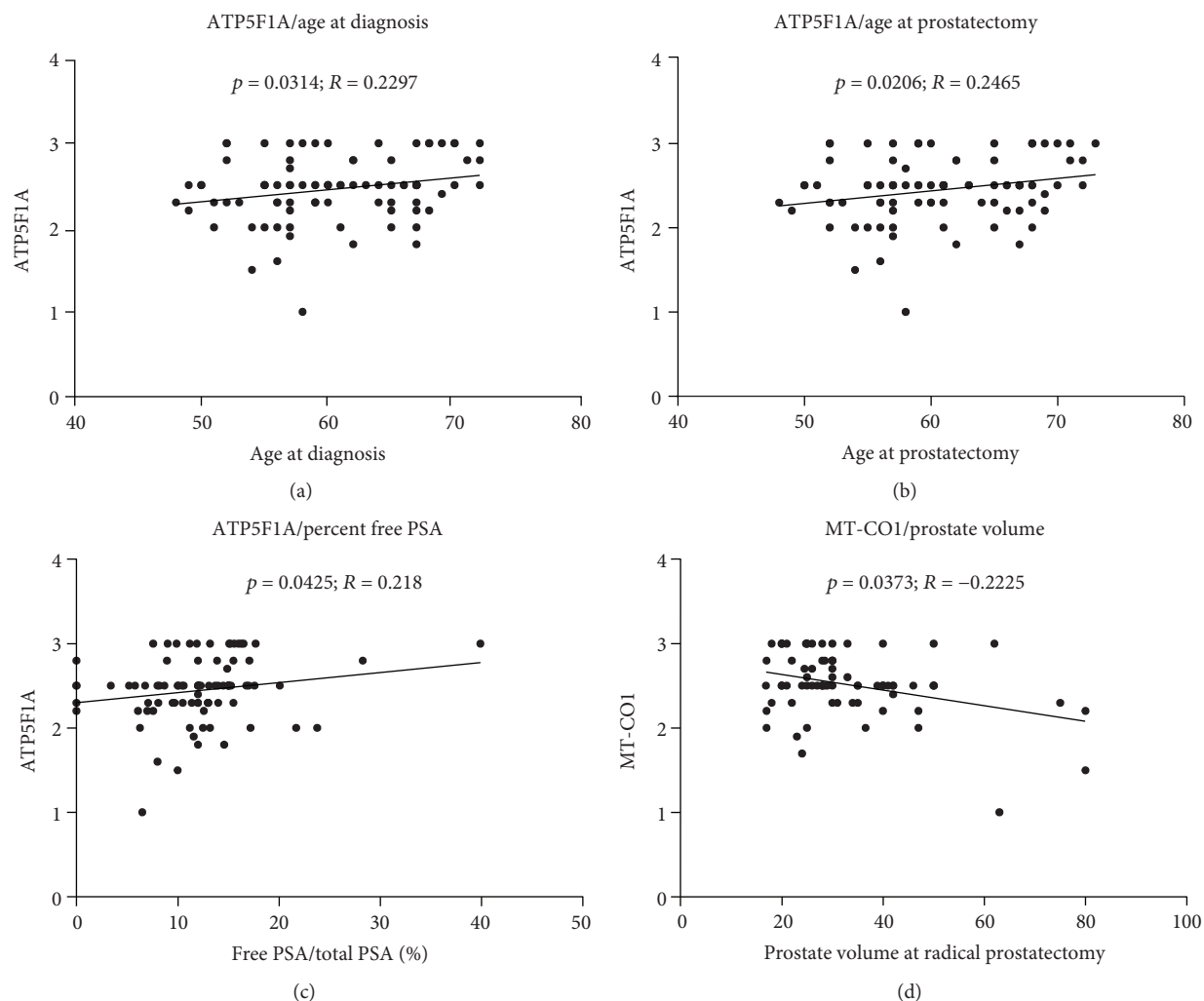


FIGURE 5: Correlation between clinical parameters and the levels of OXPHOS complexes. Correlation between ATP5F1A level and age at diagnosis (a), age at prostatectomy (b), and percent free PSA in relationship to total PSA (c). (d) Correlation between MT-CO1 levels and prostate volume at prostatectomy.

deficiencies are potentially enormous because these tumors should be prone to metabolic therapies used to selectively kill tumor cells.

Data Availability

The data used to support the findings of this study are included in the article.

Conflicts of Interest

The authors declare no competing interest.

Authors' Contributions

René G. Feichtinger and Georg Schäfer contributed equally to the work.

Acknowledgments

This research was supported by grants from the “Vereinigung zur Förderung der pädiatrischen Forschung und Fortbildung Salzburg” and the Austrian Research Promotion Agency (822782/THERAPEP).

Supplementary Materials

Supplementary Figure 1: OXPHOS complex expression in prostate carcinomas of different Gleason scores. (a) VDAC1, (b) NDUFS4, (c) SDHA, (d) UQCRC2, (e) MT-CO1, and (f) ATP5F1A. The intensities of the stainings are given as the median \pm SD. $**p < 0.01$ and $*p < 0.05$. Supplementary Figure 2: frequency distribution of the lowest staining intensities found in prostate carcinoma tissue punches of different Gleason scores. (a) VDAC1, (b) NDUFS4, (c) SDHA, (d) UQCRC2, (e) MT-CO1, and (f) ATP5F1A. The frequencies are given as percentages. The staining intensities are as follows: 0 = no staining, 1 = weak staining,

2 = moderate staining, 3 = strong staining, and 4 = very strong staining. Supplementary Figure 3: staining of OXPHOS complexes, VDAC1, and AMACR/p63 in a prostate carcinoma of Gleason score 7 and adjacent benign prostate tissue. (a, b) NDUFS4; (c, d) SDHA; (e, f) UQCRC2; (g, h) MT-CO1; (i, j) ATP5F1A; (k, l) VDAC1; and (m, n) AMACR/p63. (a, c, e, g, i, k) carcinoma and (b, d, f, h, j, l, n) benign prostate tissue. The punches are 0.6 mm in diameter. AMACR/p63 staining was used to visualize carcinoma cells (brown) and benign prostate tissue (blue). Supplementary Table 1: staining intensities of each tissue punch and mean staining intensities with clinical data. Supplementary Table 2: comparison of the expression levels of OXPHOS subunits and VDAC1 in benign prostate tissue and carcinomas of different Gleason scores. (*Supplementary Materials*)

References

- [1] R. G. Feichtinger, R. Lang, R. Geilberger et al., "Melanoma tumors exhibit a variable but distinct metabolic signature," *Experimental Dermatology*, vol. 27, no. 2, pp. 204–207, 2018.
- [2] R. G. Feichtinger, D. Neureiter, J. A. Mayr et al., "Loss of mitochondria in ganglioneuromas," *Frontiers in Bioscience*, vol. 3, pp. 179–186, 2011.
- [3] R. G. Feichtinger, D. Neureiter, B. Royer-Pokora et al., "Heterogeneity of mitochondrial energy metabolism in classical triphasic Wilms' tumor," *Frontiers in Bioscience*, vol. 3, pp. 187–193, 2011.
- [4] R. G. Feichtinger, D. Neureiter, T. Skaria et al., "Oxidative phosphorylation system in gastric carcinomas and gastritis," *Oxidative Medicine and Cellular Longevity*, vol. 2017, Article ID 1320241, 14 pages, 2017.
- [5] R. G. Feichtinger, S. Weis, J. A. Mayr et al., "Alterations of oxidative phosphorylation complexes in astrocytomas," *Glia*, vol. 62, no. 4, pp. 514–525, 2014.
- [6] R. G. Feichtinger, S. Weis, J. A. Mayr et al., "Alterations of oxidative phosphorylation in meningiomas and peripheral nerve sheath tumors," *Neuro-Oncology*, vol. 18, no. 2, pp. 184–194, 2016.
- [7] R. G. Feichtinger, F. Zimmermann, J. A. Mayr et al., "Low aerobic mitochondrial energy metabolism in poorly- or undifferentiated neuroblastoma," *BMC Cancer*, vol. 10, no. 1, p. 149, 2010.
- [8] R. G. Feichtinger, F. A. Zimmermann, J. A. Mayr et al., "Alterations of respiratory chain complexes in sporadic pheochromocytoma," *Frontiers in Bioscience*, vol. 3, pp. 194–200, 2011.
- [9] W. Habano, T. Sugai, S.-I. Nakamura, N. Uesugi, T. Yoshida, and S. Sasou, "Microsatellite instability and mutation of mitochondrial and nuclear DNA in gastric carcinoma," *Gastroenterology*, vol. 118, no. 5, pp. 835–841, 2000.
- [10] K. Polyak, Y. Li, H. Zhu et al., "Somatic mutations of the mitochondrial genome in human colorectal tumours," *Nature Genetics*, vol. 20, no. 3, pp. 291–3, 1998.
- [11] D. J. Tan, R. K. Bai, and L. J. Wong, "Comprehensive scanning of somatic mitochondrial DNA mutations in breast cancer," *Cancer Research*, vol. 62, no. 4, pp. 972–976, 2002.
- [12] F. A. Zimmermann, J. A. Mayr, R. Feichtinger et al., "Respiratory chain complex I is a mitochondrial tumor suppressor of oncogenic tumors," *Frontiers in Bioscience*, vol. 3, pp. 315–325, 2011.
- [13] F. A. Zimmermann, J. A. Mayr, D. Neureiter et al., "Lack of complex I is associated with oncogenic thyroid tumours," *British Journal of Cancer*, vol. 100, no. 9, pp. 1434–1437, 2009.
- [14] D. Martinvalet, D. M. Dykxhoorn, R. Ferrini, and J. Lieberman, "Granzyme A cleaves a mitochondrial complex I protein to initiate caspase-independent cell death," *Cell*, vol. 133, no. 4, pp. 681–692, 2008.
- [15] J. E. Ricci, C. Muñoz-Pinedo, P. Fitzgerald et al., "Disruption of mitochondrial function during apoptosis is mediated by caspase cleavage of the p75 subunit of complex I of the electron transport chain," *Cell*, vol. 117, no. 6, pp. 773–786, 2004.
- [16] K. Fiedorczuk, J. A. Letts, G. Degliesposti, K. Kaszuba, M. Skehel, and L. A. Sazanov, "Atomic structure of the entire mammalian mitochondrial complex I," *Nature*, vol. 538, no. 7625, pp. 406–410, 2016.
- [17] D. B. Zorov, M. Juhaszova, and S. J. Sollott, "Mitochondrial reactive oxygen species (ROS) and ROS-induced ROS release," *Physiological Reviews*, vol. 94, no. 3, pp. 909–950, 2014.
- [18] Y. H. Wei, "Oxidative stress and mitochondrial DNA mutations in human aging," *Proceedings of the Society for Experimental Biology and Medicine*, vol. 217, no. 1, pp. 53–63, 1998.
- [19] J. A. Mayr, T. B. Haack, P. Freisinger et al., "Spectrum of combined respiratory chain defects," *Journal of Inherited Metabolic Disease*, vol. 38, no. 4, pp. 629–640, 2015.
- [20] R. G. Feichtinger, M. Brunner-Krainz, B. Alhaddad et al., "Combined respiratory chain deficiency and UQCRC2 mutations in neonatal encephalomyopathy: defective supercomplex assembly in complex III deficiencies," *Oxidative Medicine and Cellular Longevity*, vol. 2017, Article ID 7202589, 11 pages, 2017.
- [21] P. Freisinger, N. Fütterer, E. Lankes et al., "Hepatocerebral mitochondrial DNA depletion syndrome caused by deoxyguanosine kinase (DGUOK) mutations," *Archives of Neurology*, vol. 63, no. 8, pp. 1129–1134, 2006.
- [22] E. Gilhooley, C. Fahy, E. Hanrahan, M. Keane, N. Swan, and A. Lally, "Multiple cutaneous and uterine leiomyomata with features of benign metastasizing leiomyomatosis: a novel mutation of the fumarate hydratase gene," *Clinical and Experimental Dermatology*, vol. 43, no. 3, pp. 334–335, 2018.
- [23] S. Nassereddine, C. J. Lap, F. Haroun, and I. Tabbara, "The role of mutant IDH1 and IDH2 inhibitors in the treatment of acute myeloid leukemia," *Annals of Hematology*, vol. 96, no. 12, pp. 1983–1991, 2017.
- [24] L. A. Torre, F. Bray, R. L. Siegel, J. Ferlay, J. Lortet-Tieulent, and A. Jemal, "Global cancer statistics, 2012," *CA: a Cancer Journal for Clinicians*, vol. 65, no. 2, pp. 87–108, 2015.
- [25] J. F. Hopkins, V. Y. Sabelnykova, J. Weischenfeldt et al., "Mitochondrial mutations drive prostate cancer aggression," *Nature Communications*, vol. 8, no. 1, p. 656, 2017.
- [26] A. M. F. Kalsbeek, E. F. K. Chan, J. Grogan et al., "Mutational load of the mitochondrial genome predicts pathological features and biochemical recurrence in prostate cancer," *Aging*, vol. 8, no. 11, pp. 2702–2712, 2016.
- [27] A. Kloss-Brandstätter, G. Schäfer, G. Erhart et al., "Somatic mutations throughout the entire mitochondrial genome are associated with elevated PSA levels in prostate cancer patients," *American Journal of Human Genetics*, vol. 87, no. 6, pp. 802–812, 2010.
- [28] J. A. Mayr, D. Meierhofer, F. Zimmermann et al., "Loss of complex I due to mitochondrial DNA mutations in renal oncocytoma," *Clinical Cancer Research*, vol. 14, no. 8, pp. 2270–2275, 2008.

- [29] G. Bartsch, W. Horninger, H. Klocker et al., "Tyrol prostate cancer demonstration project: early detection, treatment, outcome, incidence and mortality," *BJU International*, vol. 101, no. 7, pp. 809–816, 2008.
- [30] M. S. Reuter, J. O. Sass, T. Leis et al., "HIBCH deficiency in a patient with phenotypic characteristics of mitochondrial disorders," *American Journal of Medical Genetics. Part A*, vol. 164A, no. 12, pp. 3162–3169, 2014.
- [31] J. Koch, P. Freisinger, R. G. Feichtinger et al., "Mutations in *TTC19*: expanding the molecular, clinical and biochemical phenotype," *Orphanet Journal of Rare Diseases*, vol. 10, no. 1, p. 40, 2015.
- [32] C. L. Alston, A. G. Compton, L. E. Formosa et al., "Biallelic mutations in *TMEM126B* cause severe complex I deficiency with a variable clinical phenotype," *American Journal of Human Genetics*, vol. 99, no. 1, pp. 217–227, 2016.
- [33] W. Habano, S. Nakamura, and T. Sugai, "Microsatellite instability in the mitochondrial DNA of colorectal carcinomas: evidence for mismatch repair systems in mitochondrial genome," *Oncogene*, vol. 17, no. 15, pp. 1931–1937, 1998.
- [34] A. M. F. Kalsbeek, E. K. F. Chan, N. M. Corcoran, C. M. Hovens, and V. M. Hayes, "Mitochondrial genome variation and prostate cancer: a review of the mutational landscape and application to clinical management," *Oncotarget*, vol. 8, no. 41, pp. 71342–71357, 2017.
- [35] J. M. Cuezva, G. Chen, A. M. Alonso et al., "The bioenergetic signature of lung adenocarcinomas is a molecular marker of cancer diagnosis and prognosis," *Carcinogenesis*, vol. 25, no. 7, pp. 1157–1163, 2004.
- [36] J. M. Cuezva, M. Krajewska, M. L. de Heredia et al., "The bioenergetic signature of cancer: a marker of tumor progression," *Cancer Research*, vol. 62, no. 22, pp. 6674–6681, 2002.
- [37] A. Isidoro, E. Casado, A. Redondo et al., "Breast carcinomas fulfill the Warburg hypothesis and provide metabolic markers of cancer prognosis," *Carcinogenesis*, vol. 26, no. 12, pp. 2095–2104, 2005.
- [38] A. Isidoro, M. Martínez, P. L. Fernández et al., "Alteration of the bioenergetic phenotype of mitochondria is a hallmark of breast, gastric, lung and oesophageal cancer," *The Biochemical Journal*, vol. 378, no. 1, pp. 17–20, 2004.
- [39] G. Chen, T. G. Gharib, C. C. Huang et al., "Proteomic analysis of lung adenocarcinoma: identification of a highly expressed set of proteins in tumors," *Clinical Cancer Research*, vol. 8, no. 7, pp. 2298–2305, 2002.
- [40] D. R. Faksvåg Haugen, Ø. Fluge, L. J. Reigstad, J. E. Varhaug, and J. R. Lillehaug, "Increased expression of genes encoding mitochondrial proteins in papillary thyroid carcinomas," *Thyroid*, vol. 13, no. 7, pp. 613–620, 2003.
- [41] H. J. Chang, M. R. Lee, S. H. Hong et al., "Identification of mitochondrial FoF1-ATP synthase involved in liver metastasis of colorectal cancer," *Cancer Science*, vol. 98, no. 8, pp. 1184–1191, 2007.
- [42] G. Gasparre, L. Iommarini, A. M. Porcelli et al., "An inherited mitochondrial DNA disruptive mutation shifts to homoplasmy in oncogenic tumor cells," *Human Mutation*, vol. 30, no. 3, pp. 391–396, 2009.
- [43] A. Baracca, S. Barogi, V. Carelli, G. Lenaz, and G. Solaini, "Catalytic activities of mitochondrial ATP synthase in patients with mitochondrial DNA T8993G mutation in the ATPase 6 gene encoding subunit *a*," *The Journal of Biological Chemistry*, vol. 275, no. 6, pp. 4177–4182, 2000.
- [44] A. I. Jonckheere, G. H. Renkema, M. Bras et al., "A complex V *ATP5A1* defect causes fatal neonatal mitochondrial encephalopathy," *Brain*, vol. 136, no. 5, pp. 1544–1554, 2013.
- [45] J. A. Mayr, V. Havlickova, F. Zimmermann et al., "Mitochondrial ATP synthase deficiency due to a mutation in the *ATP5E* gene for the F1 ϵ subunit," *Human Molecular Genetics*, vol. 19, no. 17, pp. 3430–3439, 2010.
- [46] L. Sánchez-Cenizo, L. Formentini, M. Aldea et al., "Up-regulation of the ATPase inhibitory factor 1 (IF1) of the mitochondrial H⁺-ATP synthase in human tumors mediates the metabolic shift of cancer cells to a Warburg phenotype," *The Journal of Biological Chemistry*, vol. 285, no. 33, pp. 25308–25313, 2010.
- [47] R. Song, H. Song, Y. Liang et al., "Reciprocal activation between ATPase inhibitory factor 1 and NF- κ B drives hepatocellular carcinoma angiogenesis and metastasis," *Hepatology*, vol. 60, no. 5, pp. 1659–1673, 2014.
- [48] T. Yin, L. Lu, Z. Xiong, S. Wei, and D. Cui, "ATPase inhibitory factor 1 is a prognostic marker and contributes to proliferation and invasion of human gastric cancer cells," *Biomedicine & Pharmacotherapy*, vol. 70, pp. 90–96, 2015.

Review Article

Possible Clues for Brain Energy Translation via Endolysosomal Trafficking of APP-CTFs in Alzheimer's Disease

Senthilkumar Sivanesan ¹, Ravi Mundugaru,¹ and Jayakumar Rajadas ^{2,3}

¹Department of Research and Development, Saveetha Institute of Medical and Technical Sciences, Chennai 602 105, India

²Biomaterials and Advanced Drug Delivery Laboratory, Stanford University School of Medicine, Stanford, CA 94305, USA

³Department of Bioengineering and Therapeutic Sciences, Schools of Pharmacy and Medicine, University of California San Francisco, San Francisco, CA 94158, USA

Correspondence should be addressed to Senthilkumar Sivanesan; senbio@gmail.com and Jayakumar Rajadas; jayraja@stanford.edu

Received 10 April 2018; Revised 14 July 2018; Accepted 19 August 2018; Published 21 October 2018

Academic Editor: Marcelo Mori

Copyright © 2018 Senthilkumar Sivanesan et al. This is an open access article distributed under the Creative Commons Attribution License, which permits unrestricted use, distribution, and reproduction in any medium, provided the original work is properly cited.

Vascular dysfunctions, hypometabolism, and insulin resistance are high and early risk factors for Alzheimer's disease (AD), a leading neurological disease associated with memory decline and cognitive dysfunctions. Early defects in glucose transporters and glycolysis occur during the course of AD progression. Hypometabolism begins well before the onset of early AD symptoms; this timing implicates the vulnerability of hypometabolic brain regions to beta-secretase 1 (BACE-1) upregulation, oxidative stress, inflammation, synaptic failure, and cell death. Despite the fact that ketone bodies, astrocyte-neuron lactate shuttle, pentose phosphate pathway (PPP), and glycogenolysis compensate to provide energy to the starving AD brain, a considerable energy crisis still persists and increases during disease progression. Studies that track brain energy metabolism in humans, animal models of AD, and *in vitro* studies reveal striking upregulation of beta-amyloid precursor protein (β -APP) and carboxy-terminal fragments (CTFs). Currently, the precise role of CTFs is unclear, but evidence supports increased endosomal-lysosomal trafficking of β -APP and CTFs through autophagy through a vague mechanism. While intracellular accumulation of $A\beta$ is attributed as both the cause and consequence of a defective endolysosomal-autophagic system, much remains to be explored about the other β -APP cleavage products. Many recent works report altered amino acid catabolism and expression of several urea cycle enzymes in AD brains, but the precise cause for this dysregulation is not fully explained. In this paper, we try to connect the role of CTFs in the energy translation process in AD brain based on recent findings.

1. Introduction

Alzheimer's disease (AD), a progressive neurodegenerative disorder, evolves over many years and is characterized by episodes of memory impairments, loss of cognitive skills [1], and personality changes [2]. Although both tau and amyloid beta ($A\beta$) reportedly play normal functions at the synapse, the transsynaptic spread of pathogenic tau aggregates and accumulation of toxic $A\beta$ oligomers are together believed to be crucial for synapse loss and neurodegeneration in AD [3]. Despite marked neuronal death during late AD, it is worthwhile to examine the survival of a limited number of $A\beta$ -resistant neurons via increased glucose uptake [4]. Unfortunately, it is difficult to understand how and why only certain nerve cells become resistant to $A\beta$ toxicity, a fact that

emphasizes the need to identify precise therapeutic targets for AD. Notably, the toxicity of $A\beta$ oligomer species occurs within seconds to minutes, although it takes several years to attain disease severity. This inequality, along with disparate results of anti-amyloid clinical trials, questions the centrality of $A\beta$ as the chief mediator of neuronal cell death [5]. Moreover, whether $A\beta$ oligomeric species directly cause AD is still arguable [6].

Early stages of AD include white matter changes that involve pericyte degeneration and vascular defects with loss of myelinated axons and oligodendrocytes [7]. Hypometabolism occurs early in AD progression, with oxidative stress and impaired mitochondrial bioenergetics [8]. Disruption of normal $A\beta$ synaptic signaling and nonfulfillment of synaptic energy demands presumably cause amyloid toxicity and

metabolic stress [5, 9]. Currently, the amyloid cascade hypothesis accentuates the role of soluble $A\beta$ oligomers [10–12] and tau aggregates [13, 14] in AD pathogenesis. However, notable emerging views on the role of insulin resistance and hypometabolism connected to AD suggest that the damage induced by pathogenic $A\beta$ entities could be a secondary effect rather than the early and precise cause of AD.

As part of normal aging, oxygen and glucose metabolic rates are consistently altered in brain cells [15] and are drastically changed in many neurodegenerative diseases [16]. Although numerous alternative pathways could fulfill brain energy needs, there will still be an unmet energy demand [17]. Adenosine triphosphate (ATP) production could be age dependently decreased owing to poor nutrient and oxygen supply as well as reduced rates of glycolysis and oxidative phosphorylation [18]. Brain hypoperfusion and loss of blood-brain barrier (BBB) integrity can diminish nutrient import and/or toxin removal [19]. Recent research focuses on AD hypometabolism-associated cognitive impairments. Reduced glucose transporter 1 (GLUT1) levels cause an age-dependent decrease in cerebral capillary density, reduced cerebral blood flow and glucose uptake, and increased BBB leakage [20]. Indeed, these metabolic and vascular alterations precede dendritic spine loss in cornu ammonis 1 (CA1) hippocampal neurons, and associated behavioral impairments implicate energy dysfunctions during the course of AD. Several seminal works also implicate alterations in spine shape, density, and size of aged neurons, indicative of gross changes in dendritic structures [18].

The precise cellular events of hypometabolism associated with AD progression are poorly understood. Unfortunately, apart from ketone bodies, astrocyte-neuron lactate shuttle, the pentose phosphate pathway (PPP), and glycogenolysis, there are no clear-cut data that support other energy compensatory mechanisms to balance the bioenergetic deficits in AD brain. Several findings substantiate that plasma levels of certain amino acids are significantly altered in mild cognitive impairment (MCI) and AD patients compared to control individuals [21–23]. The BBB restricts the entry of glutamate and other anionic excitatory amino acids from the circulation [24], although it allows selective transport of certain amino acids to support neuronal functions through transporters [25, 26]. However, whether transported amino acids could support brain energy functions during starvation/hypometabolism is not clear. A growing body of evidence suggests that starvation/hypometabolism in AD brain increases endosomal-lysosomal trafficking of β -amyloid precursor protein (β -APP) meant for clearance during autophagy. The intricate role of such events and further functions need to be further explored. Moreover, the apparent cause for abnormal β -APP processing in AD brains is relatively unclear. This review envisages the importance of vascular abnormalities, hypometabolism, insulin resistance, and altered β -APP processing in AD along with our hypothetical views on possible energy compensatory mechanisms in AD brain (Figure 1).

1.1. Hypoxia and Hypometabolism Are Early Events in AD. Cerebral amyloid angiopathy- (CAA-) associated microbleeds

are one of several causative factors attributed to brain hypometabolism and atrophy in AD [27]. Vascular risk factors, such as adversely affected hippocampus microvasculature length [28], hypoperfusion [29], hypoxia, and hypometabolism, contribute greatly to early AD progression [30–34]. A stronger correlation seems to exist between brain energy inhibition and AD severity [35, 36]. Consistently, agents used to alleviate brain energy dysfunctions are promising for the treatment of cognitive and neurological diseases including AD [37–40].

While fludeoxyglucose positron emission tomography (^{18}F -FDG-PET) helps to detect the cerebral metabolic rate of glucose metabolism (MRglc) in AD [41], voxel-based morphometry (VBM) of T1-weighted magnetic resonance imaging (MRI) could reveal brain atrophy [42]. Recent ^{18}F -FDG-PET studies confirm hypometabolism in early sporadic AD [43, 44]. Moreover, region-specific severe hypometabolism in AD brain regions shows age invariance with greatly reduced frontal cortex glucose metabolism [45, 46]. There is a strong correlation between glucose hypometabolism and atrophy in the precuneus in early AD subjects based on ^{18}F -FDG-PET studies [47]. In mild AD subjects, there is significantly lower MRglc in the parietal cortex, posterior cingulate, and thalamus [48]. Different research groups report hypometabolism in AD/probable AD subjects in the temporal cortex, bilateral middorsolateral frontal region, frontal brain, and parieto-mesial cortex regions based on ^{18}F -FDG-PET [42, 49, 50]. Although Stein et al. [51] identified energy fluctuations manifested as poor glucose metabolic rate in the limbic areas of the temporal lobe, a voxel-based study that analyzed AD brain regions revealed significant atrophy of the hippocampus and amygdala [52]. Metabolic fluctuations of key glycolytic enzymes [53] and oxygen delivery in the circulating erythrocytes could also be risk factors for brain hypometabolism in AD [54].

The “Warburg effect,” well described for cancer cells, appears to apply to neuronal cells [4], notably during the mild phase of AD where neurons with defective glucose uptake show resistance to $A\beta$ toxicity. Thus, the prodementia phase of AD provides evidence of gray matter loss and brain glucose deficits [55]. Reduced expression of energy metabolism genes that encode subunits of the mitochondrial electron transport chain is also apparent in the posterior cingulate neurons of AD brains [56]. Mitochondrial failure develops in $A\beta$ overexpressing *Caenorhabditis elegans*, a finding that demonstrates this phenomenon is not unique to human AD [57]. Using Trem2^{-/-} 5xFAD transgenic mice, mutations in triggering receptor expressed on myeloid cells 2 (TREM2) can lead to energy dysfunctions in the immune cell microglia and thereby cause impaired clearance of amyloid plaques; energy supplementation with cyclocreatine to immune cells reduces the plaque load to protect the neurons [58]. Altogether, vascular and metabolic fluctuations are well indicated during the early course of AD.

1.2. Defective Glycolytic Enzymes, Glucose Transporters, and Impaired Insulin Signaling in AD. It is difficult to determine whether brain hypometabolic status is a consequence or cause of AD pathology, but many recent works support the

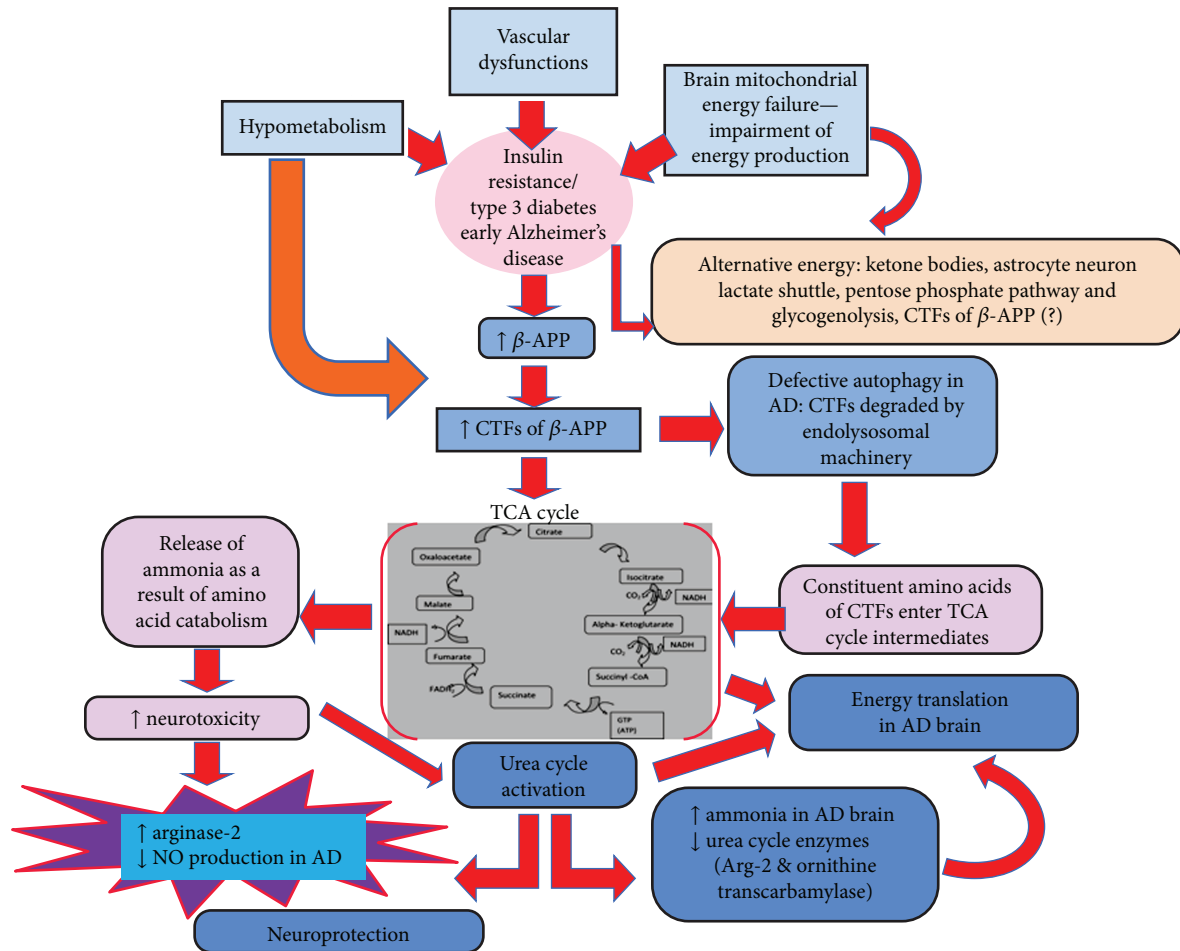


FIGURE 1: Hypothetical scheme that shows the possible energy compensatory mechanism in hypometabolic AD brain through endolysosomal trafficking of CTFs and urea cycle activation.

latter. Elevated plasma glucose concentrations in fasting conditions are attributed to increased brain glucose levels in AD, a finding that implicates insulin resistance [59]. Human and animal studies clearly show reduced expression of glucose transporters in aged [60] and AD [59] brains, including changes in the expression of key enzymes involved in glycolysis and oxidative phosphorylation [61–63]. Evidence supports considerable neuronal loss in AD brain that involves oxidative stress-mediated inhibition of glyceraldehyde-3-phosphate dehydrogenase (GAPDH) activity [64]. The reduced flux of pyruvate carboxylase (PC) in gluconeogenesis and pentose phosphate from the hexose monophosphate shunt reported in the brains of $A\beta$ PP-PS1 mice (an AD model) further indicates poor glucose metabolism [65]. A study with Thy-1 mito-CFP mice showed reduced ATP levels in white matter during aging, in correlation with ultrastructural alterations in mitochondria, as well as reduced association of mitochondria with the endoplasmic reticulum [66]. The van Gijssel-Bonnello et al. group [67] recently performed metabolomic analysis using 5xFAD transgenic mouse astrocytes and showed marked changes in the glycolytic pathway and tricarboxylic acid cycle (TCA).

A considerable number of research substantiates glucose transporter defects [20, 68–70], neurovascular dysfunctions

associated with glucose transporter defects [20], poor glucose utilization [71, 72], and cognitive dysfunctions [73] in AD. The defective insulin signaling mechanisms reported in AD [70, 74–77] further strengthen the vascular and metabolic anomalies in AD, and the disease could be described as type 3 diabetes [78, 79]. Therefore, therapeutics aimed towards curing AD would need to significantly rely on regulating insulin levels and brain cellular energy levels [80–84]. Insulin improves cognition and may be neuroprotective, yet different intranasal insulin concentrations exert varying responses in subsets of AD patients [39, 40, 84–86].

1.3. Hypoxia and Energy Stress/Starvation Influences β -APP Processing and Beta-Secretase 1 (BACE1) Levels. Defective glycolysis [59] and oxidative phosphorylation tend to be part of the metabolic adaptation process implicated as early signs of sporadic AD [15]. Substantial evidence pinpoints that hypoxia significantly increases BACE1 gene expression through hypoxia-inducible factor 1- α (Hif1 α) upregulation [32, 87–89]. Although increased BACE1 activity reduces mitochondrial glucose uptake [90], a majority of work supports the view that BACE1 upregulation accounts for energy inhibition [36, 91–93]. Gabuzda et al. [94] explored energy-related metabolic stress on APP processing using sodium

azide and agents that inhibit protein transport in the secretory pathway (monensin and brefeldin A). These agents could ultimately drive oxidative energy impairment in mitochondria to alter several-fold APP proteolytic processing into an 11.5kDa carboxy terminal fragment. In another work, Velliquette et al. [91] revealed that energy inhibition by agents such as insulin, 2-deoxyglucose, 3-nitropropionic acid, and kainic acid in wild-type and Tg2576 transgenic mice strikingly elevates cerebral BACE1 levels concomitant with progressive AD pathology. Xiong et al. [93] inhibited mitochondrial complex I, II, and IV with rotenone, nitropropionic acid, and sodium azide, respectively, to prove that mitochondrial respiratory inhibition and oxidative stress trigger BACE1 expression as well as the presence of β -APP carboxy terminal fragments. Gatta et al. [92] inhibited heme synthesis and mitochondrial energy production using small interfering RNA and N-methylprotoporphyrin IX; these actions alter APP processing and amyloid aggregation. In another work [95], fasting differentially activates macroautophagy in 5xFAD mouse neurons compared to control mice. Fasting alters the numbers and pattern of autophagosomes in neurons, although the study suggests that activated macroautophagy after fasting does not degrade intracellular A β that is increased due to enhanced uptake from the extracellular space [95]. Inhibition of the key glycolytic enzyme 6-phosphofructo-2-kinase in astrocyte cultures increases amyloidogenic processing of APP [96]. Unfortunately, the cause for increased BACE1 and β -APP processing in conditions such as energy inhibition, starvation, and hypometabolism in AD brain is still unclear. However, there is a plausible relationship between hypometabolism and autophagy. Specifically, defects in mammalian target of rapamycin (mTOR) signaling in AD brain correlate with impaired mitochondrial functions and energy metabolism [97]. Whether hypometabolism precedes defective autophagy or the vice versa requires further exploration.

1.4. Connection between Early Autophagy/Macrophagy and β -APP Processing. Macroautophagy activation occurs during conditions such as cellular stress due to nutritional deficit or cell injury [98]. This process represents a lysosomal pathway for the turnover of organelles and long-lived proteins and is a key determinant of cell survival and longevity [99]. While chaperone-mediated autophagy (CMA) involves chaperone-mediated degradation of proteins near the lysosomal lumen that have specific sequence signals [100], macroautophagy degrades misfolded and aggregated proteins by lysosomal machinery [101]. Using a fusion protein called tandem-fluorescent-APP, investigators showed that starvation triggers the trafficking of APP and APP-carboxy-terminal fragments (APP-CTFs) to the degradative endolysosomal network, a finding that provides a new hint for identifying key therapeutics for AD [102]. A more recent work indicates increased BACE1 turnover in the vicinity of suppressed autophagy after lysosomal inhibition [103]. Since BACE1 recruitment to the autophagy pathway and its comigration with autophagic vacuoles seems to occur similarly along the entire axon, autophagic induction with concomitant BACE1 retention could promote increased

β -APP cleavage processing. Taken together, the protective role of autophagy elicited under metabolic stress conditions reveals bioenergetic adaptations in the cellular environment [104]. Thus, autophagy could provide compensatory regulation of brain energy through the APP trafficking pathway.

Culminating evidence pinpoints early induction of neuronal macroautophagy in sporadic AD brains and transgenic mouse models of AD pathology even before the visualization of extracellular A β deposits [99, 105]. While dystrophic dendrites are the sites where autophagosomes and late autophagic vacuoles (AVs) accumulate, it is possible that purified AVs are the source of APP, beta-cleaved APP, presenilin 1, nicastrin, and γ -secretase activity. Nonetheless, Boland et al. [106] reveal that although neuronal macroautophagy does not directly regulate APP metabolism, there is plausible proof for an antiamyloidogenic role of lysosomal proteolysis in postsecretase APP-CTF catabolism. Indeed, agents/drugs that can reduce A β levels in the brain probably account for the increased degradation of APP-CTFs as well as A β clearance [107].

1.5. Amino Acid Sensing in Lysosomes Provides Hints about the Brain Energy Translation Process. The role of lysosomal machinery in the degradation and recycling of cellular waste is not novel. Moreover, the localization of lysosomal hydrolases within neurons is a feature of AD [108]. However, compelling evidence supports additional lysosomal machinery functions involved in secretion, plasma membrane repair, and energy metabolism [109]. While several studies provide mechanistic insights about the lysosome and cellular energy metabolism [109–112], much remains to be explored in brain regions and particularly in AD. Other studies show a favoring of amino acid sensing and mTOR signaling promoted by vacuolar H⁺-ATPase within the lysosomal compartment [113–115]. In a recent review, Carroll and Dunlop [116] detail the role of lysosomes in autophagy, in amino acid sensing by mTOR complex 1 (mTORC1), and the key signaling events associated among lysosomes, adenosine monophosphate-activated protein kinase (AMPK), and mTORC1. Considering this point of view, the events associated with endosomal-lysosomal trafficking of β -APP [102, 117] need much more exploration to support energy-related functions of cleaved APP fragments.

1.6. Culminating Work Shows Amino Acid Catabolism and Urea Cycle Activation in AD Brain. While ketone bodies [118, 119], PPP [67], and astrocyte-neuron lactate shuttle [120] try to compensate for AD brain energy deficits, there is still (to some extent) an increasing demand for brain energy. Urea cycle activation in AD brain [121–123] to remove ammonia generated from increased amino acid catabolism [121, 123, 124] provides evident and plausible insights into amino acid catabolism for energy conversion. AD brains exhibit increased expression of carbamoyl phosphate synthetase 1 (CPS-1) and peptidylarginine deiminase (PAD), which catalyzes the conversion of arginine into citrulline during ammonia formation [124]. The normal brain lacks urea-cycle-related ornithine transcarbamylase (OTC) and CPS-1 enzymes, a finding that strengthens the fact that

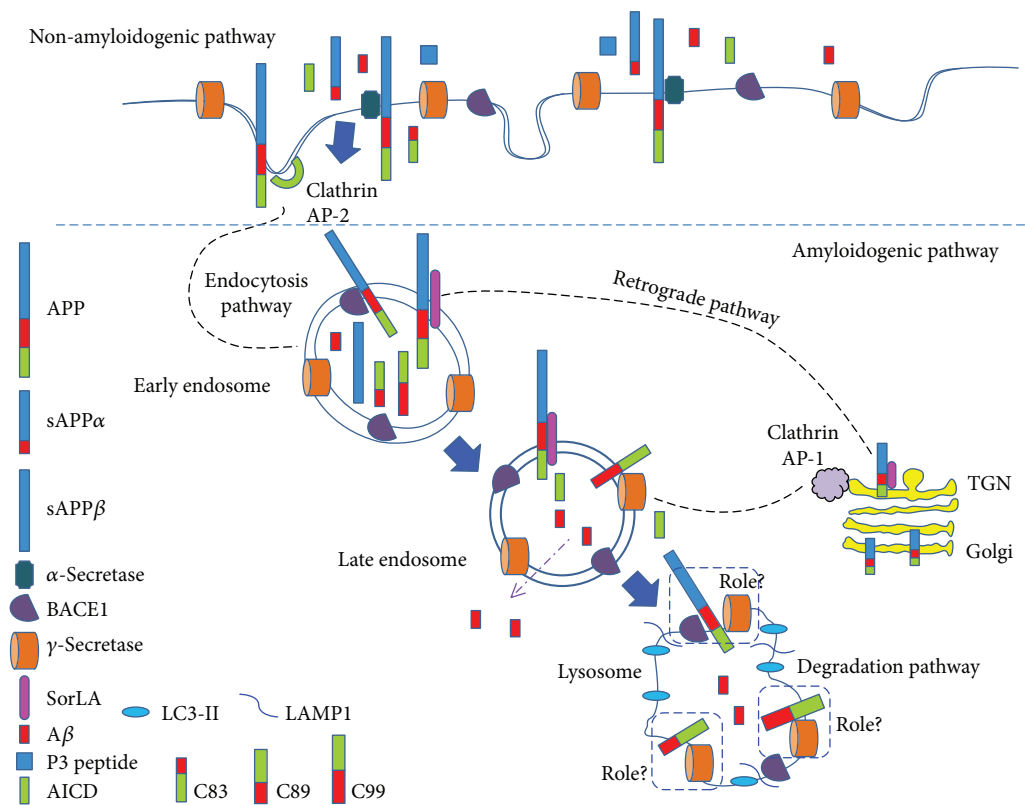


FIGURE 2: Pathways involved in the proteolytic processing of β -APP in AD.

AD brains are vulnerable to ammonia toxicity. Favorably, defects in ammonia detoxification owing to the adversely affected energy-producing pathway of glucose metabolism (involving PC and PPP) were reported in 20-month-old A β PP-PS1 mice [65].

According to Seiler [125], hyperammonemia in the blood and brain of AD subjects can provoke toxicity, contribute to AD pathogenesis, and alter β -APP processing in the lysosome. Ammonia is the major end product of cellular amino acid metabolism [126], and the brain can derive ammonia from both endogenous and exogenous pathways [125, 127]. Endogenous sources include degradation of neurotransmitters (glutamate, aspartate, and other monoamines), amino acids (e.g., glutamine, asparagine, and glycine), and hexamines. Deamination of amino-purines, amino-pyrimidines, and oxidative deamination of primary amines overall contribute to the endogenous sources of brain ammonia. Given the fact that the urea cycle in AD brains generates copious amounts of ammonia, a considerable amount of protein degradation must occur during AD pathogenesis. Increasing evidence pinpoints amino acid catabolism [128, 129] and ammonia accumulation in AD brain [128, 130, 131], although the exact processes remain unclear. However, such notable findings could indicate activation of energy compensation regulatory mechanisms in hypometabolic AD brain. Findings from Hansmannel et al. [121] strikingly reveal that all urea cycle enzymes are expressed in AD brain, with notably increased arginase-2 (Arg2) gene expression compared to control. Moreover, vulnerable AD brain regions exhibit region-specific alterations in arginase and nitric oxide

synthase (NOS) [132]. OTC induction and Arg2 upregulation in AD would attempt to reduce brain ammonia, including reduction of NO and inducible NOS levels, actions that may emphasize the intricate neuroprotective role of the urea cycle pathway [121]. In Huntington's disease (HD), another neurodegenerative disease, markedly elevated toxic urea levels in the brain before dementia onset precede brain damage in a transgenic sheep HD model and human subjects [133]. Since urea and ammonia are the key metabolic units of protein catabolism, there is a clear-cut indication for major protein catabolism in neurodegenerative HD and AD. Interestingly, a recent ongoing phase 2 clinical trials for AD is testing AMX0035 which is an oral formulation of two drugs, sodium phenylbutyrate (PB) and tauroursodeoxycholic-acid (TUDCA). While PB is an FDA-approved drug prescribed for urea-cycle disorders to reduce toxic unfolded proteins, TUDCA helps in reducing cellular energy loss.

1.7. Evidence Spotlights the Importance of APP-CTFs-Derived Amino Acids in Brain Energy Functions in AD. Serum and cerebrospinal fluid metabolomics studies reveal major alterations in canonical energy metabolism pathways, Krebs cycle, mitochondrial function and amino acid metabolism in MCI and AD patients [22]. Since starvation promotes trafficking of both APP and APP-CTFs to the degradative endolysosome [102], it provides clues for compensatory mechanisms initiated to counterbalance the energy deficits. Proteolytic processing of APP mainly involves amyloidogenic and nonamyloidogenic pathways [134, 135] as detailed below (Figure 2). BACE1 cleavage of APP within its

extracellular/luminal domain represents the amyloidogenic pathway and promotes shedding of soluble β -secreted APP (sAPP β) and membrane-associated C-terminal fragment of 99 amino acids (β CTF/C99) or 89 amino acids (β CTF/C89). After ectodomain shedding, γ -secretase (protein complex comprised of presenilin 1 or 2, Aph1 homolog A or B, nicastrin, and presenilin enhancer protein 2) cleavage occurs in the membrane-tethered C89 and C99 and thereby releasing p3 from C89 or A β peptides from C99. The nonamyloidogenic pathway at the plasma membrane involves cleavage by α -secretases (ADAM10/ADAM17) that generates soluble α -secreted APP (sAPP α) and a C-terminal membrane-bound fragment of 83 amino acids (α CTF/C83). Further cleavage of this fragment by γ -secretase releases the p3 peptide. The retrograde trafficking mechanisms that follow either α - or β -secretase cleavage allow delivery of APP-CTFs to the trans-Golgi network (TGN). Based on recent findings, the majority of γ -secretase cleavage of APP occurs in the TGN [136]. Notably, γ -secretase cleavage of both β CTF/C99 and α CTF/C83 generates the APP intracellular domain (AICD), but it is rapidly degraded similar to p3. Growing evidence depicts novel/alternative metabolic processing pathways (η -secretase, δ -secretase, and meprin pathways) during physiological processing of APP [137, 138]. Usually, carboxy-terminal fragments, such as β CTF/C89, β CTF/C99, and α CTF/C83, are targeted to the endosomal-lysosomal compartment [102, 139]. The biological importance of β CTF/C99, β CTF/C89, α CTF/C83, and p3 remains unclear [135], although many studies substantiate the neuroprotective functions of sAPP α , including in brain development, growth factor, neural cell proliferation [140, 141], and synaptic plasticity [142]. sAPP β is involved in pruning of synapses during the development of both central and peripheral neurons [143] but reported to cause suppression of neuronal stem cell differentiation [144]. Although controversies exist about the biological functions of the AICD fragment, it is reported to be involved in gene transcription, cytoskeletal dynamics, and apoptosis [145]. However, during lysosomal degradation that recruits various CTFs (β CTF/C89, β CTF/C99, and α CTF/C83), it is likely that constitutive amino acids formed after proteolytic cleavage could serve as TCA cycle intermediates to fulfill brain energy deficits [146]. It remains elusive whether cleaved amino acids from APP after degradation in endolysosomes [102] also provide energy via the TCA cycle. This could be due to the fact that during APP sorting, beclin1 promotes targeting of a smaller fraction of surface-internalized APP to microtubule-associated protein 1 light chain 3- (LC3-) positive phagophores for degradation [147]. According to Hoyer et al. [148], hypoxia/sodium azide insults in HEK293 cells stably transfected with bAPP695 show energy failure with strikingly elevated ATP turnover and adenosine levels that parallel intracellular APP increases. In another work, upon hypoglycemic induction, rat neuronal cultures increase utilization of amino acids as evidenced by ammonia formation due to amino acid catabolism [149]. Overall, there is a considerable body of evidence that supports β -APP energy-related functions during AD hypometabolism. Further detailed investigations are warranted on APP-related energy

functions in order to accurately track the pathological cascade to develop precise therapeutic targets. Recently, a study revealed that a greater number of dendritic spines in healthy brains (controls) compared to age-matched AD brains poorly correlate with symptoms such as dementia in controls, despite marked amyloid plaques and tangles observed in both types of brains [150]. This intriguing result demarcates the disease and healthy brains from the amyloid cascade hypothesis and creates avenues for further exploration in AD research.

2. Summary

AD brain is vulnerable to increased β -APP proteolytic cleavage and accumulation of various CTFs as well as APP in the endolysosomal compartment. While these intricate events are complicated, the relative cause and functions of cleavage products are poorly understood. In this paper, we hypothesize that in hypometabolic AD brains, the constitutive amino acids of CTFs and APP formed during endolysosomal degradation could compensate for metabolic demands through the TCA cycle. Our hypothetical views on APP-related brain energy functions can be justified with numerous recent works that implicate amino acid catabolism, urea cycle activation (due to increased amino acid catabolism), and ammonia toxicity propagated in AD brain. We also try to connect possible neuroprotective mechanisms in AD brain against ammonia toxicity through activation of urea cycle enzymes (Arg-2 and OTC) and decreased nitric oxide (NO) levels.

Conflicts of Interest

The authors declare no competing financial interests.

Acknowledgments

The authors sincerely thank Dr. Mathew D. Howell for providing critical English and grammar corrections in the manuscript.

References

- [1] R. Tarawneh and D. M. Holtzman, "The clinical problem of symptomatic Alzheimer disease and mild cognitive impairment," *Cold Spring Harbor Perspectives in Medicine*, vol. 2, no. 5, pp. 1–16, 2012.
- [2] F. C. Bozzola, P. B. Gorelick, and S. Freels, "Personality changes in Alzheimer's disease," *Archives of Neurology*, vol. 49, no. 3, pp. 297–300, 1992.
- [3] T. L. Spire-Jones and B. T. Hyman, "The intersection of amyloid beta and tau at synapses in Alzheimer's disease," *Neuron*, vol. 82, no. 4, pp. 756–771, 2014.
- [4] A. Atlante, L. de Bari, A. Bobba, and G. Amadoro, "A disease with a sweet tooth: exploring the Warburg effect in Alzheimer's disease," *Biogerontology*, vol. 18, no. 3, pp. 301–319, 2017.
- [5] P. A. Engel, "Does metabolic failure at the synapse cause Alzheimer's disease?," *Medical Hypotheses*, vol. 83, no. 6, pp. 802–808, 2014.

- [6] G. P. Morris, I. A. Clark, and B. Vissel, "Inconsistencies and controversies surrounding the amyloid hypothesis of Alzheimer's disease," *Acta Neuropathologica Communications*, vol. 2, no. 1, p. 135, 2014.
- [7] A. Montagne, A. M. Nikolakopoulou, Z. Zhao et al., "Pericyte degeneration causes white matter dysfunction in the mouse central nervous system," *Nature Medicine*, vol. 24, no. 3, pp. 326–337, 2018.
- [8] J. Yao and R. Diaz Brinton, "Targeting mitochondrial bioenergetics for Alzheimer's prevention and treatment," *Current Pharmaceutical Design*, vol. 17, no. 31, pp. 3474–3479, 2011.
- [9] J. Godyn, J. Jonczyk, D. Panek, and B. Malawska, "Therapeutic strategies for Alzheimer's disease in clinical trials," *Pharmacological Reports*, vol. 68, no. 1, pp. 127–138, 2016.
- [10] G. M. Shankar, S. Li, T. H. Mehta et al., "Amyloid- β protein dimers isolated directly from Alzheimer's brains impair synaptic plasticity and memory," *Nature Medicine*, vol. 14, no. 8, pp. 837–842, 2008.
- [11] D. J. Selkoe and J. Hardy, "The amyloid hypothesis of Alzheimer's disease at 25 years," *EMBO Molecular Medicine*, vol. 8, no. 6, pp. 595–608, 2016.
- [12] S. Sivanesan, A. Tan, and J. Rajadas, "Pathogenesis of Abeta oligomers in synaptic failure," *Current Alzheimer Research*, vol. 10, no. 3, pp. 316–323, 2013.
- [13] G. S. Bloom, "Amyloid- β and tau: the trigger and bullet in Alzheimer disease pathogenesis," *JAMA Neurology*, vol. 71, no. 4, pp. 505–508, 2014.
- [14] D. J. Koss, G. Jones, A. Cranston, H. Gardner, N. M. Kanaan, and B. Platt, "Soluble pre-fibrillar tau and β -amyloid species emerge in early human Alzheimer's disease and track disease progression and cognitive decline," *Acta Neuropathologica*, vol. 132, no. 6, pp. 875–895, 2016.
- [15] M. Mamelak, "Sporadic Alzheimer's disease: the starving brain," *Journal of Alzheimer's Disease*, vol. 31, no. 3, pp. 459–474, 2012.
- [16] S. Hoyer, "The young-adult and normally aged brain. Its blood flow and oxidative metabolism. A review—part I," *Archives of Gerontology and Geriatrics*, vol. 1, no. 2, pp. 101–116, 1982.
- [17] S. Hoyer, "Abnormalities of glucose metabolism in Alzheimer's disease," *Annals of the New York Academy of Sciences*, vol. 640, no. 1, pp. 53–58, 1991.
- [18] S. Camandola and M. P. Mattson, "Brain metabolism in health, aging, and neurodegeneration," *The EMBO Journal*, vol. 36, no. 11, pp. 1474–1492, 2017.
- [19] B. V. Zlokovic, "Neurovascular pathways to neurodegeneration in Alzheimer's disease and other disorders," *Nature Reviews Neuroscience*, vol. 12, no. 12, pp. 723–738, 2011.
- [20] E. A. Winkler, Y. Nishida, A. P. Sagare et al., "GLUT1 reductions exacerbate Alzheimer's disease vasculo-neuronal dysfunction and degeneration," *Nature Neuroscience*, vol. 18, no. 4, pp. 521–530, 2015.
- [21] G. Ravaglia, P. Forti, F. Maioli et al., "Incidence and etiology of dementia in a large elderly Italian population," *Neurology*, vol. 64, no. 9, pp. 1525–1530, 2005.
- [22] E. Trushina, T. Dutta, X. M. T. Persson, M. M. Mielke, and R. C. Petersen, "Identification of altered metabolic pathways in plasma and CSF in mild cognitive impairment and Alzheimer's disease using metabolomics," *PLoS One*, vol. 8, no. 5, article e63644, 2013.
- [23] G. Corso, A. Cristofano, N. Sapere et al., "Serum amino acid profiles in normal subjects and in patients with or at risk of Alzheimer dementia," *Dementia and Geriatric Cognitive Disorders Extra*, vol. 7, no. 1, pp. 143–159, 2017.
- [24] Q. R. Smith, "Transport of glutamate and other amino acids at the blood-brain barrier," *The Journal of Nutrition*, vol. 130, no. 4, pp. 1016S–1022S, 2000.
- [25] W. M. Pardridge, "Brain metabolism: a perspective from the blood-brain barrier," *Physiological Reviews*, vol. 63, no. 4, pp. 1481–1535, 1983.
- [26] M. S. Malandro and M. S. Kilberg, "Molecular biology of mammalian amino acid transporters," *Annual Review of Biochemistry*, vol. 65, no. 1, pp. 305–336, 1996.
- [27] M. Samuraki, I. Matsunari, M. Yoshita et al., "Cerebral amyloid angiopathy-related microbleeds correlate with glucose metabolism and brain volume in Alzheimer's disease," *Journal of Alzheimer's Disease*, vol. 48, no. 2, pp. 517–528, 2015.
- [28] Y. Decker, A. Müller, E. Németh et al., "Analysis of the vasculature by immunohistochemistry in paraffin-embedded brains," *Brain Structure & Function*, vol. 223, no. 2, pp. 1001–1015, 2018.
- [29] S. Vercllytte, R. Lopes, P. Lenfant et al., "Cerebral hypoperfusion and hypometabolism detected by arterial spin labeling MRI and FDG-PET in early-onset Alzheimer's disease," *Journal of Neuroimaging*, vol. 26, no. 2, pp. 207–212, 2016.
- [30] B. S. Ashok, T. A. Ajith, and S. Sivanesan, "Hypoxia-inducible factors as neuroprotective agent in Alzheimer's disease," *Clinical and Experimental Pharmacology & Physiology*, vol. 44, no. 3, pp. 327–334, 2017.
- [31] B. Snyder, B. Shell, J. T. Cunningham, and R. L. Cunningham, "Chronic intermittent hypoxia induces oxidative stress and inflammation in brain regions associated with early-stage neurodegeneration," *Physiological Reports*, vol. 5, no. 9, article e13258, 2017.
- [32] A. Salminen, A. Kauppinen, and K. Kaarniranta, "Hypoxia/ischemia activate processing of amyloid precursor protein: impact of vascular dysfunction in the pathogenesis of Alzheimer's disease," *Journal of Neurochemistry*, vol. 140, no. 4, pp. 536–549, 2017.
- [33] S. Joubert, N. Gour, E. Guedj et al., "Early-onset and late-onset Alzheimer's disease are associated with distinct patterns of memory impairment," *Cortex*, vol. 74, pp. 217–232, 2016.
- [34] P. Grammas, D. Tripathy, A. Sanchez, X. Yin, and J. Luo, "Brain microvasculature and hypoxia-related proteins in Alzheimer's disease," *International Journal of Clinical and Experimental Pathology*, vol. 4, no. 6, pp. 616–627, 2011.
- [35] C. Arias, T. Montiel, R. Quiroz-Báez, and L. Massieu, " β -amyloid neurotoxicity is exacerbated during glycolysis inhibition and mitochondrial impairment in the rat hippocampus *in vivo* and in isolated nerve terminals: implications for Alzheimer's disease," *Experimental Neurology*, vol. 176, no. 1, pp. 163–174, 2002.
- [36] T. O'Connor, K. R. Sadleir, E. Maus et al., "Phosphorylation of the translation initiation factor eIF2 α increases BACE1 levels and promotes amyloidogenesis," *Neuron*, vol. 60, no. 6, pp. 988–1009, 2008.
- [37] M. H. Rosenbloom, T. R. Barclay, M. Pyle et al., "A single-dose pilot trial of intranasal rapid-acting insulin in apolipoprotein E4 carriers with mild-moderate Alzheimer's disease," *CNS Drugs*, vol. 28, no. 12, pp. 1185–1189, 2014.

- [38] J. Freiherr, M. Hallschmid, W. H. Frey et al., "Intranasal insulin as a treatment for Alzheimer's disease: a review of basic research and clinical evidence," *CNS Drugs*, vol. 27, no. 7, pp. 505–514, 2013.
- [39] C. Benedict, W. H. Frey II, H. B. Schiöth, B. Schultes, J. Born, and M. Hallschmid, "Intranasal insulin as a therapeutic option in the treatment of cognitive impairments," *Experimental Gerontology*, vol. 46, no. 2-3, pp. 112–115, 2011.
- [40] L. R. Hanson and W. H. Frey, "Intranasal delivery bypasses the blood-brain barrier to target therapeutic agents to the central nervous system and treat neurodegenerative disease," *BMC Neuroscience*, vol. 9, Supplement 3, p. S5, 2008.
- [41] Y. Li, J. O. Rinne, L. Mosconi et al., "Regional analysis of FDG and PIB-PET images in normal aging, mild cognitive impairment, and Alzheimer's disease," *European Journal of Nuclear Medicine and Molecular Imaging*, vol. 35, no. 12, pp. 2169–2181, 2008.
- [42] S. Frisch, J. Dukart, B. Vogt et al., "Dissociating memory networks in early Alzheimer's disease and frontotemporal lobar degeneration - a combined study of hypometabolism and atrophy," *PLoS One*, vol. 8, no. 2, article e52521, 2013.
- [43] J. R. Gatchel, N. J. Donovan, J. J. Locascio et al., "Regional 18F-fluorodeoxyglucose hypometabolism is associated with higher apathy scores over time in early Alzheimer disease," *The American Journal of Geriatric Psychiatry*, vol. 25, no. 7, pp. 683–693, 2017.
- [44] M. Vanhoutte, F. Semah, A. Rollin Sillaire et al., "¹⁸F-FDG PET hypometabolism patterns reflect clinical heterogeneity in sporadic forms of early-onset Alzheimer's disease," *Neurobiology of Aging*, vol. 59, pp. 184–196, 2017.
- [45] H. Oh, C. Madison, S. Baker, G. Rabinovici, and W. Jagust, "Dynamic relationships between age, amyloid- β deposition, and glucose metabolism link to the regional vulnerability to Alzheimer's disease," *Brain*, vol. 139, no. 8, pp. 2275–2289, 2016.
- [46] Z. Chen and C. Zhong, "Decoding Alzheimer's disease from perturbed cerebral glucose metabolism: implications for diagnostic and therapeutic strategies," *Progress in Neurobiology*, vol. 108, pp. 21–43, 2013.
- [47] S. M. Adriaanse, K. R. A. van Dijk, R. Ossenkoppele et al., "The effect of amyloid pathology and glucose metabolism on cortical volume loss over time in Alzheimer's disease," *European Journal of Nuclear Medicine and Molecular Imaging*, vol. 41, no. 6, pp. 1190–1198, 2014.
- [48] C. A. Castellano, S. Nugent, N. Paquet et al., "Lower brain ¹⁸F-fluorodeoxyglucose uptake but normal ¹¹C-acetate metabolism in mild Alzheimer's disease dementia," *Journal of Alzheimer's Disease*, vol. 43, no. 4, pp. 1343–1353, 2015.
- [49] S. M. Adriaanse, A. M. Wink, B. M. Tijms et al., "The association of glucose metabolism and eigenvector centrality in Alzheimer's disease," *Brain Connectivity*, vol. 6, no. 1, pp. 1–8, 2016.
- [50] B. K. P. Woo, D. G. Harwood, R. J. Melrose et al., "Executive deficits and regional brain metabolism in Alzheimer's disease," *International Journal of Geriatric Psychiatry*, vol. 25, no. 11, pp. 1150–1158, 2010.
- [51] D. J. Stein, M. S. Buchsbaum, P. R. Hof, B. V. Siegel Jr, and L. Shihabuddin, "Greater metabolic rate decreases in hippocampal formation and proisocortex than in neocortex in Alzheimer's disease," *Neuropsychobiology*, vol. 37, no. 1, pp. 10–19, 1998.
- [52] G. B. Frisoni, M. Lorenzi, A. Caroli, N. Kemppainen, K. Nägren, and J. O. Rinne, "In vivo mapping of amyloid toxicity in Alzheimer disease," *Neurology*, vol. 72, no. 17, pp. 1504–1511, 2009.
- [53] Y. G. Kaminsky, V. P. Reddy, G. M. Ashraf et al., "Age-related defects in erythrocyte 2,3-diphosphoglycerate metabolism in dementia," *Aging and Disease*, vol. 4, no. 5, pp. 244–255, 2013.
- [54] E. A. Kosenko, L. A. Tikhonova, C. Montoliu, G. E. Barreto, G. Aliev, and Y. G. Kaminsky, "Metabolic abnormalities of erythrocytes as a risk factor for Alzheimer's disease," *Frontiers in Neuroscience*, vol. 11, p. 728, 2018.
- [55] M. A. Araque Caballero, M. Brendel, A. Delker et al., "Mapping 3-year changes in gray matter and metabolism in A β -positive nondemented subjects," *Neurobiology of Aging*, vol. 36, no. 11, pp. 2913–2924, 2015.
- [56] W. S. Liang, E. M. Reiman, J. Valla et al., "Alzheimer's disease is associated with reduced expression of energy metabolism genes in posterior cingulate neurons," *Proceedings of the National Academy of Sciences of the United States of America*, vol. 105, no. 11, pp. 4441–4446, 2008.
- [57] S. Fong, E. Teo, L. F. Ng et al., "Energy crisis precedes global metabolic failure in a novel *Caenorhabditis elegans* Alzheimer disease model," *Scientific Reports*, vol. 6, no. 1, article 33781, 2016.
- [58] T. K. Ulland, W. M. Song, S. C. C. Huang et al., "TREM2 maintains microglial metabolic fitness in Alzheimer's disease," *Cell*, vol. 170, no. 4, pp. 649–663.e13, 2017.
- [59] Y. An, V. R. Varma, S. Varma et al., "Evidence for brain glucose dysregulation in Alzheimer's disease," *Alzheimer's & Dementia*, vol. 14, no. 3, pp. 318–329, 2018.
- [60] F. Ding, J. Yao, J. R. Rettberg, S. Chen, and R. D. Brinton, "Early decline in glucose transport and metabolism precedes shift to ketogenic system in female aging and Alzheimer's mouse brain: implication for bioenergetic intervention," *PLoS One*, vol. 8, no. 11, article e79977, 2013.
- [61] W. Meier-Ruge, P. Iwangoff, K. Reichlmeier, and P. Sandoz, "Neurochemical findings in the aging brain," *Advances in Biochemical Psychopharmacology*, vol. 23, pp. 323–338, 1980.
- [62] G. Ulfert, U. Schmidt, and S. Hoyer, "Glucose and energy metabolism of rat cerebral cortex during aging," *Experimental Brain Research*, vol. 5, pp. 102–111, 1982.
- [63] A. C. Bowling, E. M. Mutisya, L. C. Walker, D. L. Price, L. C. Cork, and M. H. Beal, "Age-dependent impairment of mitochondrial function in primate brain," *Journal of Neurochemistry*, vol. 60, no. 5, pp. 1964–1967, 1993.
- [64] D. A. Butterfield, S. S. Hardas, and M. L. B. Lange, "Oxidatively modified glyceraldehyde-3-phosphate dehydrogenase (GAPDH) and Alzheimer's disease: many pathways to neurodegeneration," *Journal of Alzheimer's Disease*, vol. 20, no. 2, pp. 369–393, 2010.
- [65] V. Tiwari and A. B. Patel, "Pyruvate carboxylase and pentose phosphate fluxes are reduced in A β PP-PS1 mouse model of Alzheimer's disease: a ¹³C NMR study," *Journal of Alzheimer's Disease*, vol. 41, no. 2, pp. 387–399, 2014.
- [66] K. E. Stahon, C. Bastian, S. Griffith, G. J. Kidd, S. Brunet, and S. Baltan, "Age-related changes in axonal and mitochondrial ultrastructure and function in white matter," *The Journal of Neuroscience*, vol. 36, no. 39, pp. 9990–10001, 2016.

- [67] M. van Gijssel-Bonnello, K. Baranger, P. Benech et al., "Metabolic changes and inflammation in cultured astrocytes from the 5xFAD mouse model of Alzheimer's disease: alleviation by pantethine," *PLoS One*, vol. 12, no. 4, article e0175369, 2017.
- [68] C. R. Hooijmans, C. Graven, P. J. Dederen, H. Tanila, T. van Groen, and A. J. Kiliaan, "Amyloid beta deposition is related to decreased glucose transporter-1 levels and hippocampal atrophy in brains of aged APP/PS1 mice," *Brain Research*, vol. 1181, pp. 93–103, 2007.
- [69] Y. Liu, F. Liu, K. Iqbal, I. Grundke-Iqbal, and C. X. Gong, "Decreased glucose transporters correlate to abnormal hyperphosphorylation of tau in Alzheimer disease," *FEBS Letters*, vol. 582, no. 2, pp. 359–364, 2008.
- [70] Y. Deng, B. Li, Y. Liu, K. Iqbal, I. Grundke-Iqbal, and C. X. Gong, "Dysregulation of insulin signaling, glucose transporters, O-GlcNAcylation, and phosphorylation of tau and neurofilaments in the brain: Implication for Alzheimer's disease," *The American Journal of Pathology*, vol. 175, no. 5, pp. 2089–2098, 2009.
- [71] I. A. Simpson, K. R. Chundu, T. Davies-Hill, W. G. Honer, and P. Davies, "Decreased concentrations of GLUT1 and GLUT3 glucose transporters in the brains of patients with Alzheimer's disease," *Annals of Neurology*, vol. 35, no. 5, pp. 546–551, 1994.
- [72] S. D. Harr, N. A. Simonian, and B. T. Hyman, "Functional alterations in Alzheimer's disease: decreased glucose transporter 3 immunoreactivity in the perforant pathway terminal zone," *Journal of Neuropathology and Experimental Neurology*, vol. 54, no. 1, pp. 38–41, 1995.
- [73] S. M. Landau, D. Harvey, C. M. Madison et al., "Comparing predictors of conversion and decline in mild cognitive impairment," *Neurology*, vol. 75, no. 3, pp. 230–238, 2010.
- [74] G. S. Watson and S. Craft, "The role of insulin resistance in the pathogenesis of Alzheimer's disease: implications for treatment," *CNS Drugs*, vol. 17, no. 1, pp. 27–45, 2003.
- [75] W. Q. Zhao, F. G. de Felice, S. Fernandez et al., "Amyloid beta oligomers induce impairment of neuronal insulin receptors," *The FASEB Journal*, vol. 22, no. 1, pp. 246–260, 2008.
- [76] L. M. Chua, M. L. Lim, P. R. Chong, Z. P. Hu, N. S. Cheung, and B. S. Wong, "Impaired neuronal insulin signaling precedes A β 42 accumulation in female A β PPsw/PS1 Δ E9 mice," *Journal of Alzheimer's Disease*, vol. 29, no. 4, pp. 783–791, 2012.
- [77] S. T. Ferreira, J. R. Clarke, T. R. Bomfim, and F. G. De Felice, "Inflammation, defective insulin signaling, and neuronal dysfunction in Alzheimer's disease," *Alzheimers Dement*, vol. 10, no. 1, pp. S76–S83, 2014.
- [78] S. M. De la Monte and J. R. Wands, "Alzheimer's disease is type 3 diabetes-evidence reviewed," *Journal of Diabetes Science and Technology*, vol. 2, no. 6, pp. 1101–1113, 2008.
- [79] H. Pilcher, "Alzheimer's disease could be "type 3 diabetes"," *Lancet Neurology*, vol. 5, no. 5, pp. 388–389, 2006.
- [80] C. G. Jolivald, C. A. Lee, K. K. Beiswenger et al., "Defective insulin signaling pathway and increased glycogen synthase kinase-3 activity in the brain of diabetic mice: parallels with Alzheimer's disease and correction by insulin," *Journal of Neuroscience Research*, vol. 86, no. 15, pp. 3265–3274, 2008.
- [81] H. B. Schioth, S. Craft, S. J. Brooks, W. H. Frey, and C. Benedict, "Brain insulin signaling and Alzheimer's disease: current evidence and future directions," *Molecular Neurobiology*, vol. 46, no. 1, pp. 4–10, 2012.
- [82] T. R. Bomfim, L. Forny-Germano, L. B. Sathler et al., "An anti-diabetes agent protects the mouse brain from defective insulin signaling caused by Alzheimer's disease-associated A β oligomers," *The Journal of Clinical Investigation*, vol. 122, no. 4, pp. 1339–1353, 2012.
- [83] F. G. De Felice, "Alzheimer's disease and insulin resistance: translating basic science into clinical applications," *The Journal of Clinical Investigation*, vol. 123, no. 2, pp. 531–539, 2013.
- [84] S. M. De la Monte, "Intranasal insulin therapy for cognitive impairment and neurodegeneration: current state of the art," *Expert Opinion on Drug Delivery*, vol. 10, no. 12, pp. 1699–1709, 2013.
- [85] M. A. Reger, G. S. Watson, P. S. Green et al., "Intranasal insulin administration dose-dependently modulates verbal memory and plasma amyloid- β in memory-impaired older adults," *Journal of Alzheimer's Disease*, vol. 13, no. 3, pp. 323–331, 2008.
- [86] S. Craft, L. D. Baker, T. J. Montine et al., "Intranasal insulin therapy for Alzheimer disease and amnesic mild cognitive impairment: a pilot clinical trial," *Archives of Neurology*, vol. 69, no. 1, pp. 29–38, 2012.
- [87] X. Sun, G. He, H. Qing et al., "Hypoxia facilitates Alzheimer's disease pathogenesis by up-regulating BACE1 gene expression," *Proceedings of the National Academy of Sciences of the United States of America*, vol. 103, no. 49, pp. 18727–18732, 2006.
- [88] X. Zhang, K. Zhou, R. Wang et al., "Hypoxia-inducible factor 1 α (HIF-1 α)-mediated hypoxia increases BACE1 expression and β -amyloid generation," *The Journal of Biological Chemistry*, vol. 282, no. 15, pp. 10873–10880, 2007.
- [89] M. Guglielmotto, M. Aragno, R. Autelli et al., "The up-regulation of BACE1 mediated by hypoxia and ischemic injury: role of oxidative stress and HIF1 α ," *Journal of Neurochemistry*, vol. 108, no. 4, pp. 1045–1056, 2009.
- [90] J. A. Findlay, D. L. Hamilton, and M. L. J. Ashford, "BACE1 activity impairs neuronal glucose oxidation: rescue by beta-hydroxybutyrate and lipoic acid," *Frontiers in Cellular Neuroscience*, vol. 9, article 382, 2015.
- [91] R. A. Velliquette, T. O'Connor, and R. Vassar, "Energy inhibition elevates β -secretase levels and activity and is potentially amyloidogenic in APP transgenic mice: possible early events in Alzheimer's disease pathogenesis," *The Journal of Neuroscience*, vol. 25, no. 47, pp. 10874–10883, 2005.
- [92] L. B. Gatta, M. Vitali, R. Verardi, P. Arosio, and D. Finazzi, "Inhibition of heme synthesis alters amyloid precursor protein processing," *Journal of Neural Transmission*, vol. 116, no. 1, pp. 79–88, 2009.
- [93] K. Xiong, H. Cai, X. G. Luo, R. G. Struble, R. W. Clough, and X. X. Yan, "Mitochondrial respiratory inhibition and oxidative stress elevate β -secretase (BACE1) proteins and activity in vivo in the rat retina," *Experimental Brain Research*, vol. 181, no. 3, pp. 435–446, 2007.
- [94] D. Gabuzda, J. Busciglio, L. B. Chen, P. Matsudaira, and B. A. Yankner, "Inhibition of energy metabolism alters the processing of amyloid precursor protein and induces a potentially amyloidogenic derivative," *The Journal of Biological Chemistry*, vol. 269, no. 18, pp. 13623–13628, 1994.
- [95] X. Chen, K. Kondo, K. Motoki, H. Homma, and H. Okazawa, "Fasting activates macroautophagy in neurons of Alzheimer's

- disease mouse model but is insufficient to degrade amyloid-beta," *Scientific Reports*, vol. 5, no. 1, article 12115, 2015.
- [96] W. Fu, D. Shi, D. Westaway, and J. H. Jhamandas, "Bioenergetic mechanisms in astrocytes may contribute to amyloid plaque deposition and toxicity," *The Journal of Biological Chemistry*, vol. 290, no. 20, pp. 12504–12513, 2015.
- [97] M. Perluigi, F. Di Domenico, and D. A. Butterfield, "mTOR signaling in aging and neurodegeneration: at the crossroad between metabolism dysfunction and impairment of autophagy," *Neurobiology of Disease*, vol. 84, pp. 39–49, 2015.
- [98] D. C. Rubinsztein, M. DiFiglia, N. Heintz et al., "Autophagy and its possible roles in nervous system diseases, damage and repair," *Autophagy*, vol. 1, no. 1, pp. 11–22, 2005.
- [99] W. H. Yu, A. M. Cuervo, A. Kumar et al., "Macroautophagy—a novel β -amyloid peptide-generating pathway activated in Alzheimer's disease," *The Journal of Cell Biology*, vol. 171, no. 1, pp. 87–98, 2005.
- [100] A. M. Cuervo and J. F. Dice, "A receptor for the selective uptake and degradation of proteins by lysosomes," *Science*, vol. 273, no. 5274, pp. 501–503, 1996.
- [101] B. Loos, D. J. Klionsky, and E. Wong, "Augmenting brain metabolism to increase macro- and chaperone-mediated autophagy for decreasing neuronal proteotoxicity and aging," *Progress in Neurobiology*, vol. 156, pp. 90–106, 2017.
- [102] L. K. Hein, P. M. Apaja, K. Hattersley et al., "A novel fluorescent probe reveals starvation controls the commitment of amyloid precursor protein to the lysosome," *Biochimica et Biophysica Acta (BBA) - Molecular Cell Research*, vol. 1864, no. 10, pp. 1554–1565, 2017.
- [103] T. Feng, P. Tammineni, C. Agrawal, Y. Y. Jeong, and Q. Cai, "Autophagy-mediated regulation of BACE1 protein trafficking and degradation," *Biological Chemistry*, vol. 292, no. 5, pp. 1679–1690, 2017.
- [104] S. Giordano, M. Dodson, S. Ravi et al., "Bioenergetic adaptation in response to autophagy regulators during rotenone exposure," *Journal of Neurochemistry*, vol. 131, no. 5, pp. 625–633, 2014.
- [105] L. Holcomb, M. N. Gordon, E. McGowan et al., "Accelerated Alzheimer-type phenotype in transgenic mice carrying both mutant amyloid precursor protein and presenilin 1 transgenes," *Nature Medicine*, vol. 4, no. 1, pp. 97–100, 1998.
- [106] B. Boland, D. A. Smith, D. Mooney, S. S. Jung, D. M. Walsh, and F. M. Platt, "Macroautophagy is not directly involved in the metabolism of amyloid precursor protein," *The Journal of Biological Chemistry*, vol. 285, no. 48, pp. 37415–37426, 2010.
- [107] M. Shinohara, N. Sato, H. Kurinami et al., "Reduction of brain β -amyloid ($A\beta$) by fluvastatin, a hydroxymethylglutaryl-CoA reductase inhibitor, through increase in degradation of amyloid precursor protein C-terminal fragments (APP-CTFs) and $A\beta$ clearance," *The Journal of Biological Chemistry*, vol. 285, no. 29, pp. 22091–22102, 2010.
- [108] R. A. Nixon, J. Wegiel, A. Kumar et al., "Extensive involvement of autophagy in Alzheimer disease: an immunoelectron microscopy study," *Journal of Neuropathology and Experimental Neurology*, vol. 64, no. 2, pp. 113–122, 2005.
- [109] C. Settembre, A. Fraldi, D. L. Medina, and A. Ballabio, "Signals from the lysosome: a control centre for cellular clearance and energy metabolism," *Nature Reviews. Molecular Cell Biology*, vol. 14, no. 5, pp. 283–296, 2013.
- [110] C. Y. Lim and R. Zoncu, "The lysosome as a command-and-control center for cellular metabolism," *The Journal of Cell Biology*, vol. 214, no. 6, pp. 653–664, 2016.
- [111] V. K. Mony, S. Benjamin, and E. J. O'Rourke, "A lysosome-centered view of nutrient homeostasis," *Autophagy*, vol. 12, no. 4, pp. 619–631, 2016.
- [112] C. Settembre, R. Zoncu, D. L. Medina et al., "A lysosome-to-nucleus signalling mechanism senses and regulates the lysosome via mTOR and TFEB," *The EMBO Journal*, vol. 31, no. 5, pp. 1095–1108, 2012.
- [113] R. Zoncu, L. Bar-Peled, A. Efeyan, S. Wang, Y. Sancak, and D. M. Sabatini, "mTORC1 senses lysosomal amino acids through an inside-out mechanism that requires the vacuolar H^+ -ATPase," *Science*, vol. 334, no. 6056, pp. 678–683, 2011.
- [114] J. L. Jewell, R. C. Russell, and K. L. Guan, "Amino acid signalling upstream of mTOR," *Nature Reviews. Molecular Cell Biology*, vol. 14, no. 3, pp. 133–139, 2013.
- [115] D. C. I. Goberdhan, C. Wilson, and A. L. Harris, "Amino acid sensing by mTORC1: intracellular transporters mark the spot," *Cell Metabolism*, vol. 23, no. 4, pp. 580–589, 2016.
- [116] B. Carroll and E. A. Dunlop, "The lysosome: a crucial hub for AMPK and mTORC1 signalling," *The Biochemical Journal*, vol. 474, no. 9, pp. 1453–1466, 2017.
- [117] J. H. K. Tam, M. R. Cobb, C. Seah, and S. H. Pasternak, "Tyrosine binding protein sites regulate the intracellular trafficking and processing of amyloid precursor protein through a novel lysosome-directed pathway," *PLoS One*, vol. 11, no. 10, article e0161445, 2016.
- [118] S. C. Cunnane, A. Courchesne-Loyer, V. St-Pierre et al., "Can ketones compensate for deteriorating brain glucose uptake during aging? Implications for the risk and treatment of Alzheimer's disease," *Annals of the New York Academy of Sciences*, vol. 1367, no. 1, pp. 12–20, 2016.
- [119] K. Heininger, "A unifying hypothesis of Alzheimer's disease. IV. Causation and sequence of events," *Reviews in the Neurosciences*, vol. 11, pp. 213–328, 2000.
- [120] L. Pellerin and P. J. Magistretti, "Sweet sixteen for ANLS," *Journal of Cerebral Blood Flow and Metabolism*, vol. 32, no. 7, pp. 1152–1166, 2012.
- [121] F. Hansmann, A. Sillaire, M. I. Kamboh et al., "Is the urea cycle involved in Alzheimer's disease?," *Journal of Alzheimer's Disease*, vol. 21, no. 3, pp. 1013–1021, 2010.
- [122] F. Bensemain, D. Hot, S. Ferreira et al., "Evidence for induction of the ornithine transcarbamylase expression in Alzheimer's disease," *Molecular Psychiatry*, vol. 14, no. 1, pp. 106–116, 2009.
- [123] J. Xu, P. Begley, S. J. Church et al., "Graded perturbations of metabolism in multiple regions of human brain in Alzheimer's disease: snapshot of a pervasive metabolic disorder," *Biochimica et Biophysica Acta (BBA) - Molecular Basis of Disease*, vol. 1862, no. 6, pp. 1084–1092, 2016.
- [124] J. Cicolini, Y. Jing, H. J. Waldvogel, R. L. M. Faull, and P. Liu, "Urea cycle enzymes and peptidylarginine deiminase in Alzheimer's superior frontal gyrus," *Alzheimer's & Dementia*, vol. 12, no. 7, p. P460, 2016.
- [125] N. Seiler, "Ammonia and Alzheimer's disease," *Neurochemistry International*, vol. 41, no. 2-3, pp. 189–207, 2002.
- [126] P. A. Wright, "Nitrogen excretion: three end products, many physiological roles," *Journal of Experimental Biology*, vol. 198, Part 2, pp. 273–281, 1995.

- [127] M. J. O'Donnell, "Mechanisms of excretion and ion transport in invertebrates," in *Comparative Physiology*, W. H. Dantzer, Ed., pp. 1207–1289, Oxford University Press, New York, NY, USA, 1997.
- [128] J. W. D. Griffin and P. C. Bradshaw, "Amino acid catabolism in Alzheimer's disease brain: friend or foe?," *Oxidative Medicine and Cellular Longevity*, vol. 2017, Article ID 5472792, 15 pages, 2017.
- [129] H. Gallart-Ayala, T. Teav, F. Mehl et al., "Altered brain metabolism in Alzheimer disease: linking peripheral and central metabolic changes," in *MSACL 2017 EU Abstract*, Salzburg, Austria, September 2017.
- [130] A. J. Cooper and T. M. Jeitner, "Central role of glutamate metabolism in the maintenance of nitrogen homeostasis in normal and hyperammonemic brain," *Biomolecules*, vol. 6, no. 2, 2016.
- [131] A. Adlimoghaddam, M. G. Sabbir, and B. C. Albeni, "Ammonia as a potential neurotoxic factor in Alzheimer's disease," *Frontiers in Molecular Neuroscience*, vol. 9, p. 57, 2016.
- [132] P. Liu, M. S. Fleete, Y. Jing et al., "Altered arginine metabolism in Alzheimer's disease brains," *Neurobiology of Aging*, vol. 35, no. 9, pp. 1992–2003, 2014.
- [133] R. R. Handley, S. J. Reid, R. Brauning et al., "Brain urea increase is an early Huntington's disease pathogenic event observed in a prodromal transgenic sheep model and HD cases," *Proceedings of the National Academy of Sciences of the United States of America*, vol. 114, no. 52, pp. E11293–E11302, 2017.
- [134] B. De Strooper and W. Annaert, "Proteolytic processing and cell biological functions of the amyloid precursor protein," *Journal of Cell Science*, vol. 113, Part 11, pp. 1857–1870, 2000.
- [135] V. W. Chow, M. P. Mattson, P. C. Wong, and M. Gleichmann, "An overview of APP processing enzymes and products," *Neuromolecular Medicine*, vol. 12, no. 1, pp. 1–12, 2010.
- [136] R. W.-Y. Choy, Z. Cheng, and R. Schekman, "Amyloid precursor protein (APP) traffics from the cell surface via endosomes for amyloid β ($A\beta$) production in the trans-Golgi network," *Proceedings of the National Academy of Sciences of the United States of America*, vol. 109, no. 30, pp. E2077–E2082, 2012.
- [137] R. Coronel, A. Bernabeu-Zornoza, C. Palmer et al., "Role of amyloid precursor protein (APP) and its derivatives in the biology and cell fate specification of neural stem cells," *Molecular Neurobiology*, vol. 55, no. 9, pp. 7107–7117, 2018.
- [138] E. Norstrom, "Metabolic processing of the amyloid precursor protein – new pieces of the Alzheimer's puzzle," *Discovery Medicine*, vol. 23, no. 127, pp. 269–276, 2017.
- [139] Q. Xiao, P. Yan, X. Ma et al., "Neuronal-targeted TFEB accelerates lysosomal degradation of APP, reducing $A\beta$ generation and amyloid plaque pathogenesis," *The Journal of Neuroscience*, vol. 35, no. 35, pp. 12137–12151, 2015.
- [140] M. Gralle, M. G. Botelho, and F. S. Wouters, "Neuroprotective secreted amyloid precursor protein acts by disrupting amyloid precursor protein dimers," *The Journal of Biological Chemistry*, vol. 284, no. 22, pp. 15016–15025, 2009.
- [141] M. P. Demars, C. Hollands, K. D. (T.). Zhao, and O. Lazarov, "Soluble amyloid precursor protein- α rescues age-linked decline in neural progenitor cell proliferation," *Neurobiology of Aging*, vol. 34, no. 10, pp. 2431–2440, 2013.
- [142] S. H. Tyan, A. Y. J. Shih, J. J. Walsh et al., "Amyloid precursor protein (APP) regulates synaptic structure and function," *Molecular and Cellular Neurosciences*, vol. 51, no. 1–2, pp. 43–52, 2012.
- [143] A. Nikolaev, T. McLaughlin, D. D. M. O'Leary, and M. Tessier-Lavigne, "APP binds DR6 to trigger axon pruning and neuron death via distinct caspases," *Nature*, vol. 457, no. 7232, pp. 981–989, 2009.
- [144] Y. D. Kwak, C. L. Brannen, T. Qu et al., "Amyloid precursor protein regulates differentiation of human neural stem cells," *Stem Cells and Development*, vol. 15, no. 3, pp. 381–389, 2006.
- [145] T. Müller, H. E. Meyer, R. Egensperger, and K. Marcus, "The amyloid precursor protein intracellular domain (AICD) as modulator of gene expression, apoptosis, and cytoskeletal dynamics—relevance for Alzheimer's disease," *Progress in Neurobiology*, vol. 85, no. 4, pp. 393–406, 2008.
- [146] S. Senthilkumar and R. Jayakumar, "Can proteolytic events of β -APP pave pathway for brain energy metabolism in human Alzheimer models?," *Journal of Neurological Sciences [Turkish]*, vol. 21, pp. 147–154, 2004.
- [147] G. Swaminathan, W. Zhu, and E. D. Plowey, "BECN1/Beclin 1 sorts cell-surface APP/amyloid β precursor protein for lysosomal degradation," *Autophagy*, vol. 12, no. 12, pp. 2404–2419, 2016.
- [148] A. Hoyer, H. J. Bardenheuer, E. Martin, and K. Plaschke, "Amyloid precursor protein (APP) and its derivatives change after cellular energy depletion. An *in vitro*-study," *Journal of Neural Transmission*, vol. 112, no. 2, pp. 239–253, 2005.
- [149] P. Honegger, O. Braissant, H. Henry et al., "Alteration of amino acid metabolism in neuronal aggregate cultures exposed to hypoglycaemic conditions," *Journal of Neurochemistry*, vol. 81, no. 6, pp. 1141–1151, 2002.
- [150] B. D. Boros, K. M. Greathouse, E. G. Gentry et al., "Dendritic spines provide cognitive resilience against Alzheimer's disease," *Annals of Neurology*, vol. 82, no. 4, pp. 602–614, 2017.

Research Article

The Causal Role of Mitochondrial Dynamics in Regulating Insulin Resistance in Diabetes: Link through Mitochondrial Reactive Oxygen Species

Hung-Yu Lin ¹, Shao-Wen Weng,^{1,2} Yen-Hsiang Chang,³ Yu-Jih Su ¹, Chih-Min Chang,¹ Chia-Jen Tsai,¹ Feng-Chih Shen,¹ Jiin-Haur Chuang,⁴ Tsu-Kung Lin,⁵ Chia-Wei Liou,⁵ Ching-Yi Lin,¹ and Pei-Wen Wang ¹

¹Department of Internal Medicine, Kaohsiung Chang Gung Memorial Hospital and Chang Gung University College of Medicine, Kaohsiung 833, Taiwan

²Lee's Endocrinology Clinic, Pingtung, Taiwan

³Department of Nuclear Medicine, Kaohsiung Chang Gung Memorial Hospital and Chang Gung University College of Medicine, Kaohsiung 833, Taiwan

⁴Department of Surgery, Kaohsiung Chang Gung Memorial Hospital and Chang Gung University College of Medicine, Kaohsiung 833, Taiwan

⁵Department of Neurology, Kaohsiung Chang Gung Memorial Hospital and Chang Gung University College of Medicine, Kaohsiung 833, Taiwan

Correspondence should be addressed to Pei-Wen Wang; wangpw@adm.cgmh.org.tw

Hung-Yu Lin and Shao-Wen Weng contributed equally to this work.

Received 23 April 2018; Revised 8 August 2018; Accepted 13 August 2018; Published 30 September 2018

Academic Editor: Eric Gross

Copyright © 2018 Hung-Yu Lin et al. This is an open access article distributed under the Creative Commons Attribution License, which permits unrestricted use, distribution, and reproduction in any medium, provided the original work is properly cited.

Background. Mitochondrial dynamics (mtDYN) has been proposed as a bridge between mitochondrial dysfunction and insulin resistance (IR), which is involved in the pathogenesis of type 2 diabetes (T2D). Our previous study has identified that mitochondrial DNA (mtDNA) haplogroup B4 is a T2D-susceptible genotype. Using transmitochondrial cybrid model, we have confirmed that haplogroup B4 contributes to cellular IR as well as a pro-fission mtDYN, which can be reversed by antioxidant treatment. However, the causal relationship between mtDYN and cellular IR pertaining to T2D-susceptible haplogroup B4 remains unanswered. **Methods.** To dissect the mechanisms between mtDYN and IR, knockdown or overexpression of MFN1, MFN2, DRP1, and FIS1 was performed using cybrid B4. We then examined the mitochondrial network and mitochondrial oxidative stress (mtROS) as well as insulin signaling IRS-AKT pathway and glucose transporters (GLUT) translocation to plasma membrane stimulated by insulin. We employed Drp1 inhibitor, mdivi-1, to interfere with endogenous expression of fission to validate the pharmacological effects on IR. **Results.** Overexpression of MFN1 or MFN2 increased mitochondrial network and reduced mtROS, while knockdown had an opposing effect. In contrast, overexpression of DRP1 or FIS1 decreased mitochondrial network and increased mtROS, while knockdown had an opposing effect. Concomitant with the enhanced mitochondrial network, activation of the IRS1-AKT pathway and GLUT translocation stimulated by insulin were improved. On the contrary, suppression of mitochondrial network caused a reduction of the IRS1-AKT pathway and GLUT translocation stimulated by insulin. Pharmacologically inhibiting mitochondrial fission by the Drp1 inhibitor, mdivi-1, also rescued mitochondrial network, reduced mtROS, and improved insulin signaling of diabetes-susceptible cybrid cells. **Conclusion.** Our results discovered the causal role of mtDYN proteins in regulating IR resulted from diabetes-susceptible mitochondrial haplogroup. The existence of a bidirectional interaction between mtDYN and mtROS plays an important role. Direct intervention to reverse pro-fission in mtDYN provides a novel therapeutic strategy for IR and T2D.

1. Introduction

The mitochondrion, an organelle responsible for the production of ATP, plays a central role in cellular metabolism [1]. Mitochondria form a complex dynamic network that continuously undergoes fusion and fission events, known as mitochondrial dynamics (mtDYN). Mitochondrial dynamics is a quality control system critical for maintaining the mitochondrial population and relevant to the stability of mitochondrial DNA (mtDNA), respiratory capacity, and cell response to stress [2]. Quality control might not be the only task carried out by mtDYN. Recent studies link mtDYN to the balance between energy demand and nutrient supply [3]. Several lines of evidence revealed alterations in mtDYN in insulin-resistant states and type 2 diabetes (T2D) in humans and in animal models [4–10]. Therefore, mtDYN have been implicated in the development of insulin resistance (IR) [9, 11, 12] and the pathogenesis of T2D [7, 13, 14].

In our previous work, we have firstly recognized that subjects harboring mitochondrial haplogroup B4, consisting of 16189T→C transition and 10398A allele, are diabetes-susceptible risk factor [15]. By the construction of transmitochondrial cybrid cell, we verified the impact of haplogroup B4 on cellular IR [16] as well as the imbalance of mtDYN toward a profusion state [17]. Further, antioxidant treatment causes concomitance of the profusion manner of mtDYN and improved IR in cybrid B4 [17]. However, the causal relationship of both physiological events has not been clarified. To address whether mtDYN plays a causal role in regulating cellular IR and serves as a potential therapeutic target, we have bidirectionally manipulated the expression of dynamic proteins, including *MFN1*, *MFN2*, *DRP1*, and *FIS1* in cybrid cell harboring diabetes-susceptible haplogroup B4. We also employed Drp1 inhibitor, mdivi-1, to interfere with endogenous expression of fission to validate the pharmacological effects on IR.

2. Materials and Methods

2.1. Cell Culture and Cybrid Generation. Cells were cultured using Dulbecco's modified eagle's medium (DMEM, high glucose, Gibco, Carlsbad, CA, USA) supplemented with 10% heat-inactivated fetal bovine serum (FBS; Gibco, Carlsbad, CA, USA) at 37°C in 5% CO₂. The generation of transmitochondrial cybrid was previously described [18]. Briefly, cybrids were generated by fusing 143B- ρ^0 cells with human platelets in the absence of pyruvate and uridine. Platelets were isolated from a volunteer subject harboring mtDNA haplogroup B4 and fused with ρ^0 cells in the presence of polyethylene glycol 1500 (50% w/v; Roche, Nutley, NJ, USA). This study protocol and written informed content were reviewed and approved by the Institutional Review Board of Chang Gung Memorial Hospital (CGMH; IRB number 101-1620A3).

2.2. Experimental Procedure. Cells were starved of FBS for 16 h, followed by transfection of plasmid/siRNA or mdivi-1 treatment. Then, cells were stimulated with insulin (Sigma-Aldrich, St. Louis, MO, USA) at 0, 0.1, or 1 μ M for 1 h and then collected for experimental assays. Gene overexpression

and knockdown of Mfn1, Mfn2, Drp1, and Fis1 were performed using Lipofectamine® 2000 (Invitrogen; Thermo Fisher Scientific, Inc., Waltham, MA, USA). Transfection of plasmid (RG207184; RG202218; RG202046; RG202560; Origene Technologies, Inc., Rockville, MD, USA) and siRNA (sc-43927; sc-43928; sc-43732; sc-60643; Santa Cruz Biotechnology, Santa Cruz, CA) spanned 24 and 48 h, respectively. Mock control of gene overexpression and siRNA was GFP-expression vector (OriGene-ORIPS100010, Origene Technologies, Inc., Rockville, MD, USA) and dsRNA with scramble sequence (sc-37007; Santa Cruz Biotechnology, Santa Cruz, CA), respectively.

2.3. Mitochondrial Morphology. Mitochondria were visualized using mitochondrial-targeting fluorescent protein cox4-DsRed, which is a kind gift from Dr. David Chan (California Institute of Technology, Pasadena, CA 91125, USA). The MicroP algorithm categorized mitochondrial morphology into six types: small globe (blue), large globe (yellow), simple tube (green), twisted tube (orange), donut (red), and branching tube (purple). $N=75-400$ mitochondria from 15–30 cells and three independent experiments.

2.4. Subfractionation of Cell Membrane. The Thermo Scientific Subcellular Protein Fractionation Kit for Cultured Cells (Thermo Fisher Scientific Inc., Rockford, IL, USA) was used to stepwise separate cytoplasmic, membrane, nuclear soluble, chromatin-bound, and cytoskeletal protein extracts from the cultured cybrid B4 cells. Briefly, cell pellet (2×10^6 cells in 20 μ L packed cell volume) was incubated with 200 μ L CEB at 4°C for 10 minutes with gentle mixing and then centrifuged at 500 \times g for 5 minutes. The supernatant was immediately transferred to a clean prechilled tube on ice to get the cytoplasmic extract. The pellet was mixed with ice-cold MEB, vortexed the tube for 5 seconds, incubated at 4°C for 10 minutes with gentle mixing, and then centrifuged at 3000 \times g for 5 minutes. The supernatant was transferred to a clean prechilled tube on ice to get the membrane extract. The nuclear soluble, chromatin-bound, and cytoskeletal protein extracts were separated stepwise according to the instruction and stored at –80°C, and the cytoplasmic and membrane extracts were maintained on ice for same-day use.

2.5. Detection of Mitochondrial Reactive Oxygen Species. The levels of mitochondrial superoxide (O₂^{•-}) produced in the cells were quantified using a MitoSOX Red kit (Molecular Probes, Invitrogen), which comprises a redox-sensitive dye composed of hydroethidine linked by a hexyl carbon chain to a triphenylphosphonium group, which was used to target the mitochondrial matrix due to the negative membrane potential across the inner mitochondrial membrane. The cells were plated at a density of 8×10^4 cells per well in 12-well plates (Nunc, Denmark) with a medium containing 25 mM glucose. MitoSOX Red was added at a final concentration of 1.0 μ M in HBSS (Gibco BRL, USA). The cells were then incubated for 10 min at 37°C, and then they were harvested and washed twice with PBS. They were fixed in 4% paraformaldehyde and mounted in Fluoromount media (Sigma-Aldrich Co. LLC), which

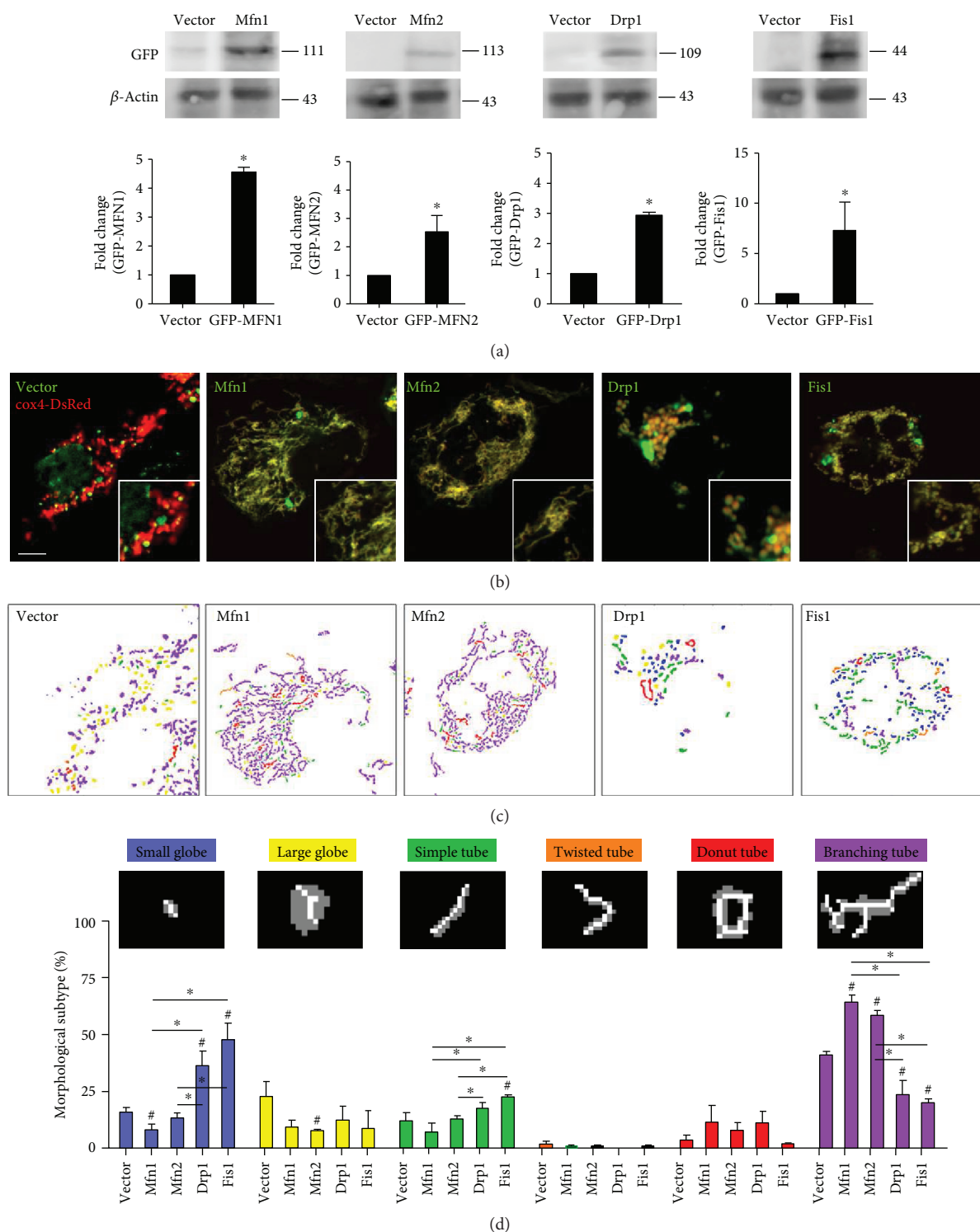


FIGURE 1: Overexpression of Mfn1/Mfn2 and Drp1/Fis1 promotes mitochondrial fusion and fission in DM cybrid, respectively. Gene overexpression was conducted by the transfecting plasmid. GFP-expressing plasmid (vector) was used as vector control. (a) Abundance of dynamic proteins Mfn1, Mfn2, Drp1, and Fis1 was determined using Western blotting. β -Actin served as loading control. (b) Mitochondrial morphology was visualized by transfecting cox4-DsRed (red fluorescence) in DM cybrid expressing GFP alone or GFP-tagged mitochondrial dynamic proteins (green fluorescence). An enlarged segment of each image was shown by a lower right square. (c) The MicroP algorithm categorized mitochondrial morphology into six types: small globe (blue), large globe (yellow), simple tube (green), twisted tube (orange), donut (red), and branching tube (purple). $N=75-400$ mitochondria from 15-30 cells and three independent experiments.

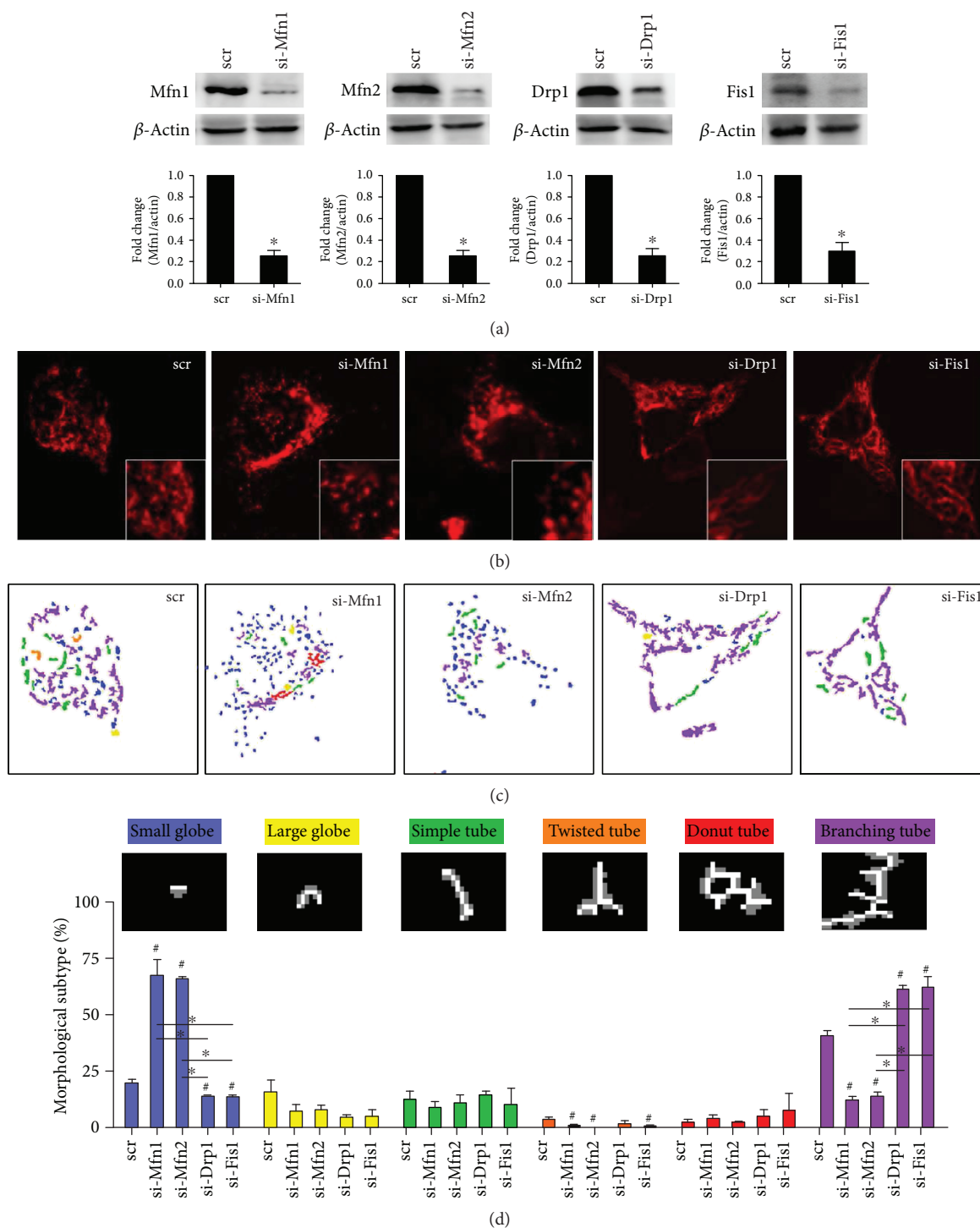


FIGURE 2: Knockdown of Mfn1/Mfn2 and Drp1/Fis1 reduces mitochondrial fusion and fission in DM cybrid, respectively. siRNA transfection was performed to knockdown target gene expression. Scramble dsRNA (scr) was used as siRNA negative control. (a) Abundance of dynamic proteins Mfn1, Mfn2, Drp1, and Fis1 was determined using Western blotting. β -Actin served as loading control. (b) Mitochondrial morphology was visualized by transfecting cox4-DsRed (red fluorescence). An enlarged segment of each image was shown by a lower right square. (c) The MicroP algorithm categorized mitochondrial morphology into six types: small globe (blue), large globe (yellow), simple tube (green), twisted tube (orange), donut (red), and branching tube (purple). $N = 75$ –400 mitochondria from 15–30 cells and three independent experiments.

assisted in the visualization of the slides under a fluorescence microscope (Leica, Wetzlar, Germany). The average fluorescence intensity was quantitatively determined using

ImageJ by counting 50–100 cells per field of view, five representative fields per experimental group, and three independent experiments.

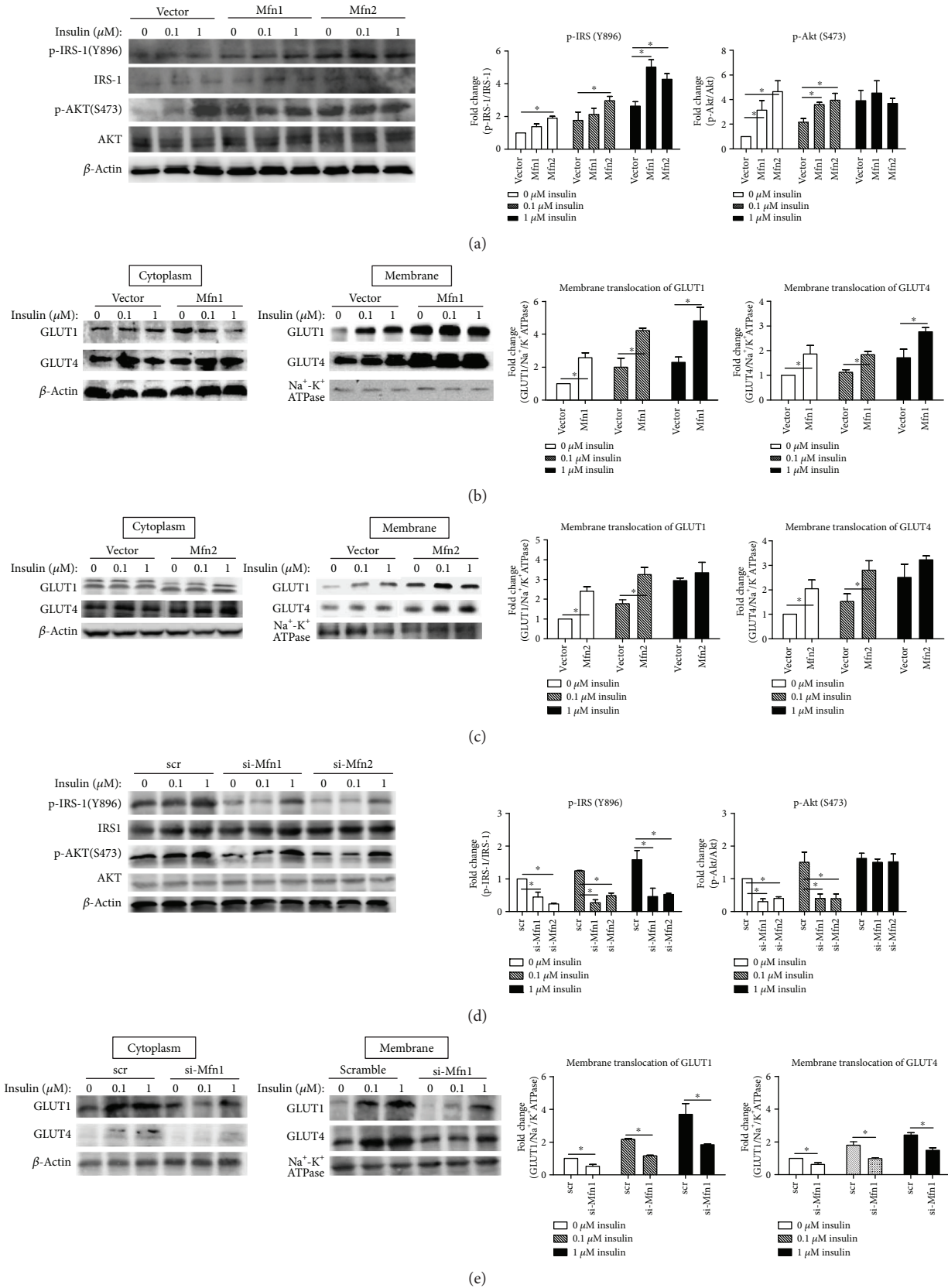
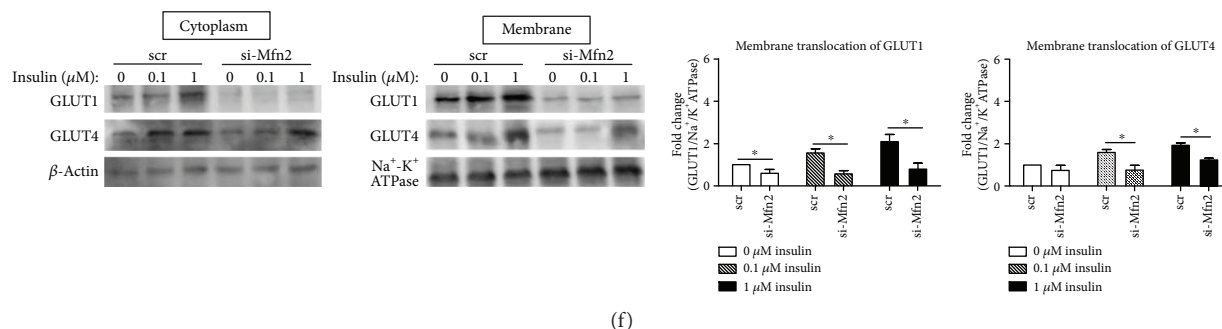


FIGURE 3: Continued.



(f)

FIGURE 3: Both Mfn1 and Mfn2 ameliorate cellular insulin resistance. Cybrid B4 was starved of FBS for 16 h, transfected with plasmid/siRNA for 24/48 h, and then treated with 0, 0.1, or 1 μM insulin for 1 h. (a, d) p-IRS1-1(Y896), IRS-1, p-AKT(S473), and AKT were determined using Western blotting. β -Actin served as loading control. (b, c, e, f) Abundance of GLUT1 and GLUT4 in cytoplasm and membrane subfractionation was probed using Western blotting. β -Actin and $\text{Na}^+\text{-K}^+\text{ATPase}$ served as loading control of cytoplasm and membrane fraction. The quantitative result (mean \pm SEM) was calculated from at least three independent experiments. * $p < 0.05$.

2.6. Western Blotting. The cells were plated at a density of 2×10^6 cells per well in 6-well plates (Nunc, Denmark). Following an overnight incubation, the cells were serum-starved for 16 h, after which they were treated with a medium containing 25 mM glucose and stimulated with 0, 0.1, and 1.0 μM insulin for 30 min. The cells were harvested, after which their protein extract was isolated using a buffer containing 150 mM NaCl, 50 mM HEPES pH 7, 1% Triton X-100, 10% glycerol, 1.5 mM MgCl_2 , 1 mM EGTA, and a protease inhibitor. The proteins were separated via SDS-PAGE by using an 8–10% polyacrylamide gel, and then they were transferred onto a polyvinylidene fluoride (PVDF) membrane (Millipore) by using a blotting apparatus. The membrane was blocked using 5% milk in TBS-T for 1 h at room temperature and then incubated overnight at 4°C with antibodies against anti-GLUT1 (1:1000 dilution from Santa Cruz Biotechnology), anti-GLUT4 (1:1000 dilution from Santa Cruz Biotechnology), anti-IRS1 (Y896) (1:1000 dilution from Epitomics, Inc.), anti-IRS1 (1:2000 dilution from Merck Millipore), p-Akt (S473) (1:1000 dilution from Santa Cruz Biotechnology), anti-Akt (1:1000 dilution from Santa Cruz Biotechnology), and anti- β -actin (1:50000 dilution from Merck Millipore). Further, following conjugation of the secondary antibody with HRP for 60 min, the signals on the membrane were detected using ECL-plus luminal solution (Advansta, USA) and exposed to an X-ray film for autoradiogram.

2.7. Statistical Analysis. The database was created using Microsoft Excel and plotted using GraphPad Prism software programs. The results were expressed as mean \pm standard error (SE). Student's *t*-test was used to compare groups, whereas a one-way analysis of variance was used when more than two groups were compared. A *P* value of less than 0.05 was considered statistically significant. The experiments were conducted at least three times to verify reproducibility.

3. Results

3.1. Mitochondrial Network Can Be Remodeled by Manipulating Mitochondrial Dynamic Genes in Diabetes-Susceptible Cybrid Cell. To examine the causal role of

mitochondrial dynamics in insulin resistance relevant to mtDNA variants, we established cybrid cell harboring diabetes mellitus- (DM-) susceptible mtDNA haplogroup B4 (thereafter DM cybrid) [18] and overexpressed Mfn1, Mfn2, Drp1, and Fis1 in cybrid B4. Overexpression significantly increased mitochondrial dynamic protein abundance (Figure 1(a)). As mitochondrial dynamic proteins govern fusion/fission manner of mitochondria [2], we thus visualized mitochondrial network by transfecting mitochondrial-targeted fluorescent protein cox4-DsRed and quantifies mitochondrial morphology. Overexpression of fusion-related Mfn1 and Mfn2 resulted in an increased tubular network of mitochondria and reduced fragmentation of mitochondria, whereas overexpression of fission-related Drp1 and Fis1 led to a reversed manner (Figures 1(b)–1(d)). Furthermore, we employed siRNA to interfere with endogenous expression of Mfn1, Mfn2, Drp1, and Fis1 to validate their role in the manner of mitochondrial dynamics. The abundance of Mfn1, Mfn2, Drp1, and Fis1 were significantly reduced by siRNA (Figure 2(a)). Knockdown of Mfn1/Mfn2 showed predominantly fragmented mitochondria, while knockdown of Drp1/Fis1 presented mainly networking mitochondria (Figures 2(b)–2(d)). These results demonstrate that manipulating mitochondrial dynamic genes significantly alter mitochondrial network in DM cybrid.

3.2. Mfn1 and Mfn2 Ameliorate Insulin Resistance of Diabetes-Susceptible Cybrid Cell. As shown in Figure 3(a), the level of insulin-induced activation of IRS-1 phosphorylation of Tyr-896 was found to be increased significantly after overexpression of fusion-related proteins (Mfn1/Mfn2). Overexpression of Mfn2 showed increased p-IRS1 in basal and insulin-treated cells, while Mfn1 increased p-IRS1 in insulin-treated cells only (1 μM). Furthermore, the Akt Ser-473 phosphorylation, which served as a downstream regulator of the PI3 kinase pathway, was also increased significantly after overexpression of fusion-related proteins (Mfn1/Mfn2) in DM-susceptible cybrids. This trend was observed both in basal or after insulin (0, 0.1 μM) treatment. The GLUT1 and GLUT4 translocation to the plasma

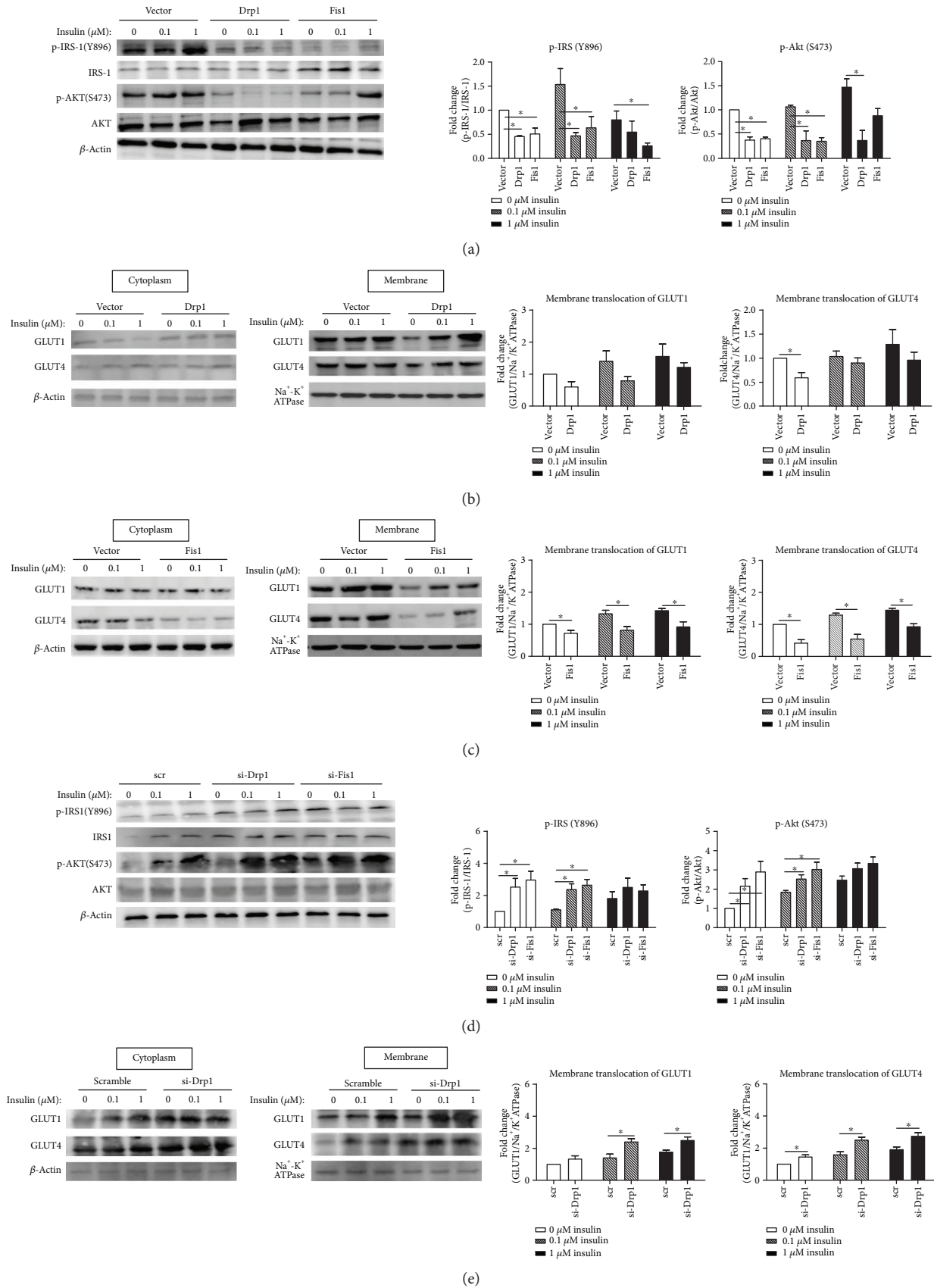


FIGURE 4: Continued.

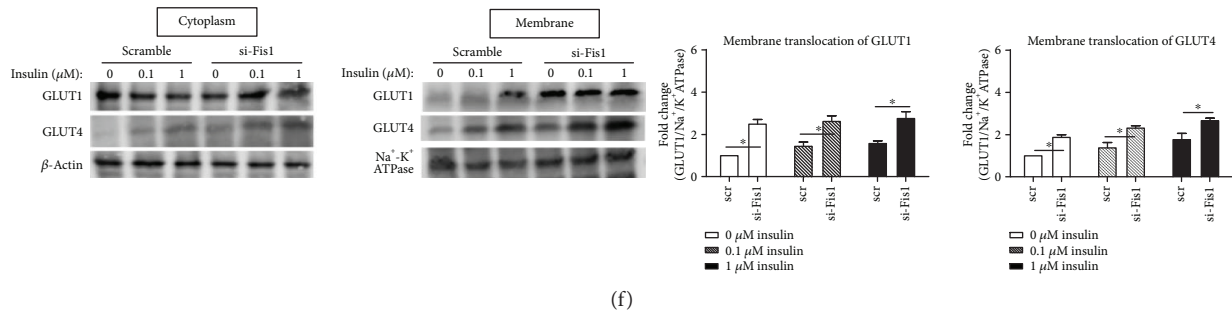


FIGURE 4: Both Drp1 and Fis1 deteriorate cellular insulin resistance. Cybrid B4 was starved of FBS for 16 h, transfected with plasmid/siRNA for 24/48 h, and then treated with 0, 0.1, or 1 μM insulin for 1 h. (a, d) p-IRS1-1(Y896), IRS-1, p-AKT(S473), and AKT were determined using Western blotting. β -Actin served as loading control. (b, c, e, f) Abundance of GLUT1 and GLUT4 in cytoplasm and membrane subfraction at ion was probed using Western blotting. β -Actin and $\text{Na}^+\text{-K}^+\text{ATPase}$ served as loading control of cytoplasm and membrane fraction. The quantitative result (mean \pm SEM) was calculated from at least three independent experiments. * $p < 0.05$.

membrane in DM-susceptible cybrids increased significantly after overexpression of fusion-related proteins (Mfn1/Mfn2) in basal and insulin-treated cells (Figures 3(b) and 3(c)). In contrast, knockdown of fusion-related molecules (Mfn1/Mfn2) significantly decreased the level of basal and insulin-induced activation of IRS-1 and Akt phosphorylation (Figure 3(d)). Furthermore, knockdown of fusion-related molecules decreased the GLUT1/GLUT4 translocation to the plasma membrane in DM-susceptible cybrids (Figures 3(e) and 3(f)). In Mfn1 overexpression cybrids, the trend was both in basal and insulin-treated cells, while the trend in Mfn2 cybrids was in insulin-treated cells only.

3.3. Drp1 and Fis1 Deteriorate Insulin Resistance of Diabetes-Susceptible Cybrid Cell. As shown in Figure 4(a), the level of both basal and insulin-induced activation of IRS-1 phosphorylation of Tyr-896 was found to be decreased significantly after overexpression of fission-related proteins (Drp1/Fis1). The Akt Ser-473 phosphorylation was also decreased significantly after overexpression of fission-related proteins (Drp1/Fis1) both in basal and after insulin treatment. The GLUT1 and GLUT4 translocation to plasma membrane decreased significantly after overexpression of Fis1 proteins in both basal and insulin-treated cells (Figure 4(c)), while only GLUT4 translocation decreased in basal condition after overexpression of Drp1 proteins (Figure 4(b)). In contrast, knockdown of fission-related molecules (Drp1/Fis1) ameliorate insulin resistance of diabetes-susceptible cybrid cells. Knockdown of Drp1/Fis1 significantly increased the level of basal and insulin-induced activation of IRS-1 and Akt phosphorylation (Figure 4(d)). Furthermore, knockdown of fission-related molecules increased the GLUT1/GLUT4 translocation to the plasma membrane in DM-susceptible cybrids (Figures 4(e) and 4(f)).

3.4. Pharmacologically Inhibiting Mitochondrial Fission Also Improves Insulin Resistance of Diabetes-Susceptible Cybrid Cell. We employed Drp1 inhibitor, mdivi-1, to interfere with endogenous expression of fission to validate the pharmacological effects on IR. The abundance of both p-Drp1 and Drp-1 were significantly reduced by mdivi-1 (Figure 5(a)).

The mitochondrial network was increased by mdivi-1 resulting in an increased tubular network of mitochondria and reduced fragmentation of mitochondria (Figures 5(b)–5(d)). As to IR, the level of activation of IRS-1 phosphorylation of Tyr-896 and the Akt Ser-473 phosphorylation were increased significantly both in basal and after insulin treatment (0, 0.1 μM) (Figure 5(e)). Furthermore, the GLUT1 and GLUT4 translocation to the plasma membrane in DM-susceptible cybrids was also increased significantly after mdivi-1 treatment both in basal and insulin-treated cells (0, 0.1 μM) (Figure 5(f)).

3.5. Dynamic Proteins Modulate Mitochondrial ROS in Cybrid B4. In our previous work [17], we have verified the imbalance of mtDYN toward a profission state in cybrid B4 and antioxidant treatment reverse it to a profusion manner. In this study, we further tested whether mtDYN may affect the expression of mtROS. As shown in Figure 6(a), overexpression of MFN1 or MFN2 reduced mtROS, while knockdown has an opposing effect (Figure 6(b)). In contrast, overexpression of DRP1 or FIS1 increased mtROS (Figure 6(a)), while knockdown has an opposing effect (Figure 6(b)). Pharmacologically inhibiting mitochondrial fission by the Drp1 inhibitor, mdivi-1 (10 μM , 24 hr), also reduced mtROS (Figure 6(c)).

3.6. The Role of Mitochondrial Dynamics in Regulating Insulin Resistance. In our previous and current reports with clinical and in vitro studies, we conclude that mitochondrial genotypes and quality control were related to insulin resistance (Figure 7).

4. Discussion

In our previous clinical studies, we found that mitochondrial haplogroup B4, consisting of 16189T \rightarrow C transition and 10398A allele, are diabetes-susceptible risk factor [15]. By the construction of transmitochondrial cybrid cell, we verified the impact of haplogroup B4 on cellular IR [16] as well as the imbalance of mitochondrial dynamics [17]. Both defects, IR and profission mtDYN, are reversed by antioxidant treatment [16, 17]. Here, we further demonstrate

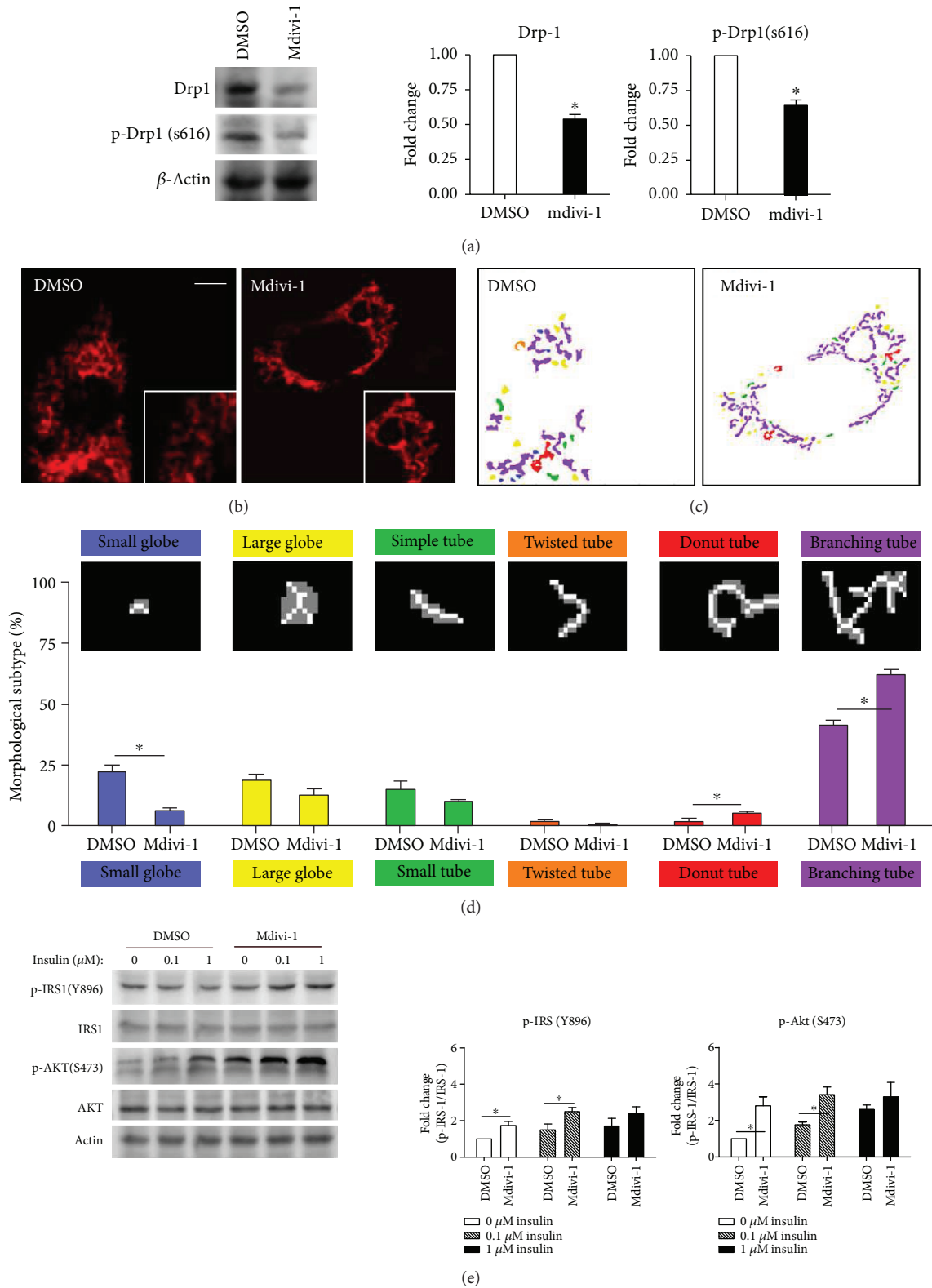
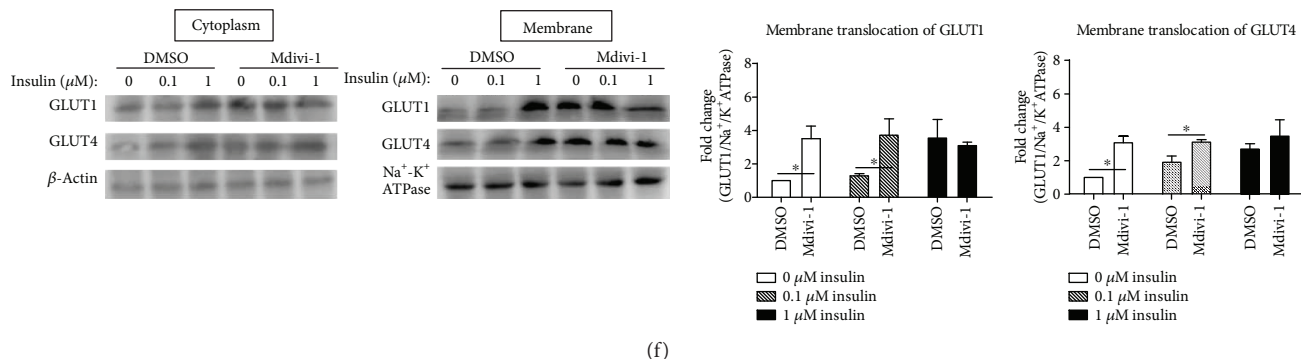


FIGURE 5: Continued.



(f)

FIGURE 5: Insulin resistance of cybrid B4 was improved by mdivi-1, which suppresses mitochondrial fission and promotes fusion. 10 μ M mdivi-1 was used to inhibit mitochondrial fission. For probing cellular insulin resistance, cybrid B4 was starved of FBS for 16 h, then incubated with mdivi-1 for 24 h, and finally treated with 0, 0.1, or 1 μ M insulin for 1 h. (a) The action of Drp1 inhibitor, mdivi-1, was determined using level of p-Drp1(S616) and Drp-1. β -Actin served as loading control. (b) Mitochondrial morphology was visualized by transfecting cox4-DsRed (red fluorescence). An enlarged segment of each image was shown by a lower right square. (c-d) The MicroP algorithm categorized mitochondrial morphology into six types: small globe (blue), large globe (yellow), simple tube (green), twisted tube (orange), donut (red), and branching tube (purple). $N = 75-400$ mitochondria from 15-30 cells and three independent experiments. (e) p-IRS1-1(Y896), IRS-1, p-AKT(S473), and AKT were determined using Western blotting. β -Actin served as loading control. (f) Abundance of GLUT1 and GLUT4 in cytoplasm and membrane subfractionation was probed using Western blotting. β -Actin and Na^+ -K⁺ATPase served as loading control of cytoplasm and membrane fraction. The quantitative result (mean \pm SEM) of Western blotting was calculated from at least three independent experiments. * $p < 0.05$.

the causal role of mitochondrial dynamics in IR by manipulating the expressions of dynamic proteins in diabetes-susceptible cybrid cells. Overexpression of fusion-related proteins (Mfn1/Mfn2) and inhibition of fission-related proteins (Drp1/Fis1) enhance mitochondria network and reverse the IR by activating the IRS1-Akt pathway and inducing the GLUT1/GLUT4 translocation to the cell membrane. Pharmacological inhibition of DRP1 by mdivi-1 also reveals improvement of IR, making it probable to be a new era of diabetes treatment.

Mitochondrial dynamics undergo fission and fusion to repair damaged components of the mitochondrial homeostasis. This regulation via the fission process allows for segregation of damaged mitochondria and the fusion process allows the exchange of material between healthy mitochondria [19, 20]. Previous reports in humans and animal models that showed the trend of dynamic proteins toward fission was related to IR/T2D. T2D patients and obese subjects show a reduction in mitofusin 2 (Mfn2) expression in skeletal muscle compared to controls [11], and exercise increases insulin sensitivity in association with a decrease in muscle dynamin-related protein 1 (Drp1) in obese and insulin-resistant humans [21]. As to animal studies, a reduction in the mitochondrial network in the skeletal muscle of obese Zucker rats [6], leptin-deficient (*ob/ob*) mice, and diet-induced obese C57BL/6 mice [9] has been reported. The mitochondria in pancreatic islets from RIP2-Opa1KO mice, which displayed hallmarks of diabetes, were shorter and fragmented with decreased ATP production [8]. Liver-specific ablation of Mfn2 in mice led to numerous metabolic abnormalities, which was characterized by glucose intolerance and enhanced hepatic gluconeogenesis [4]. An increase in Drp1-dependent mitochondrial fission in the muscle was associated with IR in rodents, and inhibition of

mitochondrial fission improved the muscle insulin signaling of obese mice [9]. More recently, in the dorsal vagal complex of the high-fat feeding rat, Drp1-dependent mitochondrial fission regulate insulin action and targeting the Drp1-mitochondrial-dependent pathway in the brain may have therapeutic potential in IR [22].

Alterations or mutations in mitochondrial fusion and fission proteins have been identified to be associated with the nutrient availability and energy demand. Mitochondrial fragmentation is caused by nutrient excess, while mitochondrial elongation is induced by nutrient withdrawal in mouse embryonic fibroblast [3, 23, 24]. Furthermore, mitochondria fuse to form elongated mitochondria to maximize ATP production during nutrient shortage, whereas mitochondria tend to form fragmented mitochondrion to prevent overt ATP synthesis during nutrient excess [25]. The molecular events causing diabetes and its complications have been focused on the oxidative stress and chronic inflammation in affected tissue [26]. Recent studies have shown that mitochondria not only generate energy for the physiological process but also emerge as a fundamental hub for innate antiviral immunity [27, 28]. Mitochondrial dynamics may be proposed as a bridge between nutrient excess and chronic inflammation in diabetes.

Before the current study, although the contribution of mitochondrial fusion and fission in IR in human and rodents is reported, it remains unclear whether changes in mtDYN directly affect insulin action with the diabetes-susceptible genotype background. Here, we further prove that restoring mitochondrial network by either overexpression of fusion-related (Mfn1/Mfn2) proteins or inhibition of fission-related proteins (Drp1/Fis1) in diabetes-susceptible cybrids, impaired insulin signaling, and GLUT1/GLUT4 translocation to cell membrane can be repaired both in basal

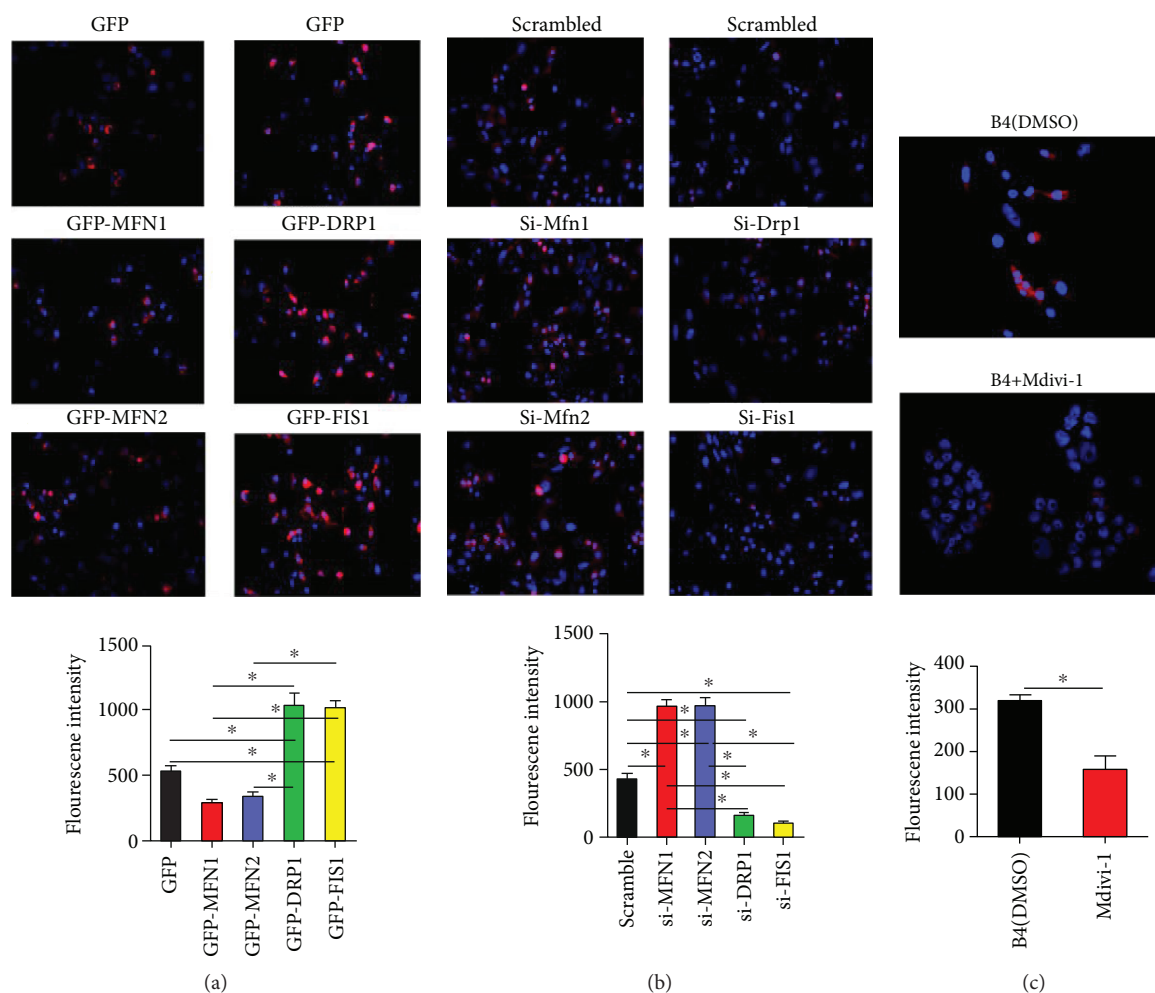


FIGURE 6: Dynamic proteins modulate mitochondrial ROS in cybrid B4. (a) Cybrid B4 was transfected with plasmid for 24 h to overexpress particular dynamic proteins. (b) Cybrid B4 was transfected with siRNA for 48 h to knockdown particular dynamic proteins. (c) Cybrid B4 was treated with 10 μ M mdivi-1 for 24 h to inhibit mitochondrial fission. Mitochondrial ROS production was visualized using MitoSOXRed, which was nuclear counterstained using DAPI. Fluorescent intensity of mitochondrial ROS was quantified using ImageJ. * $p < 0.05$ between indicated groups.

condition and in response to insulin stimulation. Furthermore, Mdivi-1, a chemical compound which attenuates mitochondrial fission by selectively blocking GTPase activity of Drp1 [29], reversed mitochondrial genotype-related imbalance of dynamics and ameliorated the impairment of insulin signal transduction in our diabetes-susceptible cybrid cells. Our data support that mitochondrial dynamic proteins per se play a causal role in IR, and the conclusion is partially supported by the previous studies [9, 22], which demonstrated that inhibition of Drp1-dependent mitochondrial fission pathway had therapeutic potential in IR in animal studies.

Besides IR, an imbalance of mitochondrial networks in neurons favoring mitochondrial fission plays a critical role in the pathogenesis of diabetic neuropathy [30, 31]. Mitochondrial fission also occurs in the kidneys and heart after acute ischemia/reperfusion injury in mice, and prevention of this process is beneficial [32, 33]. Moreover, preserving mitochondrial dynamics protected beta-cells from glucose

and palmitic acid-induced pancreatic beta-cell mitochondrial fragmentation and apoptosis [23, 34]. Genetic or pharmacological activation of Akt protected the heart against acute ischemia injury is proved by the effect of Akt-mediated mitochondrial elongation [35]. Cardiac mitochondria have been recognized to play an important role in diabetic cardiomyopathy, heart failure, and pulmonary hypertension. The potential of mitochondrial dynamics as therapeutic targets in tackling cardiovascular disease has been reviewed [36]. Therefore, Mdivi-1 may provide the potential for therapeutic use not only in IR but also in diabetes-related target organ damage. However, there are still many challenges remained to be addressed before it might be applied clinically. Its potential side effects include arrhythmia and cytotoxic to nontarget tissue [37].

Of note, a mutual interaction between mtROS and mtDYN is demonstrated in our studies. In our previous studies, cybrid harboring diabetes-susceptible mitochondrial haplogroup B4 showed fragmented mitochondrial

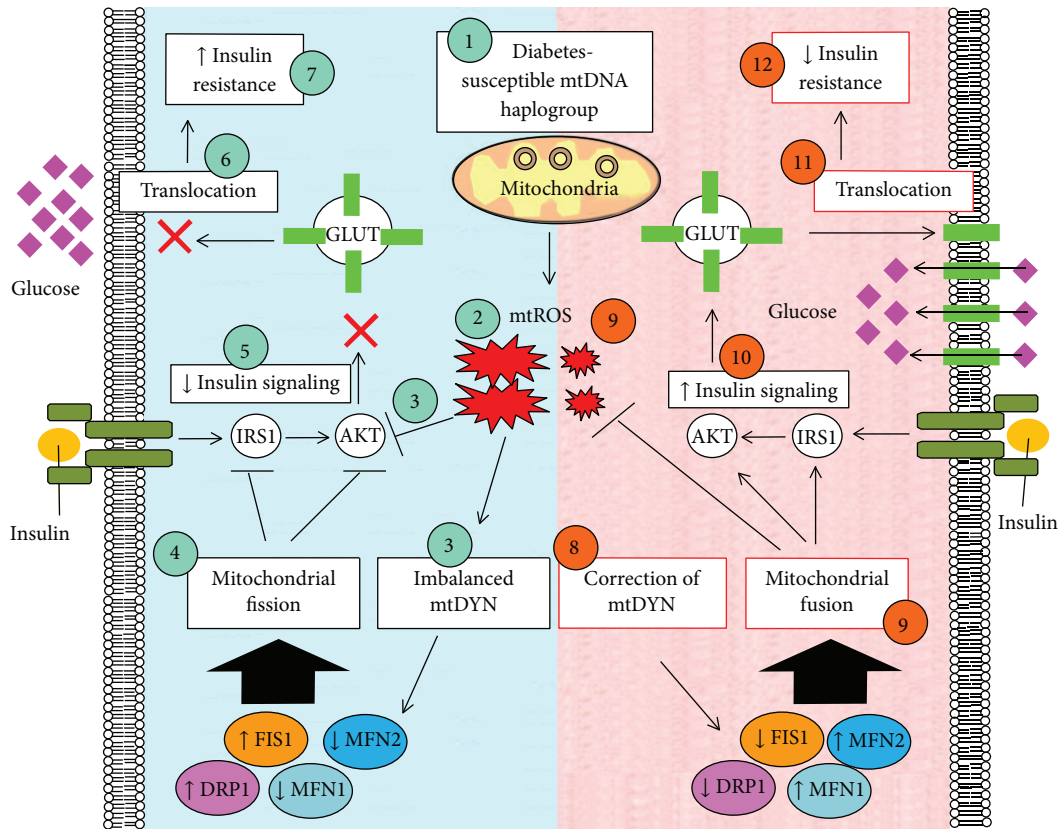


FIGURE 7: Graphic summary delineates the causal role of mitochondrial dynamics in regulating insulin resistance of diabetes through mtROS. (1-2) Diabetes-susceptible haplogroup B4 demonstrates increased mtROS expression. (3-4) Increased mtROS contributes to insulin resistance and imbalanced profile of mitochondrial dynamics: enhanced fission proteins (Drp1 and Fis1) and reduced fusion proteins (Mfn1 and Mfn2), which ultimately contributes to mitochondrial fission (Kuo et al., 2016; Weng et al., 2013). (5-7) Mitochondrial fission inhibits insulin-activated IRS1-AKT signaling, which subsequently hinders GLUTs from translocating to cellular membrane and leads to insulin resistance. (8) Either genetic manipulation or pharmacological intervention effectively (9) correct mitochondrial dynamics toward a profile of fusion and simultaneously suppresses mtROS expression, which (10) boost insulin-activated IRS1-AKT signaling, and consequently (11) activates GLUTs translocation to cellular membrane and finally (12) improving insulin resistance.

morphology, increased ROS, IR, and mitochondrial dysfunction. All the defects can be improved by antioxidant agent N-acetylcysteine (NAC) [16, 17] that is manipulating ROS, which can alter the dynamics of mitochondria. In the current study, we further prove that manipulating dynamics of mitochondria can alter mtROS. Therefore, the causal role of mtDYN in regulating IR is probably linked through mtROS.

In conclusion, mtDYN play a causal role in diabetes-susceptible mitochondrial haplogroup-related IR. Direct intervention to correct the imbalance of mtDYN, especially reversing profission, provides a novel therapeutic strategy for IR and T2D.

Abbreviations

Cybrid:	Cytoplasmic hybrid
DAPI:	4',6-diamidino-2-phenylindole
DMEM:	Dulbecco's modified eagle medium
DRP1:	Dynamin-related protein 1
FIS1:	Mitochondrial fission 1 protein
GLUT1/GLUT4:	Glut1/Glut4 glucose transporters

H ₂ O ₂ :	Hydrogen peroxide
IR:	Insulin resistance
IRS1:	Insulin receptor substrate 1
MFN1 and MFN2:	Mitofusins 1 and 2
mtDNA:	Mitochondrial DNA
NAC:	N-acetyl-L-cysteine
OCR:	Oxygen consumption rate
OPA1:	Optic atrophy gene 1
PI3K:	Phosphatidylinositol 3 (PI3)-kinase
ROS:	Reactive oxygen species
SE:	Standard error
T2DM:	Type 2 diabetes.

Data Availability

All the data supporting the results were shown in the paper and can be applicable to the corresponding author.

Conflicts of Interest

The authors declare no competing financial interest.

Authors' Contributions

H.Y.L. and S.W.W. conducted and designed the experiments, performed the data analyses, and wrote the manuscript. J.H.C., T.K.L., and C.W.L. designed the experiments and contributed to the discussion. Y.H.C., Y. J.S., F.C.S., C.M.C., C.J.T., and C.Y.L. assisted in the experiments and contributed to the discussion. P.W.W. supervised the project, designed the experiments, and edited the manuscript.

Acknowledgments

This work was supported by grants from Chang Gung Memorial Hospital (CMRPG891113, CMRPG8D0891, and CMRPG8D0892) and the Ministry of Science and Technology, Taiwan (MOST 101-2314-B-182A-123-MY3, 104-2314-B-182A-065-MY2). The authors acknowledge the kind gifts, Cox4-DsRed, from Dr. David Chan (California Institute of Technology, Pasadena, CA 91125, USA).



References

- [1] S. B. Vafai and V. K. Mootha, "Mitochondrial disorders as windows into an ancient organelle," *Nature*, vol. 491, no. 7424, pp. 374–383, 2012.
- [2] D. C. Chan, "Fusion and fission: interlinked processes critical for mitochondrial health," *Annual Review of Genetics*, vol. 46, no. 1, pp. 265–287, 2012.
- [3] M. Liesa and O. S. Shirihai, "Mitochondrial dynamics in the regulation of nutrient utilization and energy expenditure," *Cell Metabolism*, vol. 17, no. 4, pp. 491–506, 2013.
- [4] D. Sebastian, M. I. Hernandez-Alvarez, J. Segales et al., "Mitofusin 2 (Mfn2) links mitochondrial and endoplasmic reticulum function with insulin signaling and is essential for normal glucose homeostasis," *Proceedings of the National Academy of Sciences of the United States of America*, vol. 109, no. 14, pp. 5523–5528, 2012.
- [5] D. Sebastián, E. Soriano, J. Segalés et al., "Mfn2 deficiency links age-related sarcopenia and impaired autophagy to activation of an adaptive mitophagy pathway," *The EMBO Journal*, vol. 35, no. 15, pp. 1677–1693, 2016.
- [6] D. Bach, S. Pich, F. X. Soriano et al., "Mitofusin-2 determines mitochondrial network architecture and mitochondrial metabolism. A novel regulatory mechanism altered in obesity," *Journal of Biological Chemistry*, vol. 278, no. 19, pp. 17190–17197, 2003.
- [7] R. Liu, P. Jin, L. Yu et al., "Impaired mitochondrial dynamics and bioenergetics in diabetic skeletal muscle," *PLoS One*, vol. 9, no. 3, article e92810, 2014.
- [8] Z. Zhang, N. Wakabayashi, J. Wakabayashi et al., "The dynamin-related GTPase Opa1 is required for glucose-stimulated ATP production in pancreatic beta cells," *Molecular Biology of the Cell*, vol. 22, no. 13, pp. 2235–2245, 2011.
- [9] H. F. Jheng, P. J. Tsai, S. M. Guo et al., "Mitochondrial fission contributes to mitochondrial dysfunction and insulin resistance in skeletal muscle," *Molecular and Cellular Biology*, vol. 32, no. 2, pp. 309–319, 2012.
- [10] L. Wang, T. Ishihara, Y. Ibayashi et al., "Disruption of mitochondrial fission in the liver protects mice from diet-induced obesity and metabolic deterioration," *Diabetologia*, vol. 58, no. 10, pp. 2371–2380, 2015.
- [11] A. Zorzano, M. Liesa, and M. Palacin, "Mitochondrial dynamics as a bridge between mitochondrial dysfunction and insulin resistance," *Archives of Physiology and Biochemistry*, vol. 115, no. 1, pp. 1–12, 2009.
- [12] L. Stiles and O. S. Shirihai, "Mitochondrial dynamics and morphology in beta-cells," *Best Practice & Research Clinical Endocrinology & Metabolism*, vol. 26, no. 6, pp. 725–738, 2012.
- [13] B. B. Lowell and G. I. Shulman, "Mitochondrial dysfunction and type 2 diabetes," *Science*, vol. 307, no. 5708, pp. 384–387, 2005.
- [14] N. Diaz-Morales, S. Rovira-Llopis, C. Bañuls et al., "Are mitochondrial fusion and fission impaired in leukocytes of type 2 diabetic patients?," *Antioxidants & Redox Signaling*, vol. 25, no. 2, pp. 108–115, 2016.
- [15] C. W. Liou, J. B. Chen, M. M. Tiao et al., "Mitochondrial DNA coding and control region variants as genetic risk factors for type 2 diabetes," *Diabetes*, vol. 61, no. 10, pp. 2642–2651, 2012.
- [16] S. W. Weng, H. M. Kuo, J. H. Chuang et al., "Study of insulin resistance in cybrid cells harboring diabetes-susceptible and diabetes-protective mitochondrial haplogroups," *Mitochondrion*, vol. 13, no. 6, pp. 888–897, 2013.
- [17] H. M. Kuo, S. W. Weng, A. Y. W. Chang et al., "Altered mitochondrial dynamics and response to insulin in cybrid cells harboring a diabetes-susceptible mitochondrial DNA haplogroup," *Free Radical Biology & Medicine*, vol. 96, pp. 116–129, 2016.
- [18] T. K. Lin, H. Y. Lin, S. D. Chen et al., "The creation of cybrids harboring mitochondrial haplogroups in the Taiwanese population of ethnic Chinese background: an extensive *in vitro* tool for the study of mitochondrial genomic variations," *Oxidative Medicine and Cellular Longevity*, vol. 2012, Article ID 824275, 13 pages, 2012.
- [19] A. M. van der Bliek, Q. Shen, and S. Kawajiri, "Mechanisms of mitochondrial fission and fusion," *Cold Spring Harbor Perspectives in Biology*, vol. 5, no. 6, 2013.
- [20] H. M. Ni, J. A. Williams, and W. X. Ding, "Mitochondrial dynamics and mitochondrial quality control," *Redox Biology*, vol. 4, pp. 6–13, 2015.
- [21] C. E. Fealy, A. Mulya, N. Lai, and J. P. Kirwan, "Exercise training decreases activation of the mitochondrial fission protein dynamin-related protein-1 in insulin-resistant human skeletal muscle," *Journal of Applied Physiology*, vol. 117, no. 3, pp. 239–245, 2014.
- [22] B. M. Filippi, M. A. Abraham, P. N. Silva et al., "Dynamin-related protein 1-dependent mitochondrial fission changes in the dorsal vagal complex regulate insulin action," *Cell Reports*, vol. 18, no. 10, pp. 2301–2309, 2017.
- [23] A. J. A. Molina, J. D. Wikstrom, L. Stiles et al., "Mitochondrial networking protects beta-cells from nutrient-induced apoptosis," *Diabetes*, vol. 58, no. 10, pp. 2303–2315, 2009.
- [24] L. C. Gomes, G. Di Benedetto, and L. Scorrano, "Essential amino acids and glutamine regulate induction of mitochondrial elongation during autophagy," *Cell Cycle*, vol. 10, no. 16, pp. 2635–2639, 2011.
- [25] P. Mishra and D. C. Chan, "Metabolic regulation of mitochondrial dynamics," *The Journal of Cell Biology*, vol. 212, no. 4, pp. 379–387, 2016.
- [26] M. Brownlee, "Biochemistry and molecular cell biology of diabetic complications," *Nature*, vol. 414, no. 6865, pp. 813–820, 2001.

- [27] E. L. Mills, B. Kelly, and L. A. J. O'Neill, "Mitochondria are the powerhouses of immunity," *Nature Immunology*, vol. 18, no. 5, pp. 488–498, 2017.
- [28] M. Pourcelot and D. Arnoult, "Mitochondrial dynamics and the innate antiviral immune response," *The FEBS Journal*, vol. 281, no. 17, pp. 3791–3802, 2014.
- [29] A. Cassidy-Stone, J. E. Chipuk, E. Ingerman et al., "Chemical inhibition of the mitochondrial division dynamin reveals its role in Bax/Bak-dependent mitochondrial outer membrane permeabilization," *Developmental Cell*, vol. 14, no. 2, pp. 193–204, 2008.
- [30] J. L. Edwards, A. Quattrini, S. I. Lentz et al., "Diabetes regulates mitochondrial biogenesis and fission in mouse neurons," *Diabetologia*, vol. 53, no. 1, pp. 160–169, 2010.
- [31] A. M. Vincent, J. L. Edwards, L. L. McLean et al., "Mitochondrial biogenesis and fission in axons in cell culture and animal models of diabetic neuropathy," *Acta Neuropathologica*, vol. 120, no. 4, pp. 477–489, 2010.
- [32] S. B. Ong, S. Subrayan, S. Y. Lim, D. M. Yellon, S. M. Davidson, and D. J. Hausenloy, "Inhibiting mitochondrial fission protects the heart against ischemia/reperfusion injury," *Circulation*, vol. 121, no. 18, pp. 2012–2022, 2010.
- [33] C. Brooks, Q. Wei, S. G. Cho, and Z. Dong, "Regulation of mitochondrial dynamics in acute kidney injury in cell culture and rodent models," *The Journal of Clinical Investigation*, vol. 119, no. 5, pp. 1275–1285, 2009.
- [34] X. Men, H. Wang, M. Li et al., "Dynamin-related protein 1 mediates high glucose induced pancreatic beta cell apoptosis," *The International Journal of Biochemistry & Cell Biology*, vol. 41, no. 4, pp. 879–890, 2009.
- [35] S. B. Ong, A. R. Hall, R. K. Dongworth et al., "Akt protects the heart against ischaemia-reperfusion injury by modulating mitochondrial morphology," *Thrombosis and Haemostasis*, vol. 113, no. 3, pp. 513–521, 2015.
- [36] S. B. Ong and D. J. Hausenloy, "Mitochondrial dynamics as a therapeutic target for treating cardiac diseases," *Handbook of Experimental Pharmacology*, vol. 240, pp. 251–279, 2017.
- [37] A. A. Rosdah, J. K. Holien, L. M. D. Delbridge, G. J. Dusting, and S. Y. Lim, "Mitochondrial fission - a drug target for cytoprotection or cytodestruction?," *Pharmacology Research & Perspectives*, vol. 4, no. 3, article e00235, 2016.

Research Article

Superoxide Anion Production and Bioenergetic Profile in Young and Elderly Human Primary Myoblasts

Mariangela Marrone,^{1,2} Rita Maria Laura La Rovere,³ Simone Guarnieri ¹,
Ester Sara Di Filippo,^{1,2} Giovanni Monaco,³ Tiziana Pietrangelo,^{1,2} Geert Bultynck,³
Stefania Fulle ,^{1,2} and Rosa Mancinelli^{1,2}

¹Department of Neuroscience Imaging and Clinical Sciences, University “G. d’Annunzio” Chieti-Pescara, Via dei Vestini 29, 66100 Chieti, Italy

²Interuniversity Institute of Myology (IIM), Chieti, Italy

³Laboratory of Molecular and Cellular Signaling, KU Leuven, Campus Gasthuisberg O/N-I bus 802, Herestraat 49, 3000 Leuven, Belgium

Correspondence should be addressed to Stefania Fulle; stefania.fulle@unich.it

Received 10 March 2018; Revised 23 May 2018; Accepted 25 June 2018; Published 24 July 2018

Academic Editor: Julio C. B. Ferreira

Copyright © 2018 Mariangela Marrone et al. This is an open access article distributed under the Creative Commons Attribution License, which permits unrestricted use, distribution, and reproduction in any medium, provided the original work is properly cited.

Sarcopenia is the age-related loss of skeletal muscle mass, strength, and function. It is associated with regenerative difficulties by satellite cells, adult muscle stem cells, and alteration of oxidative management, mainly the increase in superoxide anions ($O_2^{\bullet-}$). We aimed to investigate the relation between regenerative deficit in elderly and increase in $O_2^{\bullet-}$ production along with mitochondrial alterations. Myoblasts and myotubes from skeletal muscle of young and elderly healthy subjects (27.8 ± 6 and 72.4 ± 6.5 years old) were measured: (1) superoxide dismutase activity and protein content, (2) mitochondrial $O_2^{\bullet-}$ production levels, (3) $O_2^{\bullet-}$ production variability, and (4) mitochondrial bioenergetic profile. Compared to young myoblasts, elderly myoblasts displayed decreased SOD2 protein expression, elevated mitochondrial $O_2^{\bullet-}$ baseline levels, and decreased oxidative phosphorylation and glycolysis. Additionally, elderly versus young myotubes showed elevated mitochondrial $O_2^{\bullet-}$ levels when stressed with N-acetyl cysteine or high glucose and higher glycolysis despite showing comparable oxidative phosphorylation levels. Altogether, the elderly may have less metabolic plasticity due to the impaired mitochondrial function caused by $O_2^{\bullet-}$. However, the increased energy demand related to the differentiation process appears to activate compensatory mechanisms for the partial mitochondrial dysfunction.

1. Introduction

Sarcopenia is defined as the age-related loss of muscle mass, strength, and function [1]. In particular, the aging process is associated with a consistent decrease in the ability of muscle tissue to regenerate following injury or overuse due to the impairment of intervening satellite cells [2]. In response to muscle damage, satellite cells, undifferentiated quiescent mononucleated cells present in muscle [3], which have properties of stem cells, are activated to proliferate as human primary myoblasts. Proliferating myoblasts migrate to the damaged region of the fiber, where they differentiate and fuse

to form myotubes via a similar process to that of myogenesis [4]. However, this capacity is reduced in the elderly, where satellite cells are unable to execute the complete repair process or they exhibit a slow recovery [5–7]. Activation and proliferation stages of satellite cells are characterized by the expression of myogenic regulatory factors (MRFs), and the phases of this process typically involve the sequential expression of proteins, including Pax3 (quiescent satellite cells), myoD (proliferating primary myoblasts), and myogenin (differentiated myoblasts). We previously demonstrated that the impaired regenerative potential in elderly primary myoblasts is related to dysregulation in myogenin and miR-1 and 133b

gene expression together with an overproduction of reactive oxygen species (ROS) [8]. Indeed, the mechanisms behind the impaired myogenic differentiation process of elderly people are multifactorial and they appear to involve an imbalance between ROS production and antioxidant enzyme activity. Thus, oxidative stress can be generated in the cells as a result of one or more of three factors: (i) increase in oxidant generation, (ii) decrease in antioxidant protection, and (iii) failure to repair oxidative damage. ROS cause damage to lipids, nucleic acids, and proteins [9]. Mitochondria are commonly considered as the source and target of ROS in many cell models including skeletal muscle cells. Noteworthy, as myoblast differentiation is accompanied by intensive mitochondrial biogenesis, the generation of intracellular ROS is also increased during myogenesis [10], thus playing a fundamental role in aging. Aging is associated with a decline in mitochondrial function and the accumulation of abnormal mitochondria [11]. Indeed, several studies demonstrate that a link exists between increased mitochondrial dysfunction and increased ROS production in sarcopenic skeletal muscle [12]. The electron transfer for complete reduction of oxygen by mitochondrial complexes I and III–IV could be the main source of ROS, and specifically $O_2^{\bullet-}$ [13]. The major class of enzymatic antioxidants is the superoxide dismutase (SOD) family that catalyze the dismutation of $O_2^{\bullet-}$ to hydrogen peroxide (H_2O_2) [14]. Subsequently, H_2O_2 is quickly reduced to water by two other enzymes, catalase and glutathione peroxidase. The isoforms of SOD are different in their cellular location: SOD1 is located in cytosol and mitochondrial intermembrane space, SOD2 in mitochondrial matrix, and SOD3 in extracellular space. Mitochondria are also the “powerhouse” of the cells producing energy in the form of adenosine triphosphate (ATP) [15, 16]. In eukaryotes, ATP is mainly produced by two different processes: through the breakdown of glucose or other sugars in the cytosol (anaerobic glycolysis) or by the metabolism of fatty acids, sugars (aerobic glycolysis), and proteins in the mitochondria, solely in the presence of oxygen (oxidative phosphorylation (OXPHOS)). The glycolytic pathway converts glucose to pyruvate in an oxygen-independent biochemical reaction resulting in ATP production. One fate of the pyruvate is reduction to lactate in the cytosol with net proton production, acidifying the medium. Protons are pumped out of the cell by various mechanisms to maintain the intracellular pH [17], and the efflux of the protons into the extracellular space or medium surrounding the cells causes extracellular acidification [18, 19]. The major nutrient substrates glucose, glutamine, and fatty acids can be completely oxidized into CO_2 and H_2O via the mitochondrial tricarboxylic acid cycle (TCA) and associated OXPHOS. OXPHOS takes place through the respiratory chain, namely, complexes I–V, that transfers electrons obtained from TCA NADH or $FADH_2$ across the mitochondrial inner membrane and the terminal electron acceptor, oxygen (O_2). More in detail, the electron transport chain passes a high energy electron at the inner mitochondrial membrane pumping hydrogen out of the matrix space, creating a proton motive force (Δp) across the inner membrane with both electrical ($\Delta \Psi_m$) and chemical (ΔpH) components [20]. The gradient created drives

hydrogen back through the membrane, through ATP synthase that couples it to ATP production by OXPHOS. The CO_2 produced can be converted to bicarbonate and protons as catalyzed by carbonic anhydrase [17], another source of protons causing medium acidification. The OXPHOS is a process through which ADP is phosphorylated in ATP by the energy derived from the oxidation of nutrients in aerobic condition. It takes place through the respiratory chain, named complexes I–V conducting electron transfer across the mitochondrial inner membrane.

Although the major part of oxygen is used for ATP synthesis (coupled respiration), the mitochondrial membrane is leaky and protons may leak back through the membrane, increasing oxygen consumption (uncoupled respiration). There are three leak events: complex I leaks $O_2^{\bullet-}$ towards the mitochondrial matrix, while complex III leaks $O_2^{\bullet-}$ towards both the intermembrane space and the mitochondrial matrix [21, 22].

We hypothesized that the deficit in regeneration in elderly could be related to the increased $O_2^{\bullet-}$ production and mitochondrial alterations. To verify this, primary myoblasts were isolated from human skeletal muscle of young and aged healthy subjects and measured as undifferentiated and differentiated cells: (1) SOD activity and protein content, (2) mitochondrial $O_2^{\bullet-}$ production, (3) variability in $O_2^{\bullet-}$ production, and (4) mitochondrial bioenergetics profile. The data from this study suggest that in elderly primary myoblasts, the metabolic machinery may not work properly. The analysis of the bioenergetic profile in elderly myoblasts seems to suggest a defect in mitochondrial function and a different metabolic plasticity with respect to young ones. Although elderly and young myotubes showed a similar oxidative metabolism, surprisingly in elderly myotubes, we found an increased level of mitochondrial superoxide anion relying more on the glycolysis processes. Taken together, these findings would suggest a glycolytic compensation in response to mitochondrial oxidative damage.

2. Materials and Methods

2.1. Muscle Samples. Biopsies from vastus lateralis muscles were obtained from 13 male healthy untrained subjects who voluntarily participated in the study. Based on age, the subjects were divided into two experimental groups:

- (1) Young subjects, 27.8 ± 6 years old ($n = 8$)
- (2) Elderly subjects, 72.4 ± 6.5 years old ($n = 5$)

Biopsies were performed following the procedure described in Pietrangelo et al. [23] and treated to collect satellite cell populations as previously described in Fulle et al. [9]. All of the subjects provided written, informed consent before participating in the study. The study was conducted according to the Helsinki Declaration (as amended in 2000), and it was approved by Ethic Committee of “G. d’Annunzio” University of Chieti-Pescara, Italy (PROT 1233/06, 1634/08, 1884/09 COET). The inclusion criteria were normal ECG and blood pressure and absence of metabolic, cardiovascular, chronic bone/joint, and muscular diseases. Exclusion

criteria were the presence of metabolic and/or cardiovascular diseases, evidence of hereditary or acquired muscular disease, or diagnosis of respiratory or psychiatric disorders. No subject was under treatment with testosterone or other pharmacological interventions or training protocols known to influence skeletal muscle. All subjects were Caucasian and nonsmokers. They presented BMI (body mass index) and % FM (fat mass) values that were not statistically different (BMI: 24.2 ± 1.5 and 27.6 ± 1.7 , young and elderly, resp.; % FM 23.0 ± 2.1 and 26.3 ± 2.1 young and elderly, resp.).

2.2. Satellite Cell Populations. The satellite cells were obtained, expanded as myoblasts in growth medium, and differentiated as previously described [9, 24]. Briefly, the percentages of myogenicity of the cell cultures were obtained using an immunocytochemistry assay, with the marker desmin and with biotinylated streptavidin-AP kits (Dako REAL™ Detection System Peroxidase/DAB+, Rabbit/Mouse; cat. number K5001; DAKO, DakoCytomation, Glostrup) [25]. Desmin is a cytoskeleton intermediate filament protein expressed early in myogenic populations [26, 27]. Differentiation of the cell populations was determined by counting the number of nuclei in the myotubes after 7 days of differentiation, as percentages with respect to the total number of nuclei, with the ratio between these two values (nuclei in myotubes/total nuclei $\times 100\%$) giving the fusion index. We only considered myotubes that were positive to the primary antibody against myosin heavy chain (MHC), using the MF20 anti-MHC monoclonal antibody (diluted 1:50; Developmental Studies Hybridoma Bank, University of Iowa, Iowa City, IA, USA), and that contained three or more nuclei [6].

2.3. Fluorescence-Activated Cell Sorting. Myogenic precursors expressing both CD56 and 5.1H11 were isolated by fluorescence-activated cell sorting (FACS) at FACSaria III (BD) as described in di Filippo et al. [8]. The primary antibodies used for this technique are specific for human myoblasts that targeted a cell surface protein, as CD56 and 5.1H11. These human CD56⁺/5.1H11⁺ cells were replaced in petri dishes and cultured in growth or differentiation medium for further analysis.

2.4. Ca²⁺ Imaging and Videomicroscopy Experiments. Videomicroscopy experiments are performed on cells plated on the bottom of special 96-well plates at a confluence of 10,000 cells/cm². The loading procedure is previously described by di Filippo et al. [28]. After registration of baseline, 40 mM KCl was added to the cells and the registration was continued [29]. The living cells, loaded with Fura-2, were sequentially excited at 340 or 380 nm with a high-speed wavelength switcher Polychrome II (Till Photonics, Germany). Fluorescence images were collected using a 40x oil objective lens, acquired using an intensified CCD camera (Hamamatsu Photonics, Hamamatsu, Japan), stored on a PC, and analyzed off-line. The acquisition time for each fluorescence emission was 0.5 s. It has been taken into consideration the ratio fluorescence (340/380 nm) signal in a selected representative cellular area after the subtraction of background fluorescence.

2.5. Protein Isolation and Quantitation. Antioxidant enzyme assays and Western blotting were performed using myoblasts and myotubes lysed in RIPA buffer (number R0278, Sigma-Aldrich), supplemented with 1:100 protease and phosphatase inhibitor cocktail (number P8340, Sigma-Aldrich), incubated 1 hour at 4°C, and centrifuged at 10000 rpm for 10 minutes at 4°C. Cytosol protein concentrations were measured on the resulting supernatant according to Bradford's method (Bradford Reagent, number B6916, Sigma-Aldrich).

2.6. Superoxide Enzyme Activities. Superoxide dismutase (SOD) activity was determined using the modified method of L'Abbé and Fischer [30, 31]. The final assay volume (1 ml) contained 20 mM Na₂CO₃, pH 10, 10 mM cytochrome c (number C7752, Sigma Aldrich), and 1 mM xanthine (number X0626, Sigma-Aldrich) and xanthine oxidase (number X4500, Sigma-Aldrich). As the xanthine oxidase activity varies, the amount used for the assay was sufficient to stimulate cytochrome c reduction at 550 nm at a rate of 0.025 per minute without SOD addition. SOD units were calculated on the basis of the definition that one unit represents the activity that inhibits cytochrome c reduction by 50%.

2.7. Western Blotting. Western blotting (WB) analysis was performed on 40 µg lysates from young and old myoblasts and myotubes, using SOD1 (71G8) mouse mAb (number 4266, Cell Signalling Technology, Danvers, MA, USA) at 1:1000, SOD2 (D9V9C) rabbit mAb (number 13194, Cell Signalling Technology) at 1:1000, and β-actin (8H10D10) mouse mAb (number 3700, Cell Signalling Technology) at 1:1000, as primary antibody, and secondary HRP-conjugated antibodies (Cell Signalling Technology) at 1:5000. Bands were detected and pictured at Bio-Rad GelDoc by LiteAblot PLUS enhanced chemiluminescent substrate (EuroClone); densitometry analyses were performed with ImageJ software.

2.8. Measurements of Mitochondrial Superoxide Anion Production. Superoxide production was measured using the indicator MitoSOX Red (number M36008, Thermo Fisher Scientific, USA) according to the manufacturer's instructions. Satellite cells were cultured as both myoblasts and myotubes. Before experiments, some of the cultures receive a treatment with 200 µM N-acetyl cysteine (NAC) for 24 hours or with NES containing 10 mM glucose plus 5 mM sodium pyruvate (BURST) solution, as acute stimulus and for 15 minutes and 2 hours. The cells were loaded with 5 µM MitoSOX and incubated for 10 min at 37°C in culture media and washed twice with normal external solution (NES, containing in mM: 140 NaCl, 2.8 KCl, 2 CaCl₂, 2 MgCl₂, 10 glucose, 10 N-2-hydroxyethylpiperazine-N'-2-ethanesulfonic acid- (HEPES-) NaOH, pH 7.3). During measurements, samples that received NAC or BURST pretreatment were in NES plus 200 µM NAC or BURST solution. Images were acquired at 512 \times 512 pixels using a LSM 510 META system (Zeiss, Jena, Germany) equipped with an Axiovert 200 inverted microscope and a Plan Neofluar oil immersion objective (40x/1.3 NA), and they were

TABLE 1: Myogenicity, fusion index, unfused desmin^{ve+} percentage, and proliferation rate (PDL).

Samples	Desmin ^{ve+} cell %	CD56 ⁺ /5.1H11 ⁺ cell %	Fusion index %	Unfused desmin ^{ve+} cell %	PDL at 25 days of culture
Young	67.5 ± 4.6	70.1 ± 5.6	48.2 ± 4.7	32.6 ± 6.1	13.2 ± 1.2
Elderly	70.3 ± 8.7	68.4 ± 4.3	24.3 ± 6.3*	66.8 ± 13.6*	9.0 ± 0.4*

pseudocolored in green. In a typical time-series recording, 14 frames were collected at frame rate of 0.1 Hz. MitoSOX fluorescence was acquired by exciting at 543 nm and collecting the emission using an LP filter set to 560 nm. Image analysis was performed by LSM 3.0 software (Zeiss). For each sample, fluorescence images were acquired from five randomly selected fields and off-line analysis of intensity was performed in ROI-representing cell areas, while in time lapse experiment ROIs were selected inside obvious mitochondrial areas. All experiments were performed at room temperature (22–26°C).

2.9. Seahorse XF Cell Mito Stress Test. The XF Cell Mito Stress Test was used to measure the oxygen consumption rate (OCR) of myoblasts and myotubes using the Seahorse XF Extracellular Flux Analyzer (number 102745-100, Seahorse Bioscience, Santa Clara, California). This technique uses specific mitochondrial inhibitors which enable the determination of six parameters for describing the key aspects of mitochondrial function: basal OCR, ATP-linked OCR, spare respiratory capacity (SRC), maximal respiratory capacity, proton leak, and nonmitochondrial respiration. Extracellular flux technology enables rapid, real-time detection of metabolic changes in cellular respiration and glycolysis rate. Cells were seeded in an XFp 8-well cell culture miniplate (Seahorse Bioscience) in three replicates at 25×10^4 /well density in 100 μ l of growth medium and incubated for 24 hours at 37°C, 5% CO₂. Before the performance of the Cell Mito Stress Test, some of the cultures received a 200 μ M NAC treatment for 24 h. Briefly, myoblasts and myotubes were incubated for 45 min at 37°C in ambient CO₂ in free-buffered DMEM (number 102353-100, Seahorse Bioscience, Santa Clara, California) (pH = 7.4) containing 1.0 mM sodium pyruvate (number S8636, Sigma-Aldrich), 10 mM glucose, and 2 mM glutamine (number G8540, Sigma-Aldrich). Baseline oxygen consumption (basal OCR) rate and parameters calculated after the addition of each drug were measured 3 times for 3 min each separated by a 3 min mix (18 min total). Following the baseline, 1.6 μ M oligomycin (number O4876, Sigma-Aldrich), the ATP synthase inhibitor, was injected into each well, followed by 3 cycles of 3 min mix and 3 min measurement. Then, 0.5 μ M of carbonyl cyanide-4-(trifluoromethoxy)phenylhydrazone (FCCP, number C2920, Sigma-Aldrich) was injected to uncouple the mitochondrial inner membrane and measure maximal respiration (maximal OCR = maximum electron flux through the electron transfer chain). Lastly, 1 μ M antimycin A (number A8674, Sigma-Aldrich) is injected to inhibit electron flux through complex III and so measurement of nonmitochondrial O₂ consumption. At the end of each experiment, the cells were lysed to determinate the total protein content (BCA assay). The

mitochondrial OCR is referred to μ g of total cellular proteins and reported as $\text{pmol} \cdot \text{min}^{-1} \cdot \mu\text{g}^{-1}$.

2.10. Seahorse XF Glycolysis Stress Test. In order to quantify changes in the glycolytic function, the glycolysis stress test was performed. It measures the extracellular acidification rate (ECAR, defined as the rate of change in proton excretion from the cell), which reflects the rate of glycolysis. It was carried out under similar conditions as the mitochondrial stress test with some differences. The assay media contained no glucose or pyruvate but supplemented with 2 mM glutamine. After the measurement of the basal ECAR, the cells enter into glycolysis with the injection of 10 mM glucose. Then, 1 μ M oligomycin was injected to inhibit OXPHOS and further shift the energy production to glycolysis; the consequent increase in ECAR would reveal the cellular maximum glycolytic capacity. Finally, 50 mM 2-deoxy-glucose (2-DG, number D6134, Sigma-Aldrich) was added; such compound is a glucose analogue that inhibits glycolysis through competitive binding to glucose hexokinase. The resulting decrease in ECAR confirms that the ECAR produced in the experiment is due to glycolysis. The ECAR is referred to μ g of total cellular proteins and reported as $\text{mpH} \cdot \text{min}^{-1} \cdot \mu\text{g}^{-1}$.

2.11. Statistical Analysis. The Seahorse XF instrument was controlled by Seahorse software for the generation of data files. For data processing, Seahorse Wave software (version 2.3.0) was used. The analysis of OCR and ECAR data was carried out also using the XF Stress Test Report Generator (version 3.0.6). Figure and statistical analyses were generated with the help of GraphPad Prism version 5.0 (GraphPad Software, La Jolla, USA). Results are presented as means \pm standard errors (SEM) or as representative traces. The statistical analysis was carried out using the *t* test ($*p \leq 0.05$, $**p \leq 0.005$, and $***p \leq 0.0005$). Analysis of mitochondrial fragmentation has been performed using Bonferroni's multiple comparison test. The significance has been codified as $*p \leq 0.05$ and $**p \leq 0.005$.

3. Results

3.1. Characterization and Functionality of Human Myoblast and Myotubes. Human myoblasts from muscle biopsies were isolated, expanded in culture, and characterized by myogenic purity, calculated as the number of cells expressing desmin (% of desmin^{ve+} cells); ability to fuse, calculated as fusion index (% FI), % of unfused desmin^{ve+} cells; and population doubling level at day 25 of culture. In Table 1 are summarized the results of myogenic purity and FI percentage for young and elderly cell cultures. Interestingly, even if the number of myogenic cells (desmin^{ve+} cell %) does not significantly change with

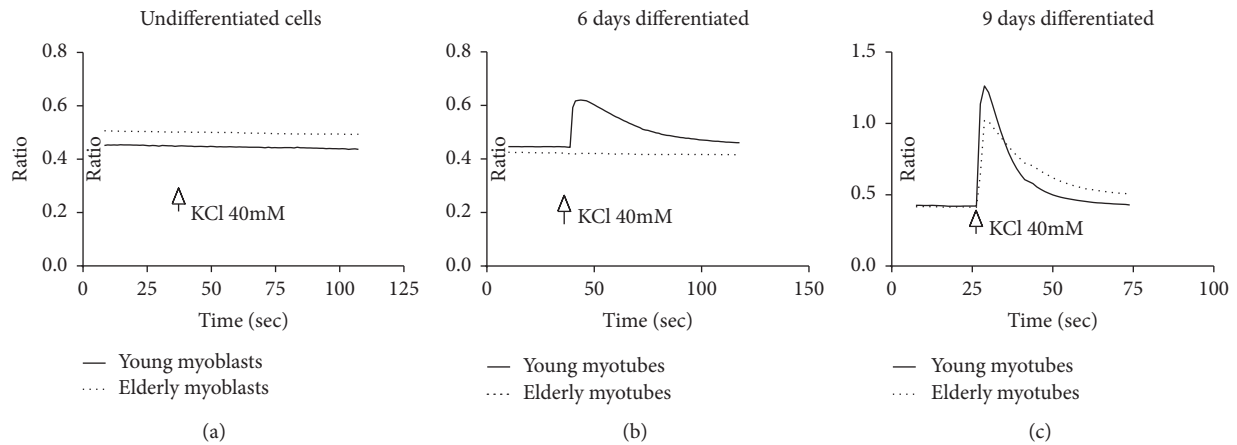


FIGURE 1: Ca^{2+} imaging and videomicroscopy experiments. Examples of Ca^{2+} transient following depolarization from KCl 40 mM on myoblasts (a) and 6 (b) and 9 (c) in vitro differentiated myotubes obtained from young (solid line) and elderly (dotted line) donors. The figure shows the 340/380 ratio as a function of time (see Methods).

the donor's age, the fusion index was significantly lower in primary human elderly myoblasts differentiated for 7 days (resp., 48.2% in young versus 24.3% in elderly). Moreover, as we previously reported [6, 8, 9, 29, 32], we observed a defected regeneration process since from elderly samples myotubes were smaller in number and thinner, containing only few myonuclei (data not shown). Furthermore, the percentage of unfused desmin^{ve+} cells calculated after 7 days of differentiation increased with age (from 32.6% in young versus 66.8% in elderly), while the myoblasts' proliferative rate (PDL) at 25 days of culture was significantly decreased.

Moreover, for our experiments, we have used myogenic precursors sorted for two specific surface markers: CD56 and 5.1H11. CD56 is a surface marker expressed by human satellite cells either in situ or upon dissociation [33]. 5.1H11 is a specific human myoblast and myotube marker [34]. As it can be seen, in young and old samples, the percentage of desmin^{ve+} cells (67.5 ± 4.6 and 70.3 ± 8.7 , resp.) and CD56^{ve+}/5.1H11^{ve+} cells (70.1 ± 5.6 and 68.4 ± 4.3 , resp.) was not significantly different, confirming a good myogenicity of our cultures and the validity of the choice of characterization markers.

The table summarizes the characterization parameters obtained from young and elderly samples. The percentage of myogenic cells (desmin^{ve+} cell %) is shown for young and elderly cultures and analyzed by the expression of desmin. To validate whether the expression of desmin was enough and sufficient as myogenic purity index, we further sorted by FACS the primary myoblast for two surface myogenic markers (CD56 and 5.1H11). The fusion index was determined by counting the number of nuclei in differentiated myotubes (positive for MyHC) after 7 days of culture in differentiation medium and reported as a percentage of the total number of nuclei; further, the unfused desmin-positive cells were counted after 7 days of differentiation. Population doubling level calculation at day 25 of culture was used to assess cell proliferative capability. Immunostaining and FI data were derived from at least 1000 cells counted in at least 10 different randomly chosen optical fields of each culture. All data ($n = 8$ young; $n = 5$ old) are presented as mean \pm SEM, $*p < 0.05$.

To verify the functionality of the primary myoblast and myotubes used in our experiments, we evaluated the capability to respond at depolarization due to the addition of KCl by generating characteristic Ca^{2+} transients. Here, we assessed the KCl-induced Ca^{2+} elevation in Fura-2-loaded young and elderly myoblasts and myotubes using single cells ($n = 51$ young and $n = 31$ elderly myoblasts; $n = 26$ young and $n = 47$ elderly myotubes after 6 days of differentiation; and $n = 13$ young and $n = 10$ elderly myotubes after 9 days of differentiation). In Figure 1 are reported representative traces of cytosolic Ca^{2+} transients in undifferentiated cells and 6- and 9-day-old differentiated cells. KCl 40 mM caused a transient rise in cytosolic Ca^{2+} levels in myotubes but not in myoblasts as expected (Figure 1(a)). Moreover, 6 days of differentiation were not enough for elderly myotubes to be fully functional since no cytosolic Ca^{2+} rise was observed after KCl addition (Figure 1(b)). Finally, this Ca^{2+} rise was less prominent in elderly myotubes after 9 days of differentiation (Figure 1(c)) with an uncompleted response and delay to return to baseline, conversely in young myotubes.

3.2. SOD Antioxidant Enzymatic Activity. We measured the activity of the cytosolic isoform of the antioxidant enzyme SOD1 in cell lysates obtained from myoblast and myotubes both from young and elderly donors. No difference was found comparing young versus old myoblasts or young versus old myotubes. A significant increase in SOD1 activity was observed comparing myoblasts versus myotubes on both young and elderly conditions ($*p \leq 0.05$).

3.3. Protein Expression of SOD1 and SOD2. We distinguished the two different forms of intracellular SOD, SOD1 and SOD2, cytosolic and mitochondrial protein, respectively. The protein expression was determined on young and elderly samples as both myoblasts and myotubes using Western blot (Figure 2). We observed a statistically significant decrease of SOD2 in elderly myoblasts with respect to young ones (Figure 2(b)). Representative SOD1 and SOD2 bands obtained by myoblasts and myotubes are shown in Figures 2(e) and 2(f), respectively.

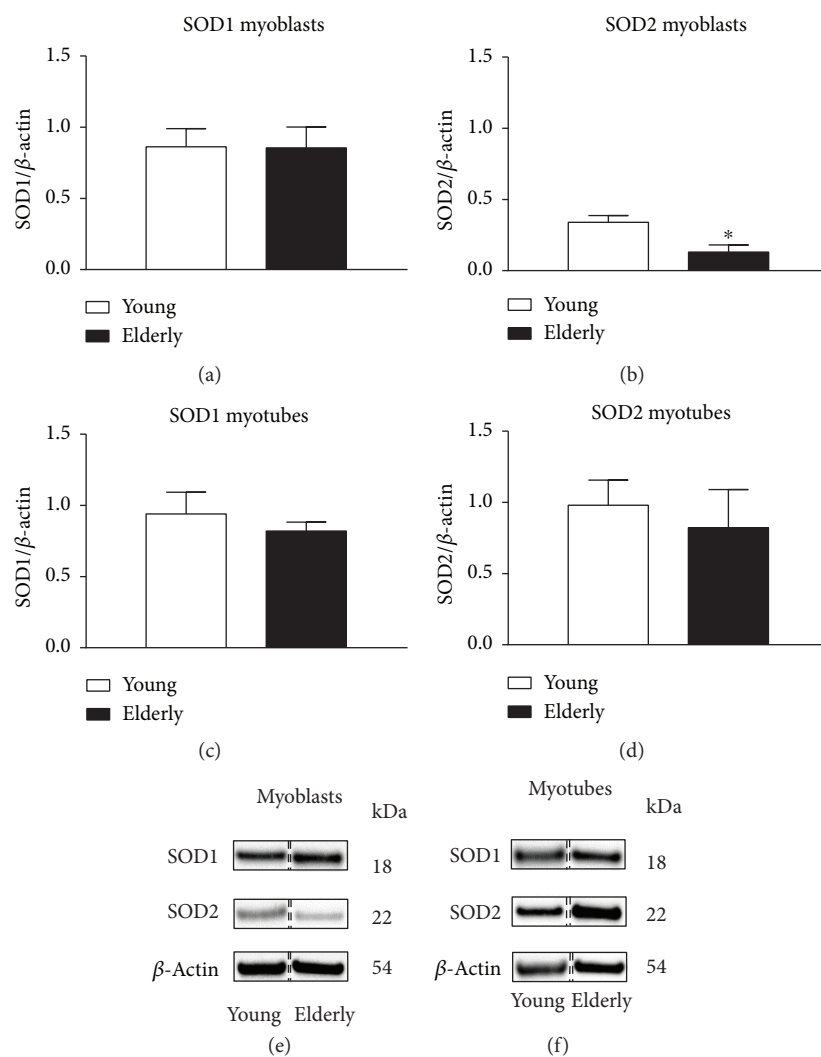


FIGURE 2: SOD1 and SOD2 protein expression. Western blotting analysis of superoxide enzymes cytosolic type 1 and mitochondrial type 2 was performed on young and elderly myoblasts and myotubes. β -Actin content was used for normalization. Panels (a), (b), (c), and (d) show SOD1 and SOD2 densitometric analysis of Western blots performed on three young and three old samples expressed as mean \pm SEM. Representative patterns of SOD1, SOD2, and β -actin (as loading control) expression in young and elderly myoblasts and myotubes are shown in panels (e) and (f). The bands were taken from two nonadjacent lanes originating from exactly the same gel and blot with exactly the same exposure time, but spliced together indicated with double-dotted lines. Moreover, we performed no change in contrast ($*p \leq 0.05$).

3.4. Mitochondrial Superoxide Anion Quantification with MitoSOX Red. We investigated the production of $O_2^{\bullet-}$ by the mitochondria in living cells using the MitoSOX Red Indicator. We first determined the mean fluorescence intensity (MFI) of the images at basal condition in untreated control condition at time zero of the time series recordings (Figure 3), and we found that in elderly myoblasts the fluorescence was significantly higher compared to the other samples ($*, p \leq 0.05$).

In addition, myoblasts (Figure 4(a)) or myotubes (Figure 4(b)) of young and elderly subjects were compared for $O_2^{\bullet-}$ production when treated for 24 hours with 200 μ M of the general antioxidant NAC or for 2 hours with high glucose and sodium pyruvate solution to BURST the increase in mitochondrial superoxide.

Elderly myoblasts in the control condition showed a statistically significant decrease in the MFI compared to young

samples (Figure 4(a); young $n = 357$, elderly $n = 111$, $***p \leq 0.0005$). The pretreatment with 200 μ M NAC (young $n = 199$, elderly $n = 111$) and BURST (young $n = 121$, elderly $n = 129$) statistically increased the $O_2^{\bullet-}$ production in the elderly with respect to the young ones ($*p \leq 0.05$ in NAC condition and $***p \leq 0.0005$ in BURST condition). In myotubes (Figure 4(b)), there was a statistically significant increase in mean intensity fluorescence in the elderly with respect to the young samples for all experimental conditions (young CTRL $n = 229$, elderly CTRL $n = 143$, $**p \leq 0.005$; young NAC $n = 187$, elderly NAC $n = 113$, $***p \leq 0.0005$; and young BURST $n = 137$, elderly BURST $n = 154$, $***p \leq 0.0005$). The MFI of myoblasts (panel c) and myotubes (panel d) are compared to the control and NAC sample conditions. Young myoblasts and myotubes in NAC condition showed a statistically significant decrease in MFI compared to the control condition ($***p \leq 0.0005$). The NAC

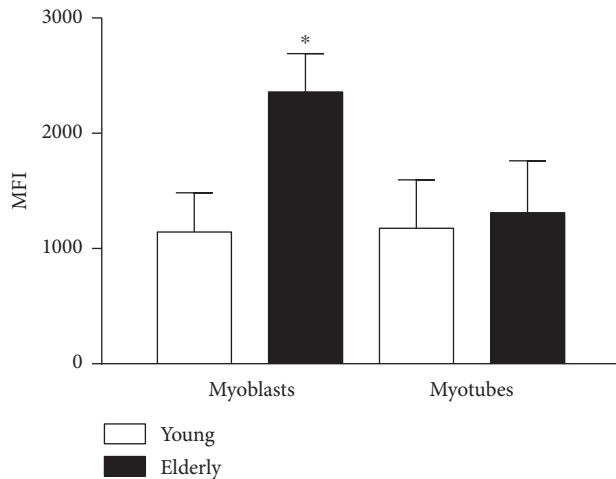


FIGURE 3: Mitochondrial superoxide anion quantification through MitoSOX Red as basal level. Mitochondrial superoxide anion production was assessed using a MitoSOX Red fluorescent probe. The baseline fluorescence level emitted by MitoSOX when it is oxidized by $O_2^{\bullet-}$ was measured at the beginning of the time series recordings performed on 3 randomly selected spot on the cells' area. Data are mean fluorescence \pm SEM of three independent experiments on elderly samples and of five experiments on young ones ($*p \leq 0.05$).

exposure of elderly myotubes resulted in a statistically significant increase in MFI compared to the control condition ($**p \leq 0.005$).

3.5. Superoxide Anion Coefficient of Variation. While performing our MitoSOX analysis, we also acquired short videos recording 14 frames every 3.5 seconds (about 50 seconds) of the MitoSOX signal. We graphed the MFI of young and elderly primary myoblasts versus time (Figure 5) observing that trace's profile differed significantly among samples. To quantify this observation, we used the coefficient of variation (CV), as it is a measure of dispersion of a frequency distribution. This analysis on myoblast-nontreated samples showed that in the elderly, the $O_2^{\bullet-}$ CV was statistically significantly increased versus young (panel b, $*p \leq 0.05$). On the contrary, elderly myotubes showed a statistically significant reduction of this parameter with respect to the young (panel d, $*p \leq 0.05$).

3.6. Mitochondrial Bioenergetics. Young and elderly samples (either myoblasts or myotubes) were assayed in untreated control condition and 24 hours after NAC treatment (Figures 6–9). In the control condition (Figure 6), the OCR parameters showed a decreasing trend in elderly versus young. However, only the nonmitochondrial respiration was significantly lower in the elderly ($***p \leq 0.0005$). Concerning the ECAR profile, the glycolysis parameter is a measure of extracellular acidification reached by the cells following the addition of saturating amounts of glucose. We found that glycolysis was significantly lower in the elderly compared to the young ($*p \leq 0.05$).

Following NAC exposure (Figure 7), the differences between elderly and young became statistically significant

in most of OCR parameters, such as the basal respiration, the spare respiratory capacity, and the maximal respiratory capacity ($*p \leq 0.05$), suggesting that NAC is more effective in scavenging ROS in the young than in the elderly. The glycolysis parameter, obtained by the ECAR profile, was found significantly decreased in elderly myoblasts compared to young ones ($**p \leq 0.005$).

Other glycolytic parameters (glycolytic capacity, glycolytic reserve, and nonglycolytic acidification, not shown) were not statistically different comparing young versus elderly myoblasts.

After 7 days of differentiation (Figure 8), we did not observe statistically significant differences in OCR parameters in our control condition samples. Surprisingly, the glycolysis was statistically significant higher in elderly myotubes compared to young ones ($*p \leq 0.05$).

After NAC treatment (Figure 9), the spare respiratory capacity and nonmitochondrial respiration were significantly decreased ($*p \leq 0.05$ and $***p \leq 0.0005$, resp.) in elderly versus young ones, suggesting that the scavenging activity of the antioxidant may be more considerable on the young than on the elderly. After NAC exposure, glycolysis value did not change comparing young and elderly myotubes.

Similarly to the values obtained for myoblasts, also in myotubes other glycolytic parameters (glycolytic capacity, glycolytic reserve, and nonglycolytic acidification, not shown) were not statistically different comparing young versus elderly.

4. Discussion

Aging is known to be characterized by an increase in oxidative stress related to an imbalance between ROS production, in particular $O_2^{\bullet-}$, and scavenger activity of antioxidant enzymes [35, 36]. This altered oxidative management is also reflected in the regenerative capacity of the skeletal muscle of the elderly, which shows an impairment in the primary myoblast-differentiating process responsible for regeneration [9, 29]. The characterization of our primary myoblast populations shows in the elderly a less regenerative capability with respect to the young ones, demonstrated by a slower proliferative rate and difficulty in differentiation (reduced % of FI and increased % of unfused desmin^{ve+} cells). The difficulty in functional differentiation, which we already previously demonstrated [29, 37], is confirmed by the response at depolarization stimuli (40 mM KCl) of the elderly myotubes that it is not yet complete and delays to return to baseline (Figure 1).

The $O_2^{\bullet-}$ radical, which we had already shown to be higher in the elderly's whole myoblasts [8], could therefore represent, if not adequately contrasted, a potential harmful agent. On the other hand, a transient increase in $O_2^{\bullet-}$, readily reduced by scavenger enzymes, seems to be positively correlated with a sustained metabolism, as occurs during the normal mitotic process or during the early phase of regeneration [38], whereas a subsequent switch-off may accelerate the muscle differentiation [39]. On the contrary, its prolonged presence, due to poor or insufficient antioxidant activity, can cause damage and impair the differentiation process.

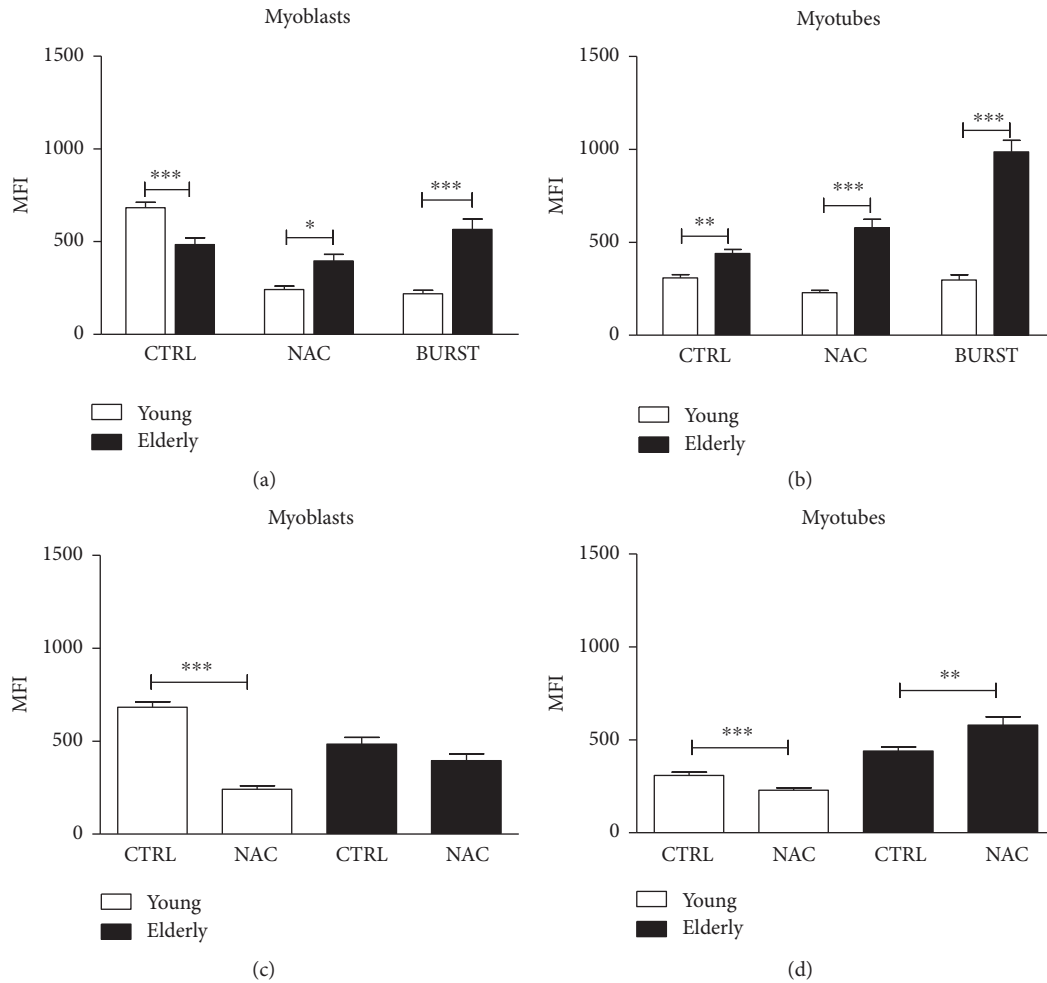


FIGURE 4: Mitochondrial superoxide anion quantification through MitoSOX Red during time series recordings. Mitochondrial superoxide anion production was assessed using a MitoSOX Red fluorescent probe. Mean fluorescence intensity (MFI) quantitation of confocal images of whole myoblasts (panels a and c) and myotubes (panels b and d) and primary myoblasts as control (CTRL), treated with 200 μ M NAC for 24 hours and BURST for 2 hours, were represented. Data are mean \pm SEM of three independent experiments on elderly samples and of five experiments on young ones. * $p \leq 0.05$, ** $p \leq 0.005$, and *** $p \leq 0.0005$.

In this study, we analyzed the activity of SOD1, noting that the differentiation process per se increases SOD1 activity independently of the donor age (Figure 10). On the other hand, we have highlighted a higher basal level of $O_2^{\bullet-}$ in the mitochondria of elderly myoblasts (Figure 3) that correlates with a low expression of SOD2. These data lead us to hypothesize that the highest $O_2^{\bullet-}$ levels observed in the whole myoblasts may be due to a mitochondrial production not sufficiently contrasted by SOD2 (Figures 2(a) versus 2(b)), thus preventing its switch-off useful for differentiation. Consistent with this, other studies show that a complete differentiation process occurs only in young samples, while it is impaired in elderly ones [8, 9]. The unexpected high mitochondrial $O_2^{\bullet-}$ level found in young myoblasts could be explained considering that they are characterized by an increased rate of proliferation [32] together with a higher oxygen consumption rate with respect to elderly ones [40], as we demonstrated in the present study through bioenergetics analysis (Figure 6). Conversely, the lower $O_2^{\bullet-}$ levels found in young myotubes compared to myoblasts

could be justified by the increase in SOD activity and the lack of proliferation rate effect as we are considering the differentiation phenotype.

As antioxidant and oxidant agents can affect the $O_2^{\bullet-}$ production and thus activate its scavenging by SOD enzyme, we stimulated our myoblasts and myotubes with NAC and BURST solution, respectively.

Elderly myoblasts and myotubes (Figures 4(c) and 4(d)) did not show lower $O_2^{\bullet-}$ levels after the NAC treatment, while young myoblasts and myotubes properly responded to NAC exposure by significantly reducing the production of $O_2^{\bullet-}$ (** $p \leq 0.0005$). These results suggest that first, an increase in $O_2^{\bullet-}$ production might be not associated with a proportional increase in SOD, and second, solely in samples from young donors might NAC be able to promote cell fitness and viability, since elderly cells even showed significantly higher $O_2^{\bullet-}$ levels in the presence of NAC compared to the control condition (** $p \leq 0.005$).

In aged muscles [35] as well as in primary myoblasts [9, 29], the impairment of the antioxidant machinery was

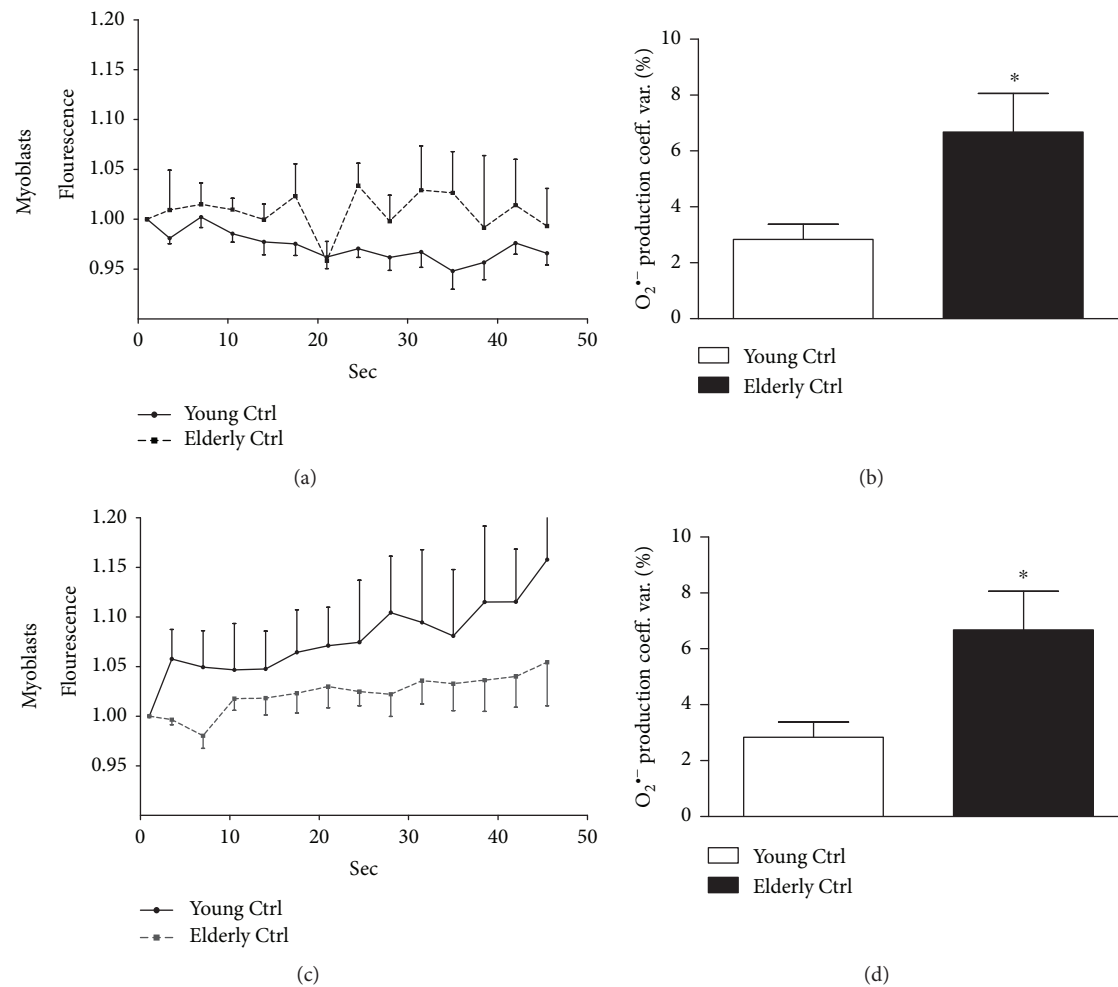


FIGURE 5: Superoxide anion coefficient of variation. The superoxide anion coefficient of variation was calculated on a short video acquired during the MitoSOX experiment. Traces of the fluorescence registered in 50 seconds of young (panel a) and elderly (panel c) myoblasts and myotubes were represented. The quantification, expressed as percentage of coefficient of variation, was shown in myoblasts (panel b) and in myotubes (panel d). In myoblasts, the $O_2^{\bullet-}$ coefficient of variation expressed as percentage increased in elderly samples comparing young ones ($*p \leq 0.05$) while in myotubes a significant reduction of this parameter was shown in elderly versus young ($*p \leq 0.05$).

already demonstrated. Therefore, when elderly primary myoblasts are treated with a high glucose solution (BURST) that enhances their cellular metabolism, they will uncontrollably reach the highest levels of $O_2^{\bullet-}$ production. Consistently, treatment with an antioxidant agent like NAC, which acts as glutathione precursor [41, 42], might not significantly affect elderly primary myoblasts due to the impaired activity of glutathione-dependent enzymes and the accumulation of hydrogen peroxide [9]. Furthermore, short videos acquired during MitoSOX experiments allowed us to investigate the variation of the response in $O_2^{\bullet-}$ production expressed as coefficient of variation (CV) in young and elderly samples under control conditions. The CV was found higher in elderly myoblasts with respect to young myoblasts, while an opposite result was observed in myotubes. We can argue that the increased variability in $O_2^{\bullet-}$ production in elderly myoblasts could be due to a large dispersion in the frequency distribution of $O_2^{\bullet-}$ flickering or, in other words, we can imagine that the elderly mitochondria produce $O_2^{\bullet-}$ in a slow and continuous regimen with respect to young

mitochondria. In elderly myotubes, the $O_2^{\bullet-}$ flickering has a narrow frequency distribution, significantly reduced with respect to the young ones, probably because those rely more on glycolysis than mitochondrial OXPHOS.

ROS not only have a detrimental effect on biological molecules, such as DNA, proteins, and lipids [36], due to their accumulation but also affect myogenic regeneration at several stages. Specifically, ROS enhanced NF- κ B transcription factor-activating I κ B kinase (IKK) that phosphorylates the I κ B inhibitor in turn upregulating NF- κ B [39]. In the skeletal muscle, the role of this transcription factor is related to the activation of protein degradation pathways [43]. Consequently, we can argue that a high level of $O_2^{\bullet-}$ found in our elderly myotubes with respect to young ones ($**p \leq 0.005$) could result in the activation of NF- κ B that in turn could boost cell catabolism. Consistent with this, we and other groups previously demonstrated that elderly samples' upregulation of FOXO1A, myostatin genes, and NF- κ B protein expression, together with downregulation of AKT1/PIK3CA/MTOR genes and phospho-Akt protein

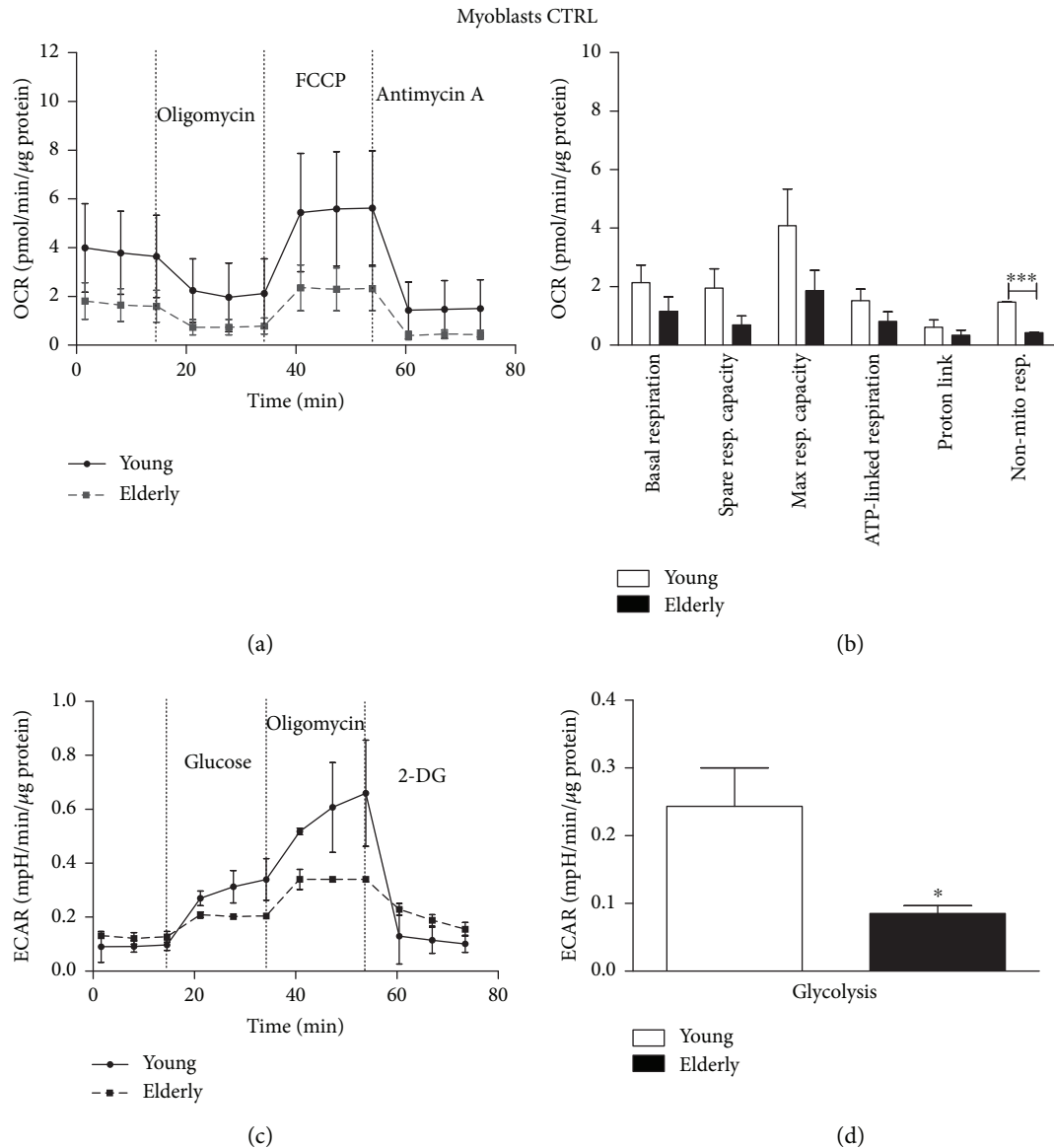


FIGURE 6: Bioenergetic profiles and parameters in young and elderly myoblasts in the control condition. Mitochondrial respiration (panels a and b) and glycolytic function (panels c and d) of young and elderly myoblasts are represented. OCR trace shows basal OCR condition and OCR recordings after 3 sequential additions of, respectively, ATP synthase inhibitor oligomycin, ECT uncoupler FCCP, and complex III inhibitor antimycin A. ECAR trace shows basal ECAR condition and ECAR recordings after 3 sequential additions of, respectively, glucose, oligomycin, and 2-DG. For each sample ($N = 3$ young and $N = 3$ elderly), cells were seeded on an XFp 6-well cell culture miniplate in three replicates at 25×10^4 /well density. Results are expressed as mean \pm SEM of three independent experiments each performed in triplicate. The OCR and the glycolysis values were normalized to cellular protein content. $*p \leq 0.05$ and $***p \leq 0.0005$.

expression, could lead to the activation of the atrophic/catabolic pathway at the expense of the anabolic ones and finally inhibit muscle differentiation [8, 9, 32]. Overall, our data, along with the results of previous studies, suggest that the failure to differentiate *in vitro* and to regenerate muscle *in vivo* [9, 10] could be associated with the oxidative damage accumulation, impaired antioxidant activity, and insufficient repair capability observed in the elderly. As all the above-mentioned events take place in mitochondria, a brief video of MitoSOX experiments performed on primary myoblasts from young or elderly donors was inserted in

the manuscript (link to movies here as supplementary material; young and elderly myoblasts) to show their relative mitochondrial dynamic.

Furthermore, to deeply investigate mitochondria's functions, we also analyzed mitochondrial bioenergetics in our samples via the Seahorse Flux analyzer. This instrument monitors OXPHOS by measuring in real time OCR and glycolysis by measuring in real time ECAR. Revising literature on aged muscle bioenergetics, many studies demonstrated a significant decrease in the activity of several respiratory chain complexes and a substantial increase in ROS production,

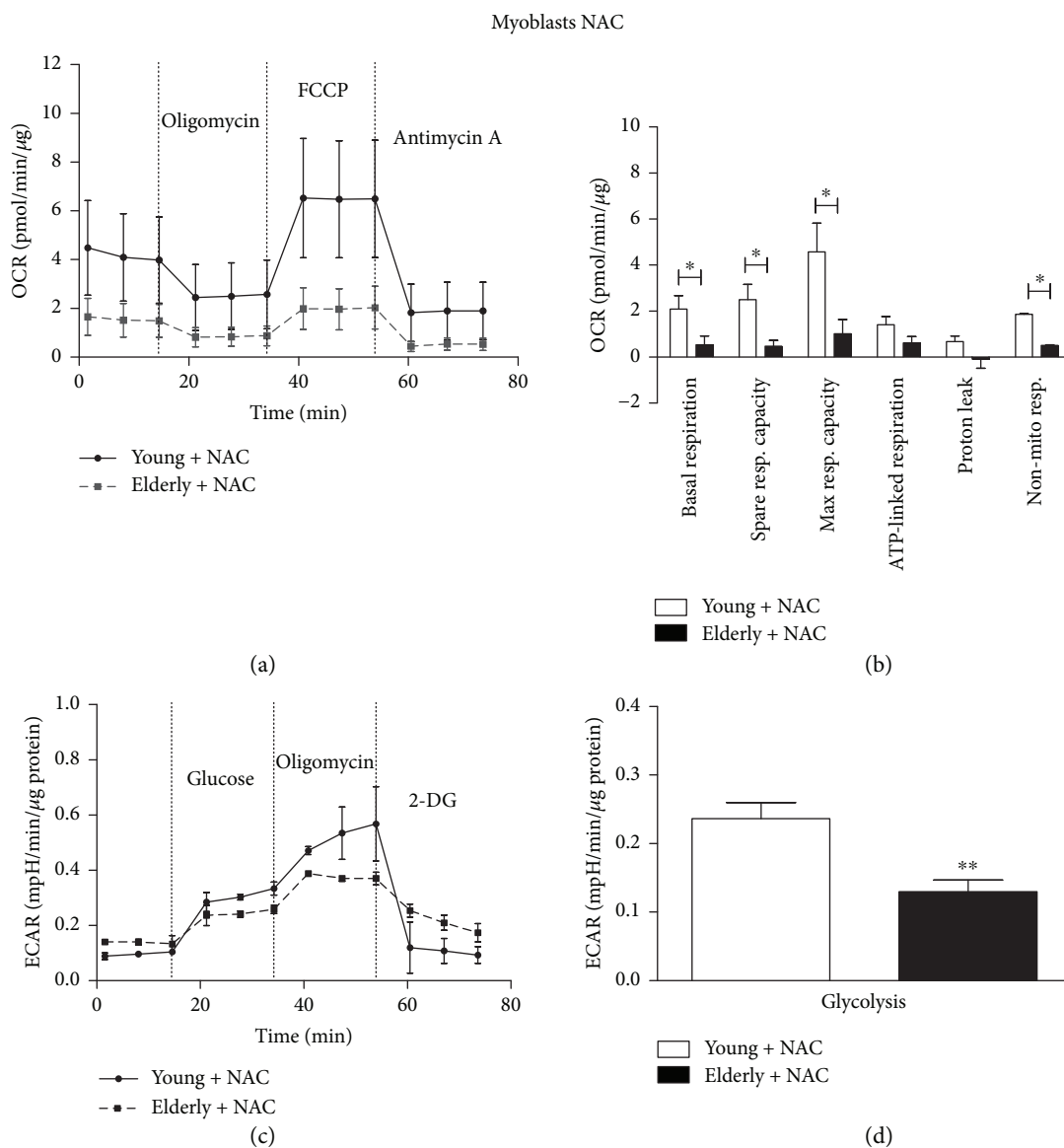


FIGURE 7: Bioenergetic profiles and parameters in young and elderly myoblasts following NAC exposure. Mitochondrial respiration (panels a and b) and glycolytic function (panels c and d) of young and elderly myoblasts are represented. OCR parameters were calculated using the data generated in respiratory flux traces (panel a). OCR trace shows basal OCR condition and OCR recordings after 3 sequential additions of, respectively, ATP synthase inhibitor oligomycin, ECT uncoupler FCCP, and complex III inhibitor antimycin A. ECAR trace shows basal ECAR condition and ECAR recordings after 3 sequential additions of, respectively, glucose, oligomycin, and 2-DG. For each sample ($N = 3$ young and $N = 3$ elderly), cells were seeded on an XFp 6-well cell culture miniplate in three replicates at 25×10^4 /well density. Results are expressed as mean \pm SEM of three independent experiments each performed in triplicate. The OCR and the glycolysis values were normalized to cellular protein content. * $p \leq 0.05$ and ** $p \leq 0.005$.

thus confirming the mitochondrial theory of aging [44, 45]. Measurements of mitochondrial respiration are strong indicators of the functional bioenergetic capacity of mitochondria and of overall cellular health. The Seahorse Mito Stress Test uses modulators of cellular respiration that specifically target components of the electron transport chain to reveal key parameters of metabolic function. The first compound injected is oligomycin that inhibits ATP synthase. The second compound is FCCP, an uncoupling agent that permeabilizes the inner mitochondrial membrane to protons, forces the mitochondria to increase the flow of electrons (and thus

oxygen consumption) to maintain the membrane potential. As a result, electron flow through the ETC is constant and oxygen is maximally consumed by complex IV. The last drug injected is antimycin A, a complex III inhibitor that shuts down the mitochondrial respiration. Parameters from the cellular mitochondrial function assay give insights into different aspects of mitochondrial functions.

In myoblasts, we observed a decreasing trend for many OCR parameters when elderly and young samples were compared, especially considering the nonmitochondrial respiration (Figures 6(a) and 6(b)). Notably, the

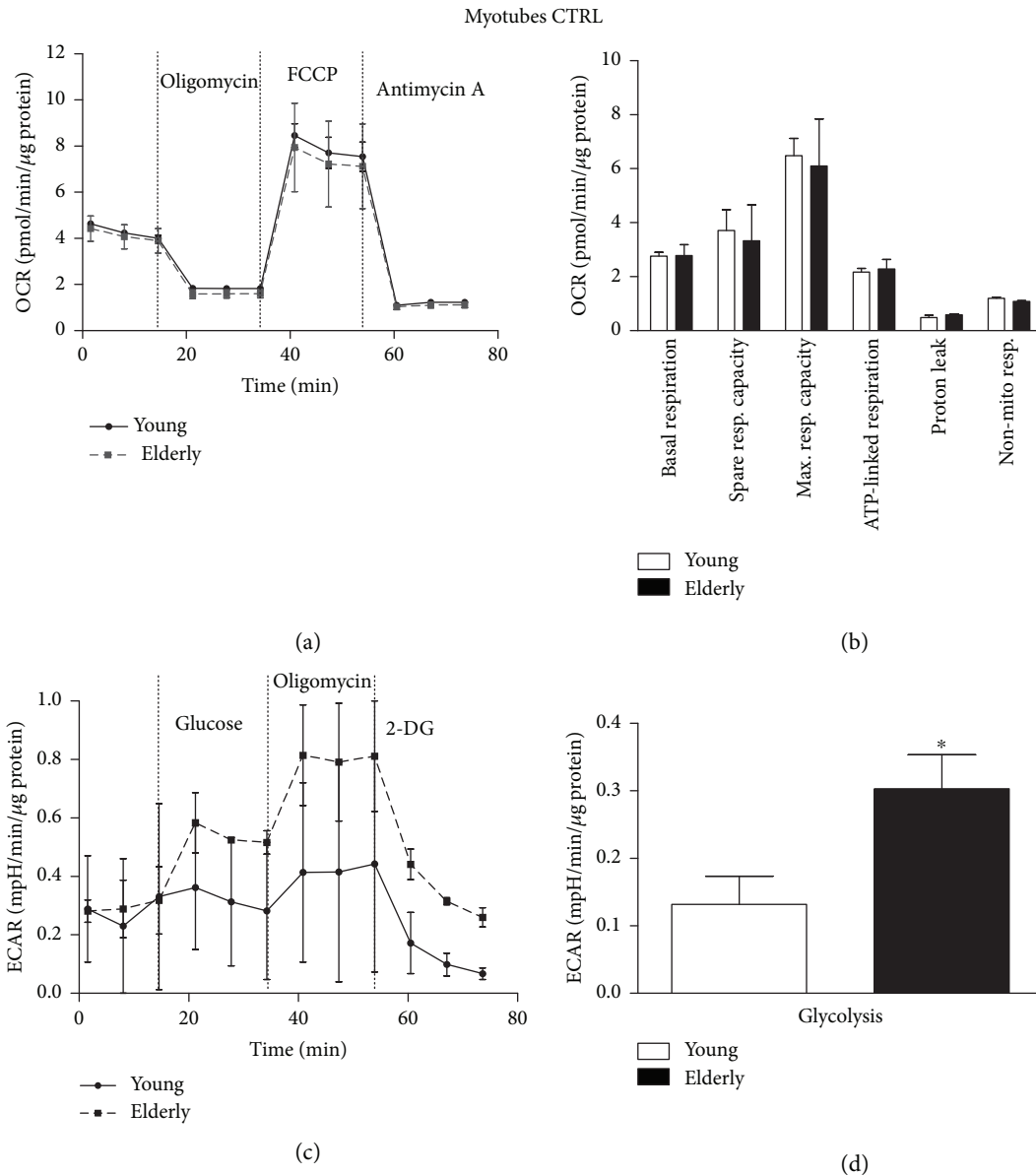


FIGURE 8: Bioenergetic profiles and parameters in young and elderly myotubes in the control condition. Mitochondrial respiration (panels a and b) and glycolytic function (panels c and d) of young and elderly myotubes are represented. OCR trace shows basal OCR condition and OCR recordings after 3 sequential additions of, respectively, ATP synthase inhibitor oligomycin, ECT uncoupler FCCP, and complex III inhibitor antimycin A. ECAR trace shows basal ECAR condition and ECAR recordings after 3 sequential additions of, respectively, glucose, oligomycin, and 2-DG. For each sample ($N = 3$ young and $N = 3$ elderly), cells were seeded on an XFp 6-well cell culture miniplate in three replicates at 25×10^4 /well density. Results are expressed as mean \pm SEM of three independent experiments each performed in triplicate. The OCR and the glycolysis values were normalized to cellular protein content. * $p \leq 0.05$.

lower values for spare respiratory and maximal respiratory capacity, which are considered as indicators of metabolic plasticity, would indicate compromised mitochondrial mass or integrity [46] and defective mitochondria in elderly samples. Moreover, we found that the glycolytic rate was significantly lower in elderly compared to young samples (Figures 6(c) and 6(d)).

After the NAC exposure, we observed that basal respiration, spare respiratory capacity, maximal respiration capacity, and nonmitochondrial respiration became significantly

lower in elderly myoblasts versus young ones (Figures 7(a) and 7(b)), together with a more pronounced decrease in glycolysis (Figures 7(c) and 7(d)). As highlighted before, NAC is solely effective in scavenging $O_2^{\bullet-}$ produced by young myoblasts (Figure 4(c)); therefore, the exclusive activity of NAC on young myoblasts could lead to a boost in their viability whose occurrence would justify their improved mitochondrial performance. On the contrary, we observed no differences between untreated and NAC-treated elderly myoblast in terms of OCR parameters, in agreement with

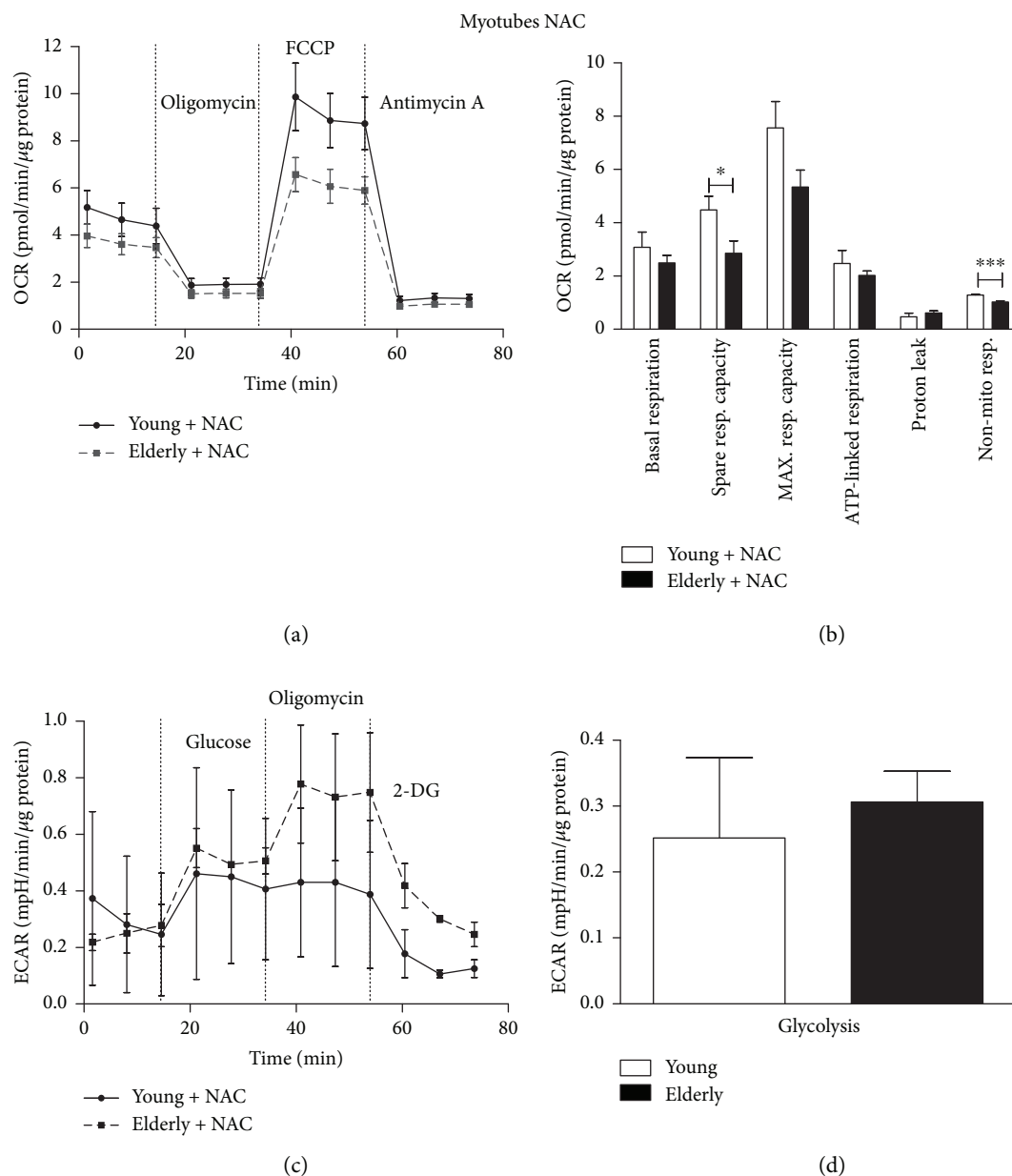


FIGURE 9: Bioenergetic profiles and parameters in young and elderly myotubes following NAC exposure. Mitochondrial respiration (panels a and b) and glycolytic function (panels c and d) of young and elderly myoblasts are represented. OCR parameters were calculated using the data generated in respiratory flux traces (panel a). OCR trace shows basal OCR condition and OCR recordings after 3 sequential additions of, respectively, ATP synthase inhibitor oligomycin, ECT uncoupler FCCP, and complex III inhibitor antimycin A. ECAR trace shows basal ECAR condition and ECAR recordings after 3 sequential additions of, respectively, glucose, oligomycin, and 2-DG. For each sample ($N = 3$ young and $N = 3$ elderly), cells were seeded on an XFp 6-well cell culture miniplate in three replicates at 25×10^4 /well density. Results are expressed as mean \pm SEM of three independent experiments each performed in triplicate. The OCR and the glycolysis values were normalized to cellular protein content. * $p \leq 0.05$ and *** $p \leq 0.0005$.

the comparable $O_2^{\bullet-}$ levels detected for both conditions (Figure 4(c)), due to a possibly partially compromised antioxidant machinery. This may lead to the hypothesis that the lower OXPHOS which we see in myoblasts associated to a whole decreased glycolysis could result in a less aerobic glycolytic component, leaving perhaps the role of energy production almost exclusively to the anaerobic component.

This hypothesis would be in agreement with the recent study conducted by Pääsuke et al. [40] on primary myoblasts

from young and elderly subjects demonstrating that the proliferation of myoblasts *in vitro* (from passages 2 to 6, simulating an *in vitro* senescence) is associated with downregulation of OXPHOS, and aging *in vivo* (young versus elderly) caused an altered metabolic profile by favoring the glycolytic pathway. Our results are in agreement also with another recent study demonstrating that senescent myoblasts show a metabolic shift leading to glycolytic enzymes a pronounced downregulation in glycolysis [47].

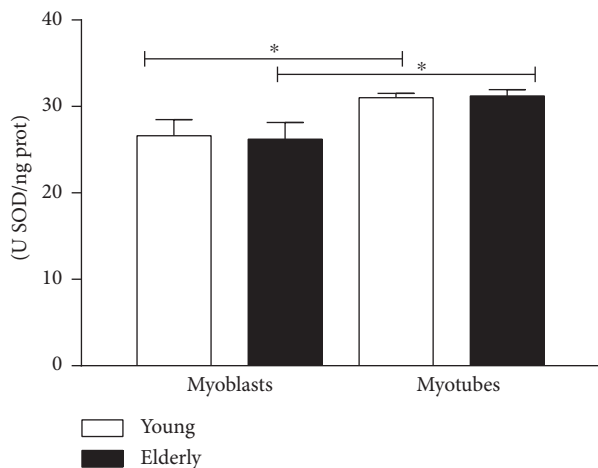


FIGURE 10: Superoxide dismutase activity. Quantitative analyses from young and elderly myoblasts and myotubes for the activity of the superoxide dismutase enzyme, SOD1. The SOD units (U SOD) were calculated considering that 1 SOD unit is defined as the quantity that inhibits the rate of cytochrome c reduction by 50% per ng of protein. The activity of the superoxide dismutase was expressed as U SOD/ng protein. * $p \leq 0.05$.

In myotubes, we found a similar trend for the OCR parameters of elderly versus young donors. The myogenic differentiation process is usually accompanied by an increase in oxidative metabolism with a shift from glycolysis to OXPHOS, as the major energy demand occurs [38, 48]. This phenomenon is not observed in our samples, where elderly myotubes have an OXPHOS metabolism trend similar to young ones, but a significantly increased glycolytic rate. These findings could suggest a different energetic plasticity of elderly myotubes with respect to young ones and the increased energy demand could not be covered only by OXPHOS metabolism but require an incremented glycolytic process maybe because their mitochondrial machine is subcritically impaired. Accordingly, Korolchuk and collaborators demonstrated that in senescent cells, the fraction of ATP produced by OXPHOS decreases, while relatively more ATP is generated by anaerobic glycolysis as a compensatory response to mitochondrial dysfunction. Furthermore, early occurrence of mitochondrial dysfunction during the induction of cell senescence could set off a number of different cellular responses and signaling pathways as well as reducing capacity to respond to peak energy demands [49]. Similarly, to myoblasts, NAC treatment disclosed the real differences in few of the measured mitochondrial parameters (e.g., spare respiratory capacity and nonmitochondrial respiration) between elderly versus young myotubes, confirming the hypothesis that the antioxidant acts by improving the whole physiological fitness of young cells.

5. Conclusions

The aging process produces increased mitochondrial $O_2^{\bullet-}$ levels, neither contrasted by an adequate amount of SOD2 nor scavenged by a NAC or BURST stressor. The proliferative state shows a slower metabolism characterized by less

OXPHOS and glycolysis, probably to the detriment of the aerobic glycolytic component.

The metabolic burst due to the onset of differentiation leads to a pronounced increase in glycolysis which does not occur in young myotubes. This result suggests that OXPHOS in elderly myotubes may not be as effective at producing ATP as it is in young myotubes. The increased glycolytic rate observed in elderly myotubes could be therefore considered as part of a compensatory mechanism mounted by the aging cells in response to the sudden increase in energy demand and in the absence of an extra OXPHOS support.

The data collected in the present study lead us to conclude that the elderly may have less metabolic plasticity due to the impaired mitochondrial function caused by oxidative stress. Further studies on the expression and activity of mitochondrial complexes in myotubes with respect to myoblasts could lay the foundations for future investigations about the detailed causes of impaired muscle regeneration during aging.

Abbreviations

ROS: Reactive oxygen species
 O₂^{•-}: Superoxide anion
 SOD: Superoxide dismutase
 OXPHOS: Oxidative phosphorylation.

Data Availability

The data related to “elderly sample myotubes were smaller in number and thinner, containing only few myonuclei (data not shown)” used to support the findings of this study are available from the corresponding author upon request.

Conflicts of Interest

The authors declare that there is no conflict of interest regarding the publication of this paper.

Acknowledgments

This work was supported by FIRB (Grant no. RBF12BUMH, 2012), PRIN (Grant no. 2010R8JK2X_007, 2010–2011), and PRIN (Grant no. 2012N8YJC3_003, 2012) from MIUR; “G. d’Annunzio” University (Grant 2016). The authors thank Dr. Vittore Verratti for muscle needle biopsies.

Supplementary Materials

Video: in the first part of the video, group A includes myoblasts of the young control sample showing the mitochondrial dynamics during a brief recording; in the second one, we can appreciate group B which includes myoblasts of the elderly control sample showing the mitochondrial dynamics during a brief recording. The video shows the different mitochondrial dynamics, with a less activity in the elderly sample with respect to young ones, confirming a reduction of plasticity and metabolism of the elderly. The videos were acquired recording 14 frames every 3.5 seconds (for about 50 seconds). The recordings are compressed 1 : 10 with Zeiss LSM 3.0 SP3 software. (*Supplementary Materials*)

References

- [1] A. J. Cruz-Jentoft, J. P. Baeyens, J. M. Bauer et al., "Sarcopenia: European consensus on definition and diagnosis: report of the European Working Group on Sarcopenia in Older People," *Age and Ageing*, vol. 39, no. 4, pp. 412–423, 2010.
- [2] R. N. Cooper, G. S. Butlerbrowne, and V. Mouly, "Human muscle stem cells," *Current Opinion in Pharmacology*, vol. 6, no. 3, pp. 295–300, 2006.
- [3] A. Mauro, "Satellite cell of skeletal muscle fibers," *The Journal of Biophysical and Biochemical Cytology*, vol. 9, no. 2, pp. 493–495, 1961.
- [4] S. B. P. Chargé and M. A. Rudnicki, "Cellular and molecular regulation of muscle regeneration," *Physiological Reviews*, vol. 84, no. 1, pp. 209–238, 2004.
- [5] I. M. Conboy and T. A. Rando, "Aging, stem cells and tissue regeneration: lessons from muscle," *Cell Cycle*, vol. 4, no. 3, pp. 407–410, 2005.
- [6] T. Pietrangelo, C. Puglielli, R. Mancinelli, S. Beccafico, G. Fanò, and S. Fulle, "Molecular basis of the myogenic profile of aged human skeletal muscle satellite cells during differentiation," *Experimental Gerontology*, vol. 44, no. 8, pp. 523–531, 2009.
- [7] S. Joannisse, J. P. Nederveen, T. Snijders, B. R. McKay, and G. Parise, "Skeletal muscle regeneration, repair and remodeling in aging: the importance of muscle stem cells and vascularization," *Gerontology*, vol. 63, no. 1, pp. 91–100, 2016.
- [8] E. S. di Filippo, R. Mancinelli, T. Pietrangelo et al., "Myomir dysregulation and reactive oxygen species in aged human satellite cells," *Biochemical and Biophysical Research Communications*, vol. 473, no. 2, pp. 462–470, 2016.
- [9] S. Fulle, S. Didonna, C. Puglielli et al., "Age-dependent imbalance of the antioxidative system in human satellite cells," *Experimental Gerontology*, vol. 40, no. 3, pp. 189–197, 2005.
- [10] J. Y. Moon, S. J. Choi, C. H. Heo, H. M. Kim, and H. S. Kim, "α-Syntrophin stabilizes catalase to reduce endogenous reactive oxygen species levels during myoblast differentiation," *The FEBS Journal*, vol. 284, no. 13, pp. 2052–2065, 2017.
- [11] D. Sebastián, M. Palacín, and A. Zorzano, "Mitochondrial dynamics: coupling mitochondrial fitness with healthy aging," *Trends in Molecular Medicine*, vol. 23, no. 3, pp. 201–215, 2017.
- [12] J. H. Huang and D. A. Hood, "Age-associated mitochondrial dysfunction in skeletal muscle: contributing factors and suggestions for long-term interventions," *IUBMB Life*, vol. 61, no. 3, pp. 201–214, 2009.
- [13] F. L. Muller, Y. Liu, and H. Van Remmen, "Complex III releases superoxide to both sides of the inner mitochondrial membrane," *The Journal of Biological Chemistry*, vol. 279, no. 47, pp. 49064–49073, 2004.
- [14] A. J. Case, "On the origin of superoxide dismutase: an evolutionary perspective of superoxide-mediated redox signaling," *Antioxidants*, vol. 6, no. 4, 2017.
- [15] D. R. Thorburn, C. Sugiana, R. Salemi et al., "Biochemical and molecular diagnosis of mitochondrial respiratory chain disorders," *Biochimica et Biophysica Acta (BBA) - Bioenergetics*, vol. 1659, no. 2–3, pp. 121–128, 2004.
- [16] M. Kompore and W. B. Rizzo, "Mitochondrial fatty-acid oxidation disorders," *Seminars in Pediatric Neurology*, vol. 15, no. 3, pp. 140–149, 2008.
- [17] J. R. Casey, S. Grinstein, and J. Orlowski, "Sensors and regulators of intracellular pH," *Nature Reviews. Molecular Cell Biology*, vol. 11, no. 1, pp. 50–61, 2010.
- [18] P. W. Hochachka and T. P. Mommsen, "Protons and anaerobiosis," *Science*, vol. 219, no. 4591, pp. 1391–1397, 1983.
- [19] G. A. Brooks, "What does glycolysis make and why is it important?," *Journal of Applied Physiology*, vol. 108, no. 6, pp. 1450–1451, 2010.
- [20] A. S. Divakaruni and M. D. Brand, "The regulation and physiology of mitochondrial proton leak," *Physiology*, vol. 26, no. 3, pp. 192–205, 2011.
- [21] N. R. Madamanchi and M. S. Runge, "Mitochondrial dysfunction in atherosclerosis," *Circulation Research*, vol. 100, no. 4, pp. 460–473, 2007.
- [22] D. Han, R. Canali, D. Rettori, and N. Kaplowitz, "Effect of glutathione depletion on sites and topology of superoxide and hydrogen peroxide production in mitochondria," *Molecular Pharmacology*, vol. 64, no. 5, pp. 1136–1144, 2003.
- [23] T. Pietrangelo, L. D'Amelio, C. Doria, R. Mancinelli, S. Fulle, and G. Fanò, "Tiny percutaneous needle biopsy: an efficient method for studying cellular and molecular aspects of skeletal muscle in humans," *International Journal of Molecular Medicine*, vol. 27, no. 3, pp. 361–367, 2011.
- [24] R. Mancinelli, T. Pietrangelo, R. La Rovere et al., "Cellular and molecular responses of human skeletal muscle exposed to hypoxic environment," *Journal of Biological Regulators and Homeostatic Agents*, vol. 25, no. 4, pp. 635–645, 2011.
- [25] T. Pietrangelo, E. S. Di Filippo, R. Mancinelli et al., "Low intensity exercise training improves skeletal muscle regeneration potential," *Frontiers in Physiology*, vol. 6, article 399, 2015.
- [26] T. Behr, P. Fischer, W. Muller-Felber, M. Schmidt-Achert, and D. Pongratz, "Myofibrillogenesis in primary tissue cultures of adult human skeletal muscle: expression of desmin, titin, and nebulin," *Clinical investigator*, vol. 72, no. 2, pp. 150–155, 1994.
- [27] S. J. Kaufman and R. F. Foster, "Replicating myoblasts express a muscle-specific phenotype," *Proceedings of the National Academy of Sciences of the United States of America*, vol. 85, no. 24, pp. 9606–9610, 1988.
- [28] E. S. Di Filippo, R. Mancinelli, M. Marrone et al., "Neuromuscular electrical stimulation improves skeletal muscle regeneration through satellite cell fusion with myofibers in healthy elderly subjects," *Journal of Applied Physiology*, vol. 123, no. 3, pp. 501–512, 2017.
- [29] S. Beccafico, C. Puglielli, T. Pietrangelo, R. Bellomo, G. Fanò, and S. Fulle, "Age-dependent effects on functional aspects in human satellite cells," *Annals of the New York Academy of Sciences*, vol. 1100, no. 1, pp. 345–352, 2007.
- [30] M. R. L'Abbé and P. W. F. Fischer, "An automated method for the determination of Cu,Zn-superoxide dismutase in plasma and erythrocytes using an ABA-200™ discrete analyzer," *Clinical Biochemistry*, vol. 19, no. 3, pp. 175–178, 1986.
- [31] A. Shakirzyanova, G. Valeeva, A. Giniatullin et al., "Age-dependent action of reactive oxygen species on transmitter release in mammalian neuromuscular junctions," *Neurobiology of Aging*, vol. 38, pp. 73–81, 2016.
- [32] S. Beccafico, F. Riuzzi, C. Puglielli et al., "Human muscle satellite cells show age-related differential expression of S100B protein and RAGE," *Age*, vol. 33, no. 4, pp. 523–541, 2011.
- [33] J. Verney, F. Kadi, N. Charifi et al., "Effects of combined lower body endurance and upper body resistance training on the

- satellite cell pool in elderly subjects,” *Muscle & Nerve*, vol. 38, no. 3, pp. 1147–1154, 2008.
- [34] F. S. Walsh and M. A. Ritter, “Surface antigen differentiation during human myogenesis in culture,” *Nature*, vol. 289, no. 5793, pp. 60–64, 1981.
- [35] S. Fulle, F. Protasi, G. Di Tano et al., “The contribution of reactive oxygen species to sarcopenia and muscle ageing,” *Experimental Gerontology*, vol. 39, no. 1, pp. 17–24, 2004.
- [36] P. Mecocci, G. Fanó, S. Fulle et al., “Age-dependent increases in oxidative damage to DNA, lipids, and proteins in human skeletal muscle,” *Free Radical Biology & Medicine*, vol. 26, no. 3-4, pp. 303–308, 1999.
- [37] P. Lorenzon, E. Bandi, F. de Guarrini et al., “Ageing affects the differentiation potential of human myoblasts,” *Experimental Gerontology*, vol. 39, no. 10, pp. 1545–1554, 2004.
- [38] A. Wagatsuma and K. Sakuma, “Mitochondria as a potential regulator of myogenesis,” *The Scientific World Journal*, vol. 2013, Article ID 593267, 9 pages, 2013.
- [39] M. Kozakowska, K. Pietraszek-Gremplewicz, A. Jozkowicz, and J. Dulak, “The role of oxidative stress in skeletal muscle injury and regeneration: focus on antioxidant enzymes,” *Journal of Muscle Research and Cell Motility*, vol. 36, no. 6, pp. 377–393, 2015.
- [40] R. Pääsuke, M. Eimre, A. Piirsoo et al., “Proliferation of human primary myoblasts is associated with altered energy metabolism in dependence on ageing *in vivo* and *in vitro*,” *Oxidative Medicine and Cellular Longevity*, vol. 2016, Article ID 8296150, 10 pages, 2016.
- [41] K. Q. de Andrade, F. A. Moura, J. M. dos Santos, O. R. de Araújo, J. C. de Farias Santos, and M. O. Goulart, “Oxidative stress and inflammation in hepatic diseases: therapeutic possibilities of N-acetylcysteine,” *International Journal of Molecular Sciences*, vol. 16, no. 12, pp. 30269–30308, 2015.
- [42] S. P. Patel, P. G. Sullivan, J. D. Pandya et al., “N-Acetylcysteine amide preserves mitochondrial bioenergetics and improves functional recovery following spinal trauma,” *Experimental Neurology*, vol. 257, pp. 95–105, 2014.
- [43] M. Sandri, “Signaling in muscle atrophy and hypertrophy,” *Physiology*, vol. 23, no. 3, pp. 160–170, 2008.
- [44] A. Navarro and A. Boveris, “The mitochondrial energy transduction system and the aging process,” *American Journal of Physiology. Cell Physiology*, vol. 292, no. 2, pp. C670–C686, 2007.
- [45] Y. Yaniv, M. Juhaszova, and S. J. Sollott, “Age-related changes of myocardial ATP supply and demand mechanisms,” *Trends in Endocrinology and Metabolism*, vol. 24, no. 10, pp. 495–505, 2013.
- [46] B. K. Chacko, P. A. Kramer, S. Ravi et al., “The bioenergetic health index: a new concept in mitochondrial translational research,” *Clinical Science*, vol. 127, no. 6, pp. 367–373, 2014.
- [47] M. A. Baraibar, J. Hyzewicz, A. Rogowska-Wrzesinska et al., “Impaired energy metabolism of senescent muscle satellite cells is associated with oxidative modifications of glycolytic enzymes,” *Aging*, vol. 8, no. 12, pp. 3375–3389, 2016.
- [48] A. H. V. Remels, R. C. J. Langen, P. Schrauwen, G. Schaart, A. M. W. J. Schols, and H. R. Gosker, “Regulation of mitochondrial biogenesis during myogenesis,” *Molecular and Cellular Endocrinology*, vol. 315, no. 1-2, pp. 113–120, 2010.
- [49] V. I. Korolchuk, S. Miwa, B. Carroll, and T. von Zglinicki, “Mitochondria in cell senescence: is mitophagy the weakest link?,” *eBioMedicine*, vol. 21, pp. 7–13, 2017.

Review Article

Mitochondrial Antioxidants and the Maintenance of Cellular Hydrogen Peroxide Levels

Ryan J. Mailloux 

Department of Biochemistry, Memorial University of Newfoundland, St. John's, NL, Canada

Correspondence should be addressed to Ryan J. Mailloux; rjmailloux@mun.ca

Received 5 April 2018; Accepted 15 May 2018; Published 2 July 2018

Academic Editor: Marcelo Mori

Copyright © 2018 Ryan J. Mailloux. This is an open access article distributed under the Creative Commons Attribution License, which permits unrestricted use, distribution, and reproduction in any medium, provided the original work is properly cited.

For over 40 years, mitochondrial reactive oxygen species (ROS) production and balance has been studied in the context of oxidative distress and tissue damage. However, research over the past decade has demonstrated that the mitochondria have a more complicated relationship with ROS. Superoxide ($O_2^{\bullet-}$) and hydrogen peroxide (H_2O_2) are the proximal ROS formed by the mitochondria, and the latter molecule is used as a secondary messenger to coordinate oxidative metabolism with changes in cell physiology. Like any other secondary messenger, H_2O_2 levels need to be regulated through its production and degradation and the mitochondria are enriched with the antioxidant defenses required to degrade ROS formed by nutrient oxidation and respiration. Recent work has also demonstrated that these antioxidant systems also carry the capacity to clear H_2O_2 formed outside of mitochondria. These observations led to the development of the postulate that the mitochondria serve as “ROS stabilizing devices” that buffer cellular H_2O_2 levels. Here, I provide an updated view on mitochondrial ROS homeostasis and discuss the “ROS stabilizing” function of the mitochondria in mammalian cells. This will be followed by a hypothetical discussion on the potential function of the mitochondria and proton motive force in degrading cellular H_2O_2 signals emanating from cytosolic enzymes.

1. Introduction

ROS genesis by the mammalian mitochondria relies on the same electron transfer pathways that are also involved in nutrient oxidation and the biosynthesis of ATP. Electrons mobilized from the combustion of carbon are transferred to complexes I and II of the respiratory chain through the carriers NADH and succinate, respectively. After entry into the electron transport chain (ETC), electrons are ferried through the ubiquinone (UQ) pool and complex III to complex IV, reducing molecular oxygen (O_2) to water [1]. Electron transfer through this chain is a thermodynamically favorable process and coupled with the pumping of protons by complexes I, III, and IV [2]. This creates an electrochemical difference of protons across the mitochondrial inner membrane (MIM), called a proton motive force (PMF), that is used by complex V to make ATP [2]. After its production, ATP is exported into the cytosol through the ADP/ATP translocase, also known as adenine nucleotide translocator (ANT), to perform useful “work” in the cell [3]. The proton

gradient formed by the flux of electrons through the respiratory chain is also used for the selective uptake of solutes and proteins into the matrix. Proton return to the matrix also plays a critical role in the regulation of ROS levels. For instance, proton return through nicotinamide nucleotide transhydrogenase (NNT) is required for the provision of NADPH, a vital component of H_2O_2 -degrading antioxidant systems [4].

Mitochondria are equipped with antioxidant defenses to quench ROS [5]. However, these defenses are not used exclusively to clear ROS formed by nutrient metabolism and respiration. Several studies have demonstrated that matrix antioxidant defenses can also quench extramitochondrial H_2O_2 [6–8]. Clearance of extramitochondrial H_2O_2 depends on the redox buffering capacity of the matrix which is influenced by the availability of ROS and NADPH. Therefore, the degradation of cellular H_2O_2 by the mitochondria (rate of uptake, $rate_u$) depends on (1) rate of mitochondrial H_2O_2 production ($rate_{p,mito}$) and (2) the rate of mitochondrial H_2O_2 degradation ($rate_{consumption}$) (Figure 1). Here,

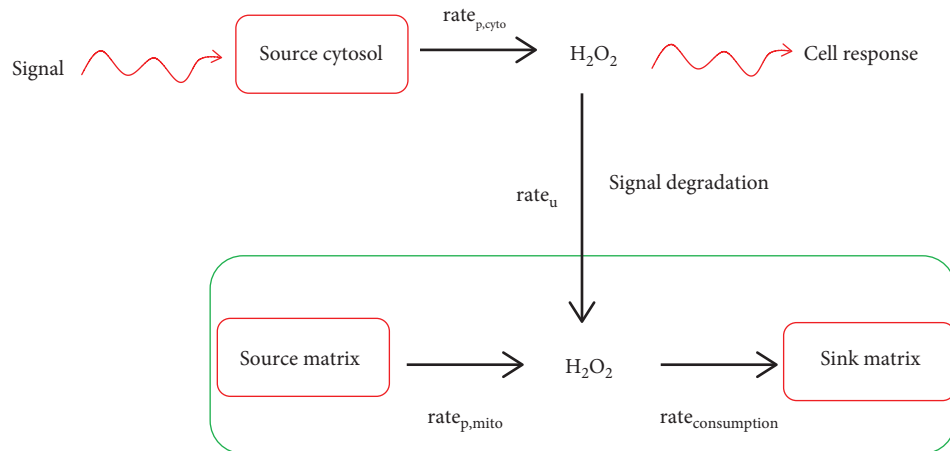


FIGURE 1: Mitochondria are a sink for cellular hydrogen peroxide. The function of mitochondria as a cellular ROS stabilizer depends on the rate of H_2O_2 production ($rate_{p,mito}$) and consumption ($rate_{consumption}$). Accumulation of cellular H_2O_2 serves as an important signal, which can be desensitized by mitochondrial antioxidant defenses. The rate of H_2O_2 uptake by the mitochondria ($rate_u$) is dependent on the redox buffering capacity of the matrix.

I review our current understanding of how the mitochondria buffer cellular H_2O_2 using the glutathione (GSH), thioredoxin (TRX), and catalase systems. I also discuss how this buffering capacity relies on mitochondrial respiration for the provision of NADPH through NNT. Finally, I elaborate on how this H_2O_2 buffering function of the mitochondria can potentially quench redox signals emanating from cytosolic ROS producers in response to physiological stimuli (Figure 1).

2. Mitochondrial H_2O_2 Homeostasis

2.1. Sources of Mitochondrial ROS. Mitochondria can contain up to 12 potential sources of ROS associated with nutrient oxidation (Table 1). These individual sites of production can be classified into two groups; the NADH/NAD⁺ isopotential group and the UQH₂/UQ isopotential group (Table 1). The ROS-producing properties of these different enzymes have recently been reviewed extensively [9, 10]. ROS producers that fall in the former group generate $O_2^{\bullet-}/H_2O_2$ in the presence of NADH. Group two enzymes on the other hand use the UQH₂ pool to make ROS (Table 1) [10]. Some of these enzymes are high capacity sites for ROS release whereas others have low rates of production. In addition, which enzyme serves as a high capacity site for production can vary between different tissues, which may be related to substrate availability and mitochondrial bioenergetics (Table 1). For example, α -ketoglutarate dehydrogenase complex (KGDH), pyruvate dehydrogenase complex (PDH), and complex III account for ~90% of the ROS released by liver mitochondria (Table 1) [8]. Complexes I and III and to a lesser extent complex II display high rates for ROS production in heart mitochondria (Table 1) [11]. It has also been documented that KGDH and PDH produce ROS in cardiac mitochondria, with the former generating more than the latter [12]. However, it has been recently estimated that KGDH and PDH make minor contributions

to overall ROS release from cardiac mitochondria [11]. Finally, complexes I, II and III, KGDH and PDH, and *sn*-glycerol-3-phosphate dehydrogenase (G3PDH) serve as high capacity sites in the muscle and KGDH and PDH produce ~8x and ~4x more ROS than complex I in these mitochondria [10]. The rate of production from these sites can vary considerably in response to different physiological conditions, which can affect the strength and duration of the H_2O_2 signal. The concentration and type of the substrate being oxidized and concentration and redox state of the electron-donating site are the most important factors that influence the rate of ROS release from the mitochondria [10]. Other factors like membrane potential strength, NADH availability, allosteric regulators, or posttranslational modifications, like protein S-glutathionylation, also affect ROS production [13, 14]. Conditions that mimic rest or exercise in the muscle have been shown to dictate which sites form the most ROS in muscle mitochondria, which can affect how much H_2O_2 is released into the extramitochondrial space [15]. This is associated with variations in the availability of different substrates and ions that ultimately influence the rate of ROS release from these sites [15]. Overall, up to 12 sites of production can contribute to the overall rate for ROS production ($rate_{p,mito}$) in the mitochondria (Figure 1). In addition, $rate_{p,mito}$ depends on the bioenergetics of the mitochondria and can vary in response to different physiological cues.

2.2. Antioxidant Defense Systems. The overall concentration of mitochondrial H_2O_2 also depends on the rate of its consumption ($rate_{consumption}$) (Figure 1). The routine degradation of H_2O_2 is vital for controlling its secondary signaling properties and preventing oxidative distress. Mitochondrial ROS producers, like KGDH, PDH, and complexes I and II, have been shown to produce a mixture of $O_2^{\bullet-}$ and H_2O_2 , which is related to the free radical properties of flavin nucleotides [12, 16]. Recent estimates indicate that ~75% of

TABLE 1: Mitochondria can contain up to twelve sources of $O_2^{\bullet-}/H_2O_2$. The twelve different enzymes are associated with nutrient metabolism and can be subcategorized in two groups: the NADH/NAD⁺ isopotential group and UQH₂/UQ isopotential group. The different sites make variable contributions to overall ROS release in different tissues.

Isopotential group	Enzyme	Site of production	High capacity site?
NADH/NAD ⁺	α -Ketoglutarate dehydrogenase	FAD (K _F)	Yes: liver, muscle [8, 10] No: cardiac [11]
	Pyruvate dehydrogenase	FAD (P _F)	Yes: liver, muscle [8] No: cardiac [11]
	Branched-chain keto acid dehydrogenase	FAD (B _F)	Moderate: muscle [10] Unknown: liver, cardiac.
	2-Oxoadipate dehydrogenase	FAD (O _F)	Moderate: muscle [10] Unknown: liver, heart
UQH ₂ /UQ	Complex I	FMN (I _F)	Yes: cardiac [11] No: muscle, liver [8]
	Complex I	UQ binding site (I _Q)	Yes: muscle [10] Unknown: liver, cardiac
	Complex II	FAD (II _F)	Yes: muscle, liver (129 mice only), cardiac [61]. No: liver (C57Bl6N) [11].
	Complex III	UQ outer leaflet binding site (III _{Qo})	Yes: muscle, liver, cardiac [8]
	Electron transfer flavoprotein: ubiquinone oxidoreductase	FAD (E _F)	No: muscle [10] Unknown: liver, cardiac
	<i>sn</i> -Glycerol-3-phosphate dehydrogenase	FAD (G _F)	Yes: muscle, liver, cardiac [10]
	Proline dehydrogenase	FAD (P _F)	No: muscle [10] Unknown: liver, cardiac
	Dihydroorotate dehydrogenase	FAD (D _F)	No: muscle [10] Unknown: liver, cardiac

the total ROS released by PDH and KGDH is H₂O₂ [17, 18]. However, mitochondria also form $O_2^{\bullet-}$ nonetheless which needs to be removed rapidly to avoid the deactivation of Fe-S cluster-containing proteins. Mitochondria contain two superoxide dismutase isozymes (SOD), MnSOD (matrix-bound) and Cu/ZnSOD (intermembrane space) that catalyze the dismutation of two $O_2^{\bullet-}$ to H₂O₂ [13]. SOD is highly concentrated in the mitochondria (10 μ M) and displays rapid kinetics ($k \approx 1.8 \times 10^9 M^{-1} s^{-1}$), maintaining the concentration of $O_2^{\bullet-}$ at ~10–200 pM [13]. Therefore, although mitochondria do produce $O_2^{\bullet-}$ via the univalent reduction of O₂, the dominant ROS in the matrix environment is H₂O₂.

Mitochondria are equipped with two main H₂O₂ degrading pathways, the GSH and TRX2 systems [19]. Liver and cardiac mitochondria have also been found to contain catalase, which plays an important role in eliminating H₂O₂ [8, 20]. In contrast to catalase, the GSH and TRX2 systems require the reductive power of NADPH to eliminate ROS. The glutathione system relies on the oxidation of two GSH molecules in the presence of H₂O₂-forming glutathione disulfide (GSSG), a reaction catalyzed in the mitochondria by glutathione peroxidase (GPX). Mitochondria contain two GPX isozymes, GPX1 and GPX4. Both isozymes catalyze the sequestration of H₂O₂ with high efficiency ($k_{GPX1} \approx 6 \times 10^7 M^{-1} s^{-1}$ and $k_{GPX4} \approx 3 \times 10^6 M^{-1} s^{-1}$) [21]. Restoration of GSH levels after a round of H₂O₂ clearance is catalyzed by glutathione reductase (GR) in the presence of NADPH. The TRX system utilizes the catalytic activity

of peroxiredoxin (PRX), which contains a peroxidic cysteine (Cys_p) in its active site to sequester H₂O₂ [22]. The oxidized Cys_p is resolved by a neighboring cysteine residue (resolving cysteine, Cys_R) forming an intermolecular disulfide bridge. In the matrix, PRX3 and PRX5 are responsible for catalyzing these reactions ($k_{PRX3} \approx 2 \times 10^7 M^{-1} s^{-1}$ and $k_{PRX5} \approx 3 \times 10^5 M^{-1} s^{-1}$) [21]. In the matrix of the mitochondria, the reductive power stored in TRX2 reactivates PRX3 or 5 through a simple disulfide exchange reaction [23]. TRX2 is then reactivated by thioredoxin reductase-2 (TR2) in the presence of NADPH. Mitochondria have also been reported to use α -keto acids to spontaneously eliminate H₂O₂ [24]. Unfortunately, α -keto acids display slow kinetics for H₂O₂ degradation [25]. In addition, millimolar amounts are required to quench H₂O₂. Pyruvate has been reported to accumulate to ~0.5 mM but α -ketoglutarate typically occurs in the low μ M range [26]. By contrast, GPX1 and PRX3 occur at ~2 μ M and ~60 μ M, respectively, in the matrix and display high rates for H₂O₂ elimination. Therefore, it is unlikely that α -keto acids make any real contribution to H₂O₂ removal *in vivo*.

The contributions of the GSH and TRX2 systems to H₂O₂ elimination has been enthusiastically debated for several years. Competitive kinetic analyses contended that PRX accounts for ~90% of the H₂O₂ removal in the mitochondria [21]. Moreover, genetic ablation of the *Trx2* gene is embryonically lethal whereas loss of the *Gpx1* and *Gpx4* genes only sensitizes cells towards oxidative distress [27]. However, it needs to be emphasized that GPX1 and 4 are

used exclusively for the elimination of H_2O_2 and lipid hydroperoxides whereas TRX2 is required to reduce disulfide bridges in a multitude of enzymes including ribonucleotide reductase. In addition, the impact of ablating the *Prx3* gene has not been examined and recent work utilizing cell lines has demonstrated that both systems are equally important at eliminating H_2O_2 [28]. Recent work has also found that the TRX2 system may fulfill a secondary function in eliminating H_2O_2 formed by respiration [8]. Indeed, Slade et al. found that only GSH and catalase were involved in eliminating H_2O_2 in mouse liver mitochondria whereas the TRX2 system made a negligible contribution [8]. Similar observations were made with rat liver mitochondria [29]. In fact, Rigobello et al. showed that the TRX2 system contributed to H_2O_2 elimination only when ROS was overproduced by liver mitochondria following treatment with the electron transport chain blocker, antimycin A [29]. These findings, however, do contradict studies conducted with muscle mitochondria. In two separate studies, it was demonstrated that the TRX2 system is integral for eliminating H_2O_2 formed by respiration [7, 30]. In addition, the GSH system was also found to play an important part in H_2O_2 removal in skeletal muscle mitochondria [7]. Similar observations were also made with neural mitochondria and skeletal muscle fibers [6, 30]. Although speculative, it is possible that different tissues rely on different systems for the elimination of H_2O_2 . Hepatocytes are routinely exposed to high ROS due to their normal physiological functions and thus may rely on catalase and GSH to maintain the steady-state level of H_2O_2 with the TRX2 system serving as the third line of defense in case levels get too high. As indicated above, TRX2 is vital for reducing disulfide bridges formed in various proteins including PRX enzymes. Therefore, it is possible that liver cells may reserve TRX2 for the reduction of disulfide bonds and utilize it for antioxidant defense when other systems are overwhelmed by H_2O_2 . By contrast, muscle and neural mitochondria are not routinely exposed to high ROS like hepatocytes and may simply utilize the GSH and TRX2 systems for H_2O_2 elimination.

2.3. Provision of NADPH and the Importance of Transhydrogenase. Antioxidant defenses depend on the reductive power stored in NADPH. Therefore, H_2O_2 degradation ultimately relies on the provision of NADPH. Mitochondria contain an entire suite of NADPH-producing enzymes that support antioxidant defenses. The complement of enzymes involved in producing NADPH in the matrix of mitochondria includes malic enzyme (ME), glutamate dehydrogenase (GDH), $NADP^+$ -dependent isocitrate dehydrogenase (IDH2), and NNT [31, 32]. It has also been found that mitochondria contain a matrix-associated glucose-6-phosphate dehydrogenase (G6PDH) isozyme, which has been speculated to play a role in the production of mitochondrial ribose sugars for nucleotide biosynthesis [33]. Unlike the other NADPH producers, which simply couple the oxidation of carbon to the reduction of $NADP^+$, NNT actually assembles in the mitochondrial inner membrane and couples proton return to the matrix to the transfer of a hydride from NADH to $NADP^+$ [34].

Work over the past decade has demonstrated that NNT is an important NADPH supplier in the mitochondria. This importance was first recognized when it was discovered that the C57Bl/6J mouse strain carries a loss-of-function variance in the *Nnt* gene [35]. These mice are glucose intolerant and have a glucocorticoid deficiency [36, 37]. Variances in the *Nnt* gene in humans are also associated with familial glucocorticoid deficiency [38]. The observation that the loss of the *Nnt* gene results in glucocorticoid deficiency is intriguing from a redox signaling perspective since it was recently found that mitochondrial ROS signals play a critical role in glucocorticoid biosynthesis and that oxidative distress hinders steroidogenesis [39]. Loss of NNT sensitizes mitochondria to oxidative distress, increases ROS release, and induces abnormalities in mitochondrial redox buffering capacity [32]. Deletion of the *Nnt* gene diminishes NADPH recovery time in liver mitochondria challenged with *tert*-butyl hydroperoxide [31]. In addition, there are no compensatory increases in the activities of IDH2, ME, or GDH in liver mitochondria from mice homozygous or heterozygous for the *Nnt* gene unless their cognate substrates are supplied at high concentrations [31, 32]. Loss of NNT also leads to spontaneous NADPH oxidation and sensitizes the mitochondria to permeability pore opening [32]. In addition, substrate supply plays an integral role in driving NADPH formation by NNT. It has been estimated that NNT accounts for most of the NADPH production in the mitochondria. This, however, depends on the bioenergetic state of the mitochondria [31]. For instance, up to 100% of the total NADPH can be produced by NNT in the mitochondria operating under state 4 respiratory conditions [31]. Induction of state 3 respiration diminishes the contribution of NNT towards NADPH production (accounting for ~50% or lower) [31]. At this point, it should be emphasized that state 3 respiratory conditions are highly artificial and do not represent a natural bioenergetic state of the mitochondria in cells. It has been estimated that the mitochondria actually operate between state 3 and 4 respiration in neural and muscle tissue and cultured cells (referred to as state_{apparent} to reflect the intermediary state of respiration in cells) [40–42]. Therefore, NNT is likely to be the major supplier for NADPH under physiological conditions. Finally, collapsing the mitochondrial membrane potential abolishes the NADPH-producing activity of NNT [31]. In fact, in one intriguing study, it was observed that collapsing the membrane potential reverses NNT [4]. In this case, it was found that it transfers a hydride from NADPH to NAD^+ resulting in the pumping of protons into the intermembrane space [4]. This results in the depletion of mitochondrial NADPH, leaving cells vulnerable to oxidative attack. This also demonstrates the importance of NNT in maintaining the NADPH pool since its reversal results in oxidation of ROS clearing systems culminating with oxidative damage and development of heart disease.

Other sources of NADPH can, to a certain degree, compensate for the loss of NNT. C57Bl/6J mice are still viable regardless of the loss-of-function mutation for the *Nnt* gene. In addition, liver mitochondria from NNT knockout mice can maintain normal NADPH levels if isocitrate, malate, or

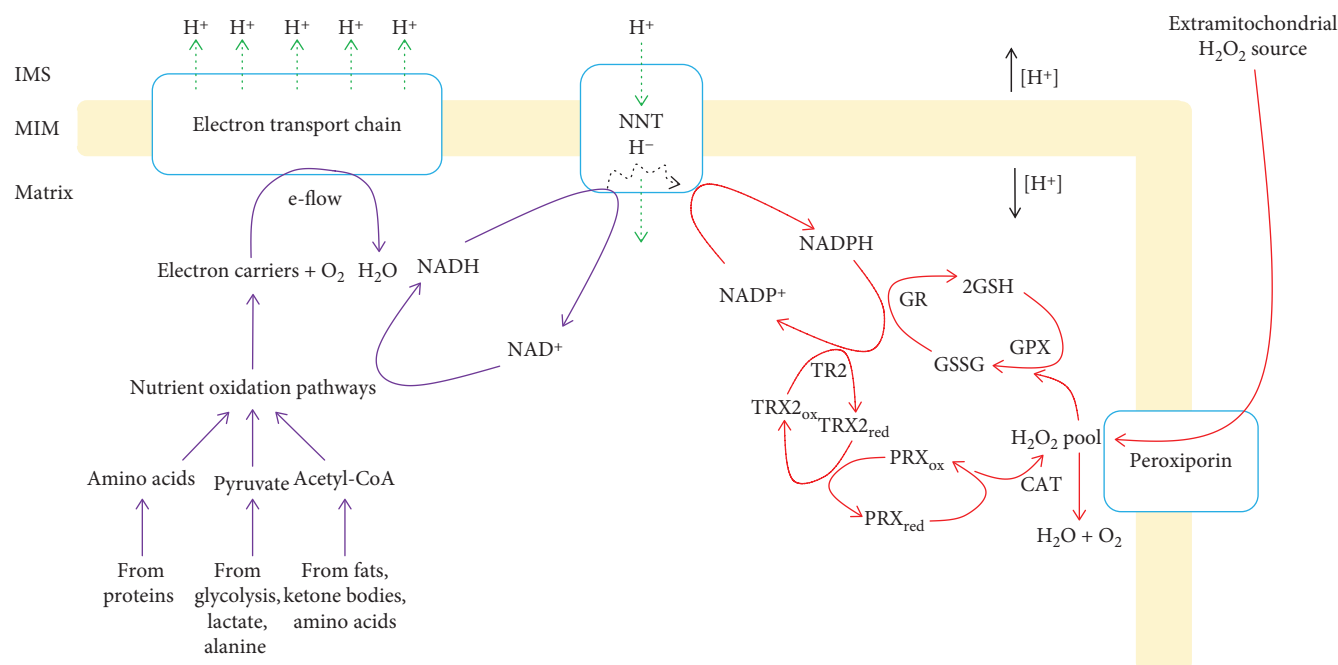


FIGURE 2: Nicotinamide nucleotide transhydrogenase (NNT) plays a central role in clearing cellular hydrogen peroxide. The combustion of carbon yielded from the metabolism of different nutrients generates electron carriers that are oxidized by respiratory chain enzymes. The electrons liberated by carrier oxidation results in the pumping of protons into the intermembrane space. Protons are returned to the matrix through NNT which powers the transfer of a hydride from NADH to NADP⁺, forming NADPH. Hydrogen peroxide generated in the cytoplasm is imported into the matrix by peroxiporin and then degraded by three different antioxidant pathways. NADPH is used to reduce oxidized GSH and TRX2 after a round of H₂O₂ elimination. Catalase can also remove H₂O₂.

glutamate are added to the reaction mixtures [31]. However, as noted above, compensation by these other NADPH-forming enzymes is limited [31]. Other pathways can also serve as NADPH suppliers in the mitochondria. Matrix-associated G6PDH was found to be an important source of NADPH in cultured myoblasts, human myotubes, and HEK293 cells cultured in a high glucose medium [33]. By contrast, exposure of cells to a low glucose medium rich in Krebs cycle-linked substrates upregulates IDH2 [33]. Therefore, mitochondria do have the ability to use various carbon sources to sustain NADPH production. However, it is likely that NNT is the major supplier *in vivo* since it utilizes a central and sustainable energy source, the proton gradient, to form NADPH.

3. Mitochondria as a Sink for Cellular Hydrogen Peroxide

Because the mitochondria are abundant in mammalian cells and enriched in antioxidant defenses, these organelles can serve as an ideal sink for cytosolic or extracellular H₂O₂. The rate for H₂O₂ uptake by the mitochondria depends on its redox buffering capacity (Figure 1). The capacity of mammalian mitochondria to clear H₂O₂ from the surrounding environment was initially proposed by Jezek and Hlavata in 2005 [43]. In this seminal article, it was hypothesized that the mitochondria can quench cytosolic H₂O₂ when the rate for ROS release from the respiratory chain (or potentially

other sources) was low [43]. This would maintain mitochondrial redox buffering capacity in a more reduced state promoting clearance of H₂O₂ formed in the cytosol or extracellular milieu. The authors based this hypothesis on findings showing that uncoupling the PMF diminishes ROS release from the respiratory chain, allowing the clearance of H₂O₂ outside of the mitochondria [43]. These concepts were then tested with brain mitochondria where it was found that matrix antioxidant defenses can stabilize the steady-state concentration of H₂O₂ in the surrounding medium [6]. Through a series of well-designed experiments, it was demonstrated that the mitochondria serve as a “dampening device” for ROS, sequestering H₂O₂ when it is at a higher than normal concentration in the surrounding medium (Figure 2) [6]. Another key finding from this study was that the “ROS-stabilizing” feature of the mitochondria relied on substrate oxidation and respiration (Figure 2) [6]. This would allow for the provision of NADPH, a key ingredient for the maintenance of antioxidant defenses. The concept that the mitochondria can clear H₂O₂ from the surrounding medium was also demonstrated with muscle and liver mitochondria. Several studies found that rat muscle mitochondria can quench H₂O₂ from the surrounding buffer using both the GSH and TRX2 systems [7, 30]. It is also possible that catalase also aids in eliminating H₂O₂ external to muscle mitochondria as well [44]. The GSH and TRX2 systems play key roles in maintaining the steady-state level of extramitochondrial H₂O₂ levels in rat and mouse liver

mitochondria [8]. Slade et al. also showed that catalase plays an integral role in eliminating extramitochondrial H_2O_2 when it is in excess [8]. Indeed, liver mitochondria isolated from C57Bl/6N mice were able to clear $2\ \mu\text{M}$ H_2O_2 within 2.5 minutes and catalase comprised $\sim 55\text{--}60\%$ of this quenching activity [8]. At lower levels, GSH and TRX2 systems were crucial at maintaining H_2O_2 steady-state levels (sub μM range) outside of the mitochondria [8]. The caveat to the studies described above is that this H_2O_2 clearance feature was tested *in vitro* bringing into question the physiological relevance of mitochondria as cellular ROS-dampening devices. However, a recent study demonstrated that the mitochondria retain their capacity to clear cytosolic H_2O_2 in cardiac myoblasts [28]. In this seminal study, different mitochondrial antioxidant defenses and NADPH producers were knocked down to assess if the mitochondria are required to maintain the steady-state concentration of cytosolic H_2O_2 . The authors found that maintenance of the cytosolic redox environment is highly dependent on mitochondrial H_2O_2 buffering capacity [28]. Moreover, it was documented that mitochondrial antioxidant defenses play a central role in clearing cellular H_2O_2 . In addition, it was shown that this capacity is highly dependent on mitochondrial substrate oxidation and NADPH production by NNT [28]. Taken together, mitochondria have an innate ability to take up and degrade H_2O_2 , a feature that depends on the provision of NADPH by NNT.

The redox code is defined as a “*set of principles that describes the spatiotemporal positioning, in terms of the redox state, of the nicotinamide pool (NAD^+ and NADP^+) and thiols/disulfides relative to the redox proteome in biological systems*” [45]. At its core, the redox code is influenced by the rate of H_2O_2 production and consumption, both of which rely on nutrient oxidation and the proton motive force [45]. One critical observation made regarding the H_2O_2 -clearing abilities of the mitochondria is that it relies on substrate catabolism and respiration. The catabolism of carbon is required for the provision of NADPH and the maintenance of mitochondrial redox buffering networks in a reduced/active state. It is, therefore, also important to consider the source of this NADPH. Dey et al. demonstrated that knocking down IDH2, ME, or NNT does compromise the H_2O_2 quenching capacity of the mitochondria [28]. However, it was also observed that NNT was the largest contributor towards the degradation of H_2O_2 [28]. This agrees with the *in vitro* studies conducted with liver mitochondria that demonstrated that NNT is the chief supplier, and ME and IDH2 make minor contributions to the NADPH pool in the matrix [31]. Moreover, a study that was conducted with permeabilized muscle fibers found that NNT is crucial for mitochondrial H_2O_2 clearance and disabling this redox circuit can lead to the development of metabolic disorders [46]. Therefore, the ability of the mitochondria to clear H_2O_2 from the cytosolic environment is likely to be highly dependent on the NADPH-forming capacity of NNT. This would mean that cellular redox balance hinges on the capacity of the mitochondria to form a proton gradient (Figure 2).

4. Role of the Mitochondria in Degrading Cytosolic H_2O_2 Signals

It is now widely recognized that H_2O_2 produced by cytosolic enzymes serves as a critical secondary messenger required to regulate a wide range of cellular functions [47]. A variety of hormones including growth factors (platelet-derived growth factor (PDGF), epidermal growth factor (EGF), insulin, and IGF) and cytokines (tumour necrosis factor- α ; TNF α , and angiotensin II) can stimulate $\text{O}_2^{\bullet-}$ production by nonimmune cell NADPH oxidases (NOX) [47]. The $\text{O}_2^{\bullet-}$ formed by NOXs is then rapidly converted to H_2O_2 by SOD for the induction of oxidative eustress signaling pathways [48]. Hydrogen peroxide signals emanating from cytosolic enzymes have been proposed to proceed via two mechanisms: (1) the floodgate model and (2) the redox relay model (Figure 3). Empirical evidence has demonstrated that both systems are used by mammalian cells for information transmission. Work on the floodgate model can be traced back to a landmark study by Irani et al. where it was shown that PDGF can stimulate cellular H_2O_2 production in vascular smooth muscle cells leading to the induction of chemotaxis and DNA synthesis [49]. Later studies demonstrated that this was associated with increased growth factor receptor phosphorylation, which was related to the H_2O_2 -mediated deactivation of the protein tyrosine phosphatases [50–52]. The accumulation of H_2O_2 for signaling was found to be facilitated by the temporary oxidative deactivation of cytosolic peroxiredoxin (PRX1) [52]. This involves the oxidation of the catalytic Cys_p to sulfinic acid (SO_2H) through a sulfenic acid intermediate (SOH). The SO_2H can be reduced back to its corresponding thiol by sulfiredoxin (SRX), but the reaction is slow (Figure 3) [53]. This allows H_2O_2 to accumulate to a high enough concentration to serve as a secondary messenger. The redox relay mechanism basically involves a series of disulfide exchange reactions between PRX and a target protein (Figure 3). For instance, Sobotta et al. observed that the cytokine-mediated activation of STAT3, and its subsequent deactivation, involves a series of disulfide exchange reactions with oxidized PRX2 and TRX1 [54]. In this case, cytokine signaling induces a burst in H_2O_2 generation resulting in its degradation by the peroxidatic cysteine in PRX2 [54]. The resulting disulfide bridge formed between the peroxidatic cysteine and the resolving cysteine in PRX2 is reduced by STAT3, activating the protein [54]. This disulfide bridge is then reduced by TRX1 in the presence of NADPH, deactivating STAT3.

It is not known if mitochondrial antioxidant defenses are required to degrade cytosolic H_2O_2 signals formed by NOX (or other cytosolic enzymes) even though interactions between the mitochondria and NOX have been documented. For instance, mitochondria have been found to crosstalk with NOX through a process called “*feed forward cycling*” [55]. This mechanism involves crosstalk between NOX and the mitochondria resulting in the activation of ROS production from both sources. Mitochondria have several properties that allow it to serve as a sink for cellular H_2O_2 signals. First, respiring mitochondria can generate NADPH quickly. NNT is a major supplier for NADPH and plays a critical role in

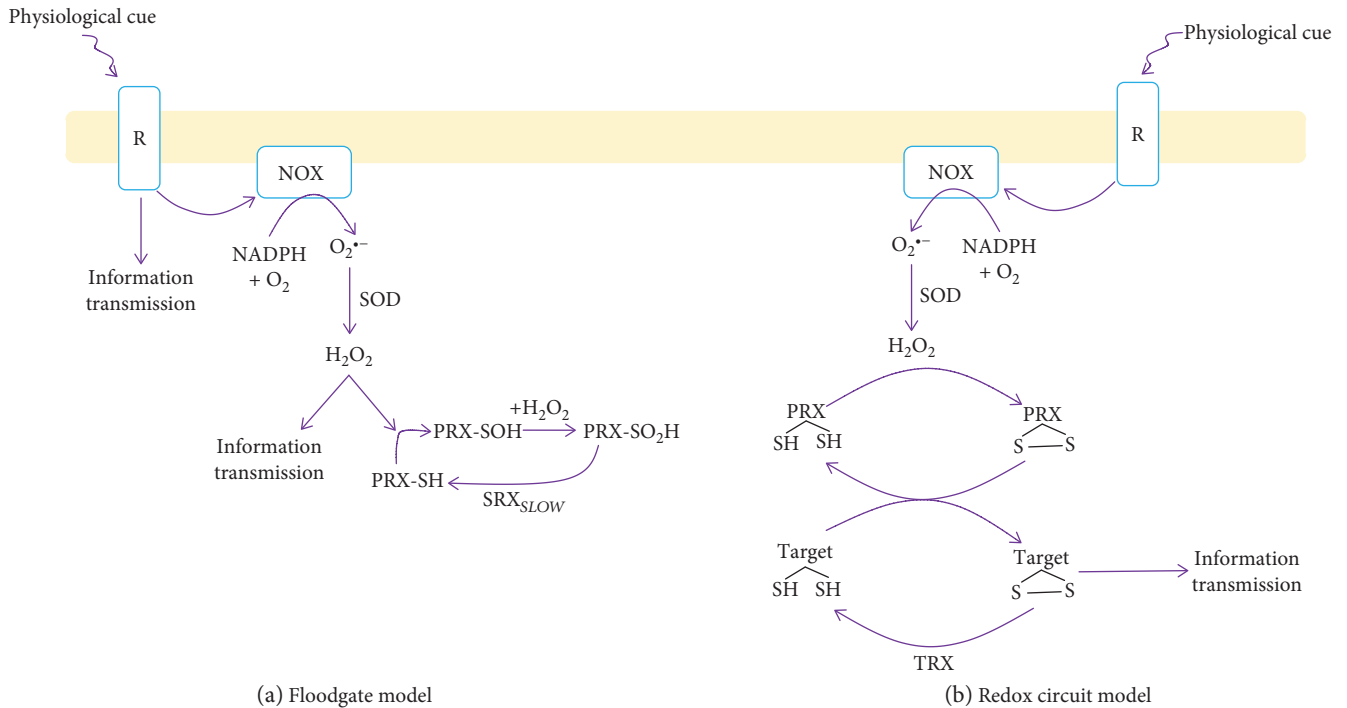


FIGURE 3: Hydrogen peroxide is a secondary messenger that transmits information in the cytosol using two different mechanisms: the floodgate and redox relay models. The floodgate model involves the activation of cell surface receptors by a physiological stimulus. This induces cell signaling cascades that also activate NADPH oxidase (NOX), activating the production of H₂O₂. The hydrogen peroxide yielded from NOX activation, results in the oxidative deactivation of peroxiredoxin-1 (PRX1). Hydrogen peroxide subsequently accumulates, inducing cell signaling pathways or reinforcing others through the deactivation of phosphatases. Reactivation of PRX1 requires sulfiredoxin (SRX). The redox relay model uses a series of thiol disulfide exchange reactions to activate or deactivate a target protein. Hydrogen peroxide generated by a physiological stimulus is first quenched by PRX2 forming a sulfenic acid on the peroxidatic catalytic cysteine. The sulfenic acid is resolved by a second cysteine forming a disulfide bridge. PRX2 is then reduced by STAT3 by a thiol disulfide exchange reaction.

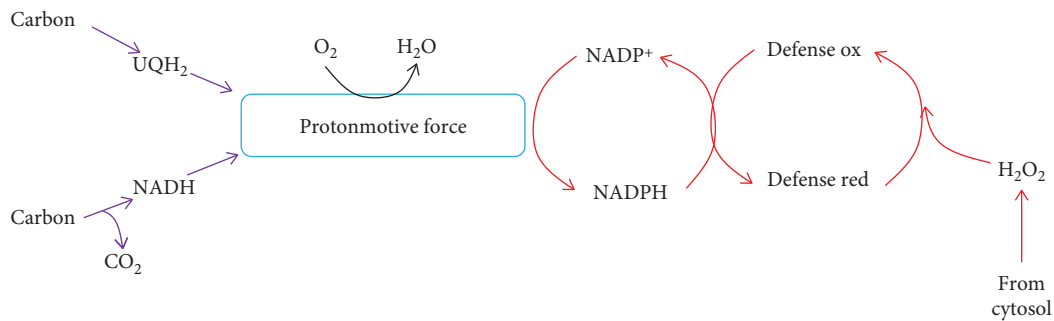


FIGURE 4: The proton gradient plays a central role in the cellular ROS stabilizing function of the mitochondria. Carbon oxidation forms the electron carriers, NADH and UQH₂, which are then oxidized by the electron transport chain. Electron flow creates a proton motive force which is tapped by transhydrogenase for the provision of NADPH for antioxidant defenses which degrades cellular H₂O₂ signals.

quenching cellular H₂O₂. When NNT is active, liver mitochondria can replenish matrix NADPH levels within a few minutes [31]. However, deletion of the *Nnt* gene induces a considerable lag in NADPH recovery in actively respiring mitochondria [31]. In addition, Dey et al. showed that NNT is a major NADPH supplier in cultured cells and plays an important role in cellular H₂O₂ degradation [28]. As noted in Section 3, several other enzymes can tap into various carbon sources to produce NADPH. However, using the proton gradient for NADPH production is advantageous

since it is a readily accessible form of sustainable energy that can be produced by the oxidation of a number of different carbon sources (Figure 2). Therefore, the capacity of the mitochondria to degrade cellular H₂O₂ signals may ultimately rely on the PMF and polarity of the mitochondrial inner membrane (Figure 4). A second important consideration is the resistance of PRX3 and 5 towards oxidative deactivation and the abundance of GSH in the matrix. The redox relay and floodgate systems in the cytosol rely on the temporary oxidative deactivation of PRX1 and 2 for signal

propagation. The caveat to this mechanism is the hindrance of an important H_2O_2 clearing system in the cytosol. Disabling a PRX1 and 2 could be dangerous since it can prolong redox signals that could potentially damage the cell. Mitochondria are not only enriched in antioxidant defenses but also contain PRX isoforms that are highly resistant to oxidative deactivation. It has been shown that PRX1 can rapidly undergo oxidative deactivation by H_2O_2 [56]. The matrix-associated isoform PRX3, on the other hand, is highly resistant to oxidative deactivation [56]. This would mean that the mitochondria can maintain their H_2O_2 -clearing capacity even when cytosolic systems may be deactivated by high H_2O_2 levels. Mitochondria are also rich in GSH (~5 mM) and contain high concentrations of the individual enzymes involved in antioxidant defenses (discussed in Section 3). Finally, liver, cardiac, and potentially muscle mitochondria contain catalase, which can also eliminate cytosolic H_2O_2 rapidly. Another important factor is that the thiol oxidoreductase, glutaredoxin-2 (GRX2), can substitute for TR2 if it is deactivated by lipid hydroperoxides and reactivate the TRX2 antioxidant system [57]. Finally, the same factors that induce cytosolic H_2O_2 signals have also been documented to activate mitochondrial respiration. Growth factor deprivation hinders mitochondrial respiration [58]. In addition, growth factors like IGF have been found to activate mitochondrial respiration through the induction of the PI3K signaling pathway [59]. Mitochondria are also equipped with regulatory mechanisms, including proton leaks, supercomplex assemblies, and protein S-glutathionylation reactions, that rapidly suppress ROS release from sites of production [60]. By suppressing ROS release, regulatory systems can promote the provision of NADPH for antioxidant defenses and the clearance of H_2O_2 . Therefore, although hypothetical at this point, mitochondria have a number of redox attributes that could potentially play a significant role in modulating cytosolic H_2O_2 signals by facilitating the desensitization of these signals.

5. Conclusion

Mitochondria are dynamic organelles that fulfill a myriad of cell functions. This includes serving as a platform for the transmission of cell signals. Mitochondria also serve as a critical source and sink for H_2O_2 , a secondary messenger that mediates cellular redox signals. Hydrogen peroxide is often dubbed a mitokine since its release from the mitochondria modulates cell functions in response to physiological cues. It is also apparent that the mitochondria have the capacity to serve as a cellular H_2O_2 stabilizing device. This is related to the high concentration of antioxidant defense enzymes in the matrix and its capacity to rapidly regenerate NADPH. Here, I have outlined how the ROS quenching capacity of the mitochondria can be utilized to degrade H_2O_2 signals emanating from cytosolic enzymes like NOX. Mitochondria are well equipped to serve as a cellular H_2O_2 signal dampener. The ability of the mitochondria to quench cellular H_2O_2 signals depends on the establishment of a proton motive force to support NADPH production for antioxidant

defenses (Figure 4). It is obvious that more research is required to understand how the mitochondria clear H_2O_2 from the surrounding environment, the role of NNT in this process, and the function of this ROS dampening feature in controlling cellular redox signals. Based on its bioenergetic properties and high amount of antioxidant enzymes, mitochondria are an excellent candidate for the modulation of cellular H_2O_2 signals.

Conflicts of Interest

The author declares that he has no conflicts of interest.

Acknowledgments

This article is dedicated to the memory of Richard Mailloux—he will be missed but never forgotten. This work was funded by the Natural Sciences and Engineering Research Council of Canada (Grant no. RGPIN-2016-04829).

References

- [1] M. D. Brand and D. G. Nicholls, "Assessing mitochondrial dysfunction in cells," *The Biochemical Journal*, vol. 435, no. 2, pp. 297–312, 2011.
- [2] D. G. Nicholls, "Forty years of Mitchell's proton circuit: from little grey books to little grey cells," *Biochimica et Biophysica Acta (BBA) - Bioenergetics*, vol. 1777, no. 7-8, pp. 550–556, 2008.
- [3] M. Klingenberg, "The ADP and ATP transport in mitochondria and its carrier," *Biochimica et Biophysica Acta (BBA) - Biomembranes*, vol. 1778, no. 10, pp. 1978–2021, 2008.
- [4] A. G. Nickel, A. von Hardenberg, M. Hohl et al., "Reversal of mitochondrial transhydrogenase causes oxidative stress in heart failure," *Cell Metabolism*, vol. 22, no. 3, pp. 472–484, 2015.
- [5] M. P. Murphy, "Mitochondrial thiols in antioxidant protection and redox signaling: distinct roles for glutathionylation and other thiol modifications," *Antioxidants & Redox Signaling*, vol. 16, no. 6, pp. 476–495, 2012.
- [6] A. A. Starkov, A. Y. Andreyev, S. F. Zhang et al., "Scavenging of H_2O_2 by mouse brain mitochondria," *Journal of Bioenergetics and Biomembranes*, vol. 46, no. 6, pp. 471–477, 2014.
- [7] D. Munro, S. Banh, E. Sotiri, N. Tamanna, and J. R. Treberg, "The thioredoxin and glutathione-dependent H_2O_2 consumption pathways in muscle mitochondria: involvement in H_2O_2 metabolism and consequence to H_2O_2 efflux assays," *Free Radical Biology & Medicine*, vol. 96, pp. 334–346, 2016.
- [8] L. Slade, J. Chalker, N. Kukulski, A. Young, D. Gardiner, and R. J. Mailloux, "Examination of the superoxide/hydrogen peroxide forming and quenching potential of mouse liver mitochondria," *Biochimica et Biophysica Acta (BBA) - General Subjects*, vol. 1861, no. 8, pp. 1960–1969, 2017.
- [9] H. S. Wong, P. A. Dighe, V. Mezera, P. A. Monternier, and M. D. Brand, "Production of superoxide and hydrogen peroxide from specific mitochondrial sites under different bioenergetic conditions," *The Journal of Biological Chemistry*, vol. 292, no. 41, pp. 16804–16809, 2017.
- [10] M. D. Brand, "Mitochondrial generation of superoxide and hydrogen peroxide as the source of mitochondrial redox signaling," *Free Radical Biology & Medicine*, vol. 100, pp. 14–31, 2016.

- [11] J. Chalker, D. Gardiner, N. Kuksal, and R. J. Mailloux, "Characterization of the impact of glutaredoxin-2 (GRX2) deficiency on superoxide/hydrogen peroxide release from cardiac and liver mitochondria," *Redox Biology*, vol. 15, pp. 216–227, 2018.
- [12] R. J. Mailloux, D. Gardiner, and M. O'Brien, "2-Oxoglutarate dehydrogenase is a more significant source of $O_2^{\bullet-}/H_2O_2$ than pyruvate dehydrogenase in cardiac and liver tissue," *Free Radical Biology & Medicine*, vol. 97, pp. 501–512, 2016.
- [13] M. P. Murphy, "How mitochondria produce reactive oxygen species," *The Biochemical Journal*, vol. 417, no. 1, pp. 1–13, 2009.
- [14] R. J. Mailloux and J. R. Treberg, "Protein S-glutathionylation links energy metabolism to redox signaling in mitochondria," *Redox Biology*, vol. 8, pp. 110–118, 2016.
- [15] R. L. S. Goncalves, C. L. Quinlan, I. V. Perevoshchikova, M. Hey-Mogensen, and M. D. Brand, "Sites of superoxide and hydrogen peroxide production by muscle mitochondria assessed ex vivo under conditions mimicking rest and exercise," *The Journal of Biological Chemistry*, vol. 290, no. 1, pp. 209–227, 2015.
- [16] V. G. Grivennikova and A. D. Vinogradov, "Partitioning of superoxide and hydrogen peroxide production by mitochondrial respiratory complex I," *Biochimica et Biophysica Acta (BBA) - Bioenergetics*, vol. 1827, no. 3, pp. 446–454, 2013.
- [17] J. R. Treberg, C. L. Quinlan, and M. D. Brand, "Hydrogen peroxide efflux from muscle mitochondria underestimates matrix superoxide production—a correction using glutathione depletion," *The FEBS Journal*, vol. 277, no. 13, pp. 2766–2778, 2010.
- [18] A. A. Starkov, G. Fiskum, C. Chinopoulos et al., "Mitochondrial alpha-ketoglutarate dehydrogenase complex generates reactive oxygen species," *The Journal of Neuroscience*, vol. 24, no. 36, pp. 7779–7788, 2004.
- [19] D. E. Handy and J. Loscalzo, "Redox regulation of mitochondrial function," *Antioxidants & Redox Signaling*, vol. 16, no. 11, pp. 1323–1367, 2012.
- [20] P. M. Rindler, A. Cacciola, M. Kinter, and L. I. Szveda, "Catalase-dependent H_2O_2 consumption by cardiac mitochondria and redox-mediated loss in insulin signaling," *American Journal of Physiology Heart and Circulatory Physiology*, vol. 311, no. 5, pp. H1091–H1096, 2016.
- [21] A. G. Cox, C. C. Winterbourn, and M. B. Hampton, "Mitochondrial peroxiredoxin involvement in antioxidant defence and redox signalling," *The Biochemical Journal*, vol. 425, no. 2, pp. 313–325, 2009.
- [22] Z. A. Wood, E. Schroder, J. Robin Harris, and L. B. Poole, "Structure, mechanism and regulation of peroxiredoxins," *Trends in Biochemical Sciences*, vol. 28, no. 1, pp. 32–40, 2003.
- [23] S. G. Rhee, "Overview on Peroxiredoxin," *Molecules and Cells*, vol. 39, no. 1, pp. 1–5, 2016.
- [24] N. I. Fedotcheva, A. P. Sokolov, and M. N. Kondrashova, "Nonezymatic formation of succinate in mitochondria under oxidative stress," *Free Radical Biology & Medicine*, vol. 41, no. 1, pp. 56–64, 2006.
- [25] J. Vasquez-Vivar, A. Denicola, R. Radi, and O. Augusto, "Peroxynitrite-mediated decarboxylation of pyruvate to both carbon dioxide and carbon dioxide radical anion," *Chemical Research in Toxicology*, vol. 10, no. 7, pp. 786–794, 1997.
- [26] R. J. Mailloux, S. L. McBride, and M. E. Harper, "Unearthing the secrets of mitochondrial ROS and glutathione in bioenergetics," *Trends in Biochemical Sciences*, vol. 38, no. 12, pp. 592–602, 2013.
- [27] R. T. Hamilton, M. E. Walsh, and H. Van Remmen, "Mouse models of oxidative stress indicate a role for modulating healthy aging," *Journal of Clinical & Experimental Pathology*, vol. 1, no. S4, 2012.
- [28] S. Dey, A. Sidor, and B. O'Rourke, "Compartment-specific control of reactive oxygen species scavenging by antioxidant pathway enzymes," *The Journal of Biological Chemistry*, vol. 291, no. 21, pp. 11185–11197, 2016.
- [29] M. P. Rigobello, A. Folda, M. C. Baldoiu, G. Scutari, and A. Bindoli, "Effect of auranofin on the mitochondrial generation of hydrogen peroxide. Role of thioredoxin reductase," *Free Radical Research*, vol. 39, no. 7, pp. 687–695, 2009.
- [30] K. H. Fisher-Wellman, L. A. A. Gilliam, C.-T. Lin, B. L. Cathey, D. S. Lark, and P. Darrell Neuffer, "Mitochondrial glutathione depletion reveals a novel role for the pyruvate dehydrogenase complex as a key H_2O_2 -emitting source under conditions of nutrient overload," *Free Radical Biology & Medicine*, vol. 65, pp. 1201–1208, 2013.
- [31] J. A. Ronchi, A. Francisco, L. A. C. Passos, T. R. Figueira, and R. F. Castilho, "The contribution of nicotinamide nucleotide transhydrogenase to peroxide detoxification is dependent on the respiratory state and counterbalanced by other sources of NADPH in liver mitochondria," *The Journal of Biological Chemistry*, vol. 291, no. 38, pp. 20173–20187, 2016.
- [32] J. A. Ronchi, T. R. Figueira, F. G. Ravagnani, H. C. F. Oliveira, A. E. Vercesi, and R. F. Castilho, "A spontaneous mutation in the nicotinamide nucleotide transhydrogenase gene of C57BL/6J mice results in mitochondrial redox abnormalities," *Free Radical Biology & Medicine*, vol. 63, pp. 446–456, 2013.
- [33] R. J. Mailloux and M. E. Harper, "Glucose regulates enzymatic sources of mitochondrial NADPH in skeletal muscle cells; a novel role for glucose-6-phosphate dehydrogenase," *The FASEB Journal*, vol. 24, no. 7, pp. 2495–2506, 2010.
- [34] Q. Zhang, P. S. Padayatti, and J. H. Leung, "Proton-translocating nicotinamide nucleotide transhydrogenase: a structural perspective," *Frontiers in Physiology*, vol. 8, p. 1089, 2017.
- [35] A. A. Toye, J. D. Lippiat, P. Proks et al., "A genetic and physiological study of impaired glucose homeostasis control in C57BL/6J mice," *Diabetologia*, vol. 48, no. 4, pp. 675–686, 2005.
- [36] H. Freeman, K. Shimomura, E. Horner, R. D. Cox, and F. M. Ashcroft, "Nicotinamide nucleotide transhydrogenase: a key role in insulin secretion," *Cell Metabolism*, vol. 3, no. 1, pp. 35–45, 2006.
- [37] E. Meimaridou, J. Kowalczyk, L. Guasti et al., "Mutations in NNT encoding nicotinamide nucleotide transhydrogenase cause familial glucocorticoid deficiency," *Nature Genetics*, vol. 44, no. 7, pp. 740–742, 2012.
- [38] E. Meimaridou, C. R. Hughes, J. Kowalczyk et al., "Familial glucocorticoid deficiency: new genes and mechanisms," *Molecular and Cellular Endocrinology*, vol. 371, no. 1–2, pp. 195–200, 2013.
- [39] I. S. Kil, S. K. Lee, K. W. Ryu et al., "Feedback control of adrenal steroidogenesis via H_2O_2 -dependent, reversible inactivation of peroxiredoxin III in mitochondria," *Molecular Cell*, vol. 46, no. 5, pp. 584–594, 2012.
- [40] V. P. Skulachev, "Cationic antioxidants as a powerful tool against mitochondrial oxidative stress," *Biochemical and*

- Biophysical Research Communications*, vol. 441, no. 2, pp. 275–279, 2013.
- [41] J. Truong, R. J. Mailloux, and H. M. Chan, “Impact of methylmercury exposure on mitochondrial energetics in AC16 and H9C2 cardiomyocytes,” *Toxicology In Vitro*, vol. 29, no. 5, pp. 953–961, 2015.
- [42] B. G. Hill, G. A. Benavides, J. R. Lancaster et al., “Integration of cellular bioenergetics with mitochondrial quality control and autophagy,” *Biological Chemistry*, vol. 393, no. 12, pp. 1485–1512, 2012.
- [43] P. Jezek and L. Hlavata, “Mitochondria in homeostasis of reactive oxygen species in cell, tissues, and organism,” *The International Journal of Biochemistry & Cell Biology*, vol. 37, no. 12, pp. 2478–2503, 2005.
- [44] D. Munro and J. R. Treberg, “A radical shift in perspective: mitochondria as regulators of reactive oxygen species,” *The Journal of Experimental Biology*, vol. 220, no. 7, pp. 1170–1180, 2017.
- [45] D. P. Jones and H. Sies, “The redox code,” *Antioxidants & Redox Signaling*, vol. 23, no. 9, pp. 734–746, 2015.
- [46] K. H. Fisher-Wellman, C.-T. Lin, T. E. Ryan et al., “Pyruvate dehydrogenase complex and nicotinamide nucleotide transhydrogenase constitute an energy-consuming redox circuit,” *The Biochemical Journal*, vol. 467, no. 2, pp. 271–280, 2015.
- [47] E. A. Veal, A. M. Day, and B. A. Morgan, “Hydrogen peroxide sensing and signaling,” *Molecular Cell*, vol. 26, no. 1, pp. 1–14, 2007.
- [48] H. Sies, “Hydrogen peroxide as a central redox signaling molecule in physiological oxidative stress: oxidative eustress,” *Redox Biology*, vol. 11, pp. 613–619, 2017.
- [49] K. Irani, Y. Xia, J. L. Zweier et al., “Mitogenic signaling mediated by oxidants in Ras-transformed fibroblasts,” *Science*, vol. 275, no. 5306, pp. 1649–1652, 1997.
- [50] S. R. Lee, K. S. Yang, J. Kwon, C. Lee, W. Jeong, and S. G. Rhee, “Reversible inactivation of the tumor suppressor PTEN by H₂O₂,” *The Journal of Biological Chemistry*, vol. 277, no. 23, pp. 20336–20342, 2002.
- [51] F. Antunes and P. M. Brito, “Quantitative biology of hydrogen peroxide signaling,” *Redox Biology*, vol. 13, pp. 1–7, 2017.
- [52] H. S. Marinho, C. Real, L. Cyrne, H. Soares, and F. Antunes, “Hydrogen peroxide sensing, signaling and regulation of transcription factors,” *Redox Biology*, vol. 2, pp. 535–562, 2014.
- [53] C. Lennicke, J. Rahn, R. Lichtenfels, L. A. Wessjohann, and B. Seliger, “Hydrogen peroxide - production, fate and role in redox signaling of tumor cells,” *Cell Communication and Signaling: CCS*, vol. 13, no. 1, p. 39, 2015.
- [54] M. C. Sobotta, W. Liou, S. Stöcker et al., “Peroxiredoxin-2 and STAT3 form a redox relay for H₂O₂ signaling,” *Nature Chemical Biology*, vol. 11, no. 1, pp. 64–70, 2015.
- [55] S. Dikalov, “Cross talk between mitochondria and NADPH oxidases,” *Free Radical Biology & Medicine*, vol. 51, no. 7, pp. 1289–1301, 2011.
- [56] A. C. Haynes, J. Qian, J. A. Reisz, C. M. Furdul, and W. T. Lowther, “Molecular basis for the resistance of human mitochondrial 2-Cys peroxiredoxin 3 to hyperoxidation,” *The Journal of Biological Chemistry*, vol. 288, no. 41, pp. 29714–29723, 2013.
- [57] H. Zhang, Y. Du, X. Zhang, J. Lu, and A. Holmgren, “Glutaredoxin 2 reduces both thioredoxin 2 and thioredoxin 1 and protects cells from apoptosis induced by auranofin and 4-hydroxynonenal,” *Antioxidants & Redox Signaling*, vol. 21, no. 5, pp. 669–681, 2014.
- [58] E. Gottlieb, S. M. Armour, and C. B. Thompson, “Mitochondrial respiratory control is lost during growth factor deprivation,” *Proceedings of the National Academy of Sciences of the United States of America*, vol. 99, no. 20, pp. 12801–12806, 2002.
- [59] H. Unterluggauer, E. Hutter, H. P. Viertler, and P. Janssen-Durr, “Insulin-like growth factor-induced signals activate mitochondrial respiration,” *Biotechnology Journal*, vol. 3, no. 6, pp. 813–816, 2008.
- [60] N. Kuksal, J. Chalker, and R. J. Mailloux, “Progress in understanding the molecular oxygen paradox - function of mitochondrial reactive oxygen species in cell signaling,” *Biological Chemistry*, vol. 398, no. 11, pp. 1209–1227, 2017.
- [61] N. Kuksal, D. Gardiner, D. Qi, and R. J. Mailloux, “Partial loss of complex I due to NDUFS4 deficiency augments myocardial reperfusion damage by increasing mitochondrial superoxide/hydrogen peroxide production,” *Biochemical and Biophysical Research Communications*, vol. 498, no. 1, pp. 214–220, 2018.